

Backfill Development: Evaluation of Potential Shaft Backfilling Materials

NWMO-TR-2023-03

April 2023

David Dixon and Jeff Stone

WSP – Golder

nwmo

NUCLEAR WASTE
MANAGEMENT
ORGANIZATION

SOCIÉTÉ DE GESTION
DES DÉCHETS
NUCLÉAIRES



Nuclear Waste Management Organization
22 St. Clair Avenue East, 4th Floor
Toronto, Ontario
M4T 2S3
Canada

Tel: 416-934-9814
Web: www.nwmo.ca

Backfill Development: Evaluation of Potential Shaft Backfilling Materials

NWMO-TR-2023-03

April 2023

David Dixon and Jeff Stone
WSP – Golder

This report has been prepared under contract to NWMO. The report has been reviewed by NWMO, but the views and conclusions are those of the authors and do not necessarily represent those of the NWMO.

All copyright and intellectual property rights belong to NWMO.

Document History

Title:	Backfill Development: Evaluation of Potential Shaft Backfilling Materials		
Report Number:	NWMO-TR-2023-03		
Revision:	R000	Date:	Month Year: April 2023
Author Company(s)			
Authored by:	David A. Dixon and Jeff Stone		
Verified by:	George Schneider		
Approved by:	George Schneider		
Nuclear Waste Management Organization			
Reviewed by:	Chang Seok Kim, Ken Birch, Mihaela Ion, Peter Keech		
Accepted by:	Paul Gierszewski		

Revision Summary

Revision Number	Date	Description of Changes/Improvements
R000	2023-04	Initial issue

ABSTRACT

Title: Backfill Development, Evaluation of Potential Shaft Backfilling Materials
Report No.: NWMO-TR-2023-03
Author(s): David A. Dixon and Jeff Stone
Company: WSP - Golder
Date: April 2023

The testing described in this report provides an evaluation of the potential for use of blends of Wyoming MX80 and aggregate materials (crushed limestone and granitic sand) as backfill in the shafts of a Deep Geological Repository. MX80-aggregate blends containing 40 to 90% MX80 were examined.

Compaction testing of the MX80-aggregate blends selected for evaluation were completed using Standard Compaction and Modified Compaction standards using low (~11 g/L) and high (~335 g/L) salinity mixing fluids. The results were used to evaluate the potential for these materials to meet the swelling pressure (>100 kPa) and hydraulic conductivity (<10⁻¹⁰ m/s) specifications set for backfill materials and to define subsequent swelling pressure and hydraulic conductivity tests.

It was determined that there was no discernible difference in the hydraulic and swelling pressure characteristics for MX80-limestone or MX80-granite sand blends where density and sand-clay ratio and porefluid composition were the same. Swelling pressure and hydraulic conductivity were measured for MX80-aggregate mixtures and pressures were found to be consistent with values previously reported for both CR-10 and SR-Sh systems.

For low salinity conditions (i.e., reference groundwater CR-10), compaction to 98% of Standard Compaction Maximum Dry Density or 95% of Modified Maximum Dry Density will be sufficient to achieve the swelling pressure (Ps) and hydraulic conductivity (k) targets set for the clay-aggregate blends, provided low salinity conditions persist and the clay content exceeds approximately 60%.

Under high salinity such as for SR-Sh conditions, none of the materials compacted to 98% of Standard Compaction Maximum Dry Density will meet the Ps and k requirements set for shaft backfill (<100 kPa and <1E-10 m/s). Materials compacted to 95% of Modified Compaction Maximum Dry Density will achieve targeted Ps and k behaviour.

In an ongoing study to determine if discernible change in the mineralogical or chemical composition of MX80 bentonite occurs as the result of soaking in low salinity (CR-10) and high salinity (SR-Sh) groundwater, samples were analysed following 54 and 82 months of testing. There is no discernible change in the mineralogical composition and the chemical composition remains similarly unchanged except for elevated Ca and K and reduced Na contents that developed soon after soaking of clay was started. These changes are attributable to cation exchange on the montmorillonite clay surfaces with Na being lost to Ca and K being gained from the groundwater.

A further series of soil water characteristic curves (SWCC) were generated for potential shaft backfilling materials and a new set of tests that have measured the gas (methane) permeability have been completed. These measurements will provide reference values for use in conducting gas transport evaluations in the future.

CONTENTS

ABSTRACT	i
CONTENTS	ii
LIST OF TABLES	iv
LIST OF FIGURES	v
1. BACKGROUND.....	1
2. MATERIALS	2
2.1 TEST PLAN	2
2.2 POREFLUID SOLUTIONS USED IN TESTING.....	2
2.3 Sand and Crushed Limestone.....	3
3. BASIC INDEX PROPERTIES.....	6
4. MINERALOGICAL AND CHEMICAL CHARACTERIZATION OF CLAY AND SAND	7
4.1 Methods and Materials.....	7
4.2 MX80 Bentonites: XRD and XRF Analyses of As Received Materials.....	8
4.2.1 XRD Analysis	9
4.2.2 XRF Analyses.....	12
4.3 Influence of Exposure of Bentonite to Saline Solutions.....	18
4.3.1 Mineralogical Composition of Brine Soaked MX80 as Determined using XRD...	19
4.3.2 Chemical Composition of Brine-Soaked MX80 as Determined using XRF	21
5. COMPACTION PROPERTIES OF BENTONITE – AGGREGATE MIXTURES.....	25
5.1 Standard Compaction Testing (SCT).....	26
5.2 Modified Compaction Tests (MCT)	28
5.3 Estimation of Swelling and Hydraulic Behaviour Based on Compaction Tests 28	
6. MEASUREMENT OF SWELLING PRESSURE AND HYDRAULIC CONDUCTIVITY	31
6.1 Testing Matrix, Testing Methods and Experimental Details.....	31
6.2 Hydraulic Conductivity Tests.....	34
6.3 Swelling Pressure Measurement	38
6.4 Summary of Ps and k Behaviour	43
7. SOIL WATER CHARACTERISTICS CURVES AND GAS PERMEABILITY	46
7.1 Background and Approach to SWCC and GP Testing.....	46
7.2 Soil Water Characteristics Curves (SWCC)	46
7.2.1 Background, Testing Methods and Experimental Details.....	46
7.2.1.1 GCTS Device	47
7.2.1.2 WP4 Dewpoint Potentiometer Device	48
7.2.2 SWCC Test Results.....	48
7.2.2.1 MX80 Granitic Sand 50:50 with CR-10.....	51

7.2.2.2	MX80 Crushed Limestone with SR-Sh.....	52
7.2.3	Summary of SWCC Results	52
7.3	Gas Permeability Measurements	54
7.3.1	Background, Testing Methods and Experimental Details.....	54
7.3.2	Gas Permeability Test Results	55
7.3.2.1	MX80 Granitic sand 50:50 with CR-10	56
7.3.2.2	MX80 Crushed Limestone with SR-Sh.....	57
7.3.2.3	Summary of Gas Conductivity and Permeability Testing	58
7.4	SWCC and Gas Conductivity Results Interpretation	60
8.	SUMMARY.....	62
	REFERENCES	64
	APPENDIX A: XRD and XRF Reports	67
	APPENDIX B: Results of Compaction Testing.....	91
	APPENDIX C: Swelling Pressure Plots	115
	APPENDIX D: Water Uptake Measurements.....	127
	APPENDIX E: Summary of Ps and K Testing	139
	APPENDIX F: Summary of SWCC and Gas Permeability Test Data.....	146

LIST OF TABLES

	Page
Table 2.1. Materials Evaluated and Properties Determined	4
Table 2.2. Chemical Composition of CR-10 and SR-Sh Porefluids	5
Table 4.1. X-Ray Diffraction Results for Bulk MX80 Bentonite	11
Table 4.2. Mineralogical Composition of Granitic Sand and Crushed Limestone	12
Table 4.3. Major Oxides Composition of MX80 Bentonite	15
Table 4.4. Comparison of Major Oxides Composition of MX80 Bentonite used in Current Study to Literature Values	16
Table 4.5. Major Oxides Composition as Oxide% for Granitic Sand and Crushed Limestone ...	17
Table 4.6 XRD-Determined Mineralogy of MX80 Samples Soaked in Brine Solution	20
Table 4.7. Chemical Composition of Untreated MX80 Determined Using XRF	23
Table 4.8. Change in MX80 Chemical Composition Following Brine-Soaking	24
Table 5.1. Standard Compaction Test Results and Initially Estimated Ps and k behaviour*	27
Table 5.2. Modified Compaction Test Results and Anticipated Ps and k Values	29
Table 6.1. Testing Matrix for Ps and k Tests	33
Table 6.2. Results of Hydraulic Conductivity and Swelling Pressure Testing	35
Table 6.3. Best-Fit and Prediction Limit Equations for k of MX80-Based Materials.....	38
Table 6.4. Best-Fit and Prediction Limit Equations for Ps of MX80-Based Materials	42
Table 6.5. Ability of Bentonite-Sand mixtures compacted using low salinity water to meet Ps and k requirements	44
Table 6.6. Effect of changing montmorillonite content of predicted Ps and k.	45
Table 7.1. Fitting parameters used to generate SWCC's	49
Table 7.2. Materials examined in current study and air entry values previously obtained	50
Table 7.3. Specimen density and fitting parameters used to generate GP curves	55
Table 7.4. Density and saturation effects on gas permeability	57

LIST OF FIGURES

	Page
Figure 1.1. Generic illustration of the NWMO DGR concept (Naserifard et al 2021)	1
Figure 2.1. Grain-size distribution of granitic sand and crushed limestone.....	3
Figure 4.1. Example of raw, unprocessed Wyoming bentonite.....	9
Figure 4.2. Soluble salt removal from brine-soaked specimens by diffusion through dialysis membrane (Dixon et al. 2018).....	18
Figure 5.1. Miniature compaction device	25
Figure 5.2. Dry density and EMDD achieved at 98% and 95% of maximum compacted density using SCT and MCT respectively.....	30
Figure 6.1. Examples of Ps/k test cells (Left) and flow monitoring equipment (Right)	32
Figure 6.2. Hydraulic conductivity of MX80-based materials: CR-10 porefluid	36
Figure 6.3. Hydraulic conductivity of MX80-based materials: comparison of CR-10 to other 10- 15 g/L porefluids.....	36
Figure 6.4. Hydraulic conductivity of MX80-based materials: High salinity (SR-Sh and NaCl) ...	37
Figure 6.5. Comparison of hydraulic conductivity data for high TDS conditions	38
Figure 6.6. Swelling pressure developed by MX80-based materials: freshwater conditions	41
Figure 6.7. Swelling pressures developed by MX80-based materials: 11-12 g/L TDS	42
Figure 6.8. Swelling pressures of MX80-based materials: High (>335 g/L TDS) salinity.....	43
Figure 7.1. Air entry value determination on a typical SWCC.....	47
Figure 7.2. GCTS apparatus used to measure the SWCC in low suction range and a typical SWCC specimen.....	47
Figure 7.3. WP4 device used to measure the SWCC in the high-suction range and example of specimen used	48
Figure 7.4. SWCC curves for MX80:Granitic Sand 50:50 with CR-10, Standard Compaction (1.58 Mg/m ³ dry density)	51
Figure 7.5. SWCC curves for MX80:Granitic Sand 50:50 with CR-10, Modified Compaction (1.85 Mg/m ³ dry density)	51
Figure 7.6. SWCC curves for MX80:Crushed Limestone 50:50 with SR-Sh, Modified Compaction (1.85 Mg/m ³ dry density)	52
Figure 7.7. SWCC curves for MX80:Crushed Limestone 60:40 with SR-Sh, Modified Compaction (1.79 Mg/m ³ dry density)	52
Figure 7.8. Comparison of SWCC tests – degree of liquid saturation vs capillary pressure.....	53
Figure 7.9. Comparison SWCC tests – capillary pressure vs degree of liquid saturation.....	53
Figure 7.10. Gas permeability equipment showing triaxial cell and methane test apparatus	54
Figure 7.11. Gas conductivity and permeability curves for granitic sand 50-50 with CR-10 compacted to standard compaction (1.58 Mg/m ³ dry density)	56
Figure 7.12. Gas conductivity and permeability curves for granitic sand 50-50 with CR-10 compacted to modified compaction (1.85 Mg/m ³ dry density).....	56
Figure 7.13. Gas conductivity and permeability curves for crushed limestone 50-50 with SR-Sh at modified compaction (1.85 Mg/m ³ dry density)	57
Figure 7.14. Gas conductivity and permeability curves for crushed limestone 60-40 with SR-Sh at modified compaction (1.79 Mg/m ³ dry density)	58
Figure 7.15. Summary of Gas Conductivity testing – Gas Conductivity versus Degree of Liquid Saturation.....	59
Figure 7.16. Summary of Gas Permeability Testing— Coefficient of Gas Permeability versus Degree of Liquid Saturation	59
Figure 7.17. Coefficient of gas permeability – Gas conductivity versus capillary pressure.....	60

1. BACKGROUND

The Nuclear Waste Management Organization (NWMO) is responsible for all technical and licensing support activities associated with the long-term management of Canada's used nuclear fuel. The generic repository concept involves the excavation of a series of placement rooms deep underground where the used nuclear fuel is contained by corrosion-resistant used fuel containers and then further isolated by a series of engineered barriers including the Highly Compacted Bentonite (HCB) and also a crushed bentonite product, referred to as Gap Fill Material (GFM), as shown in Figure 1.1. Beyond the placement room, backfill materials will be used to fill the horizontal openings as well as the vertical access shafts. This project explores the effect of groundwaters expected for two siting regions: northwestern Ontario, Wabigoon Lake Ojibway Nation – Ignace in crystalline rock (referred to herein as “crystalline”) and southwestern Ontario, Saugeen Ojibway Nation – South Bruce in sedimentary rock, (referred to herein as “sedimentary”).

The composition of these bentonite-based barrier materials is anticipated to differ with location in the repository, with bentonite-aggregate mixtures used to fill the regions beyond the placement rooms (e.g., access tunnels, service areas and shafts).

The work undertaken in this study was done in support of the development and evaluation of materials and materials-options for use in filling the shafts in the Deep Geological Repository (DGR) as it moves in a stepwise manner from conceptual design to an operational facility and then through to final closure that includes shaft backfilling.

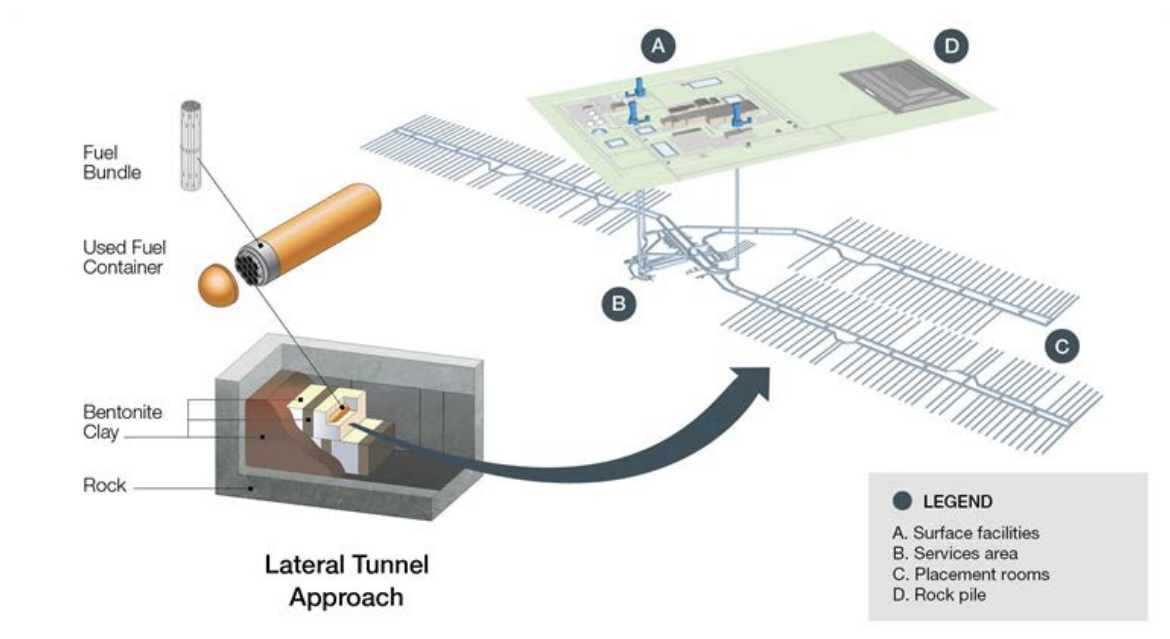


Figure 1.1. Generic illustration of the NWMO DGR concept (Naserifard et al 2021)

2. MATERIALS

2.1 TEST PLAN

The materials testing and optimization study described in this document is tasked with confirming some of the fundamental materials properties and assumptions for the Wyoming MX80 and MX80-aggregate mixtures. This is followed by determination of swelling pressure, hydraulic and gas permeability properties of various bentonite-sand and bentonite-crushed limestone blends. Specifically, the materials studied were 50:50, 60:40; 70:30, 80:20 and 90:10 mixtures of MX80 bentonite and granitic sand and similar clay-aggregate blends where crushed limestone rather than granitic sand is used as the aggregate component. The swelling, hydraulic, soil-water characteristic curves and gas permeabilities were determined for these materials using two different saline porefluids (CR-10 (11±1 g/L TDS) and SR-Sh (approximately 335 g/L TDS)). These solutions simulate groundwaters that are anticipated to be encountered in the shafts of repositories in the crystalline and sedimentary sites respectively. These data were then compared to previously generated or literature-reported values for these and similar materials and groundwater conditions.

In addition to the testing of MX80-aggregate blends, there were two sets of analyses completed on MX80 that has undergone long-term soaking at high water to solids ratio in CR-10 and SR-Sh solutions. This exposure to brine began in 2013 and subsamples have been recovered periodically since then for conduct of mineralogical and chemical analysis. These are done in order to determine if discernible compositional changes have occurred as the result of extended exposure to saline groundwater. Samples were analysed in mid-2019 and again in late 2021.

The materials blends and specifications that were tested in this study as part of shaft backfill evaluation are summarized in Table 2.1.

2.2 POREFLUID SOLUTIONS USED IN TESTING

The two reference groundwaters, CR-10 and SR-Sh used in this study were specified by the NWMO. Batches of the CR-10 and SR-Sh porefluids were prepared and chemically analysed to confirm that the stock solutions closely matched these groundwater compositions. It should be noted that the SR-Sh has very high total dissolved solids (TDS) concentration (approximately 335 g/L TDS), and so it was necessary to dilute the groundwater in order to complete chemical analysis. This is done to a high degree of accuracy by the analytical laboratory and the results are then reported as values associated with the original undiluted groundwater. All groundwaters used in subsequent testing are the full-strength solutions described and have not been subject to any dilution.

Table 2.2 presents the analytical results obtained for batches of CR-10 and SR-Sh solutions, showing that solutions prepared and accepted for use in this study. For comparison purposes, the chemical composition of saline solutions used in a previous testing program (Dixon et al. 2019) is also provided. It is noted that the current CR-10 solution exhibits a slightly higher pH (8.2) than previous batches (7 to 7.9), even though the same chemical formulation was used in its preparation. While there is no readily identifiable reason for the change, minor variations near neutral pH are not uncommon and this slight increase in pH is not enough to discernibly affect material behaviour or mineral solubility over the time taken to complete this study.

2.3 Sand and Crushed Limestone

The NWMO provided specifications for the particle-size gradations for the granitic sand and crushed limestone components. Figure 2.1 presents these target specifications and the achieved gradation for the granitic sand and crushed limestone materials.

Production of materials that meet these gradations required careful screening and blending of natural granitic sand materials as well as the custom crushing and screening of limestone from the Cobourg formation in Ontario. The limestone was supplied as bulk crushed material by CBM Aggregates of Bowmanville Ontario. This material was subsequently further crushed and screened to produce a material that closely followed specifications. Grain size analysis was done following ASTM D6913.

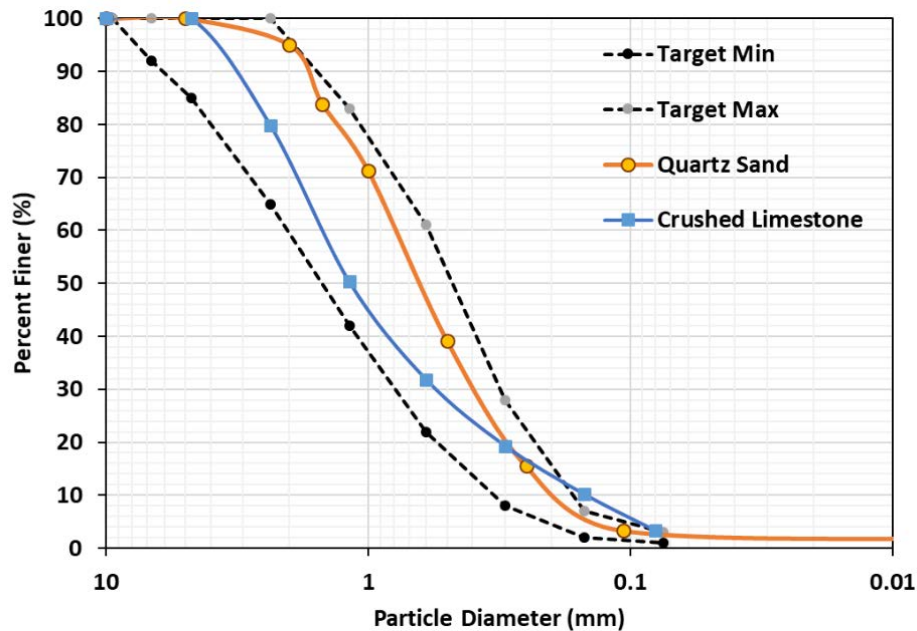


Figure 2.1. Grain-size distribution of granitic sand and crushed limestone

Table 2.1. Materials Evaluated and Properties Determined

Material/ Solution	As-delivered Materials			40% MX80 60% Aggregate*		50% MX80 50% Aggregate*		60% MX80 40% Aggregate*		70% MX80 30% Aggregate*		80% MX80 20% Aggregate*		90% MX80 10% Aggregate*	
	MX80	CRL	GS	CR-10	SR-Sh	CR-10	SR-Sh	CR-10	SR-Sh	CR-10	SR-Sh	CR-10	SR-Sh	CR-10	SR-Sh
Analysis															
Grain-size Distribution		√ (3)	√ (3)												
Standard Compaction (ASTM D698)				√	√	√	√	√	√	√	√	√	√	√	√
Modified Compaction (ASTM D1557)+				√	√	√	√	√	√	√	√	√	√	√	√
Specific Gravity of Minerals (ASTM D1188)	√ (3)	√ (3)	√ (3)												
Methylene Blue (ASTM C837)	√ (3)														
Free Swell (ASTM D5890)	√ (3)														
Consistency Limits (ASTM D4318)	√ (3)														
Mineralogy: XRD	√ (3)	√	√												
Chemical Composition XRF	√ (3)	√	√												
Swelling Pressure (32)*				√	√	√	√	√	√	√	√	√	√	√	√
Hydraulic. Conductivity* (32)				√	√	√	√	√	√	√	√	√	√	√	√
Soil-Water Characteristic Curve (4)						√ (2)	√		√						
Gas Permeability (4)						√ (2)		√	√						
Brine-Soaked Material* XRD (4) XRF (4)	√ √														

* Tests include both GS and CRL specimens,

Numbers in brackets indicate the number of tests or replicates completed.

+ Test completed using miniature compaction device that was calibrated against ASTM D1557

Table 2.2. Chemical Composition of CR-10 and SR-Sh Porefluids

Client Sample ID			SAMPLE 1 - CR-10			SAMPLE 2 - SR-SH-2013			Notes
Date Sampled			17-Apr-2018			17-Apr-2018			
Time Sampled			12:00			12:00			
ALS Sample ID			L2081434-1			L2081434-2			
Parameter	Lowest Detection Limit	Units	2018 Batch	NWMO Target	Historical Batch	2018 Batch	NWMO Target	Historical Batch	
Anions and Nutrients (Water)			CURRENT	TARGET	2014	CURRENT	TARGET	2014	
Alkalinity, Total (as CaCO3)	2	mg/L	10.0			502.0			diluted sample
Bicarbonate (HCO3)	5	mg/L	12.2			612.0			
Carbonate (CO3)	5	mg/L	<5.0			<5.0			
Chloride (Cl)	50	mg/L	6470	6100	6080	196000	205600	204000	
Conductivity (EC)	2	uS/cm	17900.0			229000.0			
Hardness (as CaCO3)		mg/L	5350			137000			
Hydroxide (OH)	5	mg/L	<5.0			<5.0			
Nitrate+Nitrite-N	0.5	mg/L	<0.50			0.70			
Nitrate-N	0.5	mg/L	<0.50			0.61			
Nitrite-N	0.05	mg/L	<0.050			0.096			
pH	0.1	pH	8.22	7.00	7.88	6.96	7.00	6.43	
TDS (Calculated)		mg/L	11700			324000			
Cation - Anion Balance		%	-3.9			0.8			
Dissolved Metals (Water)									
Calcium (Ca)	20	mg/L	2050	2130	2050	44700	48100	45000	diluted sample
Magnesium (Mg)	20	mg/L	55	60	67	6050	6080	5660	diluted sample
Potassium (K)	20	mg/L	58	15	85	22500	19500	20800	diluted sample
Sodium (Na)	40	mg/L	1900	1900	1850	53800	55200	51700	diluted sample
Sulfur (as SO4)	60	mg/L	1140	1000	923	760	960	750	diluted sample
TDS (mg/L)			11673	11212.0	11062.9	323810	335447.0	327916.4	
TDS (g/L)			11.7	11.2	11.1	323.8	335.4	327.9	

Qualifier Legend

DLDS

Detection Limit Raised: Dilution required due to high Dissolved Solids / Electrical Conductivity.

3. BASIC INDEX PROPERTIES

As part of material characterization and acceptance testing prior to initiation of testing to determine the swelling pressure (Ps), hydraulic conductivity (k), soil-water characteristic curve (SWCC) and gas permeability (GP) characteristics of the MX80-aggregate mixtures, the basic index properties of the components were determined. This included Specific Gravity (SG) (ASTM D854), Free Swell (FS) (ASTM D4829), Consistency Limits (CL) (ASTM D4318) and Methylene Blue (MB) (ASTM D837) tests on the bentonite. The FS, CL and MB tests provide an indication of the swelling clay (smectite) content, which will strongly affect the swelling pressure and hydraulic conductivity of sealing materials installed in a repository environment. The specific gravity of the component materials of the bentonite-sand mixture is needed in order to calculate the porosity of the compacted materials. The FS, CL and MB test data for both MX80 materials is provided in Table 3.1. Tests were done in triplicate in order to have confidence in the results obtained as well as to get a sense of the testing-related variability that might be expected in these parameter values.

The specific gravity (SG) determined using ASTM D854, for the MX80, granitic sand and crushed limestone is provided in Table 3.1. As for the other basic index properties tests, each was done in triplicate to provide an indication of the testing-related variability of these parameters for identical materials. In addition to the MX80 bentonite used in this study, measurements obtained for an 80-mesh, lower montmorillonite content Wyoming bentonite have been included. These measurements provide a basis for evaluation of the potential for various index tests to detect deviations in bentonite quality.

It should be noted that the SG analyses were completed using ASTM D854-Test Method B, which uses kerosene as the test fluid rather than water. This was necessary in order to eliminate the effects of adsorbed and structured water that would otherwise develop on the charged surfaces of the particles, resulting in inaccurate density determination.

The FS and MB tests done on the lower smectite content 80-mesh bentonite obtained values that were generally lower than would be expected for an MX80 product. The x-ray diffraction (XRD) and x-ray fluorescence (XRF) characterization of the lower quality bentonite also indicated that this was not an MX80 product. The characteristics of the lower-quality material are such that it would have potentially been unsuitable for use.

The comparison of index properties of two 80-mesh bentonites of differing quality allows for evaluation of a quality lab's ability to quickly (and inexpensively) identify sub-standard materials. Also, although the lower quality material was not used in the main testing program, the data generated can aid in developing methods to screen bentonite shipments for quality.

Table 3.1 – Quality Test Results for MX80 Bentonites

Material	Free Swell (cc/2g)	Specific Gravity	Consistency Limits Liquid, Plastic (%)	Methylene Blue (meq/100g)	CEC* (meq/100g)	Soluble Calcium* meq/100 g
Low Quality 80-mesh bentonite**	28**	2.73 2.71 2.71	364, 36	48	-	-
2018 High Quality MX80	26 25-26** 27*	2.69 2.69 2.69	375, 36 376, 36 375, 36 430, 36** 345, 35**	71- 72 73** 73.5** 77.5** 76**	104*	23*
MX80 Bentonite Literature Values+	28-42 32.5** 12-26*** 21***	2.70-2.82 2.72**	400-450, 32 280, 27**	-	60-110 85-90** 64*** 75***	
Crushed Limestone	-	2.71 2.71 2.71	-	-	-	-
Granitic Sand	-	2.70 2.70 2.69	-	-	-	-

Note: all index tests are done using freshwater as mixing fluid if needed.

* data supplied by CETCO for this batch of high-quality MX80; ** data from current study; *** Karnland et al. (2006)

+ data listed in Dixon (2019); ** data from Dixon et al. (2018) TR-2018-20; *** Rowe and Brachman. (2019) CNSC R613.4

- measurements not part of this testing program.

4. MINERALOGICAL AND CHEMICAL CHARACTERIZATION OF CLAY AND SAND

4.1 Methods and Materials

The mineralogical and chemical composition of each material examined MX80 bentonite (2 products), granitic sand and crushed limestone) were determined by X-ray diffraction (XRD) and X-ray fluorescence (XRF) respectively.

MX80 bentonite is predominantly a hydrous aluminum silicate comprised of clay minerals of the smectite group including montmorillonite, nontronite and sodium aluminum silicate hydroxide. This specific product has been used extensively for more than 40 years as a reference product for application in sealing of nuclear fuel waste repositories. As a result, there is a large body of mineralogical and chemical data available for this material. Being a natural material, it varies compositionally with time and location, making exact definition of mineralogical composition problematic, especially given the known presence of x-ray invisible amorphous mineral phases which result in an over-estimate of the crystalline mineral content. Literature does however provide a well-established range in mineralogical composition for the crystalline components of high-quality MX80. It is typically reported to consist of between 75 and 90% smectite clay minerals (Karnland (2010), Dixon et al. (2018; 2022)). Based on measurements of a large

number of subsamples from 11 batches of MX80 completed in a separate study (publication pending), the montmorillonite content of MX80 averaged approximately $80\% \pm 5\%$.

The presence or absence of certain accessory minerals (e.g., zeolite) in bentonite can be used in confirming the source locations for bentonite products as these vary geographically. For example, MX80 from eastern Wyoming typically has little or no zeolite present while deposits to the west have discernible zeolite presence.

Of more limited use in terms of establishing mineralogical composition are the results of major oxide analyses (by XRF) of the soil. It should be noted that this analytical tool does not provide a direct means of determining the smectite (or any other mineral) content but does provide an indication of the overall elemental composition. The XRF will also identify the non-mineral chemical components that are present in the bulk sample and so can provide some information regarding soluble salts. All MX80 products should exhibit similar elemental composition and so deviations from the norm (particularly the silica to alumina ratio), can be used to identify changes in material composition and product quality. The analytical reports, including quality checks provided by the laboratories used in this testing are provided in Appendix A.

4.2 MX80 Bentonites: XRD and XRF Analyses of As Received Materials

Commercial mineralogical analytical laboratories were used to provide a basic mineralogical check on the MX80 bentonite, granitic sand (GS) and crushed limestone (CRL) used in this study. As required for this study, three qualified and registered laboratories (James Hutton Institute, Saskatchewan Research Council (SRC) and Activation Laboratories (ActLab) were selected and subsamples of the same batch of clay were submitted for random orientation bulk powder analysis in 2018 followed by a single re-analysis of the higher quality material in 2019. As noted previously, two very different "MX80" materials were characterized and only the high-quality material was used in subsequent testing. Both bentonite products were submitted for XRD and XRF analyses in 2018 and the results provide a valuable basis for quality comparison. As a further check on analytical consistency a further analysis of the archived MX80 used in this study was completed in 2019.

Figure 4.1 shows an example of the appearance of raw-excavated and as-yet unprocessed sodium bentonite from Wyoming. This material is subsequently dried, mechanically crushed and screened to provide grain-size specific commercial products. Of note in Figure 4.1 are visually obvious inclusions of darker, coarser-texted materials, likely of different mineralogical composition than the bulk material. Such materials would typically be broken down and dispersed during processing, but should small fragments be incorporated into a subsample, they can result in some degree of apparent mineralogical variability in results obtained by XRD. This may be the reason for the variation in feldspar content observed and as feldspar is a strongly crystalline mineral the presence of small quantities of highly crystalline material could skew the calculated mineralogy.



Figure 4.1. Example of raw, unprocessed Wyoming bentonite

4.2.1 XRD Analysis

The XRD data for the two 80-mesh bentonites examined in this study are provided in Table 4.1. Both materials are clearly montmorillonite-dominated, but there is a notable difference between them (~62% and ~88% montmorillonite content for low quality and high-quality materials respectively). The data clearly show the compositional differences between the two samples and clearly establishes the ability of XRD to quickly identify potential quality issues.

The high-quality MX80 product used in this study has a measured mineralogical composition that is consistent with that reported in literature (Dixon et al. 2022). The variability in the reported values for various analyses on the same batch of clay can be attributed to sample preparation (a more oriented sample will provide a higher montmorillonite value) and perhaps the method used by the software used in calculating mineral contents. As noted previously, the presence of even a few grains of larger, well crystallized mineral could affect the results since they provide a stronger diffraction response (see Figure 4.1). The laboratory-provided traces associated with the XRD analyses are provided in Appendix A.

These data illustrate the challenges in assessing bentonite materials for small (<10%) changes in montmorillonite content. It should also be noted that the semi-quantitative analyses are generally not able to determine minor mineral proportioning to an accuracy greater than approximately $\pm 1\%$ and swelling clay composition is accurate to $\sim \pm 5\%$ (Karnland et al. 2006). In the current study a $\pm 8\%$ was observed. A montmorillonite content of 80% has been used in evaluation of swelling pressure, hydraulic conductivity, SWCC and gas permeability tests conducted in this study as it represents the lower bound of composition as defined by standard deviation determination (Table 4.1).

It should also be noted that the XRD results provided are for the crystalline component of the clay only. Bentonite is known to contain quantities of x-ray invisible (amorphous) materials (e.g., iron-oxides, hydroxides, silica). The presence of x-ray amorphous materials in MX80 bentonite was noted by Olsson and Karnland (2009) and Karnland (2010). These amorphous materials are not accounted for in semi-quantitative XRD analyses and so depending on their quantity, discernible over-estimation of the proportion of crystalline minerals in a clay mass may occur (Kaufhold et al. 2002). The poorly crystalline state of many of the iron-based minerals is indicated by the range of analytical values for the various iron-based minerals (e.g., siderite, goethite, hematite, magnetite and lepidocrocite), which is taken to be indicative of their generally poor crystallinity. While not detected by XRD analysis, the amorphous components will be included in the results of chemical analysis using XRF.

The presence of an amorphous component is recognized in the analytical reports provided by the testing laboratories and in one case (ActLab 2018 report on low-quality bentonite), an ~11% amorphous content by mass was reported (Table 4.1). These non-crystalline minerals represent a normally unquantified, but potentially significant mineral component. Of particular interest are the amorphous iron and silica components that have the potential to affect the swelling and hydraulic behaviour of the bentonite. For the purposes of consistent terminology, the contents of the crystalline mineral components have been recalculated based on proportions not including amorphous materials, the originally reported values are provided in brackets for reference purposes.

Included in the evaluation of mineralogical composition is a retest of the 2018 order of MX80 bentonite that was done in 2019 on a separate sample from the stockpile of material at the Golder laboratory in Mississauga. This is the same shipment (but different bag), of high-quality material provided for and used in this study. It was handled and analysed in the same manner as the 2018 tests by one of the labs used in 2018, but a discernibly different mineralogical composition was determined. Specifically, it indicates a lower than previously identified montmorillonite content and notably higher feldspar content. This may be a real difference indicating variability within the same shipment or may be a function of textural and other factors noted above (e.g., a couple of grains of feldspar in the small sample taken), but these results highlight the risk to basing quality-evaluation of these materials using a single methodology. It should be noted that the low montmorillonite and high feldspars observed in the 2019 retest were not identified in the subsequent analyses of materials that had been soaked in brine or were not associated with any discernible difference in its chemical composition (see Section 4.1.1.2).

XRD analyses were also completed on the granitic sand and crushed limestone. The results of XRD analysis are provided in Table 4.2 and show generally consistent results, but again there is notable variation in the quantities reported, illustrating again some of the challenges related to use of XRD for quality-control purposes. The results confirm that the limestone is, as expected, calcite-dominated (averaging $81 \pm 5\%$ calcite) with minor contents of quartz, dolomite, illite and other non-swelling minerals. The granitic sand is a mixture dominated by quartz and feldspar (main components of granite, $90 \pm 5\%$) with small quantities of other secondary minerals normally associated with granite (e.g., muscovite, chlorite, amphibole). Both the granitic sand and crushed limestone meet the compositional requirements set for this study.

Table 4.1. X-Ray Diffraction Results for Bulk MX80 Bentonite

	ActLab Low quality MX80 (2018)	Hutton Low quality MX80 (2018)	ActLab High Quality MX80 (2018)	ActLab High Quality MX80 (2019)	Hutton High Quality MX80 (2018)	SRC High Quality MX80 (2018)	Average High Quality MX80 (2018)	MX80 Dixon et al. (2018)	MX80 Dixon et al. (2022) ++	MX80 SKB (2006)
Mineral	%	%	(%)	(%)	(%)	(%)	(%)	(%)	(%)	(%)
Montmorillonite	60.7	68.9	95	76.3	91.6	87	87.5±8.1	87.4±8.0	70 - 89	81.1 - 85.8
Calcite	2.7	1.3	-	1.1	0.6	-	<0.6	2.9±0.7	0.6 - 1.4	0.1 - 0.5
Dolomite	-	-	-	-	-	-	-	TR	-	-
Bassanite (CaSO ₄)	-	0.8	-	-	-	-	-	-	-	-
Quartz	7.6	2.4	1.5	2.7	2.2	5.6	3.0±1.8	2.5±1.0	1.5 – 6.1	4.6 - 7*
Biotite	-	-	-	-	-	-	-	<1.4	-	-
Muscovite (+illite)	6.7	3.2	1.3	-	0.8	-	<1.3	0.3 - 7.1	0 – 3.3	2.1 - 3.9
Chlorite	-	-	-	-	-	-	-	-	-	-
Chlinoptilite ⁺	-	3.8	-	-	-	-	-	-	0	-
Plagioclase	18.8	9.5	2.2	15.2	3.6	7.3	7.1±5.8	0 - 6.8	8.9 – 9.3 ⁺⁺⁺	1.8 - 4.2
K-Feldspar	-	2.2	-	4.7	0.4	-	<4.7	<3		0.3 - 2.1*
Siderite	-	-	-	-	-	-	-	<2	-	-
Pyrite	-	0.1	-	-	0.4	-	<0.4	<0.6	-	0.5 - 0.6
Gypsum	Tr	-	-	-	-	-	-	<0.4	-	0.5 - 1.3
Iron minerals ^{**}	-	-	-	-	0.4	-	<0.4	-	-	0.8 - 2.6
Cristobalite	3.5	7.8	Tr	-	-	-	Tr	-	-	-
Amorphous	(11)	NR	NR	NR	NR	NR	??	NR	NR	NR
Total	100	100	100	100	100	99.9	100	99.9	100	100

Note: Tr = trace; '-' = not detected; NR = not reported., ?? detected but not quantifiable

* values are sum of polymorphs of the indicated mineral group (e.g., quartz, cristobalite and tridymite; microcline and orthoclase feldspars)

** sum of iron minerals goethite, hematite, magnetite and lepidocrocite

* member of zeolite family of minerals. ** results from 11 separate samples. *** Combined plagioclase and k-feldspar content.

Table 4.2. Mineralogical Composition of Granitic Sand and Crushed Limestone

Mineral	Limestone				Granitic Sand			
	ActLab	Hutton	SRC	Avg	ActLab	Hutton	SRC	Avg
	(%)	(%)	(%)	(%)	(%)	(%)	(%)	(%)
Calcite	84.8	75.5	82.6	81	-	-	-	-
Dolomite	2.7	2.0	-	1.6	-	-	-	-
Quartz	7.0	7.4	6.1	6.8	45	39.8	36.1	40.3
Biotite	-	-	-	-	-	-	-	-
Muscovite (+illite)	5.0	0.2 (10.1)*	3.9	<5	3.3	3.7	0.4	2.5
Ankerite (Carbonate)	-	-	5.6	<2	-	-	-	-
Mica	-	-	-	-	-	1.8	-	<1.8
Plagioclase	-	1.2	-	<1	34.5	32.3	-	33.4
K-Feldspar	-	1.2	-	<1	11	14	-	12.5
Total Feldspars	-	2.4	-	<1	45.5	46.3	58.6	50.1
Chlorite	-	1.7	1.9	1.2	2.5	3.4	3.0	3
Amphibole	-	-	-	-	3.7	4.3	1.8	3.3
Pyrite	-	0.7	-	<1	-	-	-	-
Total	99.5	100	100.1	100	99.8	99.3	99.9	100

* identified as Illite and Illite/Smectite mixed layer, ** total feldspars

4.2.2 XRF Analyses

The same bentonite, granitic sand and crushed limestone samples as were used in the XRD analyses also underwent XRF analysis. XRF is a measure of the total chemical composition of the specimens and hence will include those materials that were identified by XRD but also those that cannot be identified by XRD due to their poor crystallinity (e.g., amorphous materials). As a result, XRF, when combined with XRD and other analytical tools, provides a means of identifying differences in the mineralogical composition of sealing system components.

A total of seven XRF analyses were completed on MX80; two on the low-quality product received in 2018 and the remaining 5 on the higher-quality material that has been used in this study. Tests on the high-quality bentonite material include 4 completed in 2018 and a retest completed in 2019 on archived material. The results of analyses of the bentonite materials are presented in Table 4.3. For comparison purposes the results published for other MX80 materials are provided in Table 4.4.

While the as-received data values for the XRF analyses, provided in Table 4.3 indicate a discernible variation in the results obtained for “identical” bentonite specimens, many of these differences can be attributed to the water content reported for the specimens (typically referenced as LOI (loss on ignition) or water content). The range in water content reported is the result of differing laboratory conditions (and perhaps material preparation for testing) and does not relate to the basic chemical composition of the specimens. In order to address the issue of differing water contents in the samples, the water content was subtracted from the total oxide composition and the remainder was used to “adjust” or normalize the proportioning of the other components. As can be seen in Table 4.3, this results in much more consistent proportioning of the cations. The results of the five analyses indicate a high degree of consistency in the results

obtained, providing confidence in this analytical method as well as its potential for use in comparing other batches of materials to our current reference material.

Several cells in Table 4.3 are shaded to allow for ease of comparison of the results. The reference values for MX80 materials used in the current study are in green-shaded cells. Where the values obtained for the low-quality material differ substantially from the reference values, they are shaded yellow (values substantially lower) and blue (values substantially higher). The lower-quality MX80 material shows substantially lower aluminum and higher silica contents, with notably higher Na and Ca contents in the lower-quality material. The $\text{SiO}_2/\text{Al}_2\text{O}_3$ ratios provided in Tables 4.3 and 4.4 provide an indication that there are mineralogical differences between the two bentonites as Si and Al are the main building blocks of the clay minerals. Hence differences in the ratio of these two components in a sample are perhaps an indicator of mineralogical differences, (as supported by the XRD analyses presented in Section 4.1.1.1). There is also a notably higher Na and Ca oxide contents in the low-quality materials, together with a reduced Mg oxide content. These cations (particularly Na and to a lesser extent Ca) are typically associated with the surface-exchange sites of the bentonite, but Ca and Mg are also associated with calcite, sulfates and other minor minerals.

The ratio of Na/Ca remains relatively constant in the low and high-montmorillonite content bentonites but the $\text{SiO}_2/\text{Al}_2\text{O}_3$ ratio in the lower montmorillonite content bentonite is notably higher than determined for the higher-quality material (3.5 versus 2.81). This could be associated with differences in the crystalline mineral content or the presence of a higher content of x-ray invisible silicates. A $\text{SiO}_2/\text{Al}_2\text{O}_3$ ratio of approximately 3.5 was also determined for MX80 materials reported by SKB (Karnland et al. 2006) and Posiva (Kiviranta and Kumpulainen 2011).

An example of how the XRF data would be normalized (adjusted) for a sample found to have an 18% Al_2O_3 ; 17.4% LOI and total measured oxide content of 98.8%; is as follows:

$$\text{Adjusted AL}_2\text{O}_3\% = 100 * ((18 / 98.8) / (1 - (17.4 / 98.8))) = 22\%$$

In order to compare the MX80 being used in the current study to other batches of MX80, Table 4.4 is provided and contains data reported for MX80 bentonite in 2004/5 (Karnland et al. 2006) and 2010 (Kiviranta and Kumpulainen 2011) as well as an analysis of the current bentonite batch, completed by American Colloid Company in 2018. Using the MX80 used in the current study as the baseline, it is possible to compare it to previously completed analyses on the same product (not necessarily the same batch, as indicated by the dates for SKB and Posiva studies). Those components that vary notably from the range established for the current material are highlighted in Table 4.4, yellow cells indicating values that are lower than the reference and blue cells are for values that are higher.

The data provided by American Colloid Co. (ACC) are included in Table 4.4 and is for the same MX80 material as was used in the current study. The results show only minor differences from those provided by external laboratories. Slightly higher Mg and Ca oxides and slightly lower sodium (Na) and potassium (K) oxides were the main differences. The Mg and K contents are most likely to be associated with the feldspar and non-clay components. Na, while slightly lower in the ACC analyses is not really substantially different and Na is largely associated with the ion-exchange sites on the clay minerals as well as water-soluble salts. Similarly, the Ca is strongly associated with the ion-exchange sites on the clay minerals but is also present as minor but variable carbonate (and sulphate) mineral components (e.g., gypsum) that may or may not be present or x-ray detectable.

When compared to the XRF-determined composition of MX80 reported by SKB (Karnland et al. 2006) and Kumpulainen and Kiviranta (2011) there are some notable

differences in the chemical compositions determined using XRF. The main differences are the higher $\text{SiO}_2/\text{Al}_2\text{O}_3$ ratios in the SKB/Posiva values. These higher values are strong indicators of some difference in the mineralogical composition of the samples (e.g., quartz, clays, feldspar or amorphous silicates) and are actually closer to those observed for the 2018 low-quality materials listed in Table 4.3, although their montmorillonite mineral compositions are similar to the high-quality materials used in this study (Table 4.1).

It is possible that the Si/Al and Na/Ca oxide ratios will provide indicators to changes in product composition, but further study is needed to determine if this has the potential to be developed into a screening tool.

Chemical analyses were also completed on the granitic sand and crushed limestone materials. The results are provided in Table 4.5 and show nearly identical results, showing that these components can be reliably analysed using XRF in conjunction with XRD analysis.

Of note is the presence of ~ 2% total iron in both the limestone and granitic sand and <1% and ~2.5% contents of K_2O in the limestone and granitic sand respectively. Iron is not clearly associated with any crystalline mineral other than pyrite in these materials, although it may be a minor insoluble constituent in other minerals or as a soluble amorphous oxide. Potassium (K) has been identified as being potentially detrimental to bentonite longevity if it is present in readily soluble form as they can facilitate conversion of smectite to illite under certain conditions. It is likely that the majority of the potassium is present in the potassium feldspars identified in the XRD analyses rather than being in a readily accessible form (Table 4.3). The current analyses do not provide a means of identifying the location of Fe or K or the potential to influence longer-term behaviour.

Table 4.3. Major Oxides Composition of MX80 Bentonite

Low Quality Material					Material used in current study										Summary		
Oxides	Activation Labs	Normalized value	Hutton Institute	Normalized value	Activation Labs	Normalized value	Activation Labs	Normalized value	Hutton Institute	Normalized value	SRC 1	Normalized value	SRC 2	Normalized value	Average Raw Data	Normalized value	STDev
Batch Yr	2018		2018		2018		2018		2018		2018		2018		2018		
Analy. Date	11 Jul 2018		04 Jun 2018		21 Nov 2019		10 Oct 2018		12 Oct 2018		12 Oct 2018		12 Oct 2018		2018		
Description	Lo Q		Lo Q		MX80		MX80		MX80		MX80		MX80		MX80		
	(wt %)	(wt %)	(wt %)	(wt %)	(wt %)	(wt %)	(wt %)	(wt %)	(wt %)	(wt %)	(wt %)	(wt %)	(wt %)	(wt %)	(wt %)	(wt %)	(wt %)
Na ₂ O	2.68	2.93	2.55	2.77	2.29	2.52	2.16	2.50	2.30	2.50	2.04	2.41	2.03	2.41	2.16	2.47	0.05
MgO	1.92	2.10	1.85	2.01	2.83	3.11	2.59	3.00	2.76	3.01	2.43	2.87	2.44	2.89	2.61	2.98	0.09
Al ₂ O ₃	17.73	19.39	18.37	19.92	20.39	22.43	19.64	22.73	20.99	22.86	19.60	23.16	19.50	23.11	20.02	22.86	0.27
SiO ₂	62.12	67.92	64.23	69.66	58.11	63.91	55.60	64.35	58.96	64.21	54.30	64.16	54.20	64.23	56.23	64.17	0.14
P ₂ O ₅	0.07	0.08	0.06	0.07	0.07	0.08	0.07	0.08	0.08	0.09	0.07	0.08	0.08	0.09	0.07	0.08	0.01
K ₂ O	0.68	0.74	0.60	0.65	0.61	0.67	0.52	0.60	0.52	0.57	0.49	0.58	0.47	0.56	0.52	0.60	0.04
CaO	2.33	2.55	2.20	2.39	2.10	2.31	1.67	1.93	1.74	1.90	1.79	2.12	1.75	2.07	1.81	2.07	0.15
TiO ₂	0.21	0.23	0.21	0.23	0.21	0.23	0.20	0.23	0.22	0.24	0.20	0.24	0.19	0.23	0.20	0.23	0.005
MnO	0.06	0.06	0.06	0.07	0.02	0.02	0.02	0.02	<0.05	-	0.01	0.01	0.01	0.01	0.01	0.02	0.004
V ₂ O ₅	0.00	-	<0.05	-	<0.003	-	<0.003	-	<0.05	-	-	-	-	-	-	-	-
Cr ₂ O ₃	0.01	0.01	<0.05	-	0.01	0.01	<0.01	-	<0.05	-	-	-	-	-	-	-	-
Fe ₂ O ₃	3.63	3.97	3.72	4.03	4.28	4.71	3.93	4.55	4.15	4.52	3.70	4.37	3.72	4.41	3.96	4.51	0.12
FeO	-	-	-	-	-	-	-	-	-	-	-	-	-	-	-	-	-
BaO	-	-	0.12	0.13	-	-	-	-	0.05	0.05	-	-	-	-	-	-	-
C	-	-	-	-	-	-	-	-	-	-	-	-	-	-	-	-	-
SO ₃	-	-	-	-	-	-	-	-	-	-	-	-	-	-	-	-	-
other	0.02	0.02	-	-	-	-	-	-	0.05	0.05	<0.01	-	<0.01	-	-	-	-
LOD	-	-	1.77	-	-	-	-	-	9.41	-	-	-	-	-	-	-	-
LOI*	8.44	8.45	6.08	6.08	8.90	8.92	13.61	13.61	7.49	7.54	15.10	15.14	15.10	15.18	12.04	12.08	3.22
Total	99.9	100.0	100.1	100.2	99.8	100.0	100.0	100.0	99.3	100.0	99.7	100.0	99.5	100.0	99.67	100.0	-
Si/Al***	3.50		3.50		2.85		2.83		2.81		2.77		2.78		2.81		
Na/Ca***	1.15		1.16		1.09		1.29		1.32		1.14		1.16		1.20		

* sum of loss on drying at 110°C and loss on ignition

** analysis completed by Am. Colloid Company.

*** oxide mass ratio

Table 4.4. Comparison of Major Oxides Composition of MX80 Bentonite used in Current Study to Literature Values

NWMO Current Study				CETCO Data		Literature Values			
Oxides	Average Raw Data	Normalized value	STDev	MTC/ACC **	Normalized value	SKB	Normalized value	Posiva	Normalized value
Batch Yr	2018			2018		2006		2011	
Analy. Date	2018			2018		2006		2011	
Description	MX80			SA604		SKB		Posiva	
	(wt %)	(wt %)	(wt %)	(wt %)	(wt %)	(wt %)	(wt %)	(wt %)	(wt %)
Na ₂ O	2.16	2.47	0.05	1.87	2.30	2.02	2.26	2.19	2.28
MgO	2.61	2.98	0.09	3.16	3.88	2.34	2.62	2.34	2.44
Al ₂ O ₃	20.02	22.86	0.27	18.57	22.83	19.12	21.38	18.70	19.46
SiO ₂	56.23	64.17	0.14	51.46	63.26	59.52	66.56	65.37	68.03
P ₂ O ₅	0.07	0.08	0.01	0.10	0.12	0.06	0.07	-	-
K ₂ O	0.52	0.60	0.04	0.16	0.20	0.52	0.58	0.53	0.55
CaO	1.81	2.07	0.15	2.07	2.54	1.34	1.50	1.29	1.34
TiO ₂	0.20	0.23	0.005	0.16	0.20	0.16	0.18	0.15	0.16
MnO	0.01	0.02	0.004	0.02	0.02	0.02	0.02	-	-
V ₂ O ₅	-	-	-	-	-	-	-	-	-
Cr ₂ O ₃	-	-	-	-	-	-	-	-	-
Fe ₂ O ₃	3.96	4.51	0.12	3.78	4.65	3.70	4.14	3.86	4.02
FeO	-	-	-	-	-	-	-	0.53	0.55
BaO	-	-	-	-	-	-	-	-	-
C	-	-	-	-	-	0.32	0.36	0.79	0.82
SO ₃	-	-	-	-	-	0.30	0.34	0.34	0.35
other	-	-	-	-	-	-	-	-	-
LOD	-	-	-	-	-	-	-	-	-
LOI*	12.04	12.08	3.22	17.41	17.63	10.70	10.69	5.36	5.28
Total	99.67	100.0	-	98.8	100.0	100.1	100.0	101.5	100.0
Si/Al***		2.81			2.77		3.11		3.50
Na/Ca***		1.19			0.90		1.51		1.70

* sum of loss on drying at 110oC and loss on ignition

** analysis completed by Am. Colloid Company.

*** oxide mass ratio

Karnland et al 2006

Avg 5 tests

TR-2006-30

Kumpulainen & Kiviranta 2011

Table 5

WR-2011-41

Table 4.5. Major Oxides Composition as Oxide% for Granitic Sand and Crushed Limestone

	Granitic Sand		Crushed Limestone	
	Hutton Institute	ActLab	Hutton Institute	ActLab
Loss on drying @110°C	0.10	NR	0.21	NR
Loss on ignition @1000°C	1.01	1.06	36.12	36.04
Na ₂ O	3.33	3.66	0.1	0.08
MgO	1.04	1.16	1.67	1.68
Al ₂ O ₃	12.86	12.92	2.83	3.03
SiO ₂	74.42	73.24	11.76	11.57
P ₂ O ₅	0.05	0.07	0.07	0.08
K ₂ O	2.14	2.59	0.68	0.54
CaO	2.25	2.24	43.95	44.68
TiO ₂	0.30	0.30	0.13	0.14
Mn ₃ O ₄	<0.05	0.044	<0.05	0.038
V ₂ O ₅	<0.05	0.008	<0.05	0.004
CR ₂ O ₃	<0.05	0.01	<0.05	0.01
Fe ₂ O ₃	2.77	2.99	2.52	1.39
BaO	0.07	-	<0.05	-
ZrO ₂	<0.05	-	<0.05	-
SrO	0.05	-	0.06	-
CuO	-	-	-	0.005

LOI is typically reported as loss when specimen heated to 1000°C, this may or may not include the loss of mass when dried to 110°C.

NR = not reported, "-" not reported in analysis

4.3 Influence of Exposure of Bentonite to Saline Solutions

Of concern in evaluation of the effectiveness of bentonite-based materials as an isolating material is the influence of groundwater chemistry on its swelling and hydraulic properties. Associated with this is understanding what changes to the chemical and mineralogical composition of bentonite will happen as the result of ongoing exposure to saline groundwater.

As part of the current study, MX80 materials purchased in 2014 have been soaking in brine solutions for more than 81 months (6.75 years) and have been tested to determine their mineralogical and chemical composition. This is done to determine if there have been any discernible changes to them mineralogically or chemically as a result of this exposure to saline water. These salt-soaked samples are the same as were examined in the study by Dixon et al. (2018) and analysed after 18 months of exposure to SR-Sh brine. It should be noted that the bentonite used in this study of effects of salt are not the same as those used in the other tests completed as part of this study. There are slight mineralogical and chemical differences between the reference materials reported in Dixon et al. (2018) for the 2014 MX80 bentonite that is used in the effects of brine study and the 2018 MX80 bentonite shipment that is used in all the other components of the current study. For consistency of reporting and ease of separating these two bentonites they are referred to as 2014 and 2018 bentonites. This report presents the analytical results for the as-delivered 2014 bentonite (testing began in early 2016), following soaking in SR-Sh (~335 g/L TDS) for 18 months reported by Dixon et al. (2018) and data subsequently obtained by analysis of samples from the same batches of materials that had been soaking in CR-10 and SR-Sh for 54 and 81 months.

The conduct of these tests involved soaking of MX80 bentonite in sufficient brine solution that the clay's ability to absorb water (> than its free-swell capacity) is exceeded. The sealed containers of bentonite-fluid mixture were stored in the dark at constant temperature of 20°C and subsamples of bentonite were subsequently removed at 18, 54 and 81 months. Soluble salts were removed from the water-saturated bentonite sub-samples using passive soaking in a semi-permeable dialysis membrane while surrounded by deionized water. This results in the movement of ions in solution from the saline fluid diffusing outwards through the diffusion membrane to the freshwater reservoir, while keeping the clay particles inside the membrane enclosure as shown in Figure 4.2.



Figure 4.2. Soluble salt removal from brine-soaked specimens by diffusion through dialysis membrane (Dixon et al. 2018)

Monitoring of the electrical conductivity of the freshwater side and repeated replacement of the external reservoir solution with deionized water allowed for removal of almost all the soluble ions from the MX80 and measuring of the reservoir fluid's electrical conductivity and total dissolved solids (TDS), allowed for determination of the endpoint regarding soluble cation removal. The end point of ion removal by membrane diffusion was between 10 and 24 ppm TDS (24.48 microsieverts (μSv)). At that point it was assumed that the cations present in the system are almost entirely associated with the mineral component (absorbed on the surfaces of the minerals as exchangeable or non-exchangeable ions). The desalinated samples were subsequently oven dried and crushed to provide material for XRD and XRF analysis.

4.3.1 Mineralogical Composition of Brine Soaked MX80 as Determined using XRD

The results of XRD analyses of the 2014 MX80 bentonite studied previously were reported in Dixon et al. (2018). To these data the results of two further analyses have been added providing information regarding ongoing influence of saline porefluid on the mineralogical composition of MX80 bentonite.

In Table 4.6 the results of XRD analyses completed on as-received material, following 18 months of brine exposure and then following approximately 54 and 81 months of brine exposure are summarized. As noted previously, XRD is a semi-quantitative methodology that is used to estimate mineral composition and so values determined should be taken as-such, variations are to be expected. With soaking of the clay at high water/solid ratio and subsequent desalination of the porefluid by dialysis it is likely that the crystalline mineral components will show improved x-ray diffraction behaviour as the result of removal (dissolution) of amorphous coatings and hence apparent changes to the determined mineralogy (e.g., quartz, feldspar as shown in Table 4.6).

Of note in the data presented in Table 4.6 is the substantial reduction (highlighted values) in the calcite component between 18 and 54 months after the start of soaking as well as the apparent disappearance of trace minerals such as biotite, siderite, pyrite and gypsum. All but one of these minerals (biotite) are known to be more soluble in water than most other minerals present and could be expected to be lost when soaked at a high liquid to solid ratio for an extended time. With apparent loss of some of the minor components, the proportion of those left would be expressed as a slight increase in their proportion even though there is no change in the actual quantity of each component. The apparent disappearance of the very small biotite component is unexpected, but this was only reported as a trace amount initially. The very small size of the specimens tested also leaves open the potential for a single small particle of feldspar (or other mineral) originally present as an inclusion in the bentonite deposit (see visually present inclusions in raw bentonite in Figure 4.1) to skew the analytical results, this may in-part be the reason for observed scatter in analytical results for what are considered to be identical samples.

The results presented in Table 4.6 do not show any consistent change in the measured, major minerals component of the bentonite. Specifically;

- The montmorillonite contents determined were typically within the range reported for the source material prior to start of soaking in brine. There was one analysis (CR-10 @ 54 months highlighted in yellow in Table 4.6) that indicated a reduction in montmorillonite (and increase in feldspar minerals). This was not followed by a similar result when material was retested at 81 months. The materials soaked in the SR-Sh brine showed no changes in average contents of the major building blocks of the minerals present (Si, Al, Fe). It was also not apparent in the chemical (XRF) analyses for these samples (see Section 4.1.2.2) that indicated very similar chemical compositions.

- There were small apparent losses or reductions in some of the more soluble minerals (gypsum, siderite and calcite) as might be expected when fine-grained, relatively soluble minerals are placed in solution.
- Feldspars are amongst the most mineralogically-stable of minerals and soaking in saline solution should not affect them over the short-term. Feldspar mineral content (plagioclase and K-feldspar) shows the most variability of all the minerals. This may be associated with their texture and perhaps removal of some amorphous coatings (resulting in stronger diffraction pattern and interpreted higher mineral presence), as the result of extended soaking rather than mineralogical change.

Table 4.6 XRD-Determined Mineralogy of MX80 Samples Soaked in Brine Solution

Solution	Original	SR-Sh	SR-Sh	SR-Sh	CR10	CR10	Apparent change due to soaking in CR-10
Time soaked in soln.	Material	18 Mo	54 Mo.	82 Mo.	54 Mo.	82 Mo.	
Test Date	2014	2016	Nov 2019	Feb 2022	Nov 2019	Feb 2022	CR-10
Mineral		3 tests					
Montmorillonite	87.4±8	88±4	83.4	83.0	77.0	85.3	no consistent change
Zeolite	ND	ND	ND	ND	ND	ND	
Calcite	2.9±0.7	2.6±2.3	1.2	1.8	1.8	1.4	reduced Ca
Dolomite	TR	ND	ND	ND	ND	ND	loss of minor component
Quartz	2.5±1	1.2±1	2.2	2.0	2.8	2.2	no change
Quartz (Cristobalite)	ND	ND	ND	ND	ND	ND	
Biotite	<1.4	<1.7	ND	ND	ND	ND	loss of minor component
Muscovite (+illite)	0.3-7.1	0-8.2	1.8	1.5	3.1	1.3	no change
Feldspar (Plagioclase)	0-6.8	0-8.3	7.2	6.2	9.6	3.7	no change ?
Na-Feldspar	ND	ND	ND	ND	ND	ND	
K-Feldspar	<3	<2.3	4.2	4.3	5.7	5.0	increase
Siderite	<2	<3.2	ND	0.8	ND	0.6	no change
Pyrite	<0.6	<0.4	ND	0.4	ND	0.5	no change
Gypsum	<0.4	ND	ND	ND	ND	ND	loss of minor component
Amorphous	NR	NR	NR	NR	NR	NR	
Iron minerals	ND	ND	ND	ND	ND	ND	
Total	100	100	100	100	100	100	

Note: TR = trace; 'ND' = not detected; NR = not reported cannot be detected by xrd

The apparent lack of mineralogical change in the materials examined are not surprising as illitization, if it occurs is both a long-term process and also highly influenced by temperature. Studies by Karnland and Birgersson (2006) for a KBS-3 type environment (similar to NWMO crystalline option where CR-10-type groundwater is present) concluded that for the SKB groundwater environment (similar to CR-10):

"by use of realistic potassium concentrations show insignificant transformation of the montmorillonite during the lifetime of the repository. The calculated extent of montmorillonite that will be transformed is less than 1%, which should be compared with the calculated maximum acceptable illitization of 30% based on the design criterion of at least 1 MPa in swelling pressure. The margins to significant transformation is large both with respect to temperature and potassium concentrations."

Similarly, in a modelling exercise completed by Zheng et al. (2017), for a sedimentary geosphere (argillaceous clay stone) interacting with bentonite concluded that for a FEBEX bentonite:

- At room temperature, the bentonite will exhibit a volume fraction decrease of montmorillonite of approximately 1% in 1,000 years and 1.5 to 3% in 100,000 years
- At a temperature of approximately 100 °C at the canister surface, volume loss of smectite will vary depending on location but will be between 1 and 3%.

As a result, the small changes in smectite content observed in this study are consistent with other reported information and are not interpreted as being indicative of material alteration.

4.3.2 Chemical Composition of Brine-Soaked MX80 as Determined using XRF

The results of XRF analyses of the MX80 bentonite studied previously were reported in Dixon et al. (2018). The results of further analyses have been added, providing further information regarding the influence of saline porefluid on the mineralogical composition of MX80 bentonite.

Table 4.7 and Table 4.8 present the results of XRF analyses completed on as-received material and brine-soaked materials respectively, following 18 months of brine exposure and then following approximately 54 and 81 months of brine exposure. These data provide an indication of any large-scale loss of material as well as evidence of ion-exchange that has occurred as the result of extended exposure to simulated groundwaters.

The data presented in Table 4.7 shows the as-reported and adjusted oxides contents for raw, as-received MX80. The adjusted values are based on the raw analytical results of XRF analyses for each of the oxides and these are then normalized to eliminate the water content determined during loss-on-ignition (LOI). Otherwise, it is difficult to compare the results for samples having differing LOIs as this value will vary with the initial moisture content of the sample. For comparison to the MX80 used in this study, other XRF data sourced from the literature are also presented, illustrating the variability of the chemical composition of this bentonite. The data in Table 4.7 is quite consistent between samples, the bentonite examined in this study deviates from literature-derived values in its Na, Ca, Si, Al and Fe contents. The Na and Ca can be attributed to variability in the natural soluble salts present in bentonite. The Si and Al contents are more indicative of differences in the mineralogical composition of the samples (e.g., quartz, feldspar and montmorillonite). The iron content may reflect differences in the minor mineral components (e.g., pyrite). Detailed mineralogical assessment would be required in order to determine what these minor differences may be the result of, and since no reference materials are available for the literature-derived samples, this evaluation cannot be carried out.

In Table 4.8, the effects of soaking MX80 in low salinity CR-10 (~12 g/L TDS) and brine SR-Sh (~335 g/L TDS) for 18, 54 and 81 months are presented. The chemical composition of the original, untreated bentonite sample is compared to those obtained for MX80 that has been soaked in CR-10 for 54 and 81 months (there was no analysis done at 18 months) and also MX80 that has been soaked for 18, 54 and 81 months in SR-Sh brine. The data for the XRF analysis of the untreated source material shows a good repeatability, establishing that any subsequently observed differences between these data and what is obtained following soaking in artificial groundwater are real.

Cation exchange capacity (CEC) is a measure of how many cations can be retained on soil particle surfaces. The negative charges on the surfaces of the mineral particles cause positively-charged atoms or molecules (cations) to weakly bond with them, but allow them to exchange with other positively charged particles in the surrounding soil water. As a result, CEC

provides an indication of both the strength of the negative surface and the surface area available for exchange to occur on. As montmorillonite has both a high surface charge and a very high surface area per gram of clay, CEC provides an indication of clay content.

The cation compositions observed in Table 4.7 for the desalinated specimens include structural, exchangeable, and non-exchangeable cations. Those cations that would originally have been found in the bulk pore fluid have been largely removed through the desalination process. The exposure of the bentonite to brine solutions having high TDS, higher Ca and K to Na ratios relative to the raw materials will result in the release of much of the Na component (with corresponding decrease in Na in the desalinated specimen) and sorption of Ca and K to replace of the released Na (with corresponding increase in Ca and K in the XRF values of the desalinated specimen). In natural bentonites, there is generally a very low exchangeable K content and most of the K found in these materials is associated with K-feldspars and Illite and so is not readily removed/released without destruction of those very durable minerals. The K determined for the raw bentonite can therefore be assumed to be structural K and not part of the cation exchange process in that material. Subsequent increases in detected K are therefore attributable to ion-exchange onto mineral surfaces as the result of the presence of K in the groundwater solutions used.

In Table 4.8 those compositional values that differ more than the determined standard deviation from the original raw material have been highlighted. The cations that show differences beyond the anticipated levels of variation are limited to Na, Ca and K, all of which are associated with the porefluid and the exchangeable cations on the clay mineral surfaces. This means that the values reported for the raw samples reflect the sum of the total "natural" soluble salts and exchangeable cations present in the MX80 as well as the structural components in the mineral solids. It should be noted that the raw clay samples were not diffusion desalinated to remove their soluble cation components.

As anticipated, following soaking of the MX80 in SR-Sh brine and subsequent desalination of the samples, there is a notable reduction in the Na and increase in the Ca and K present in the remaining specimen following drying. The changes in Na and Ca are attributable to exchange of Na for Ca on the mineral surfaces, releasing Na for removal during desalination. The apparent increase in K is also attributed to K moving out of solution and into some of the expanded interlayers of the hydrated bentonite where they exchange for other cations (e.g., Na) associated with the mineral surfaces and are preferentially retained. It is notable that the K content does not seem to have increased substantively following the initial 18 months of soaking in artificial groundwater and that the K present in the materials soaked in CR-10 and SR-Sh solutions are similar. This seems to indicate that it is a surface-exchange process that has come into equilibration. It is also notable that the changes to the chemical composition of the bentonite seen in Table 4.6 for CR-10 soaking do not seem to extend to materials tested at 81 months and that Table 4.8 data does not show changes in silica or alumina contents in the bentonite. Such changes would not be expected but could be interpreted as such if XRD results were taken in isolation. Similarly, the Ca content determined by XRF also shows an apparent increase after exposing the bentonite to brine solution, which is not consistent with the XRD results indicating loss of calcite.

Table 4.7. Chemical Composition of Untreated MX80 Determined Using XRF

Oxides	Activation Labs	Normalized value	Hutton Institute	Normalized value	SRC 1	Normalized value	SRC 2	Normalized value	Average Norm. Value	STDev	Activation Labs	Normalized Value
Batch Yr	2016		2016		2016		2016		2016		2016	
Test Date	2016		2016		2016		2016		2016		Nov 2019**	
	(wt %)	(wt %)	(wt %)	(wt %)	(wt %)	(wt %)	(wt %)	(wt %)	(wt %)	(wt %)	(wt %)	(wt %)
Na ₂ O	1.87	2.30	1.98	2.41	1.49	1.78	1.56	1.88	2.09	0.27	2.29	2.52
MgO	3.16	3.88	3.09	3.77	2.25	2.68	2.26	2.72	3.27	0.56	2.83	3.11
Al ₂ O ₃	18.57	22.83	18.24	22.24	18.80	22.43	18.80	22.65	22.54	0.22	20.36	22.40
SiO ₂	51.46	63.26	51.76	63.11	54.40	64.92	53.10	63.98	63.82	0.71	58.11	63.94
P ₂ O ₅	0.10	0.12	0.07	0.09	0.06	0.07	0.06	0.07	0.09	0.02	0.07	0.08
K ₂ O	0.16	0.20	0.61	0.74	0.43	0.51	0.41	0.49	0.58	0.19	0.61	0.67
CaO	2.07	2.54	2.21	2.69	1.82	2.17	1.87	2.25	2.42	0.21	2.1	2.31
TiO ₂	0.16	0.20	0.16	0.20	0.19	0.22	0.18	0.21	0.21	0.01	0.21	0.23
MnO	0.02	0.02	<0.05	0.06	0.03	0.03	0.03	0.03	0.04	0.02	0.019	0.02
V ₂ O ₅	<0.003	-	<0.05	0.06	-	-	-	-	-	-	-	-
Cr ₂ O ₃	<0.001	-	<0.05	0.06	-	-	-	-	-	-	-	-
Fe ₂ O ₃	3.78	4.65	3.86	4.71	4.20	5.01	4.59	5.53	4.97	0.35	4.28	4.71
FeO	-	-	-	-	-	-	-	-	-	-	-	-
C	-	-	-	-	-	-	-	-	-	-	-	-
S	-	-	-	-	0.16	0.19	0.17	0.20	0.10	0.10	-	-
LOI*	17.41	17.63	17.19	17.33	15.80	15.86	15.90	16.08	16.72	-	8.9	8.92
Total	98.8	100.0	99.2	100.1	99.6	100.0	98.9	100.0	100.0	-	99.78	100.0
Na ₂ O/K ₂ O		11.69		3.25		3.47		3.80	3.59			3.75
Na ₂ O/CaO		0.90		0.90		0.82		0.83	0.87			1.09
SiO ₂ /Al ₂ O ₃	2.77	2.77	2.84	2.84	2.89	2.89	2.82	2.82	2.83	0.04	2.85	2.85

* Loss on ignition (heating to 1000C). This removes all water, carbonate, gypsum and organic matter from the specimen.

** A different subsample of 2016 MX80 bentonite order.

*** Data expressed as % of total non-LOI oxide content. Adjusted value = measured value / (1-LOI/100) / (1-Adj LOI)

Table 4.8. Change in MX80 Chemical Composition Following Brine-Soaking

Oxides	Raw Material, no brine exposure			Exposure to SR-Sh				Exposure to CR-10		Notes
	Initial 2016 data*		Retest 2019 data	18 Months Soaking**		54 Months	81 Months	54 Months	81 Months	
	Adj. oxides	STDev	Adj. oxides	Adj. oxides	STDev	Adj. oxides	Adj. oxides	Adj. oxides	Adj. oxides	
	(wt %)	(wt %)	(wt %)	(wt %)	(wt %)	(wt %)	(wt %)	(wt %)	(wt %)	
Na ₂ O	2.09	0.27	2.52	0.36	0.16	0.92	0.81	0.62	0.37	Substantial reduction
MgO	3.26	0.56	3.11	3.32	0.40	3.73	3.53	3.66	3.84	Slight Increase?
Al ₂ O ₃	22.54	0.22	22.40	21.67	1.09	22.64	22.31	22.35	22.33	No Change
SiO ₂	63.81	0.72	63.94	63.64	1.52	63.66	63.08	63.02	63.91	No Change
P ₂ O ₅	0.09	0.02	0.08	0.08	0.01	0.08	0.08	0.09	0.09	No change
K ₂ O	0.49	0.19	0.67	1.34	0.06	0.75	1.35	1.37	0.71	Substantial increase in k
CaO	2.42	0.21	2.31	3.84	0.34	3.25	3.91	3.89	3.64	Substantial increase in Ca
TiO ₂	0.21	0.01	0.23	0.21	0.03	0.20	0.19	0.19	0.24	No change
MnO	0.02	0.02	0.02	0.03	0.01	0.02	0.03	0.02	0.03	No change
V ₂ O ₅	-	-	-	-	-	-	-	-	-	
Cr ₂ O ₃	-	-	-	-	-	-	-	-	-	
Fe ₂ O ₃	4.97	0.35	4.71	5.41	0.94	4.76	4.72	4.77	4.78	No change
FeO	-	-	-	-	-	-	-	-	-	
C	-	-	-	-	-	-	-	-	-	
S	0.10	0.10	-	0.04	-	-	-	-	0.04	No change
LOI	16.72	-	8.9	15.75	-	13.27	13.78	11.94	12.41	
Total***	100	-	100	99.9		100	100	100	100	
SiO ₂ /Al ₂ O ₃	2.83		2.84	2.94		2.81	2.79	2.82	2.86	

* average of 4 analyses; materials purchased in 2014 but not tested until 2016.

** average of 3 analyses;

*** excluding Loss on ignition (LOI)

5. COMPACTION PROPERTIES OF BENTONITE – AGGREGATE MIXTURES

The compaction behaviour of mixtures of MX80 bentonite and aggregate (granitic sand (GS) or crushed limestone (CRL)) were examined for two compaction energies. The lower energy Standard Compaction Test (SCT) also known as the Standard Proctor (SP) test defined in ASTM D698. The higher compaction effort, Modified Compaction (MC) test was completed using the Miniature Compaction Test (Mini Proctor) described and calibrated for bentonite-aggregate materials by Dixon et al. (1985). The Mini Proctor test has been calibrated to the ASTM D1557 Modified Compaction Test (MCT) and the device is shown in Figure 5.1 was used to evaluate both the compaction behaviour of the bentonite – aggregate blends as well as the effects of porefluid salinity.

Plots showing the fluid content versus dry density achieved for each of the Standard (SCT) and Modified (MCT) compaction tests are provided in Appendix B. For the purposes of density specifications in a field-type condition, target densities are typically defined based on a percentage of SCT maximum dry density or a percentage of MCT. In this study low-density targets are based on 98% of SCT maximum density.



Figure 5.1. Miniature compaction device

Table 5.1 and Figure 5.2 present the results of SCTs on MX80-GS and MX80-CRL mixtures that had low salinity (CR-10), or high salinity (SR-Sh) fluids used in their preparation. The results obtained using MCT energy to compact the specimens are presented in Table 5.2 and in Figure 5.2.

Most conventional compaction testing is done under conditions of essentially zero total dissolved solids (TDS) in the porefluid. The mixing fluids used in this study have notable TDS contents (~12 g/L and ~335 g/L) and represent fluids that might be used if local groundwater were used to moisture-condition the material prior to its compaction. These fluids also simulate the porefluid conditions that would ultimately be present in the sealing system components once saturation is achieved, and groundwater equilibration occurs.

The use of high TDS fluid in compaction testing complicates analysis of the results as the Maximum Compacted Dry Density (MCDD) determinations need to be adjusted to take into account the potentially substantial mass of salt left behind by drying (the apparent dry density of material that is not salt-corrected is higher than is actually achieved). Similarly, defining the Optimum Moisture Content (OMC) needed to achieve maximum compacted density for a given

energy input from oven drying of the specimens is complicated by the residual salt component. For consistency of presentation, the data in this report are expressed in terms of gravimetric water content (the mass of fresh water divided by the dry mass of soil that has been corrected for any residual salt left following drying).

The dry density of a specimen was determined as follows:

Dry Density = (oven dried mass of soil and salt – mass of salt present) / specimen volume.

Gravimetric Water Content = mass of water released during oven drying / dry mass of soil particles only.

Figure 5.2 shows consistent trends of decreasing achievable maximum compacted dry density with increasing bentonite content for all the materials examined. This trend is present for both the CR-10 and SR-Sh fluid systems. The SCT produces lower maximum achievable density than the MCT, which is expected given the much lower energy imparted during compaction.

Of greater interest than dry density of the shaft backfill is how well it will function as a barrier, specifically its hydraulic conductivity and its ability to maintain a positive contact pressure with its confinement (shaft walls). These properties can be predicted through determination of the Effective Montmorillonite Dry Density (EMDD). EMDD is defined as the mass of montmorillonite in a compacted specimen divided by the volume occupied by the montmorillonite and voids (fluid and air volume), any mass and volume occupied by other materials is considered to be inert and not an influence in subsequent specimen behaviour (e.g., swelling pressure, hydraulic conductivity). There are databases that can be used to develop preliminary predictions regarding swelling pressure and hydraulic conductivity under a range of groundwater and density conditions using EMDD, but these databases have limited information regarding behaviour under conditions relevant to the anticipated DGR conditions in Canada. The swelling pressure and hydraulic behaviour of backfill materials prepared to 98% SCT and 95% MCT maximum dry density are presented in Section 6 of this report.

5.1 Standard Compaction Testing (SCT)

There are discernable differences in the maximum compacted dry density (MCDD) achievable for the various bentonite-aggregate mixtures examined when low compaction effort (SCE), is used.

- The MCDD achieved for the various bentonite-aggregate blends examined show a trend of increasing MCDD with increasing aggregate content.
- The EMDDs associated with the MCDDs achieved using SCE show a continuous trend of increasing EMDD with increasing bentonite content.
- The granitic sand – bentonite mixtures achieved slightly (5-10 %) higher MCDD than the crushed limestone (Figure 5.2). This was observed for materials prepared with both low and high-salinity fluids.
- The lower salinity CR-10 exhibits a slightly (<5%) lower MCD than observed for materials prepared using the higher salinity SR-Sh and this is observed for both granitic sand and crushed limestone aggregate admixtures.

The use of high salinity porefluid resulted in slightly higher maximum dry density for both granitic sand and crushed limestone aggregate systems. This is attributable to the effects of salts on water sorption on the montmorillonite particle surfaces, with low salinity systems having more

adsorbed water associated with the soil. This adsorbed water will require greater effort to displace. In the SCT the energy applied seems to have been insufficient to overcome some of this resistance.

Table 5.1. Standard Compaction Test Results and Initially Estimated Ps and k behaviour*

Bentonite	OMC	MCDD	98% MCDD*	EMDD @ 98% MCDD	ECDD @ 98% MCDD	k **	Suitable	Ps**	Suitable
(%)	(%)	(Mg/m ³)	(Mg/m ³)	(Mg/m ³)	(Mg/m ³)	(m/s)		(MPa)	
MX80:GS – CR-10									
50	19	1.63	1.597	1.002	1.144	4.6E-12	Yes	354	Yes
60	20	1.539	1.508	1.029	1.172	3.7E-12	Yes	409	Yes
70	20	1.506	1.476	1.096	1.241	2.1E-12	Yes	587	Yes
80	22	1.415	1.387	1.094	1.240	2.1E-12	Yes	584	Yes
90	22	1.345	1.318	1.103	1.248	2.0E-12	Yes	609	Yes
MX80:GS – SR-Sh									
50	17	1.7	1.666	1.071	1.216	8.3E-10	No	62	No
60	21	1.62	1.588	1.108	1.254	4.9E-10	No	82	No
70	15	1.56	1.529	1.148	1.295	2.8E-10	No	110	Yes
80	22	1.49	1.460	1.166	1.313	2.2E-10	No	125	Yes
90	25	1.45	1.421	1.204	1.351	1.3E-10	No	164	Yes
MX80:CRL – CR-10									
50	15	1.62	1.588	0.993	1.135	4.9E-12	Yes	337	Yes
60	17	1.54	1.509	1.030	1.173	3.7E-12	Yes	412	Yes
70	17.5	1.48	1.450	1.070	1.215	2.6E-12	Yes	512	Yes
80	20	1.39	1.362	1.110	1.070	8.3E-12	Yes	240	Yes
90	20	1.33	1.303	1.088	1.233	2.3E-12	Yes	563	Yes
MX80:CRL – SR-Sh									
50	14	1.7	1.666	1.071	1.216	8.3E-10	No	62	No
60	18	1.66	1.627	1.148	1.295	2.8E-10	No	110	Yes
70	18	1.53	1.499	1.118	1.264	4.3E-10	No	88	No
80	17.5	1.5	1.470	1.176	1.323	1.9E-10	No	134	Yes
90	23	1.4	1.372	1.156	1.302	2.6E-10	No	116	Yes

* EMDD at 98% of Standard Proctor Maximum Dry Density is based on an assumed montmorillonite content of 80% in the bentonite.

** Using equations provided in Dixon (2019).

Note: the MCDD is determined using equations provided in Dixon et al. (1985) that convert mini-compaction results to MPMCDD

5.2 Modified Compaction Tests (MCT)

Compaction of bentonite-aggregate materials using the MCT results in a different pattern of compaction behaviour than observed for materials compacted using SCT specifications. Shown in Figure 5.2, the behaviour of bentonite-aggregate materials compacted using the MCT can be summarized as follows:

- A decrease in the achievable MCDD is observed with increasing aggregate content.
- There is no clear difference in the MCDD achieved using granite sand or crushed limestone for a given bentonite-aggregate ratio.
- The same maximum densities are achieved for both low and high salinity porefluid systems for a given MX80-Aggregate ratio and compaction effort (excepting for the 90% bentonite – 10% GS mixture that for undetermined reasons exhibited a lower-than expected MCDD). Compaction tests completed for 100% MX80 were consistent with the density trend observed for bentonite-aggregate mixtures.
- No clear improvement in the EMDD achieved is observed once clay content exceeds 60-70%.

5.3 Estimation of Swelling and Hydraulic Behaviour Based on Compaction Tests

As EMDD is the main parameter in determining swelling and hydraulic performance in a given groundwater environment, the materials prepared to MCDD using 60-100% bentonite content should exhibit similar behaviours. As can be seen in Table 5.1 and Figure 5.2, the SCT results show a decreasing dry density and gradually increasing EMDD with increasing bentonite content for the entire range of MX80-aggregate specimens examined. The MCT materials have a higher dry density and EMDD than those compacted using SC energy with little evident change in EMDD once bentonite content exceeds approximately 60% (Figure 5.2). This is consistent with compaction behaviour reported by Dixon et al. (1985). Since it is EMDD that controls the swelling pressure, hydraulic conductivity and other properties of bentonite-based materials increasing the bentonite content for these materials beyond approximately 60% for materials compacted to either SC or MC specifications will result in only a slight lowering of k and increase of P_s , as can be seen in Table 5.1 and Table 5.2.

Table 5.2. Modified Compaction Test Results and Anticipated Ps and k Values

Bentonite	OMC	MCDD	95% MCDD	EMDD @ 95% MCDD*	ECDD @ 95% MCDD**	k +	Suitable	Ps+	Suitable
(%)	(%)	(Mg/m ³)	(Mg/m ³)	(Mg/m ³)	(Mg/m ³)	(m/s)		(MPa)	
MX80:GS – CR-10									
50	20	2.07	1.967	1.421	1.566	1.6E-13	Yes	3.20	Yes
60	13	1.972	1.873	1.423	1.568	1.6E-13	Yes	3.24	Yes
70	17.5	1.923	1.827	1.470	1.613	1.1E-13	Yes	4.09	Yes
80	10	1.825	1.734	1.452	1.597	1.3E-13	Yes	3.77	Yes
90	15	1.629	1.548	1.333	1.480	3.2E-13	Yes	2.04	Yes
100+		1.727	1.641	1.538	1.641	8.9E-14	Yes	4.74	Yes
MX80:GS – SR-Sh									
50	10	2.041	1.939	1.384	1.530	1.1E-11	Yes	0.60	Yes
60	10.5	1.972	1.873	1.465	1.568	6.8E-12	Yes	0.78	Yes
70	11.5	1.903	1.808	1.448	1.592	4.9E-12	Yes	0.93	Yes
80	14	1.864	1.771	1.493	1.636	2.7E-12	Yes	1.27	Yes
90	22	1.717	1.631	1.419	1.564	7.2E-12	Yes	0.76	Yes
100+		1.727	1.641	1.499	1.641	2.5E-12	Yes	1.32	Yes
MX80:CRL – CR-10									
50	20	1.992	1.892	1.326	1.473	3.4E-13	Yes	1.97	Yes
60	18	1.982	1.883	1.435	1.580	1.4E-13	Yes	3.45	Yes
70	17.5	1.894	1.799	1.488	1.582	1.4E-13	Yes	3.48	Yes
80	15	1.854	1.761	1.482	1.625	1.0E-13	Yes	4.36	Yes
90	15	1.776	1.687	1.479	1.622	1.0E-13	Yes	4.29	Yes
MX80:CRL – SR-Sh									
50	11	2.031	1.929	1.372	1.519	1.3E-11	Yes	0.55	Yes
60	12	1.972	1.873	1.423	1.568	6.8E-12	Yes	0.78	Yes
70	20	1.894	1.799	1.438	1.582	5.6E-12	Yes	0.86	Yes
80	16	1.825	1.734	1.452	1.597	4.6E-12	Yes	0.96	Yes
90	19	1.756	1.668	1.458	1.602	4.3E-12	Yes	1.00	Yes

* EMDD at 95% of Modified Proctor maximum dry density is based on an assumed montmorillonite content of 80% in the bentonite.

** Using equations provided in Dixon (2019). + Data from Dixon et. al (2018)

Note: the MCDD is determined using equations provided in Dixon et al. (1985) that convert mini-compaction results to MPMCDD

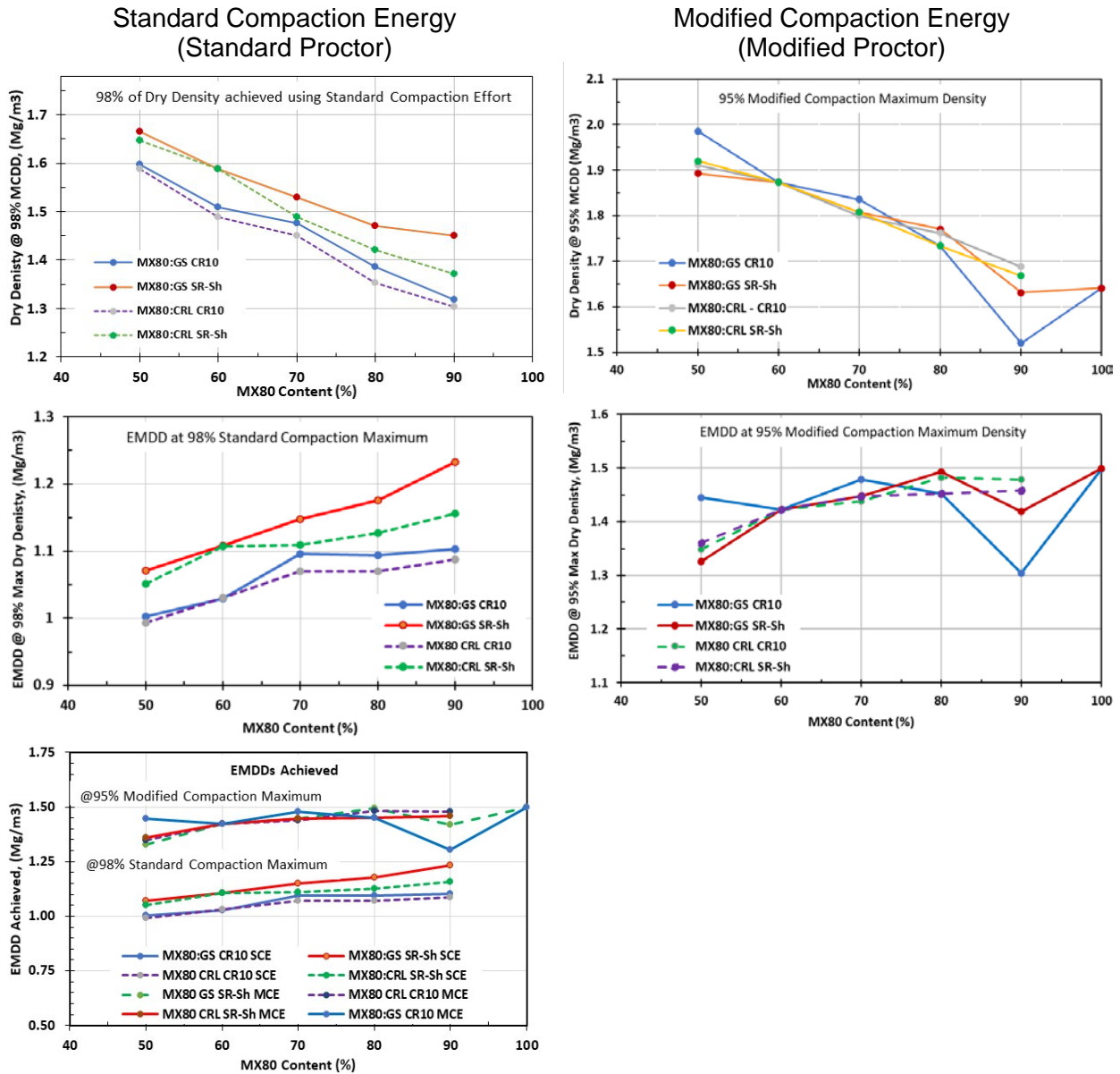


Figure 5.2. Dry density and EMDD achieved at 98% and 95% of maximum compacted density using SCT and MCT respectively

6. MEASUREMENT OF SWELLING PRESSURE AND HYDRAULIC CONDUCTIVITY

6.1 Testing Matrix, Testing Methods and Experimental Details

The swelling pressure and hydraulic conductivity properties of sealing system components outside the placement room and other key locations where higher degree of sealing effectiveness is required (e.g., room, tunnel and shaft seals), has been defined to be a minimum of 100 kPa swelling pressure on a rigidly confining medium and have advective flow velocity (hydraulic conductivity) of less than $1\text{E-}10$ m/s.

The test cells and monitoring systems used to complete the P_s and k measurements are shown in Figure 6.1. For comparison, the cell used by Rowe and Brachman (2019) is also provided in Figure 6.1. The cells used in the current study are the same as those used by Dixon et al. 2018; Barone et al. (2014) and were previously used by Dixon (1995); Dixon et al. (1996; 1999); Priyanto et al. (2013) and numerous other studies completed since the 1980s. The design details of this type of test cell vary with the laboratory using them but the cells all provide rigid confinement to the test specimen and allows for simultaneous monitoring of swelling pressure development by, and measurement of advective fluid flow through the specimen. Examples of other test cells can be found in reports by Pusch (1980) and Rowe and Brachman (2019).

Measurement of swelling pressure and hydraulic conductivity are accomplished using rigidly confined specimens that are built at a target initial degree of fluid saturation $>90\%$. The fluid used in moisture conditioning the specimens is identical to that subsequently used to complete saturation and accomplish hydraulic conductivity measurements (e.g., CR-10 used to moisture condition specimen and CR-10 used to percolate through; SR-Sh used to moisture condition specimen and SR-Sh used to percolate). This method of test preparation eliminates uncertainties regarding the porefluid composition present within the specimen and shortens testing time by allowing for relatively quick completion of the saturation process.

The P_s/k tests completed in this study are listed in Table 6.1 and are intended to provide data related to the behaviour of MX80-aggregate mixtures compacted to densities achievable using SCT and MCT as described in Section 5. Detailed plots obtained for each test are provided in Appendix C. The test matrix also includes use of MX80-aggregate blends prepared using crushed limestone (CRL) rather than granitic sand (GS). The examination of alternative aggregate materials is intended to identify if there is any discernible difference in their behaviour.

Based on the results obtained from compaction testing and using previously reported P_s and k data, target densities for 20 bentonite-aggregate specimens were identified for testing in Phase I and are listed in Table 6.1. The degree of densification for each specimen was targeted to be 98% of either SCMCD or 95% of MCMCD, depending on the material and porefluid used.

For environments where the groundwater salinity is relatively low (e.g., CR-10-type) lower densification of the backfill may provide materials exhibiting suitable behaviour. Hence half of the first series of tests completed in this study consisted of MX80-GS and MX80-CRL granitic sand systems that were tested using CR-10 fluid. The other half of the tests consisted of MX80-GS and MX80-CRL compacted to $\sim 95\%$ of Modified Proctor maximum dry density and then tested using SR-Sh fluid. These tests will provide valuable information regarding swelling pressure and hydraulic conductivity of potential backfilling materials as well as a comparison that will determine if the nature of the aggregate mixed with the MX80 affects swelling pressure development or hydraulic conductivity.

Table 6.1. Testing Matrix for Ps and k Tests

MX80:Aggregate Dry mass ratio	Sample #	Mixing and Testing Fluid ⁺	Aggregate	Target Dry Density* (Mg/m ³)	End-of-Test Dry Density** (Mg/m ³)	End-of- Test EMDD** (Mg/m ³)	Test Duration (days)
Relevant to 98% Standard Compaction Effort in Low Salinity Environment							
50:50	HC06	CR-10	GS	1.597	1.615	1.025	86
50:50	HC22	CR-10	GS	1.600	1.571	0.976	212
60:40	HC05	CR-10	GS	1.508	1.449	0.977	86
60:40	HC23B	CR-10	GS	1.51	1.550	1.074	98
70:30	HC04	CR-10	GS	1.476	1.427	1.053	86
80:20	HC12	CR-10	GS	1.387	1.375	1.160	101
90:10	HC09	CR-10	GS	1.318	1.302	1.087	127
40:60	HC32	CR-10	CRL	1.650	1.716	1.030	143
50:50	HC10X	CR-10	CRL	1.588	1.649	1.061	60
50:50	HC14	CR-10	CRL	1.588	1.569	0.980	93
60:40	HC16	CR-10	CRL	1.588	1.488	1.015	108
70:30	HC20	CR-10	CRL	1.450	1.483	1.102	135
80:20	HC19	CR-10	CRL	1.352	1.354	1.062	134
90:10	HC21	CR-10	CRL	1.303	1.290	1.076	133
Relevant to 98% Standard Compaction Effort in High Salinity Environment							
40:60	HC33	SR-Sh	GS	1.720	1.693	0.964	40
50:50	HC3X	SR-Sh	GS	1.760	1.671	1.082	83
60:40	HC2Xa	SR-Sh	GS	1.721	1.598	1.125	77
70:30	HC1X	SR-Sh	GS	1.558	1.508	1.132	60
80:20	HC7X	SR-Sh	GS	1.577	1.503	1.209	67
90:10	HC8	SR-Sh	GS	1.500	1.464	1.244	65
Relevant to 95% Modified Compaction Effort in Low Salinity Environment							
50:50	HC29	CR-10	GS	1.967	1.925	1.377	228
40:60	HC30	CR-10	CRL	1.950	1.966	1.285	213
50:50	HC28	CR-10	CRL	1.929	1.892	1.333	224
Relevant to 95% Modified Compaction Effort in High Salinity Environment							
40:60	HC31	SR-Sh	GS	1.950	1.915	1.219	65
50:50	HC25	SR-Sh	GS	1.967	1.946	1.404	180
60:40	HC27	SR-Sh	GS	1.873	1.831	1.380	130
50:50	HC11	SR-Sh	CRL	1.990	1.878	1.320	114
50:50	HC24B	SR-Sh	CRL	1.929	1.829	1.250	98
60:40	HC13	SR-Sh	CRL	1.932	1.852	1.403	106
60:40	HC26	SR-Sh	CRL	1.873	1.844	1.395	197
70:30	HC15	SR-Sh	CRL	1.865	1.808	1.455	100
80:20	HC17	SR-Sh	CRL	1.769	1.660	1.375	86
90:10	HC18	SR-Sh	CRL	1.721	1.631	1.419	127

* Target densities mainly based on maximum compacted dry density from compaction tests

** Tested dry density is based on end-of-test mass and volume measurements

+ CR-10 has a TDS of 11g/L, SR-Sh has a TDS of 335 g/L

++ EMDD calculated based on 80% montmorillonite content in bentonite

6.2 Hydraulic Conductivity Tests

The testing matrix for hydraulic conductivity and swelling pressure testing is provided in Table 6.1 and includes MX80-aggregate blends (granitic sand or crushed limestone were used as aggregate). These specimens were tested using the CR-10 (~12 g/L TDS) and SR-Sh (~335 g/L TDS) groundwaters described in Section 2.2. The results of testing were subsequently compared to data presented in previously completed studies. In many cases the montmorillonite content of literature data is not provided in reports containing Ps and k data, this may contribute to some of the scatter observed in data presented for comparison to current test results. For the purposes of determining the EMDD values for use in graphing and data comparison, unless otherwise documented, it is assumed that MX80 used in this study as well as literature-derived have a consistent montmorillonite content of 80%.

Specimens examined in this testing series were constructed using the same fluid as was subsequently percolated through them. This was done to avoid unquantifiable effects of non-equilibrated porefluid composition and to avoid the very long testing times (years) that would be required to pass multiple pore volumes through the specimens in order to achieve porefluid chemical equilibrium. The tests completed in the current study were constructed at >90% initial degree of fluid saturation and lasted from 3-7 months each. This allowed for specimen saturation to occur and a discernible quantity of fluid to be percolated through it.

Tests began with percolating fluid being introduced at a base of the specimen at a low hydraulic head of 1.5 m (15 kPa). This percolation under low gradient continued until the specimen indicated near-equilibrium in terms of total pressure and water inflow rate, this usually required several weeks of monitoring. At that time, the hydraulic head applied at the base of the specimen was increased to 5 m (50 kPa) with the drain at the top of the cell remaining open, in some tests this hydraulic head was subsequently increased to 100 and in some cases 200 kPa. The influx of fluid to the specimen was monitored using a displacement measurement system of the type shown in Figure 6.1. Regular monitoring of inflow was done to ensure that rate of inflow was consistent, and any leakage that might affect subsequently calculated hydraulic conductivity was quantified. Leakage was checked by continuing to monitor any water movement into the cell once the top drain was closed. In a properly sealed cell, the inflow rate will decrease towards zero as the hydraulic pressure becomes uniform throughout the internal volume of the cell and any occluded air in the system is compressed. Leakage would be identifiable and quantifiable as continuing inflow into a closed cell. In the data summary table provided in Appendix E the measured “leakage” of each cell is provided and shows that the volumes measured during leakage testing are much lower than the flow rate observed with the top drain open, and so the data can be used with confidence since leakage will be a small and quantified influence on the k value(s) measured.

The hydraulic conductivity determined is based on monitored time and Inflow volume recorded and assumes Darcian flow behaviour. The measured k values are provided in Table 6.2 and represent the average flow over an extended period of monitoring rather than short-term minimum or maximum values. This is particularly important with regards to eliminating the small but discernible effects of ambient temperature variations on the pressure supply and monitoring gauges at very low inflow rates. These data are plotted in Figure 6.2 and Figure 6.3, showing the data collected as well as previously collected data for systems percolated with CR-10 respectively. Detailed plots of the data collected are provided in Appendix D.

Previously determined hydraulic conductivity values for MX80-based materials completed using groundwaters comparable to CR-10 (e.g., ~ 12 g/L TDS Äspö groundwater and NaCl), (Dueck et al. 2011; Karnland et al. 2008, 2009), are also plotted in Figure 6.3. It was expected that these data would plot similarly to those for CR-10 and they do, although the literature data for

NaCl permeant tends to be slightly lower than for simulated groundwaters containing Na-Ca CL. Slightly lower k for NaCl-only solutions is not unexpected as the Ca in the CR-10 solution will tend to interact with the clay surfaces and adsorbed water layers, resulting in a slight increase in the ability of the clay to conduct groundwater. The good comparability of the current study data to literature and previous studies using CR-10 Dixon et al. (2018), shown in Figure 6.2, provides confidence in the data collected in the current study. It also indicates that consistent results have been obtained by several researchers, each using slightly different permeameter setups and testing protocols.

Table 6.2. Results of Hydraulic Conductivity and Swelling Pressure Testing

MX80:Aggregate Dry mass ratio	Sample #	Mixing and Testing Fluid ⁺	Aggregate	Specimen Dry Density** (Mg/m ³)	Specimen EMDD (Mg/m ³)	Measured k (m/s)	Measured Ps (kPa)	Test Duration (days)
40:60	HC33	SR-Sh	GS	1.693	0.964	8.5E-9	55	41
40:60	HC31	SR-Sh	GS	1.915	1.219	4.3E-13	250	218
40:60	HC30	CR-10	CRL	1.966	1.285	1.7E-12	1550	213
40:60	HC32	CR-10	CRL	1.717	0.991	6.8E-12	105	167
50:50	HC14	CR-10	CRL	1.569	0.980	1.1E-12	90	93
50:50	HC10X	CR-10	CRL	1.649	1.061	6.1E-12	100	60
50:50	HC24B	SR-Sh	CRL	1.829	1.260	3.5E-11	50	100
50:50	HC11	SR-Sh	CRL	1.878	1.320	6.5E-13	195	114
50:50	HC28	CR-10	CRL	1.892	1.333	2.7E-13	3032	229
50:50	HC22	CR-10	GS	1.571	1.019	2.9E-12	245	212
50:50	HC06	CR-10	GS	1.615	1.025	3.1E-12	330	86
50:50	HC3X	SR-Sh	GS	1.671	1.082	4.0E-10	80	83
50:50	HC29	CR-10	GS	1.925	1.377	2.7E-13	3300	229
50:50	HC25	SR-Sh	GS	1.946	1.404	1.9E-12	300	183
60:40	HC16	CR-10	CRL	1.488	1.054	3.8E-12	180	108
60:40	HC26	SR-Sh	CRL	1.844	1.395	8.4E-12	160	218
60:40	HC13	SR-Sh	CRL	1.852	1.403	2E-13	380	94
60:40	HC05	CR-10	GS	1.449	0.977	6.6E-12	200	86
60:40	HC23B	CR-10	GS	1.550	1.076	1.3E-12	272	100
60:40	HC2Xa	SR-Sh	GS	1.598	1.125	3.2E-10	90	77
60:40	HC27	SR-Sh	GS	1.831	1.380	2.6E-12	485	136
70:30	HC04	CR-10	GS	1.427	1.053	3.3E-12	270	86
70:30	HC20	CR-10	CRL	1.483	1.102	2.4E-12	270	136
70:30	HC1X	SR-Sh	GS	1.508	1.132	4.3E-11	190	60
70:30	HC15	SR-Sh	CRL	1.808	1.455	1.2E-13	453	100
80:20	HC19	CR-10	CRL	1.354	1.062	3.2E-12	310	134
80:20	HC12	CR-10	GS	1.375	1.154	1.6E-12	425	101
80:20	HC7X	SR-Sh	GS	1.503	1.209	3.0E-11	70	67
80:20	HC17	SR-Sh	CRL	1.660	1.375	5.2E-12	330	86
90:10	HC21	CR-10	CRL	1.290	1.076	5E-13	348	134
90:10	HC09	CR-10	GS	1.302	1.086	8.6E-13	350	127
90:10	HC8	SR-Sh	GS	1.464	1.244	4.4E-12	65	65
90:10	HC18	SR-Sh	CRL	1.631	1.419	3.9E-12	193	126

* Target densities mainly based on maximum compacted dry density from compaction tests

** Tested dry density is based on end-of-test mass and volume measurements

+ CR-10 has a TDS of 11g/L, SR-Sh has a TDS of 335 g/L.

Figures 6.2 and 6.3 also contain the best-fit and prediction limit regression lines (@90% degree of confidence) for the entire database of 10-15 g/L TDS fluids as well as for CR-10. Details of how these limits are calculated can be found online at <https://www.real-statistics.com/regression/confidence-and-prediction-intervals/> and are also discussed and presented in Dixon et al. (2019). The best-fit lines obtained for these two data sets are essentially identical and provide equations for use in generating conservative bounding values for the hydraulic conductivity of bentonite-based materials. These equations are similar to those provided in Dixon (2019) but are based on a much larger database and so have an increased robustness. These equations are summarized in Table 6.3.

Based on the data provided in Figure 6.3 for the combined data sets for TDS of 10-15 g/L an EMDD greater than approximately 0.75 Mg/m³ will be sufficient to maintain a k of less than 10⁻¹⁰ m/s.

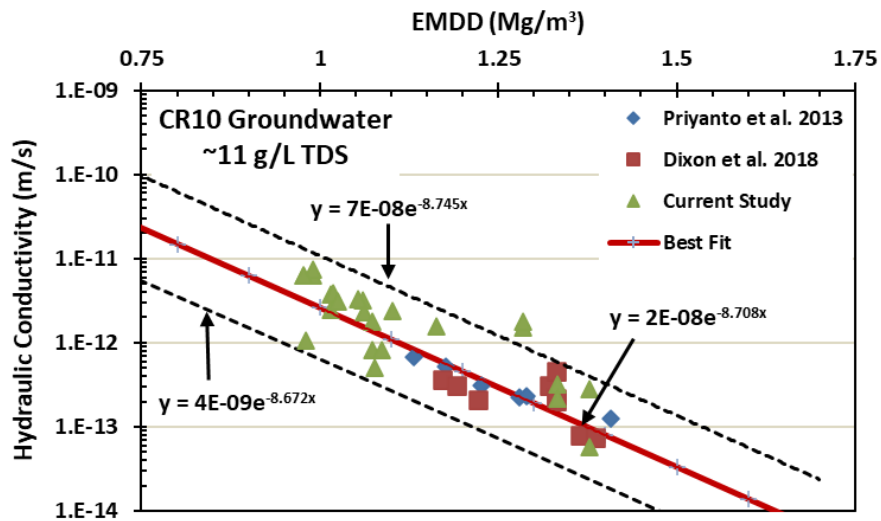


Figure 6.2. Hydraulic conductivity of MX80-based materials: CR-10 porefluid

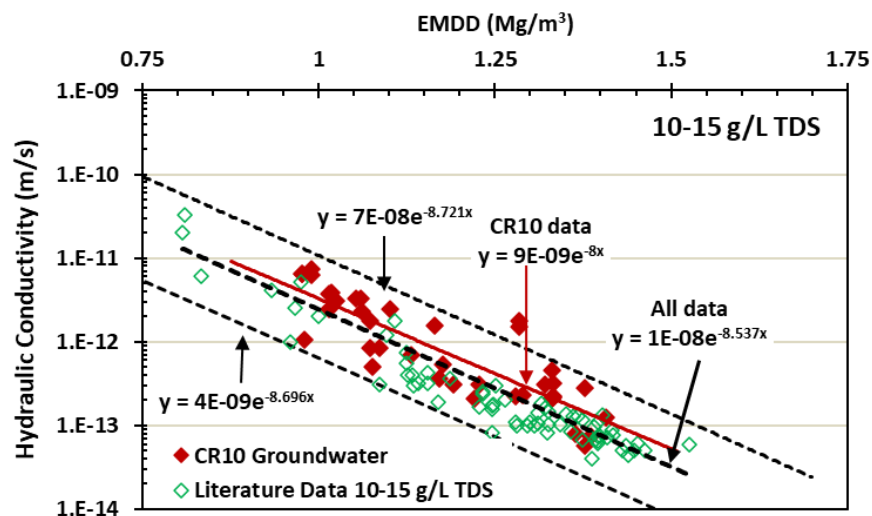


Figure 6.3. Hydraulic conductivity of MX80-based materials: comparison of CR-10 to other 10-15 g/L porefluids

Measurement of hydraulic conductivity under highly saline groundwater conditions was completed using the artificial groundwater SR-Sh (~335g/l TDS) formulation. The results are presented in Table 6.1 and plotted in Figures 6.4 and 6.5. There is a small additional database for tests previously completed using this groundwater composition (Dixon et al. 2018). This provides a basis for comparison with the current study and also provides for a larger database for use in developing generic predictive equations. Many of the previous tests were completed on bentonite-only systems (no aggregate content), and the comparability of the data provides further support to the applicability of the EMDD parameter in prediction of hydraulic behaviour.

Figure 6.4 plots the k data for specimens constructed using GS and CRL separately, showing that the hydraulic behaviour of MX80-aggregate mixtures is not discernably affected by the type of aggregate used. This is consistent with the EMDD concept where behaviour is determined by the density of the smectite content and other materials act only as inert filler (where aggregate content is 0 to approximately 60% by mass).

The data presented in Figure 6.4 contains test results from three separate testing series conducted at three different laboratories (AECL Whiteshell laboratories; WSP-Golder Mississauga, WSP-Golder Saskatoon), by different operators and separately manufactured test cells. The consistency of the results obtained is a strong indicator of the quality and reproducibility of these tests.

The most comparable literature data for tests completed using a highly saline porefluid similar to SR-Sh are provided by Rowe and Brachman (2019) who used a brine known as MW (333 g/L TDS). The data from Rowe and Brachman (2019) are not shown in Figure 6.5 or used in development of predictive equations for k-behaviour as they are notably inconsistent with those collected in the current and previous studies. This difference was attributed by Rowe and Brachman (2019) as non-stabilized flow (inflow not equal to outflow) and so not true k values. For these reasons the data from Rowe and Brachman were not used in the development of predictive equations for k.

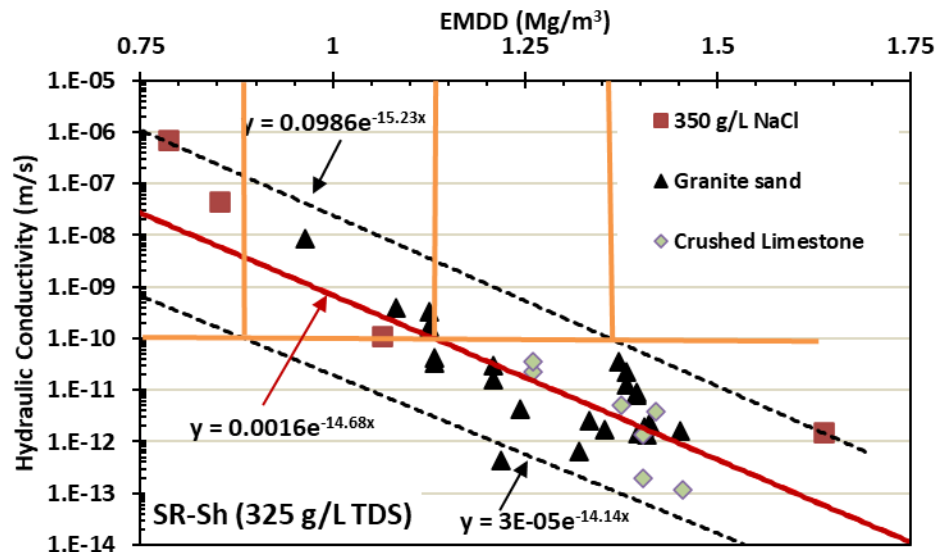


Figure 6.4. Hydraulic conductivity of MX80-based materials: High salinity (SR-Sh and NaCl)

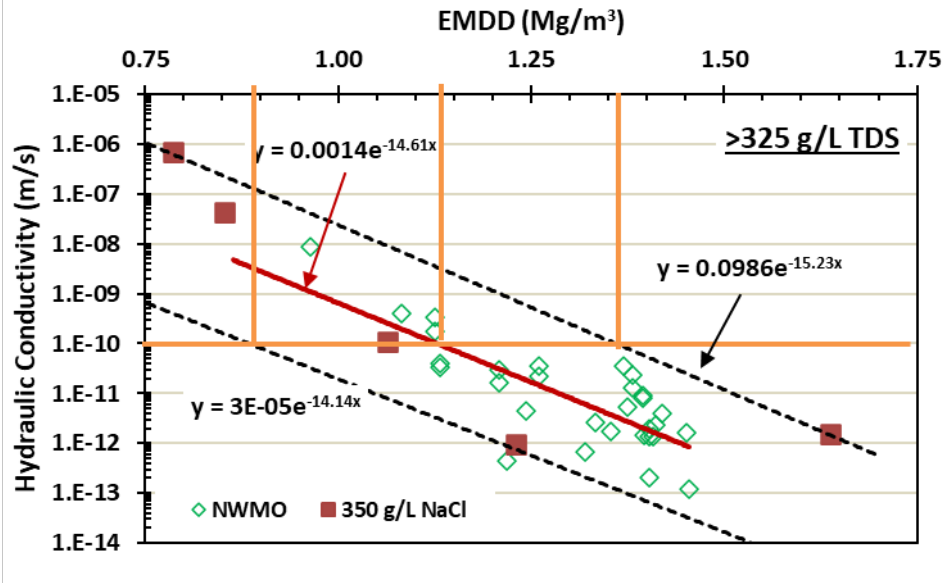


Figure 6.5. Comparison of hydraulic conductivity data for high TDS conditions

Table 6.3. Best-Fit and Prediction Limit Equations for k of MX80-Based Materials

Porefluid	Parameter			
	CR-10*	EMDD for $k < 10^{-10}$ m/s (Mg/m ³)	SR-Sh	EMDD for $k < 10^{-10}$ m/s (Mg/m ³)
Best-Fit	$k = 2E-8 * e^{(-8.708 * EMDD)}$	<0.75	$k = 0.0016 * e^{(-14.68 * EMDD)}$	1.13
Upper Prediction Limit	$k = 7E-8 * e^{(-8.745 * EMDD)}$	0.75	$k = 0.0986 * e^{(-15.23 * EMDD)}$	1.36
Lower Prediction Limit	$k = 4E-9 * e^{(-8.672 * EMDD)}$	<<0.75	$k = 3E-5 * e^{(-14.14 * EMDD)}$	0.88

* Equations are for all 10-15 g/L TDS data with 90% degree of confidence applied

** Equations are for all SR-Sh data (335 g/L)

6.3 Swelling Pressure Measurement

The testing matrix defined for the first phase of swelling pressure testing is provided in Table 6.1 and consists of MX80-aggregate blends tested using the CR-10 (~12 g/L TDS) and SR-Sh (~335 g/L TDS) groundwater formulations described in Section 2.2. The lower-salinity CR-10 solutions were used in testing lower-density specimens prepared to a target of 98% of standard proctor maximum dry density and >90% initial saturation. The higher-salinity SR-Sh solution was used in testing of higher-density specimens prepared to a target of 95% of modified proctor maximum dry density, also at >90% initial degree of fluid saturation.

The design of test cells and flow monitoring gauges used to determine swelling pressure are presented in Figure 6.1. The design of these cells allows for the measurement of both swelling pressure and hydraulic conductivity on the same specimens. In order to determine swelling

pressure, specimens were allowed unlimited access to the simulated groundwater solution (CR-10 or SR-Sh) at the base of the specimen under an initial hydraulic head of 1.5 m (15 kPa) with the top drain left open to allow for air escape during hydration. After several weeks of percolation, the total pressure measured by the loadcell comes to equilibrium, at which time the hydraulic head was increased to 5 m (50 kPa) and inflow and total pressure monitoring was continued. Once the specimen's total pressure (measured at the top of the cell under conditions of 50 kPa hydraulic pressure and top drain open), had stabilized, the drain at the top of the cell is closed and a "pseudo-B-test" was performed. This simulates the conduct of a "B" test done for triaxial compression samples to check for fluid saturation. In some tests further pressure steps to 100 and 200 kPa under no-drainage conditions were completed to provide additional "B-test" data confirmation.

The "B"-test referenced above assumes that pressures measured correspond to those attributable to the effective stress concept. This means that the total pressure measured is the sum of the mechanical (swelling) and the hydraulic pressure present. Knowing the total pressure (measured value) and the applied hydraulic pressure head the swelling pressure can be determined ($P_s = \text{total pressure} - \text{hydraulic pressure}$). Swelling pressure can also be estimated from the tests when their top-drain is open. For these conditions it is assumed that the hydraulic contribution to the total pressure is one-half (1/2) that of the hydraulic pressure at the base. These open-drainage data are not generally used to define swelling pressure excepting where the hydraulic contribution is very low (e.g., 1.5 m or less) where a hydraulic pressure component would not discernibly influence the total pressure determined. These open-drainage P_s values provide a useful additional check on the values determined using the "B" tests. It is also assumed that given the low range of hydraulic heads applied (typically 15-100 kPa) and their relatively high density that there will be no influence of altering hydraulic head on the micro or macro structure of the specimens. The response of the system to changes in pore pressure are also indicators that there is little change in the bentonite or bentonite-aggregate internal structure (i.e., changes to effective stress and hydraulic conductivity measured are nil).

At the end of monitoring, the hydraulic head was typically decreased to zero, the top drain re-opened, and internal pressure was allowed to equilibrate. This was done to provide an end-of-test swelling pressure measurement under a zero hydraulic head condition. As a result of the sequencing of these tests, at the end of each test, there were two or more swelling pressure values generated for each specimen, providing a check on data consistency. In general, the data collected at 15 kPa hydraulic head prior to initial application of 50 kPa hydraulic head were not used to generate swelling pressure values. The data for lower, initial hydraulic head (15 kPa) conditions was observed to have some limitations regarding stress transfer from the specimen to the loadcells where swelling pressures were low and often had experienced insufficient water uptake to ensure that they were fully saturated.

The swelling pressures determined have been plotted in Figure 6.5 and Figure 6.6 as a function of EMDD since this parameter provides a means of eliminating the effects of material type, non-bentonite additions (e.g., aggregate).

The Rowe and Brachman (2019) swelling pressure data plotted in Figures 6.5 and 6.6 are end-of-testing total pressure measurements and are lower than the "peak or maximum" swelling pressures observed by them. Rowe and Brachman (2019) observed an early maximum P_s value in their tests, with a subsequent trend of decreasing P_s with time after that. The apparent decay in P_s can in-part be attributed to the effects of ongoing percolation of their specimens constructed using deionized water with brine solution. The results of such percolation would be a reduction in the repulsive forces that were originally present between the clay platelets as the

surface charges are balanced by introduced cations in the percolating solution and hence an ongoing reduction in the swelling pressure could be expected as porefluid composition changes. The observed peak swelling pressures can therefore be attributed to those resulting from a lower salinity porefluid that is not representative of either a freshwater or the brine. By the end of testing, the porefluid of the specimens tested by Rowe and Brachman (2019) can be assumed to be essentially that of the percolating fluid and hence are comparable to those generated by specimens initially prepared using the same groundwater solutions as are subsequently percolated through them. It would therefore be expected that the equilibrated Ps reported would be comparable.

The current testing series described in this report do not observe any consistent pattern of ongoing change in Ps with time (see plots in Appendix C). Generally, the Ps observed seems to be a near-equilibrium value, or slightly increasing with time. This can be attributed to using the same porefluid to prepare and percolate each specimen, resulting in a shorter time to achieve chemical equilibrium and smaller change in the porewater composition present and hence smaller ongoing changes in observed Ps. Some fluctuation in the observed Ps could be expected as there will be some initial internal strain in the specimens due to localized swelling during saturation. With time, the specimen will come to density equilibrium and swelling pressure would stabilize close to the observed values.

The data collected for specimens tested using CR-10 and SR-Sh fluids in the current study are consistent with those generated previously using these fluids. The CR-10 data trends lower than observed for NaCl-only porefluid. This is to be expected as an Na-only system will exhibit higher repulsive forces between clay platelets (measured as swelling pressure) than one that has Ca present in its porewater. These same cation-mineral interactions will also result in a greater volume of structured water being present in Na-systems and hence a reduced pore volume being available for advective flow (hence lower k in a Na-dominated versus a mixed Na-Ca or Ca porefluid).

Of note when evaluating the swelling pressure developed under freshwater conditions are those data reported by Rowe and Brachman (2019). When compared to a summary compiled from many studies completed by numerous researchers over a 40-year period (see Dixon 2019), the data of Rowe and Brachman (2019) are on the lower end of reported values, as shown in Figure 6.6. This may in-part be a result of the manner in which Ps was determined as many tests do not use a combination of open-drain and closed drain (B-test) conditions at several hydraulic heads to confirm saturation and to where-possible determine Ps repeatedly on the same specimen (with Ps being defined by the effective stress principal ($P_s = \text{Total Pressure} - \text{Hydraulic Pressure}$)) as presented by Dixon et al. (1986) and Graham et al. (1991).

In terms of equilibrated swelling pressure, it has been observed that a substantial seating load can result in a high initial total pressure followed by decay in this value with time after the peak is reached. This is interpreted as being the result of slight densification of the swelling clay closest to the piston during specimen preparation, with its subsequent swelling to a lower density. This behaviour could also be induced by the method used to densify the specimen prior to testing. With hydration, the initially non-homogeneous (with respect to density along the length of the specimen) bentonite will strain slightly, decreasing the density adjacent to the piston as it compresses and densifies materials further away from the ends of the specimen, with a resulting slow “reduction” in the total pressure as the specimen moves towards density equilibrium. This is a possible explanation for the different patterns of swelling pressure development observed and discussed by Dixon et al. (1996; 2019); Lee et al. (2010); Pusch (1980) and subsequently observed by Rowe and Brachman (2019). Such system effects should not result in differences in the equilibrium Ps measured, provided that the tests were left to run

long enough to come to, or approach stress equilibrium. The pattern of total pressure decrease with time observed by Rowe and Brachman (2019) may also be the result in the effects of changing porefluid composition (and perhaps soil microstructure) as the initially-present freshwater is replaced by the percolating brine. In the tests completed in the current study there is little evidence of decreasing total pressure with time provided that the hydraulic pressure component does not change (effective stress concept). In general, the tests completed in this study are not exhibiting any marked trend to decreasing P_s with time (see data presented in Appendix E)

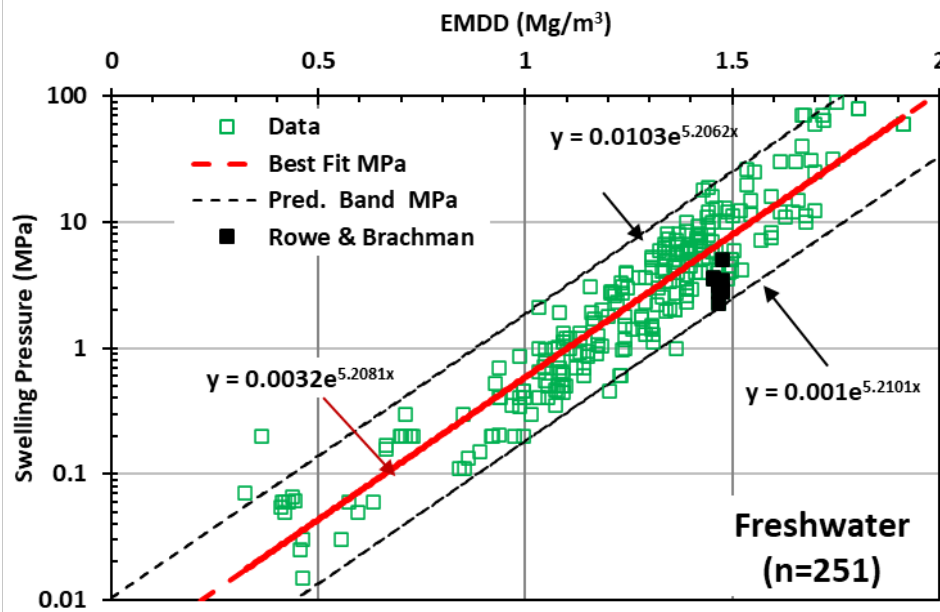


Figure 6.6. Swelling pressure developed by MX80-based materials: freshwater conditions

The P_s results of measuring P_s using CR-10 or 12 g/L NaCl permeant for MX80-GS and MX80-CRL materials are presented in Figure 6.7. The CR-10 data includes tests completed by Priyanto et al. (2013); Barone et al. (2014) and Dixon et al. (2018) as well as the current testing program (see Table 6.2). The data do not show any discernible difference between systems prepared using GS and those prepared using CRL. As with the results for hydraulic conductivity (Section 6.2), these results confirm the validity of the EMDD concept to describe swelling pressure behaviour. In order to achieve a P_s of 0.1 MPa (100 kPa) or greater, systems percolated using CR-10-type groundwater will require an EMDD of > 0.90 Mg/m³ (best-fit) to >1.06 Mg/m³ (Lower Prediction Limit) as shown in Table 6.4.

Figure 6.8 shows swelling pressure developed in the presence of very high TDS groundwater. Of note is the good comparability of the P_s data from Brachman et al. (2021), with tests completed using a porefluid very similar in TDS to the SR-Sh used in this study (where end-of-test swelling pressure is used). This indicates that the swelling pressure behaviour observed by Brachman et al. (2021), (very high initial swelling pressure followed by gradually decrease), is perhaps associated with how those samples were prepared or measurements were made rather than an intrinsic difference in the materials examined or the influence of porefluid composition.

Figure 6.8 also shows how cation composition of the porefluid used will influence the P_s developed. The limited number of tests done using a pure 350 g/L NaCl solution seems to trend towards slightly higher P_s than those for mixed cations (Ca-Na). The offset is slight but is

consistent with literature evidence on the effects of cation composition on behaviour. The data presented shows that minor variations in cation concentration and cation ratios will have a limited effect on Ps behaviour, allowing generic predictive equations to be used in estimating the swelling pressure that will develop for a material or mixture of bentonite and aggregate of known EMDD.

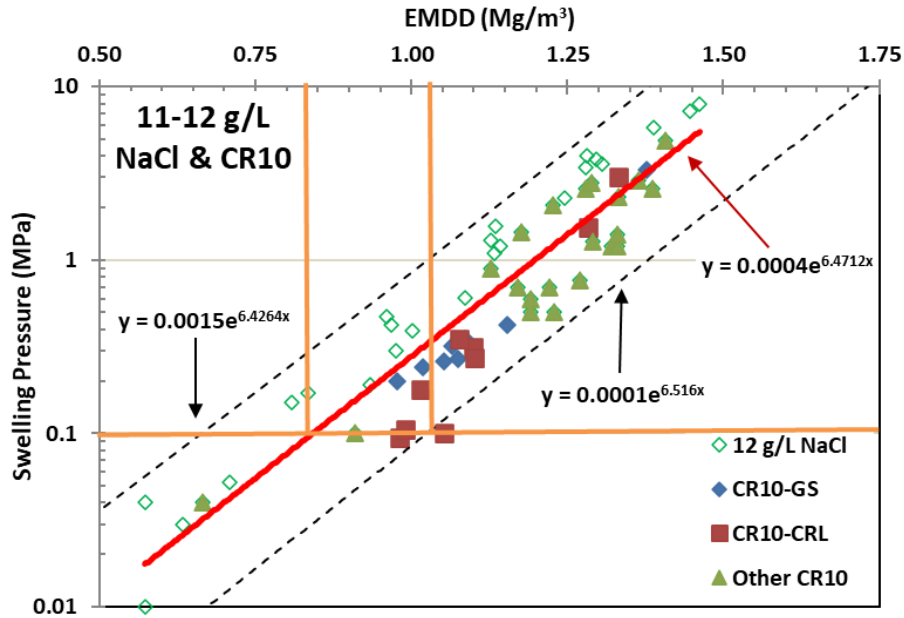


Figure 6.7. Swelling pressures developed by MX80-based materials: 11-12 g/L TDS

Table 6.4. Best-Fit and Prediction Limit Equations for Ps of MX80-Based Materials

Porefluid	CR-10*	EMDD for Ps >0.1 MPa	SR-Sh	EMDD for Ps >0.1 MPa
Best-Fit	$P_s = 0.0004 \cdot e^{6.4712 \cdot EMDD}$	0.90	$P_s = 0.0006 \cdot e^{4.519 \cdot EMDD}$	1.13
Upper Prediction Limit	$P_s = 0.0015 \cdot e^{6.4264 \cdot EMDD}$	0.78	$P_s = 0.0026 \cdot e^{4.5544 \cdot EMDD}$	0.80
Lower Prediction Limit	$P_s = 0.0001 \cdot e^{6.516 \cdot EMDD}$	1.06	$P_s = 0.0002 \cdot e^{4.4109 \cdot EMDD}$	1.38

* Equations are for all 10-15 g/L TDS data with 90% degree of confidence applied

** Equations are for all SR-Sh data (335 g/L)
Ps is calculated as MPa using EMDD in Mg/m³.

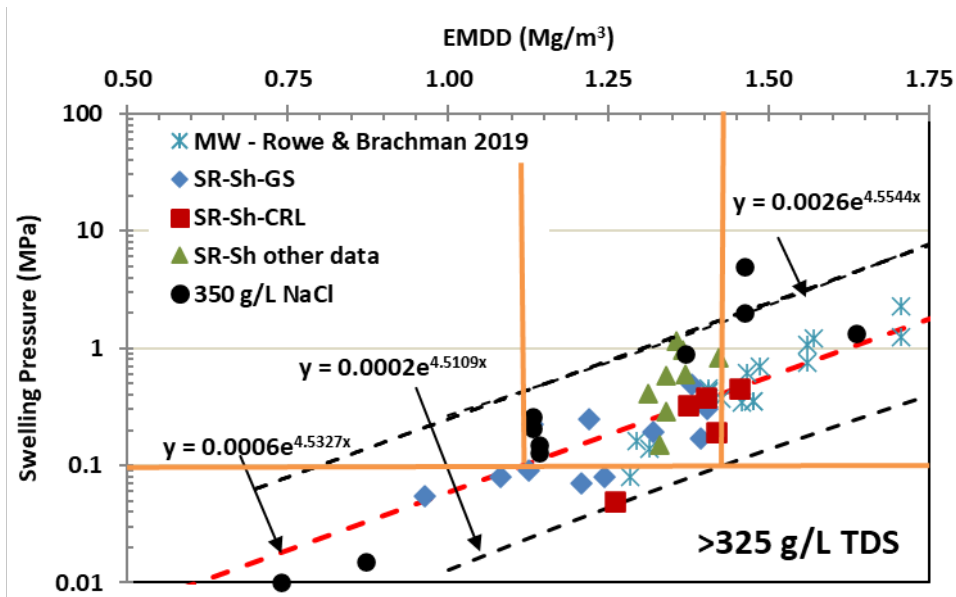


Figure 6.8. Swelling pressures of MX80-based materials: High (>335 g/L TDS) salinity

6.4 Summary of Ps and k Behaviour

A comprehensive set of laboratory tests were completed. These examined the roles of density, porefluid composition (low salinity CR-10 and brine SR-Sh), as well as the mineralogy of the material used as aggregate in the bentonite-sand mixtures.

There was no consistent, discernible effect of aggregate type on the swelling pressured developed by or the hydraulic conductivity of any of the bentonite-sand blends examined in this study. It is noted that in Figure 6.6 that there is a slight tendency of the Ps of the CRL at low density to trend towards slightly lower values than observed by GS mixtures. This is based on a very limited number of data points and so is not conclusively indicative. The overall behaviour of the materials tested is consistent with the assumption that the aggregate component acts as an inert filler and plays no substantial role in determining the Ps and k behaviour. With increase in salinity comes a clear decrease in the Ps developed and k observed. As a result, the EMDD required to achieve the targeted Ps and k values increase.

Table 6.5 compiles the information collected regarding the effects of material composition, compacted density achievable using SCE and MCE methods as well as the porefluid salinity on the Ps and k behaviour of potential shaft backfills. Predicted values that do not achieve the target performance for the backfill are highlighted in orange in Table 6.5. From these data it can be seen that shaft backfill formulations that are compacted to standard compaction effort are unable to meet the performance targets set for it should saline conditions be present or develop (shown in shaded cells). Materials prepared using SCE effort in an environment where only low (<12 g/L TDS), salinity conditions are expected to be evident will only meet performance requirements when there is a substantial (>60%) bentonite content present.

For a shaft backfill that is compacted to densities approaching MCE values, the swelling pressure and hydraulic conductivity behaviour of bentonite-sand materials is such that any formulation between 50 and 80% bentonite can meet the performance specifications under both low- and high-salinity conditions.

Table 6.5. Ability of Bentonite-Sand mixtures compacted using low salinity water to meet Ps and k requirements

Standard Compaction Effort (SCE)								
Mixture (Bentonite-Aggregate)	Max. Dry Density (Mg/m ³)	EMDD (Mg/m ³)	Ps in CR- 10* (kPa)	k in CR-10* (m/s)		Ps in SR- Sh* (kPa)	k in SR-Sh* (m/s)	
@ 98% Standard Compaction Effort (SCE)+								
90-10	1.310	1.095	BF 478 LPL 125	BF 1.4E-12 UPL 5.0E-12	ok	BF 86 LPL 30	BF 1.7E-10 UPL 5.6E-9	k high Ps low
80-20	1.370	1.078	BF 430 LPL 112	BF 1.6E-12 UPL 5.8E-12	ok	BF 79 LPL 26	BF 2.1E-10 UPL 7.3E-9	k high Ps low
70-30	1.463	1.083	BF 442 LPL 116	BF 1.6E-12 UPL 5.5E-12	ok	BF 81 LPL 26	BF 2E-10 UPL 6.8E-9	k high Ps low
60-40	1.500	1.021	BF 296 LPL 77	BF 2.6E-12 UPL 9.5E-12	ok Ps low	BF 61 LPL 20	BF 5E-10 UPL 1.7E-8	k high Ps low
50-50	1.593	0.998	BF 255 LPL 67	BF 3.1E-12 UPL 1.2E-11	k ok Ps low	BF 55 LPL 18	BF 6.9E-10 UPL 2.5E-8	k high Ps low
@ 95% Modified Compaction Effort (MCE)								
90-10	1.539	1.323	BF 2090 LPL 555	BF 2.7E-13 UPL 8.1E-13	ok	BF 241 LPL 78	BF 5.9E-12 UPL 1.8E-10	k low, Ps low
80-20	1.734	1.452	BF 4815 LPL 1285	BF 8.1E-14 UPL 2.4E-13	ok	BF 433 LPL 140	BF 8.9E-13 UPL 2.5E-11	ok
70-30	1.835	1.479	BF 5735 LPL 1530	BF 6.5E-14 UPL 2.3E-13	ok	BF 489 LPL 158	BF 6.0E-13 UPL 1.6E-11	ok
60-40	1.873	1.422	BF 3965 LPL 1057	BF 1.0E-13 UPL 2.9E-13	ok	BF 378 LPL 122	BF 1.4E-12 UPL 3.9E-11	ok
50-50	1.986	1.446	BF 4630 LPL 1235	BF 8.5E-14 UPL 2.3E-13	ok	BF 421 LPL 136	BF 9.7E-13 UPL 2.7E-11	ok

* determined using equations provided in Table 6.3 and Table 6.4.

Note that shaded cells do not meet target values for Ps or k.

+ Average of values obtained for GS and CRL aggregates,

BF-best fit to data; LPL-lower prediction limit for Ps; UPL-upper prediction limit for k.

Lacking data to the contrary, the EMDD values used to determine trendlines and prediction limits are based on an assumed montmorillonite content of 80% by mass in the bentonite clay. The lack of reported montmorillonite contents associated with some literature data induces a degree of uncertainty regarding the subsequently generated trendlines to describe Ps and k.

In order to initially evaluate the magnitude of EMDD change and hence Ps and k change resulting from uncertainty in the montmorillonite content in MX80, the effect of changing montmorillonite content by $\pm 5\%$ from the 80% used in this study (75% to 85%) was assessed.

For illustrative purposes, a 60:40 MX80:aggregate blend compacted to a dry density of 1.8 Mg/m³ was considered and the changes in Ps and k resulting from change in EMDD due to $\pm 5\%$ montmorillonite content were calculated and are shown in Table 6.6. A $\pm 5\%$ change in montmorillonite content for this blend results in an EMDD range of ± 0.045 Mg/m³ ($\pm 3.4\%$) from the value of 1.337 Mg/m³ present at 80% montmorillonite.

- In low TDS CR-10 water, the effect of $\pm 5\%$ montmorillonite content on k is an approximately $\pm 50\%$ range in calculated k.
- In low TDS CR-10 water, the effect of $\pm 5\%$ montmorillonite content on Ps is an approximately $\pm 30\%$ range in calculated Ps.
- In high TDS SR-Sh water, the effect of $\pm 5\%$ montmorillonite content on k is an approximately $\pm 50-90\%$ range in calculated k.
- In high TDS SR-Sh water, the effect of $\pm 5\%$ montmorillonite content on Ps is an approximately $\pm 20\%$ range in calculated Ps.

While an approximately 20-30% uncertainty in the Ps and 50-90% uncertainty in k is certainly notable, it is far lower than the prediction bounds calculated for the large data bases used in this evaluation. The prediction limits for the Ps and k values are in the order of $\pm 300-500\%$ for Ps and ± 1 -order of magnitude in k. Uncertainty in montmorillonite content (e.g., $\pm 5\%$ from target of 80% montmorillonite in bentonite clay) can therefore be considered as a secondary consideration with regards to prediction of Ps and k. Based on this it may be possible to use a $\pm 5\%$ bounding on montmorillonite content as a quality target for acceptance of bentonite but further evaluation should be completed once reference shaft backfill composition is defined (taking into consideration bentonite:aggregate ratio, compacted density, and anticipated groundwater composition).

Table 6.6. Effect of changing montmorillonite content of predicted Ps and k.

60% MX80 : 40% Aggregate Compacted to 1.8 Mg/m³ dry density					
Montmorillonite	EMDD	Ps in CR-10	Ps in SR-Sh	k in CR-10	k in SR-Sh
(%)	(Mg/m ³)	(kPa)	(kPa)	(m/s)	(m/s)
85	1.379	3003 (-31%)	302 (-20%)	1.2 E-13 (-50%)	2.6E-12 (-46%)
80— reference	1.337	2286	252	1.8E-13	4.8E-12
75	1.292	1710 (+25%)	206 (+20%)	2.6E-13 (+44%)	9.3E-12 (+94%)

Notes: k and Ps calculated using best-fit equation in Tables 6.3 and 6.4 respectively

7. SOIL WATER CHARACTERISTICS CURVES AND GAS PERMEABILITY

7.1 Background and Approach to SWCC and GP Testing

The characterization of gas permeability involves several interrelated components:

- Sample preparation;
- Soil-water characteristic curve (SWCC) tests;
- Gas permeability (GP) tests; and
- Derivation of a numerical relationship that describes the relative gas permeability as a function of saturation and as a function of capillary pressure.

The conduct of each of these tests requires highly specialized equipment and testing procedures in order to accommodate the materials and porefluids examined in this study. Each of the specimens used in the SWCC and gas permeability tests were prepared to a pre-calculated density and moisture (or saturation) state. The methods and equipment used are described as part of each component's discussion.

7.2 Soil Water Characteristics Curves (SWCC)

7.2.1 Background, Testing Methods and Experimental Details

The soil-water characteristic curve (SWCC) test measures the relationship between the quantity of water in a soil and the negative pore water pressure, or soil suction that is holding this water in place. The suction tests undertaken as part of this study are necessary for assessing the water retention (resistance to desaturation), water uptake and storage capacity of the bentonite materials. The SWCC is typically presented in terms of degree of liquid saturation versus capillary pressure or saturation versus suction but can also be presented as gravimetric or volumetric water content versus suction. For the purposes of data analysis, it is assumed that the capillary pressure (resistance of soil capillaries to desaturate, or suction) is equal to the air pressure used to induce desaturation in the pressure device and that the relative humidity in the air immediately above the specimens (as per WP4 device reading) is a measure of the total suction in the specimen. The measured SWCC and the specific gravity of the material are then combined to determine the relationship between degree of saturation and suction.

For this testing program, two methods were used to measure the complete SWCC. The first method used a GCTS Fredlund SWCC pressure cell to measure the lower portion of the SWCC, from 100 to 1500 kPa. The second method used a WP4 dewpoint potentiometer to measure the upper portion of the SWCC, from about 20,000 to 300,000 kPa. Data from the two methods can be combined to form the complete SWCC, from a saturated to a desaturated state.

The air entry value is a significant characteristic of an SWCC and represents the capillary pressure (or suction) where air starts to enter the largest pores in a soil and the soil begins to lose water (Fredlund and Xing, 1994). Determination of the air entry value is at the intersection of two straight lines, as shown in Figure 7.1. In this example, the air entry value is about 3,000 kPa.

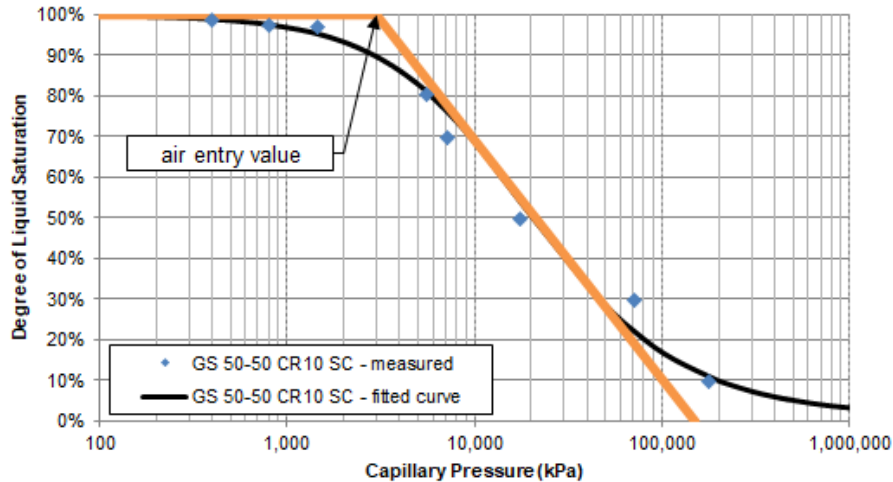


Figure 7.1. Air entry value determination on a typical SWCC

7.2.1.1 GCTS Device

The low suction ranges (100-1500 kPa) were measured using the axis translation method by pressurizing a single soil specimen in a GCTS Fredlund SWCC pressure cell. The cell and associated pressure system were developed by Geotechnical Consulting and Testing Systems (GCTS) and are shown in Figure 7.2, together with an example of the type of specimen tested.



Figure 7.2. GCTS apparatus used to measure the SWCC in low suction range and a typical SWCC specimen

The GCTS apparatus can apply a vertical stress to the specimen and any change in sample height can easily be monitored during testing. It is therefore preferred over traditional pressure cells for the type of materials being tested in this study. For each series of measurements, one saturated 64 mm diameter by 20 mm high specimen for each pore water solution material was compacted directly into stainless steel testing rings. Each specimen was placed on a 15 bar, high air entry ceramic stone for testing in the low suction range. The specimen was then

subjected to a small token load followed by the stepwise application of the appropriate suctions; namely 100, 200, 400, 800 and 1500 kPa. At each of these suctions, fluid was allowed to drain from the specimen. The vertical height of the sample was monitored during the testing.

In low- or non-bentonite soils with a low air-entry value, a significant quantity of fluid usually drains out of the specimen at suctions less than 1500 kPa, and in some cases, the specimen can be nearly dry. In fine-grained clay soils and in particular soils having substantial swelling clay content, the air-entry value is generally significantly greater, and a substantial suction can be required before specimen desaturation begins. The latter behavior was seen in all the materials tested for this program, with no significant drainage observed for suctions less than 1500 kPa.

7.2.1.2 WP4 Dewpoint Potentiometer Device

The high suction range was measured in the WP4 device, shown in Figure 7.3. The WP4 measures suction by determining the relative humidity of the air above the sample in the closed chamber (an AOAC-approved method; also conforms to ASTM D6836). The instrument determines the relative humidity using the chilled mirror method, once the sample comes into equilibrium with the vapour in the sealed chamber. A tiny mirror in the chamber is chilled until dew just starts to form on it. At the dewpoint, the WP4 measures mirror and sample temperature with 0.001°C accuracy. The relative humidity environment can be converted to an equivalent suction value using the Lord Kelvin equation. The WP4 is calibrated using saturated salt solutions to an accuracy of ± 100 kPa. The instrument will maintain good accuracy for suctions as low as 1,000 kPa, but in the current study was used over the range of $\sim 5,000$ to 200,000 kPa.



Figure 7.3. WP4 device used to measure the SWCC in the high-suction range and example of specimen used

7.2.2 SWCC Test Results

The data generated using the GCTS and WP4 devices were combined to generate a plot of saturation versus capillary pressure (actual values are negative pressure (suction) but are expressed as positive values). These data were then fitted using the van Genuchten curve fitting model to generate SWCC curves using fitting parameters provided in Table 7.1. These curves are defined by Equations 7.1 and 7.2:

$$P_c = (1 / \alpha) (S_{ec}^{-1/m} - 1)^{1/n} \quad (7.1)$$

$$S_{ec} = (S_l - S_{lr}) / (1 - S_{lr}) \quad (7.2)$$

where:

- P_c = capillary pressure, Pa;
 S_{ec} = effective saturation (volume ratio);
 S_l = liquid saturation (volume ratio);
 S_{lr} = residual liquid saturation (volume ratio);
 α = van Genuchten fitting parameter (1/Pa);
 m = van Genuchten fitting parameter (unitless); and
 n = van Genuchten fitting parameter (unitless).

It should be noted that since we are dealing with suctions rather than pressures, the equation above generates values that are negative.

SWCCs were measured for 50:50 MX80:GS with CR-10 at 98% of maximum density achieved using standard compaction (SC) and at 95% of maximum density achieved using modified compaction (MC). Curves were also measured for MX80:CRL with SR-Sh at 95% modified compaction at a bentonite:sand ratio of 50:50 and at 60:40. It should be noted that the materials selected for testing were defined based on the anticipated groundwater compositions in granitic rock (CR-10) and a sedimentary (limestone) where highly saline (SR-Sh) conditions could be expected to exist. Hence the two low salinity materials were prepared using GS as the sand component and one compacted to 98% SC and the other to 95% MC maximum dry density. The high-salinity materials were prepared using CRL and compacted to 95% of MC maximum dry density. These densities reflect the densification necessary to achieve the swelling pressure and hydraulic conductivity behaviour required of the DBF.

Table 7.1. Fitting parameters used to generate SWCC's

Material	m	n	a	S _{lr}
			(1/Pa)	
Granitic Sand 50-50 CR-10 SC	0.77	1.19	6.88E-08	0.01
Granitic Sand 50-50 CR-10 MC	1.21	1.34	1.89E-08	0.01
Crushed Limestone 50-50 SR-Sh MC	1.47	2.51	1.06E-08	0.01
Crushed Limestone 60-40 SR-Sh MC	1.15	2.58	1.32E-08	0.01

Details regarding the specimens prepared and the results of the SWCC analyses are provided in Table 7.2. A summary of the data and brief discussion of the meaning of the results are provided in Sections 7.2.2.1 and 7.2.2.2. with the full set of data collected as part of SWCC testing provided in Appendix F.

Table 7.2. Materials examined in current study and air entry values previously obtained

Specimen Name	Degree of Compaction	Sand (%)	Fluid	Dry Density (Mg/m³)	EMDD (Mg/m³)	Air Entry Value (kPa)	Saturation at Air Entry (%)
Current Study							
GS 50-50 CR-10 SC	98% SC	50 GS	CR-10	1.58	0.985	3,000	90
GS 50-50 CR-10 MC	95% MC	50 GS	CR-10	1.85	1.275	9,000	90
CRL 50-50 SR-Sh MC	95% MC	50 CRL	SR-Sh	1.85	1.275	34,000	90
CRL 60-40 SR-Sh MC	95% MC	40 CRL	SR-Sh	1.79	1.326	29,000	90
Previous Studies							
SA40 NWMO TR-2014-12		30 GS	DW	1.51	1.170	3,000	95
SA440 NWMO TR-2018-20		MX80	DW	1.5	1.396	6,000	90
SA440 NWMO TR-2018-20		MX80	SR-L	1.5	1.396	21,000	95
SA440 NWMO TR-2018-20		MX80	SR-Sh	1.5	1.396	25,000	95
SA440 NWMO TR-2018-20		30 GS	DW	1.8	1.481	15,000	95
SA440 NWMO TR-2018-20		30 GS	CR-10	1.8	1.481	15,000	95
SA440 NWMO TR-2018-20		30 GS	SR-L	1.8	1.481	20,000	95
SA440 NWMO TR-2018-20		30 GS	SR-Sh	1.8	1.481	25,000	95
SA40 NWMO TR-2014-12		30 GS	CR-10	1.55	1.211	4,000	96
SA40 NWMO TR-2014-12		30 GS	SR160	1.63	1.294	4,000	95
SA40 NWMO TR-2014-12		30 GS	SR270	1.66	1.326	10,000	95

7.2.2.1 MX80 Granitic Sand 50:50 with CR-10

SWCC tests were conducted on MX80:GS 50:50 with CR-10 at two different densities. The first test was conducted on material compacted to 1.58 Mg/m^3 (dry density), or 98% of standard Proctor. The suction-moisture curves obtained are shown in Figure 7.4 and indicate the air entry value was at about 3,000 kPa and that insignificant desaturation occurred below this suction.

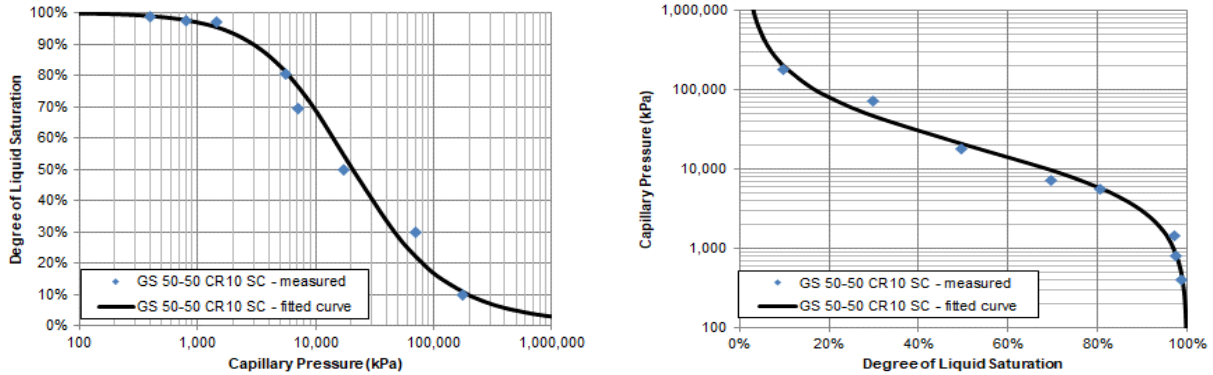


Figure 7.4. SWCC curves for MX80:Granitic Sand 50:50 with CR-10, Standard Compaction (1.58 Mg/m^3 dry density)

The second test on MX80-GS was conducted on material compacted to 1.85 Mg/m^3 (dry density), or 95% of modified Proctor. These results are shown in Figure 7.5 and indicate an air entry value at about 9,000 kPa. This higher air entry value as compared to the standard effort SWCC test would be expected as the sample had a higher density and therefore smaller pore spaces.

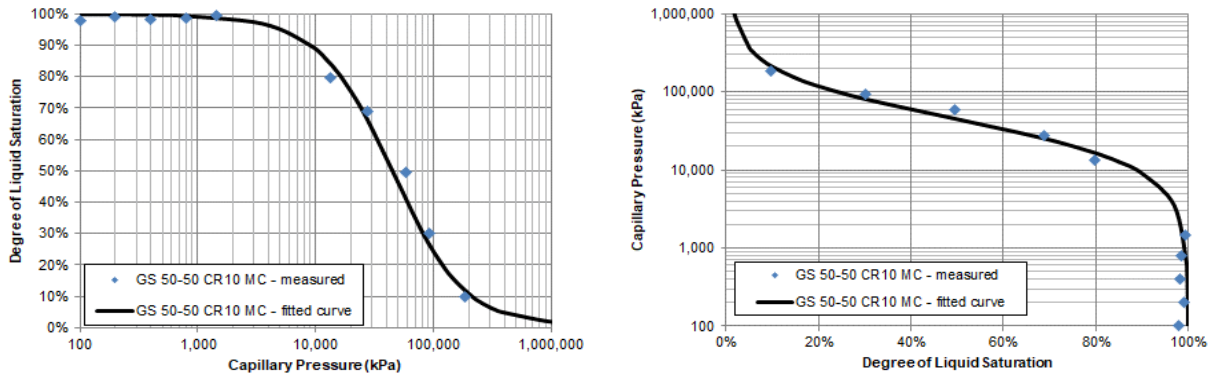


Figure 7.5. SWCC curves for MX80:Granitic Sand 50:50 with CR-10, Modified Compaction (1.85 Mg/m^3 dry density)

7.2.2.2 MX80 Crushed Limestone with SR-Sh

SWCC tests were conducted on blends of MX80 and crushed limestone with SR-Sh fluid and compacted to 95% modified Proctor. The first test was on a sample prepared at 50:50 MX80:CRL and compacted to 1.85 Mg/m^3 (dry density), and the results are shown in Figure 7.6. As can be observed, the air entry value is at about 34,000 kPa.

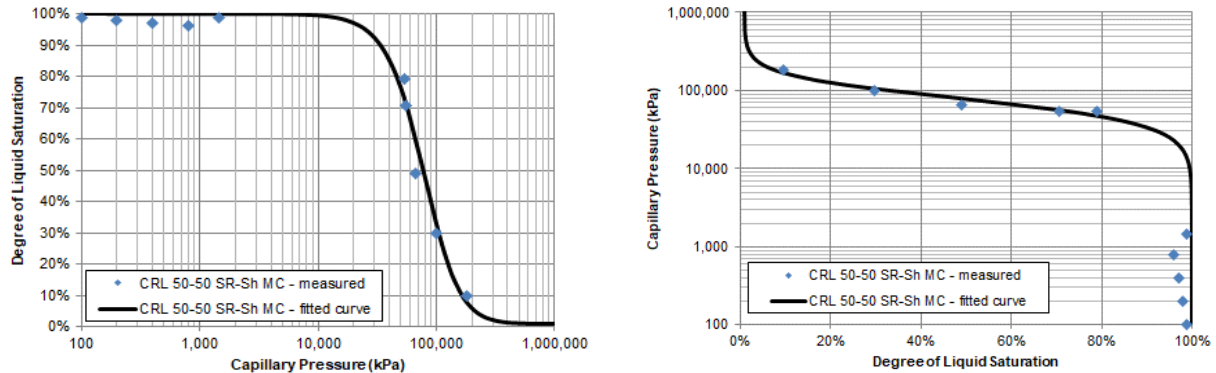


Figure 7.6. SWCC curves for MX80:Crushed Limestone 50:50 with SR-Sh, Modified Compaction (1.85 Mg/m^3 dry density)

The second test using CRL was conducted on a sample prepared at 60:40 MX80:CRL and compacted to 1.79 Mg/m^3 (dry density) and the results are shown in Figure 7.7. Similar to the 50:50 blend, the 60:40 blend has a relatively high air entry value, at about 29,000 kPa.

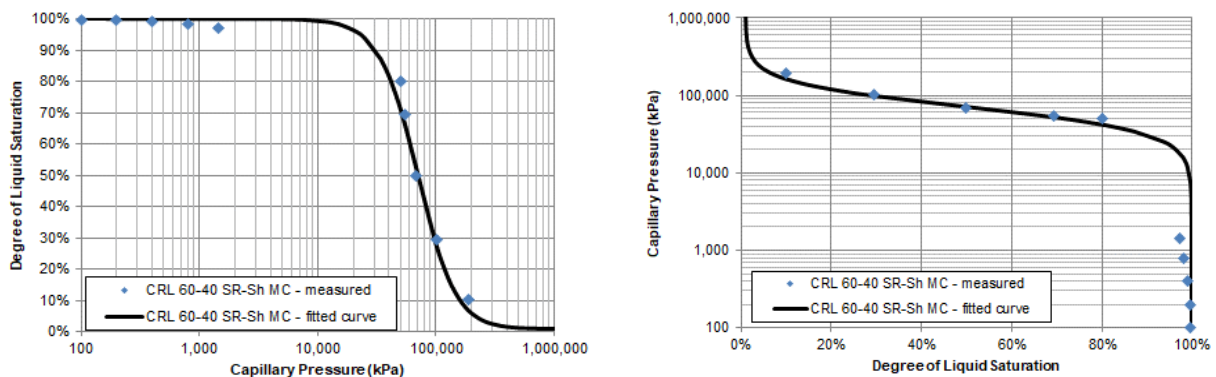


Figure 7.7. SWCC curves for MX80:Crushed Limestone 60:40 with SR-Sh, Modified Compaction (1.79 Mg/m^3 dry density)

7.2.3 Summary of SWCC Results

The data generated in the course of this testing have all be fitted using the van Genuchten curve fitting function provided as Equations 7.2 and 7.3. The fitting functions are forced to the 100% saturation line for the range of capillary pressures where no desaturation was observed (typically saturation $>90\%$ and capillary pressure below $\sim 1500 \text{ kPa}$). The data plots clearly showed that the specimens were not able to lose moisture at low pressure and liquid saturation levels above that level. This behavior can be observed in each of Figures 7.4 through 7.7. A summary of the SWCC's for the materials tested is shown in Figures 7.8 and 7.9 and show that there is a wide variation in the suction-moisture behavior. These figures show the same data but reverse the x and y axes. This was done to provide the data in both of the formats encountered in literature. The results of the two tests conducted with CRL are nearly identical,

plotting immediately adjacent to each other, suggesting that this variation in bentonite content is not significant in the moisture retention characteristics. The granitic sand material compacted with standard effort has the lowest air entry value, which can likely be attributed to the lower density.

All the tests indicate that to accomplish water removal (air-entry) such that saturation is less than 90% requires increasingly higher pressure (suction) to be applied to the porefluid. The pressure required to achieve <90% saturation (air-entry) appears to be influenced by both the density of the specimen and also the salinity of the porefluid. An increase in bentonite content from 50:50 to 60:40 did not appear to significantly change the SWCC.

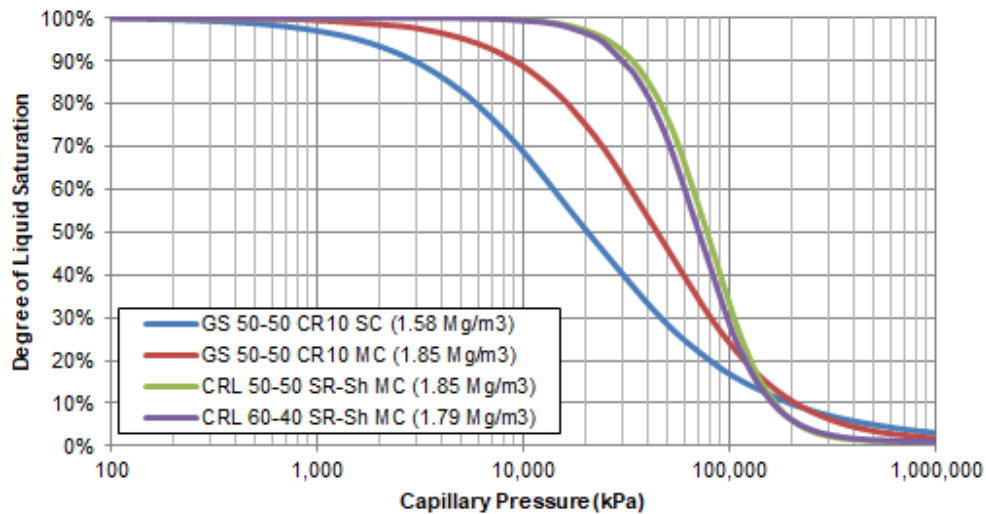


Figure 7.8. Comparison of SWCC tests – degree of liquid saturation vs capillary pressure

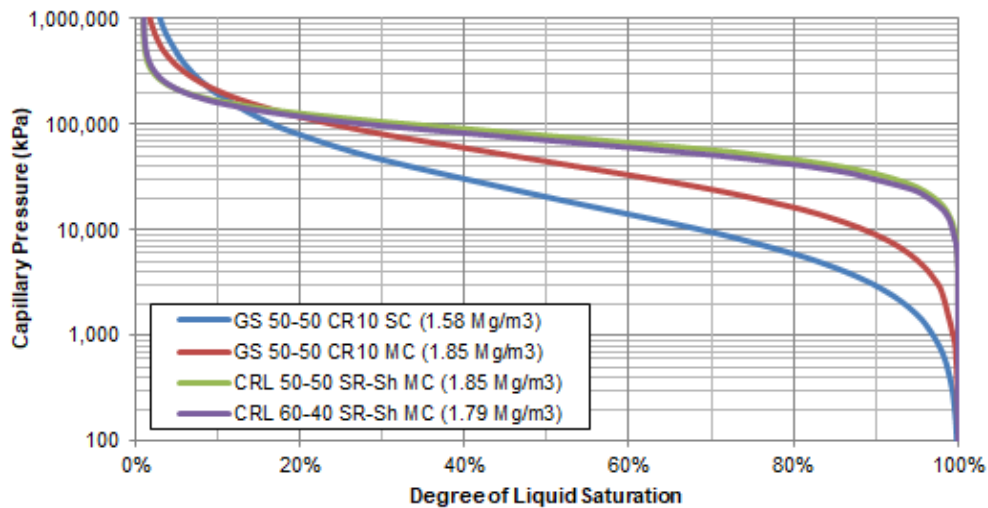


Figure 7.9. Comparison SWCC tests – capillary pressure vs degree of liquid saturation

7.3 Gas Permeability Measurements

7.3.1 Background, Testing Methods and Experimental Details

Gas permeability, K (GP used for K in text discussions in order to make clearly differentiate between gas and water permeability as both have their values presented in m^2) were made on unsaturated specimens of the reference clay using the specified porefluids. Testing was done using the setup shown in Figure 7.10 and used methane as the permeant. It should be noted that the convention for expressing gas permeability uses K (in m^2) while gas conductivity (expressed as GC in this report) uses the symbol k (expressed in m/s).



Figure 7.10. Gas permeability equipment showing triaxial cell and methane test apparatus

In Figure 7.10, the left photo shows a sample installed in the triaxial cell, with the methane tank, gas-water bladders and differential pressure transducer. The right photo shows the pressure volume controllers, computer monitor displaying pressure differential and the reservoir used for applying the cell pressure. Equipment containing methane was kept in a fume hood during testing, while all other equipment was set up outside the fume hood.

Specimens prepared to pre-defined degrees of saturation and dry density were installed in triaxial hydraulic conductivity cells and confined through application of a water pressure on its perimeter. The use of specimens of this type provided a means of accurately knowing the degree of saturation and also provided a material of more uniform degree of saturation than could be accomplished through either saturation or desaturation via the specimen ends. This technique also allowed for a more conventional confining pressure to be used on the perimeter of the specimen. Any other technique would require cell pressures capable of restraining the swelling pressure of the specimen, a technically difficult and extremely time intensive process, and would result in heterogeneous specimen density and saturation conditions. Once the pre-built specimens were installed and confined at 250 kPa using the external cell pressure, the specimen was exposed to a differential gas pressure from the specimen top to the specimen bottom and the rate of gas movement into the specimen was monitored. Through measurement of gas inflow into the specimen it is possible to calculate the gas permeability, providing a single point in the permeability-saturation curve for the material and porefluid being examined. To develop a representative curve for use in defining the saturation-permeability relationship, a minimum of five measurements at substantially different degrees of liquid saturation (10-80%) were completed.

7.3.2 Gas Permeability Test Results

The tests completed provide gas permeability values at a degree of liquid saturation from 10% to 80%, corresponding to approximately residual degree of saturation up to optimum water content conditions. The data were then fitted to a two-phase flow characterisation curve using the van Genuchten (1980) – type relationship to provide values extending beyond the range of saturation examined. Gas conductivity, expressed in m/s was also determined from these tests. Gas conductivity is derived by simple multiplication of the gas permeability value by $5.9 \text{ E}+05$ and is based on the relationship between gas conductivity (k) and coefficient of gas permeability (K), where $k = (K * \text{fluid density} * \text{gravity}) / \text{fluid viscosity}$.

In the tests completed in this study, each specimen was tested at a confining pressure of 250 kPa in order to ensure that no volume change occurred during testing. The 250 kPa confining pressure applied will have provided a seal at the outer perimeter of the specimen and should not affect the movement of gas through the specimens. As none of the specimens were water saturated and no water was added in the course of testing (each degree of saturation shown involved a unique sample that was not allowed access to any water), each specimen will have been volumetrically-stable during testing. In a repository environment it is likely that degree of saturation will vary with location, which would complicate gas movement.

The fitted gas permeability curves have been generated using the van Genuchten-Mualem-Luckner model and the best-fit parameter values used in the calculations are provided in Table 7.3, with detailed results contained in Appendix F. These curves can be given by:

$$K_{rg} = (1 - S_{ek})^{1/3} (1 - S_{ek}^{1/m})^{2m} \quad (7.3)$$

$$S_{ek} = (S_l - S_{lr}) / (1 - S_{lr} - S_{gr}) \quad (7.4)$$

where:

- K_{rg} = gas phase relative permeability (ratio);
- K_g = gas phase permeability (m^2);
- S_{ek} = effective saturation (volume ratio);
- S_l = liquid saturation (volume ratio);
- S_{lr} = residual liquid saturation (volume ratio);
- S_{gr} = residual gas saturation (volume ratio); and
- m = van Genuchten fitting parameter (unitless).

Table 7.3. Specimen density and fitting parameters used to generate GP curves

Material	Dry Density	EMDD	m	S_{gr}	K_g	S_{lr}
	(Mg/m^3)	(Mg/m^3)			(m/s)	
Granitic Sand 50-50 CR-10 SC	1.58	0.985	0.77	0.12	1.53E-06	0.01
Granitic Sand 50-50 CR-10 MC	1.85	1.275	1.21	0.04	3.47E-07	0.01
Crushed Limestone 50-50 SR-Sh MC	1.85	1.275	1.47	0.05	4.46E-07	0.01
Crushed Limestone 60-40 SR-Sh MC	1.79	1.326	1.15	0.13	5.69E-07	0.01

The gas permeability can be calculated by multiplication with the relative permeability (K_{rg}):

$$K_g = K_{rg} * K \quad (7.5)$$

7.3.2.1 MX80 Granitic sand 50:50 with CR-10

Gas permeability tests were conducted on MX80:GS 50:50 with CR-10 at two different densities. The first test was conducted on material compacted to 1.58 Mg/m^3 (dry density), or 98% of standard Proctor. The results of this testing are shown in Figure 7.11. As can be observed, the gas permeability significantly decreased at a degree of liquid saturation above approximately 75%-80%, as the gas-filled pores began to become discontinuous and gas movement through the soil became more and more restricted as saturation increased. This is consistent with the behaviour observed for bentonite material studies reported by Dixon et al. (2018). As noted previously, the specimens were each prepared to specified degrees of saturation and not allowed access to water, as a result there will have been no swelling of the specimens and the 250 kPa confining pressure will have had no influence on gas movement through the specimens.

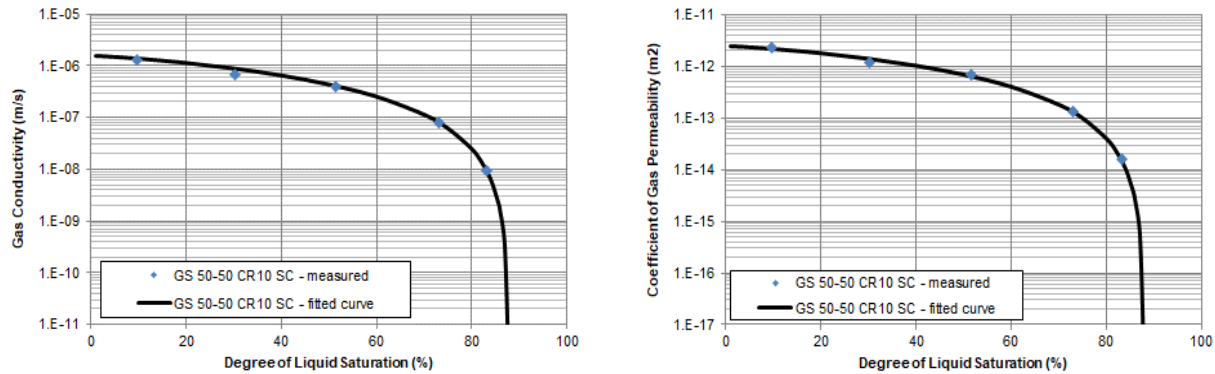


Figure 7.11. Gas conductivity and permeability curves for granitic sand 50:50 with CR-10 compacted to standard compaction (1.58 Mg/m^3 dry density)

The second test on MX80-GS was conducted on material compacted to 1.85 Mg/m^3 (dry density), or 95% of modified Proctor. These results are shown in Figure 7.12. As can be observed, the gas conductivity and permeability begins to decrease rapidly once the degree of liquid saturation increases to more than approximately 80%; this is consistent with the other tests completed.

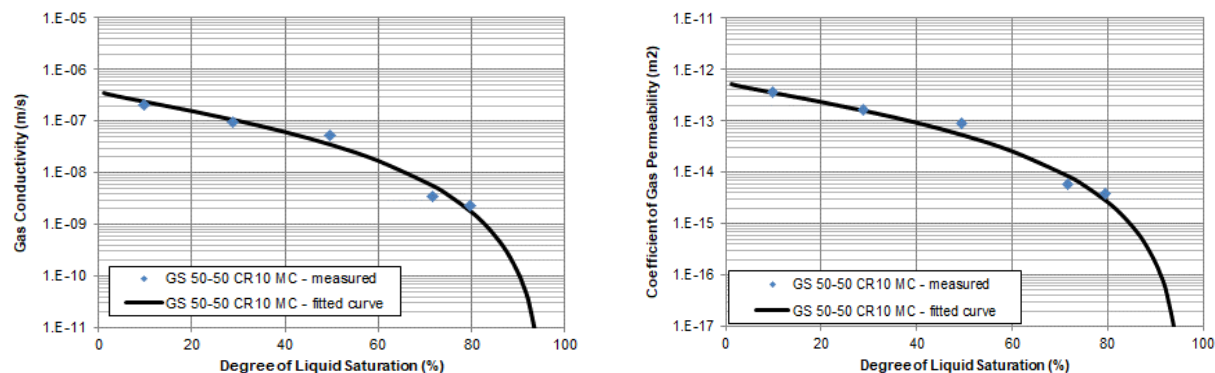


Figure 7.12. Gas conductivity and permeability curves for granitic sand 50:50 with CR-10 compacted to modified compaction (1.85 Mg/m^3 dry density)

Figures 7.11 and 7.12 show that the gas conductivity of the 50:50 bentonite:sand material compacted to a dry density of 1.85 Mg/m^3 (i.e., 95% of Modified compaction) is about half to one

order of magnitude lower than that for the same material compacted to 1.58 Mg/m³ (i.e., 98% of standard compaction), for a given degree of liquid saturation (where saturation is less than about 85%). The fitted curves above about 85% saturation are considered to be less accurate with respect to gas conductivity, as there is no test data to use to fit the curves. Measuring gas flow at high degree of fluid saturation is not reliably accomplished due to the voids being mostly filled by fluid, providing no contiguous pathways for gas flow.

The increase in compacted dry density of a 50:50 bentonite:granite aggregate mixture prepared with CR-10 solution from 1.58 Mg/m³ to 1.85 Mg/m³ results in a substantial decrease in the gas conductivity and permeability until >90% saturation is achieved, as shown in Figures 7.11 and 7.12 and in Table 7.4.

Table 7.4. Density and saturation effects on gas permeability

Material	Dry Density	EMDD	S=50	S=60	S=70	S=80	S=85*	S=90*
	(Mg/m ³)	(Mg/m ³)	(m/s)	(m/s)	(m/s)	(m/s)	(m/s)	(m/s)
Granitic Sand 50-50 CR-10 SC	1.58	0.985	4E-7	2E-7	1E-7	2.5E-8	<1E-9	<1E-11
Granitic Sand 50-50 CR-10 MC	1.85	1.275	4E-8	2E-8	6E-9	2E-9	4E-10	1E-10
Crushed Limestone 50-50 SR-Sh MC	1.85	1.275	1.5E-8	6E-9	2E-9	3E-10	1E-10	<1E-11
Crushed Limestone 60-40 SR-Sh MC	1.79	1.326	4E-8	2E-8	5E-9	6E-10	<1E-11	<1E-11

S=fluid saturation (%)

* As noted previously, data at saturation > approximately 85% is based on extrapolation and values should be considered as qualitative rather than quantitative.

7.3.2.2 MX80 Crushed Limestone with SR-Sh

Gas permeability tests were conducted on two different blends of MX80 and crushed limestone. Both blends used SR-Sh fluid and were compacted to 95% of modified Proctor. The first test was conducted on material prepared at 50:50 MX80:CRL and compacted to 1.85 Mg/m³ (dry density) (EMDD=1.275 Mg/m³), the same as for one of the tests done using granitic aggregate. The results are shown in Figure 7.13 with data provided in Table 7.4.

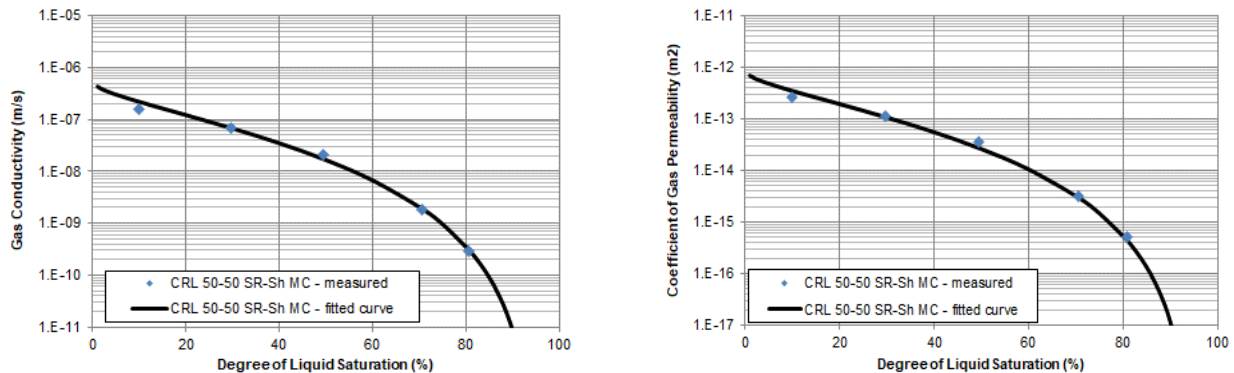


Figure 7.13. Gas conductivity and permeability curves for crushed limestone 50-50 with SR-Sh at modified compaction (1.85 Mg/m³ dry density)

The second test done using CRL as the aggregate component was conducted on a sample prepared at 60:40 MX80:CRL and compacted to 1.79 Mg/m^3 (EMDD 1.326 Mg/m^3) using SR-Sh solution and the results are shown in Figure 7.14. As can be observed, the gas conductivity of this test appears to be very similar to that observed for the 50:50 mixes prepared using GS or CRL using 95% modified compaction density. The similarity can be attributed to their nearly identical EMDDs (difference of $\sim 0.05 \text{ Mg/m}^3$), as compared to an EMDD difference of approximately 0.29 Mg/m^3 for the specimen prepared to 1.58 Mg/m^3 dry density.

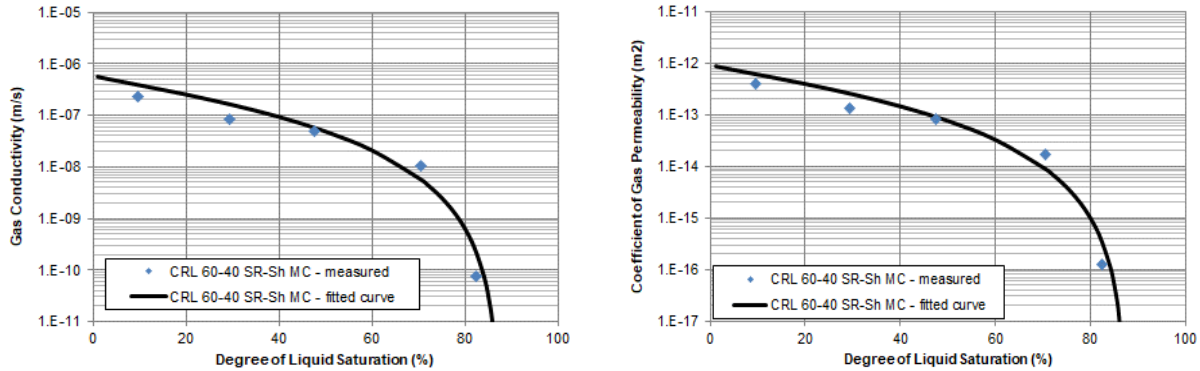


Figure 7.14. Gas conductivity and permeability curves for crushed limestone 60-40 with SR-Sh at modified compaction (1.79 Mg/m^3 dry density)

The results of testing to determine the gas conductivity and permeability behaviour of MX80:CRL aggregate materials prepared to 95% of maximum modified compaction density are summarized in Table 7.4 and show a good comparability to the results obtained for the same bentonite-aggregate ratio where granitic sand is used as the aggregate component and CR-10 used as the porefluid. This would seem to indicate that the porefluid composition has limited or perhaps no effect on gas movement, particularly when degree of fluid saturation is high. A larger body of data that includes evaluation of these variables is required in order to determine the role of porefluid composition.

7.3.2.3 Summary of Gas Conductivity and Permeability Testing

The gas conductivity and permeability curves for the materials tested are shown in Figures 7.15 and 7.16 respectively. They show the expected pattern of decreasing gas conductivity and permeability with increasing degree of liquid saturation and a trend towards rapidly decreasing values as the liquid saturation increases beyond approximately 80%. This is consistent with the expected change from interconnected voids to isolated pockets above this fluid saturation level. Below a degree of liquid saturation of 85%, the gas conductivity for all materials was less than $4 \times 10^{-9} \text{ m/s}$. The three densest specimens had an average gas conductivity of approximately $3 \times 10^{-10} \text{ m/s}$ at 85% fluid saturation, and fluid composition may have had an influence on gas conductivity. The corresponding average gas permeability for the three most dense specimens at 85% fluid saturation was approximately $4 \times 10^{-16} \text{ m}^2$.

As can be observed in Figures 7.15 and 7.16, the material compacted to a dry density of 1.58 Mg/m^3 (i.e., 50:50 MX80:Granitic Sand at 98% Standard Compaction) had the highest gas conductivity and permeability of the four materials examined (where degree of saturation was less than about 85%). The gas permeability for the low density material was approximately one order of magnitude higher over most of the range of liquid saturation (Table 7.4).

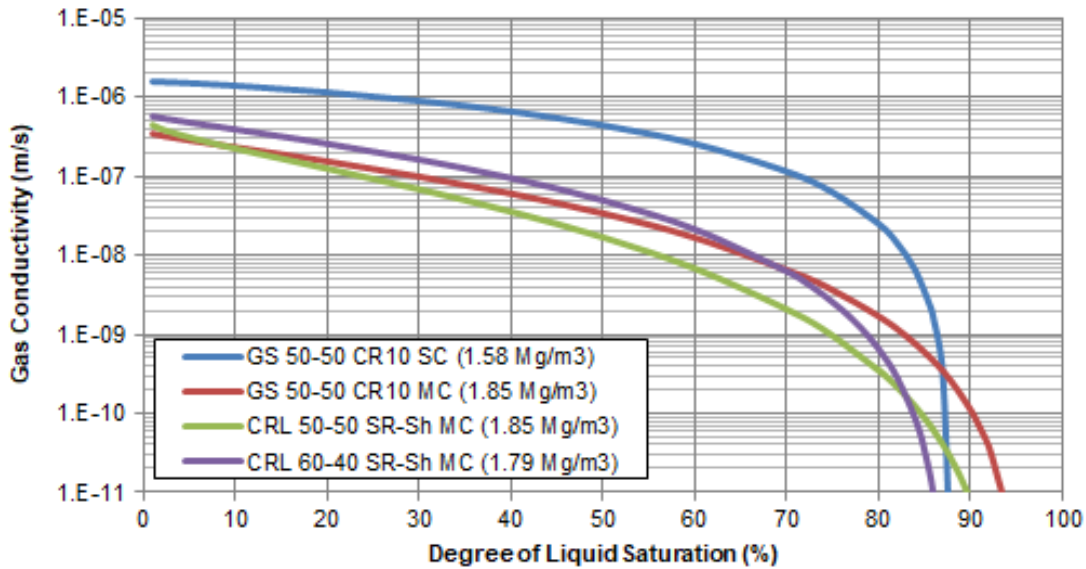


Figure 7.15. Summary of Gas Conductivity testing – Gas Conductivity versus Degree of Liquid Saturation

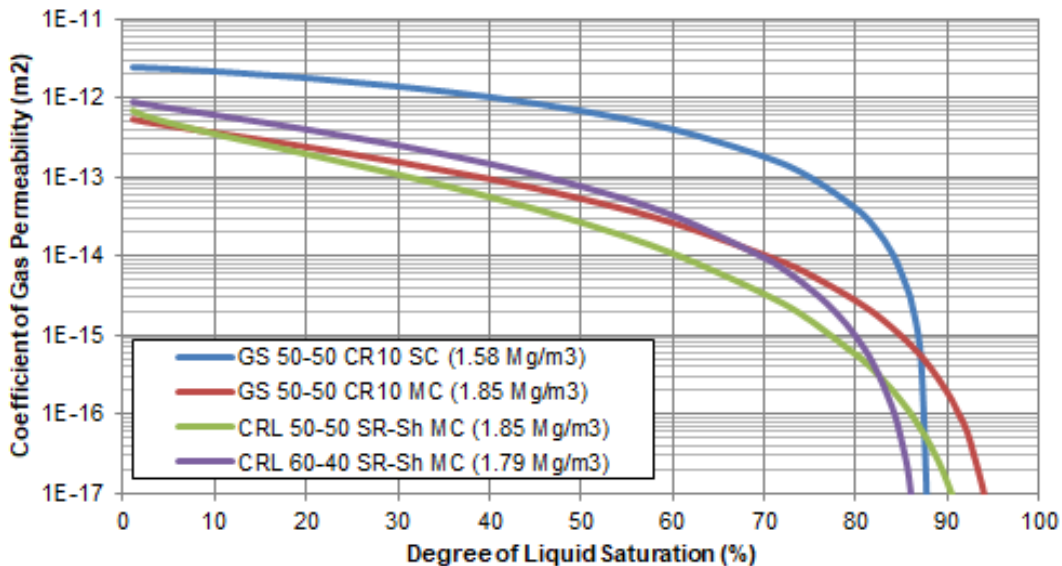


Figure 7.16. Summary of Gas Permeability Testing-- Coefficient of Gas Permeability versus Degree of Liquid Saturation

The differences observed in the plots of gas conductivity and permeability where saturation is greater than 85% are likely the result of the fitting formulations used to generate the curves, as they extend to a saturation range for which no data exists.

The three tests compacted using modified compaction had lower gas permeability values than was observed for the test compacted using standard compaction and were similar to each other (within about a half order of magnitude range for a given degree of fluid saturation), up until a degree of liquid saturation of approximately 80%, beyond which no measurements were available and k_g values were estimated using numerical extrapolation.

The two tests consisting of bentonite:crushed limestone, compacted using modified effort, exhibit a sharp decrease in gas permeability once a degree of liquid saturation of approximately 70% was exceeded. This suggests that continuous pathway(s) for gas flow are not available until degree of fluid saturation falls below 70-80%. The results for these two tests also show an approximate doubling of k_g when bentonite content was increased from 50% to 60%. The 60% bentonite specimen actually had a slightly higher EMDD than the 50% specimen making explanation of the observed behaviour problematic without more data for comparison.

7.4 SWCC and Gas Conductivity Results Interpretation

The results of the gas permeability tests can be combined with those of the SWCC tests to calculate gas conductivity versus capillary pressure functions, and these are shown in Figure 7.17 below. Detailed data is provided in Appendix F.

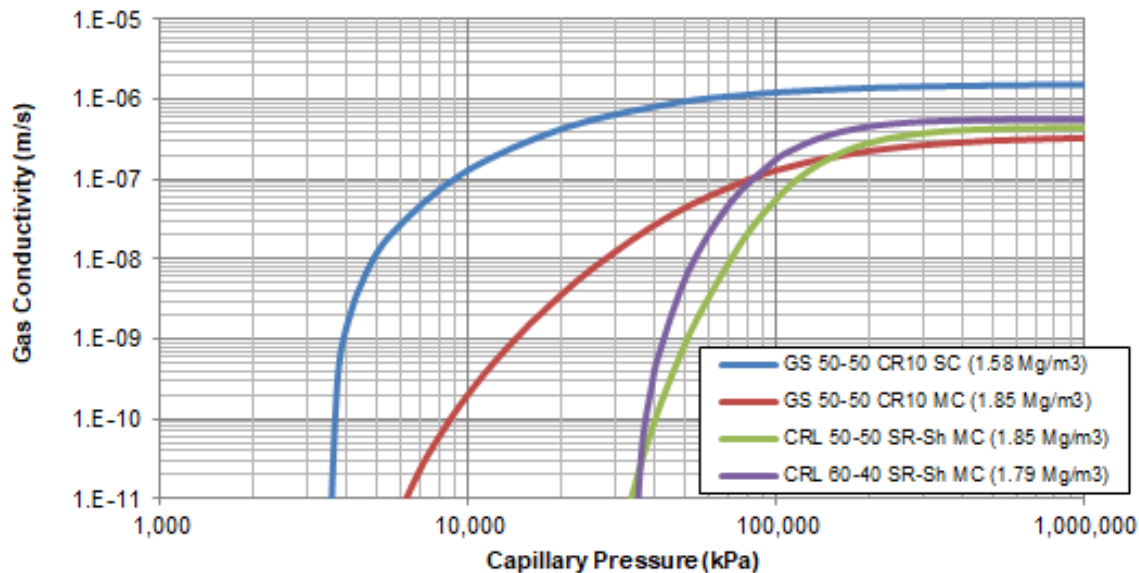


Figure 7.17. Coefficient of gas permeability – Gas conductivity versus capillary pressure

The SWCC and gas (methane) permeability tests completed in this study indicate:

- Moisture retention and gas permeability is significantly affected by density (as shown in Figures 7.8 and 7.9 and 7.15 to 7.17). The GS 50:50 CR-10 specimen compacted to standard compaction (1.58 Mg/m^3 dry density) had the lowest air entry value and highest gas permeability measured.
- At low saturation (less than about 20%), where the suction is greater than about 200,000 kPa, the gas conductivity of the blend prepared to a dry density of 1.58 Mg/m^3 was approximately an order of magnitude greater than the same blend compacted with modified effort (1.85 Mg/m^3 dry density). This difference was maintained for all saturation levels up to approximately 80%.
- The gas permeability of the three blends compacted with modified effort were similar (2 to $6 \times 10^{-7} \text{ m/s}$) at residual saturation levels (i.e., at suctions greater than 200,000 kPa), indicative of open pathway(s) for gas flow.

- As degree of fluid saturation increased, the gas conductivity for each blend decreased until saturation greater than 85% was reached, beyond which k_g was too low to reliably measure. This would indicate that no open pathways were available for gas flow through these materials at high saturation.
- A change in bentonite content from 50% to 60%, blended with crushed limestone, compacted using modified effort and in a high salinity environment had only a small affect if any, on the SWCC.
- The gas permeability results indicate an approximate doubling of the apparent k_g at any particular degree of fluid saturation less than 80%, as a result of an increase in bentonite from 50 to 60%. The reason for the apparent change in k_g is unknown.

There would be value in undertaking further assessments (lab and literature review) of the SWCC and in particular the gas permeability properties of potential shaft backfill materials. This would allow a better understanding to be developed with regards to the movement of gas (or air) from the placement rooms and subsequently through the tunnel and shaft backfill components. Comparison of the newly generated gas permeability data to air-permeability tests results previously completed and reported in the literature should be attempted to help determine if there are any intrinsic differences in behaviour of air and methane.

8. SUMMARY

A study to investigate several key behavioural properties of bentonite-sand blends has been completed. This work has focussed primarily on materials being considered as candidate shaft backfill and has examined the behaviour of two aggregate materials (granite sand and crushed limestone) in groundwaters relevant to a repository built in a granitic host rock (granite sand aggregate and CR-10 groundwater) or a sedimentary host rock (crushed limestone aggregate and SR-Sh groundwater).

This study provides information regarding the likely performance of a range of bentonite-aggregate mixtures, highlighting the importance of knowing the bentonite quality (montmorillonite content) and the groundwater environment that will be present over the longer-term.

Key findings of this study are summarized as follows.

- MX80 was apparently unaffected mineralogically by exposure for a period of approximately 7 years to CR-10 or SR-Sh at high liquid to solid ratio. Despite high k levels there was no evidence of mineralogical change of montmorillonite to illite. This is consistent with literature-reported predictions for long-term stability of smectite (Karnland and Birgersson 2006; Zheng et al. 2017).
- Soaking of MX80 at a high liquid to solids ratio in artificial groundwater for 7 years resulted in a change in the exchangeable cation composition of the clay (higher calcium and potassium present and reduced sodium).
- Compaction behaviour using Standard compaction effort or Modified compaction effort was unaffected by aggregate type (i.e., granite sand versus crushed limestone).
- The presence of highly saline porefluid resulted in a slight increase in density achieved when standard compaction (SC) effort was used.
- Materials compacted using modified compaction (MC) effort exhibited no influence of porefluid salinity on density achieved.
- The aggregate (granite sand or crushed limestone) used as the sand component did not discernibly influence the swelling pressure or hydraulic conductivity achieved for the range of densities and EMDDs examined.
- The swelling pressure and hydraulic conductivity data collected in the current study are entirely consistent with previous work done by WSP-Golder and also literature-reported data for this type of material. These properties can be estimated using the EMDD parameter if it is known.
- From evaluation of P_s and k data the range in observed P_s for an assumed 80% montmorillonite content in the bentonite will fall within a factor of 3 to 5 of the best-fit value and k will be within a factor of 5 to 10 ($1/2$ to 1-order of magnitude). These are much higher than the estimated effect of $\pm 5\%$ uncertainty in montmorillonite content.
- The swelling pressure and hydraulic conductivity of the materials tested were strongly affected by porefluid salinity at the densities of interest in a shaft backfill. Increased salinity resulted in decreased swelling pressure and increased hydraulic conductivity observed for the bentonite-sand ratios and compacted densities tested.

- The influence of uncertainty in montmorillonite content for differing shipments of MX80 was evaluated based on an assumed range of $\pm 5\%$ from a target value of 80% by mass in the bentonite. The result of such variation is discernible with respect to prediction of Ps and k. The Ps will range by approximately $\pm 25\text{-}30\%$ and k will range by approximately $\pm 50\text{-}90\%$ for a $\pm 5\%$ range in montmorillonite content. These values are much lower than the values generated for the prediction limits for the data presented in this report.
- For a low-salinity environment (e.g., CR-10), an EMDD more than 1.06 Mg/m^3 is needed in order to achieve both Ps and k targets. This is achieved when standard compaction effort is used to compact bentonite-aggregate mixtures having more than 60% bentonite content. If modified compaction effort is used to densify the backfill the target minimum EMDD values are met for all blends having more than 50% bentonite content.
- For a high salinity environment (e.g., SR-Sh), an EMDD of more than 1.36 Mg/m^3 is needed in order to achieve both Ps and k targets. This is not achieved for any bentonite-aggregate mixture prepared using standard compaction effort. If modified compaction effort is used to densify the backfill the target minimum EMDD values are met for all blends having more than 50% bentonite content.
- The SWCC tests indicate that aggregate type had no discernible effect on SWCC behaviour.
- The SWCC behaviour observed was strongly influenced by the porefluid composition (TDS).
- From the limited (4) gas permeability tests completed in this study, it appears that gas movement was:
 - a) influenced by backfill density ($>$ density results in lower gas permeability/conductivity);
 - b) influenced by aggregate content (when related to degree of fluid saturation). Change in limestone aggregate from 50 to 40% resulted in an approximate doubling of k_g at a degree of fluid saturation less than approximately 80%. The reason for this is unknown.
 - c) possibly influenced by aggregate type and/or porefluid. The k_g of the 50:50 blends were much lower for limestone aggregate systems than for granitic sand at the same density, when related to capillary pressure. The porefluids differed in the two specimens making conclusions regarding the potential significance of these factors difficult.
 - d) largely prevented when fluid saturation exceeds approximately 80 to 85%.

REFERENCES

- ASTM D6913 – 04, 2004. Standard Test Methods for Particle-Size Distribution (Gradation) of Soils Using Sieve Analysis, ASTM International, West Conshohocken, PA, 2014, www.astm.org.
- ASTM D5890–11, 2011. Standard test method for swell index of clay mineral component of geosynthetic clay liners. ASTM International, West Conshohocken, PA, 2014, www.astm.org.
- ASTM D698-12e2, 2012. Standard Test Methods for Laboratory Compaction Characteristics of Soil Using Standard Effort (12,400 ft-lbf/ft³ (600 kN-m/m³)), ASTM International, West Conshohocken, PA, 2014, www.astm.org.
- ASTM D1557-12e1, 2012. Standard Test Methods for Laboratory Compaction Characteristics of Soil Using Modified Effort (56,000 ft-lbf/ft³ (2,700 kN-m/m³)), ASTM International, West Conshohocken, PA, 2014, www.astm.org.
- ASTM D854-14, 2014. Standard test methods for specific gravity of soil solids by water pycnometer. ASTM International, West Conshohocken, PA, 2014, www.astm.org.
- ASTM C837-15, 2015. Standard test method for methylene blue index of clay, ASTM International, West Conshohocken, PA, 2014, www.astm.org.
- ASTM D-4318-17e1, 2017. Standard test methods for liquid limit, plastic limit and plasticity index of soils, ASTM International, West Conshohocken, PA, 2014, www.astm.org.
- ASTM D-4829-19, 2019. Standard test method for expansion index of soils, ASTM International, West Conshohocken, PA, 2014, www.astm.org.
- Barone, F., Stone J., and Man A. 2014. Geotechnical properties of candidate shaft backfill. Nuclear Waste Management Organization Report NWMO-TR-2014-12. Toronto, Canada.
- Dixon, D.A. 1995. Towards an understanding of water structure and water movement through dense clays. Ph.D. Thesis, Dept. Civil and Geol. Engineering. University of Manitoba, Winnipeg, Canada.
- Dixon, D.A. 2000. Porewater salinity and the development of swelling pressure in bentonite-based buffer and backfill materials. Posiva Oy Report 2000-04. Olkiluoto, Finland.
- Dixon, D.A. 2019. Review of the T-H-M-C Properties of MX80 Bentonite. Nuclear Waste Management Organization, NWMO-TR-2019-07, Toronto, Canada.
- Dixon, D.A., Gray, M.N., Baumgartner, P., and Rigby, G.L. 1986. Pressure acting on waste containers in bentonite-based materials. Proc. Canadian Nuclear Society 2nd Intl conf. on Radioactive Waste Management, pp 221-227. Winnipeg, Canada.
- Dixon, D.A., Wan, A.W-L., Gray, M.N. and Miller, S.H. 1996. Water uptake and stress development in bentonites and bentonite-sand buffer materials. Atomic Energy of Canada Limited Report, AECL-11591, COG-96-221, Chalk River, Ontario, Canada.

- Dixon, D.A., Graham, J. and Gray M.N. 1999. Hydraulic conductivity of clays in confined tests under low hydraulic gradients. *Can. Geotech. J.* 36, 815-825.
- Dixon, D.A., Man, A., Rimal, S., Stone, J. and Siemens, G. 2018. Bentonite seal properties in saline water. Nuclear Waste Management Organization Report NWMO-TR-2018-20. Toronto, Canada.
- Dixon, D.A., Stone, J., Birch, K., and Kim, C.S. 2022. Sealing materials for a deep geological repository: Evaluation of swelling pressure and hydraulic conductivity data for bentonite-based Sealing materials proposed for use in placement room, *Canadian Geotechnical Journal* Publication pending.
- Dueck, A., Johannesson, L-E., Kristensson, O., Olsson, S. and Sjolund, A. 2011, Hydro-mechanical and chemical-mineralogical analyses for the bentonite buffer from a full-scale field experiment simulating a high-level waste repository, *Clays and Clay Minerals*, V. 59 (6), pp 595-607.
- Fredlund, D.G. and Xing, A. (1994) Equations for the soil-water characteristic curve. *Canadian Geotechnical Journal*, 31 (3): 521-532.
- Graham, J., Oswell, J., and Gray, M.N., 1991. The effective stress concept in saturated sand-clay buffer, *Proc. Workshop on Stress Partitioning in Engineered Clay Barriers*, 29-31 May 1991, Duke University, Durham, North Carolina, USA.
- Karnland, O. and Birgersson M. 2006. Montmorillonite stability: With special respect to KBS-3 conditions, Swedish Nuclear Fuel and Waste Management Company Technical Report SKB TR-06-11. Stockholm, Sweden.
- Karnland, O., Olsson, S. and Nilsson, U. 2006. Mineralogy and sealing properties of various bentonites and smectite-rich clay materials. Swedish Nuclear Fuel and Waste Management Company Technical Report SKB TR-06-30. Stockholm, Sweden.
- Karnland, O., Nilsson, U., Weber, H. and Persin, P. 2008. Sealing ability of Wyoming bentonite pellets foreseen as buffer material – Laboratory results, *Physics and Chem. of the Earth, Parts A/B/C*, Vol. 33, Supplement 1, pp S472-S475.
- Karnland, O., Olsson, S., Sanden, T., Falth, B., Jansson, M., Eriksen T.E., Svardstron K., Rosborg, B., and Muurien, A. 2009. Long-term test of buffer material at the Äspö HRL, LOT project, Swedish Nuclear Fuel and Waste Management Company, Technical Report, TR-09-31, Stockholm.
- Karnland, O. 2010. Chemical and mineralogical; characterization of the bentonite buffer for the acceptance control procedure in a KBS-3 repository. Swedish Nuclear Fuel and Waste Management Company Technical Report SKB TR-10-60. Stockholm, Sweden.
- Kiviranta, L. and Kumpulainen, S. 2011. Quality control and characterization of bentonite materials. Posiva Oy Working Report WR-2011-84. Eurajoki, Finland.
- Lee, J.O., Cho, W.J., Kang, C.H. and Chun, K.S. 2010. Swelling and hydraulic properties of Ca-bentonite for the buffer of a waste repository. IAEA-SM-357/68, Vienna, Austria.

- Naserifard N., Lee A., Birch K., Chiu A., and Zhang X. 2021. Deep Geological Repository Conceptual Design Report: Crystalline / Sedimentary rock , Nuclear Waste Management Organization, NWMO APM-REP-00440-0211 R000, Toronto. Priyanto, D.G., Kim, C.S. and Dixon, D.A. 2013. Geotechnical characterization of a potential shaft backfill material. Nuclear Waste Management Organization Report NWMO-TR-2013-03. Toronto, Canada.
- Pusch, R. 1980. Swelling pressure of highly compacted bentonite, Swedish Nuclear Fuel and Waste Management Company, SKB, KBS-80-13, Stockholm, Sweden.
- Rowe, R.K. and Brachman R.W.I. 2019. Laboratory determination of seal material performance, Final report submitted to the CNSC (project R613.4), Queens University, Kingston, Ontario.
- Zheng, L., Rutqvist, J., C+Xu, H. and Birkholzer, J.T. 2017, Coupled THMC models for bentonite in an argillite repository for nuclear waste: Illitization and its effect on swelling stress under high temperature, Elsevier open-access document, 1-S2.0-S0013795217304180-Liange_Zheng_Coupled_THMC_models_2017.pdf

APPENDIX A: XRD and XRF Reports

Activation Laboratories Ltd.



Geometallurgy

X-ray Diffraction Analysis of One Sample

W.O. # A18-14254
Invoice # A18-14254

Client: Golder Associates Ltd.

Attn: Daniel Jones

Date Reported: October 16, 2018

Methods

One sample was submitted for quantitative X-ray diffraction analysis and clay speciation. For the quantitative XRD analysis, a portion of the sample was mixed with corundum and packed into a standard holder. Corundum was added as an internal standard, to estimate the X-ray amorphous and poorly crystalline content. For the clay speciation analysis, a portion of sample was dispersed in distilled water and clay minerals in the < 4 μm size fraction separated by gravity settling of particles in suspension. Oriented slides of the < 4 μm size fraction were prepared by placing a portion of the suspension onto a glass slide. In order to identify expandable clay minerals, the oriented slides were analyzed air-dried and after treatment with ethylene glycol.

The X-ray diffraction analysis was performed on a Panalytical X'Pert Pro diffractometer equipped with Cu X-ray source and an X'Celerator detector and operating at the following conditions: 40 kV and 40 mA; range 5-70 deg 2θ for random specimens and 3 – 30 deg 2θ for oriented specimens; step size 0.017 deg 2θ ; time per step 50.165 sec; fixed divergence slit, angle 0.5° or 0.25° ; sample rotation 1 rev/sec. The X'Pert HighScore plus software along with the PDF4/Minerals ICDD database were used for mineral identification. The quantities of the crystalline mineral phases were determined using Rietveld method. The Rietveld method is based on the calculation of the full diffraction pattern from crystal structure data. The amounts of the crystalline minerals were recalculated based on a known percent of corundum and the remainder to 100 % was considered poorly crystalline and X-ray amorphous material.

Results

The minerals identified in the bulk sample and their abundances are in Table 1 and the diffraction patterns are in Appendix 1.

The clay speciation procedure showed presence of mineral from the smectite group. Smectite was identified on the basis of the peak at 15 Å that shifted to 17 Å after treatment with ethylene glycol. The peak at 1.50 Å indicated that the smectite mineral was montmorillonite.

Table 1. Mineral abundances (wt %)

Client ID	Sample 4
Actlabs ID	A18-14254-1
Montmorillonite	95.0
Quartz	1.5
Plagioclase	2.2
Mica	1.3
Cristobalite	trace

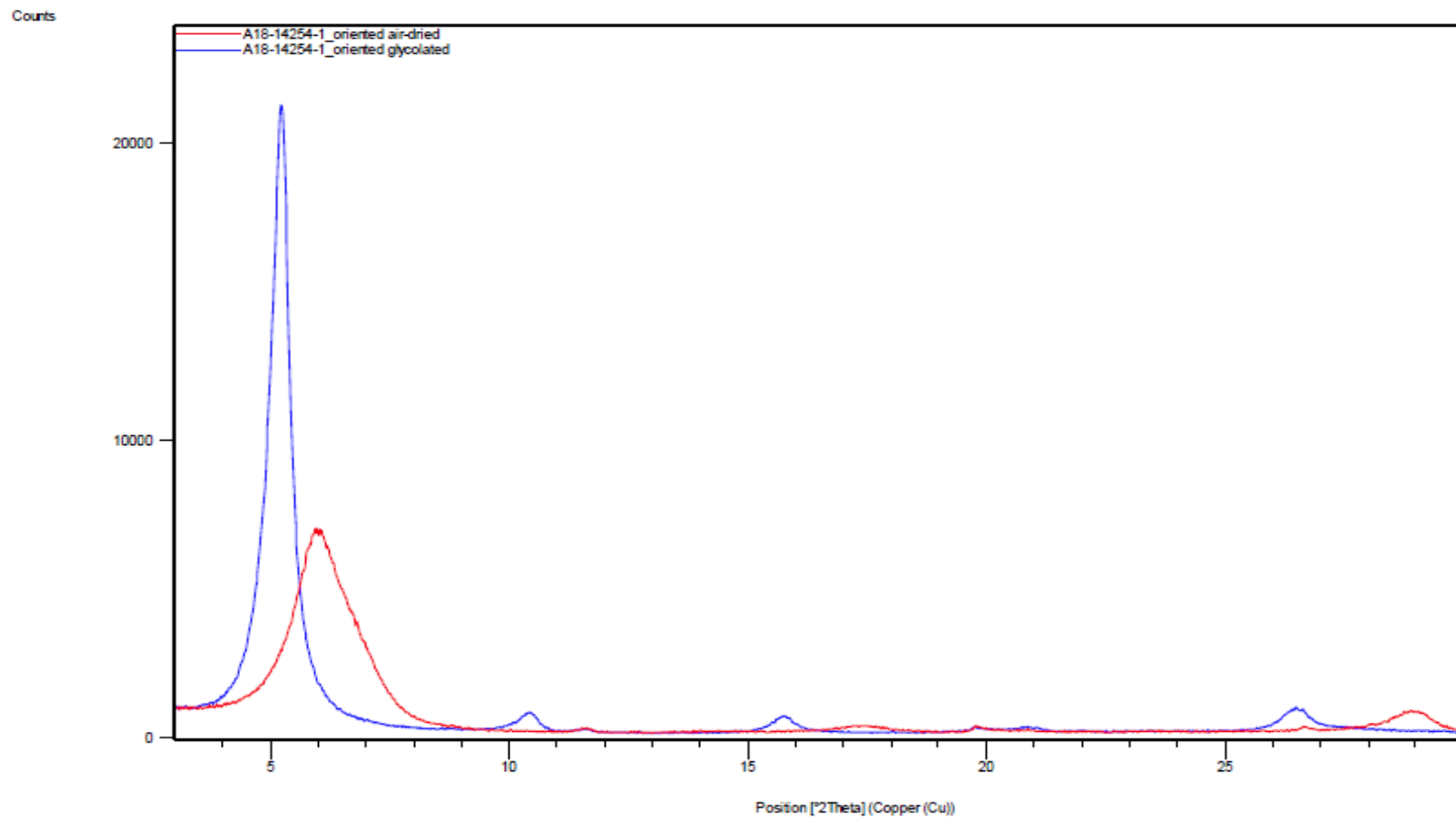
Note: Montmorillonite may include a small amount of X-ray amorphous material.

Reported by:

Elitsa Hrischeva, Ph.D.

Activation Laboratories Ltd.

APPENDIX 1
Diffraction patterns

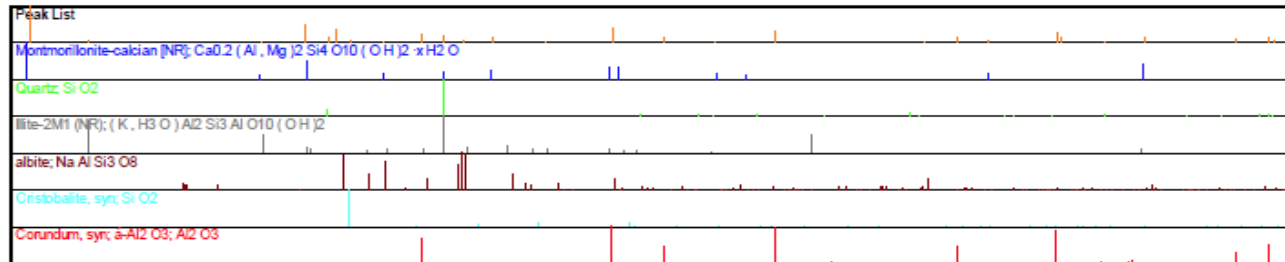
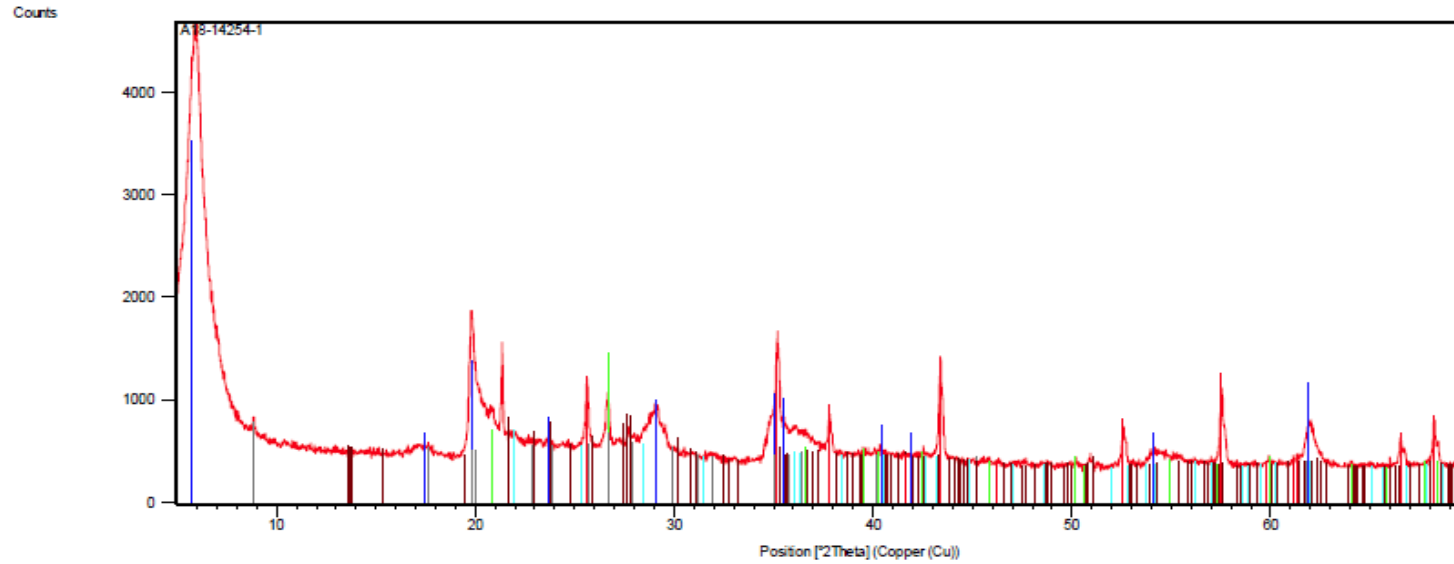


QC

Activation Laboratories Ltd.

Report: A18-14254

Analyte Symbol	Co3O4	CuO	NI0	SiO2	Al2O3	Fe2O3(T)	MnO	MgO	CaO	Na2O	K2O	TiO2	P2O5	Cr2O3	V2O5	LOI	Total
Unit Symbol	%	%	%	%	%	%	%	%	%	%	%	%	%	%	%	%	%
Lower Limit	0.005	0.005	0.003	0.01	0.01	0.01	0.001	0.01	0.01	0.01	0.01	0.01	0.01	0.01	0.003		0.01
Method Code	FUS-XRF	FUS-XRF	FUS-XRF	FUS-XRF	FUS-XRF	FUS-XRF	FUS-XRF	FUS-XRF	FUS-XRF	FUS-XRF	FUS-XRF	FUS-XRF	FUS-XRF	FUS-XRF	FUS-XRF	FUS-XRF	FUS-XRF
AN-G Meas				45.66	29.12	3.27	0.045	1.81	16.00	1.63	0.14	0.22	0.01	0.01	0.013		
AN-G Cert				46.30	29.8	3.36	0.040	1.79	15.90	1.63	0.13	0.22	0.01	0.01	0.012		
BE-N Meas	0.008	0.008	0.032	38.29	10.03	12.93	0.202	12.99	13.96	3.17	1.35	2.73	1.06	0.04	0.045		
BE-N Cert	0.008	0.009	0.034	38.2	10.1	12.8	0.200	13.1	13.9	3.18	1.39	2.61	1.05	0.0500	0.042		
BE-N Meas	0.007	0.010	0.032	38.34	10.03	13.04	0.199	13.10	14.09	3.17	1.37	2.67	1.05	0.06	0.044		
BE-N Cert	0.008	0.009	0.034	38.2	10.1	12.8	0.200	13.1	13.9	3.18	1.39	2.61	1.05	0.0500	0.042		
AC-E Meas				71.41	14.99	2.55	0.055	0.04	0.36	6.74	4.55	0.11					
AC-E Cert				70.35	14.70	2.56	0.058	0.03	0.34	6.54	4.49	0.11					
NOD-A-1 Meas	0.429		0.806	3.98	4.07		23.82	4.85	15.91			0.50	1.31		0.131		
NOD-A-1 Cert	0.424		0.809	3.81	3.87		23.9	4.76	15.4			0.530	1.37		0.137		
NOD-P-1 Meas				13.92	4.87		38.67	3.41	3.19	2.30	1.24	0.49	0.48		0.109		
NOD-P-1 Cert				13.9	4.82		37.6	3.30	3.06	2.21	1.21	0.500	0.460		0.102		
BIR-1a Meas				47.56	15.65	11.56	0.175	9.71	13.25	1.89	0.04	0.99	0.03				
BIR-1a Cert				47.96	15.50	11.30	0.175	9.700	13.30	1.82	0.030	0.96	0.021				
BIR-1a Meas				47.54	15.38	11.68	0.174	9.77	13.31	1.89	0.04	0.98	0.04				
BIR-1a Cert				47.96	15.50	11.30	0.175	9.700	13.30	1.82	0.030	0.96	0.021				
Silicon (IV) Oxide 99.8% Meas				99.73													
Silicon (IV) Oxide 99.8% Cert				99.8													
AMIS 0104 Meas				18.48	2.24	20.95	45.92		1.41		0.28	0.34					
AMIS 0104 Cert				18.30	2.20	20.78	45.580		1.34		0.26	0.27					
sample 4 Orig	< 0.005	< 0.005	< 0.003	55.80	19.83	3.94	0.015	2.61	1.68	2.16	0.53	0.20	0.07	< 0.01	< 0.003	13.61	100.4
sample 4 Dup	< 0.005	< 0.005	< 0.003	55.41	19.45	3.91	0.015	2.57	1.66	2.15	0.52	0.20	0.07	< 0.01	< 0.003	13.62	99.57
Method Blank	< 0.005	< 0.005	< 0.003	< 0.01	< 0.01	< 0.01	< 0.001	< 0.01	< 0.01	< 0.01	< 0.01	< 0.01	< 0.01	< 0.01	< 0.003		
Method Blank	< 0.005	< 0.005	< 0.003	< 0.01	< 0.01	< 0.01	< 0.001	< 0.01	< 0.01	< 0.01	< 0.01	< 0.01	< 0.01	< 0.01	< 0.003		



(Note that bentonite listed in report as Sa 2 is not the reference MX80 used in this study)

XRD results for Granitic Sand and Crushed Limestone**Table 1.** Mineral abundances in bulk samples (wt %)

Client ID	Sa 1	Sa 2	Sa 3
Actlabs ID	A18-07152-1	A18-07152-2	A18-07152-3
Calcite	84.8	2.4	n.d.
Dolomite	2.7	n.d.	n.d.
Quartz	7.0	6.8	45.0
Cristobalite	n.d.	3.1	n.d.
Muscovite/illite	5.0	6.0	3.3
Montmorillonite*	n.d.	54	n.d.
Plagioclase	n.d.	16.7	34.5
K feldspar	n.d.	n.d.	11.0
Chlorite	n.d.	n.d.	2.5
Amphibole	n.d.	n.d.	3.7
Pyrite	0.5	n.d.	n.d.
Amorphous	n.d.	11	n.d.

Note: n.d. = not detected. The amount of montmorillonite is a rough estimate calculated from the relative proportions of montmorillonite and illite in the < 4 µm size fraction. Amorphous includes opal.

Table 2. Relative proportions of clay minerals in the < 4 µm size fraction

Client ID	Sa 2
Actlabs ID	A18-07152-2
Montmorillonite	90
Illite	10

Reported by:

Elitsa Hrischeva, Ph.D.
 Scientist
 Activation Laboratories Ltd



Report Number: 2018-27371

ANALYTICAL LABORATORY SERVICES
 Assured Analytical Excellence
www.claysandminerals.com

**Report on the Bulk Mineralogy of a Single Bentonite
 Sample by X-Ray Powder Diffraction (XRPD) and Chemistry
 by X-Ray Fluorescence (XRF)**

FOR:

Daniel Jones/David Dixon
 Golder Associates Ltd
 6925 Century Avenue
 Suite #100
 Mississauga
 Ontario
 L5N 7K2
 CANADA



REPORT AUTHORS:

Ian M Phillips, BSc, PhD (Senior Analyst)
 (e-mail: ian.phillips@hutton.ac.uk T: 01224 395355)

A handwritten signature in black ink, appearing to read "S Hillier".

Prof Stephen Hillier

Report Authorisation
stephen.hillier@hutton.ac.uk
 2018-11-15 12:08Z



Tests marked "N/A" are not covered by the UKAS Schedule for this laboratory.
 Opinions and interpretations expressed herein are outside the scope of UKAS Accreditation.
 This report shall not be reproduced, except in full, without written approval of the laboratory.

James Hutton Limited, Craigmuckler, Aberdeen AB15 8QH, Scotland
 T: +44 (0)344 928 5428 W: www.huttonltd.com

Report Number: 2018-27371

Job and Sample Information:	
Job No(s):	2018-27371
Client Order No/Reference:	1895762
Date Sample(s) Received:	11-October-2018
Appendix	XRF Certificate
Lab Code	Client Code
1295625	Sample 4

Introduction

A single sample, described as 'clay', was forwarded for bulk mineralogical analysis by X-ray powder diffraction (XRPD) and chemistry by X-Ray Fluorescence (XRF).

Methods

Methods	Accreditation Reference
Identification and Quantification of polycrystalline material by XRPD	GM003 and GM004
Chemistry by X-Ray Fluorescence (Sub-Contracted)	Sub-Contracted

XRPD

The bulk sample was wet ground (in ethanol) in a McCrone mill and spray dried to produce a random powder. The X-ray powder diffraction (XRPD) pattern was recorded from 2- θ 5°2 θ using Cobalt K α radiation. Quantitative analysis was done by a normalised full pattern reference intensity ratio (RIR) method. Unless stated otherwise, expanded uncertainty using a coverage factor of 2, i.e. 95% confidence, is given by $\pm X^{(2)}$, where X = concentration in wt.%, e.g. 30 wt.% \pm 3. Note also that for phases present at the trace level (<1%) there may also be uncertainty as to whether or not the phase is truly present in the sample. This is both phase and sample dependent. It arises because at trace concentrations identification is often based on the presence of a single peak and the judgement of the analyst in assigning that peak to a likely mineral.

The XRPD pattern is identified by a labcode and by a name based on customer supplied identifiers, plus the suffix 'B' for bulk sample.

Results

The bulk XRPD results are presented in Table 1. The XRPD pattern, with the main non-clay phases identified by reference to patterns from the International Centre for Diffraction Database (ICDD), is provided for reference.

Comments and opinions

The sample is a mixture of dioctahedral smectite (91.6%) with smaller amounts of quartz, plagioclase, K-feldspar, calcite, siderite, pyrite, muscovite and a trace of gypsum.

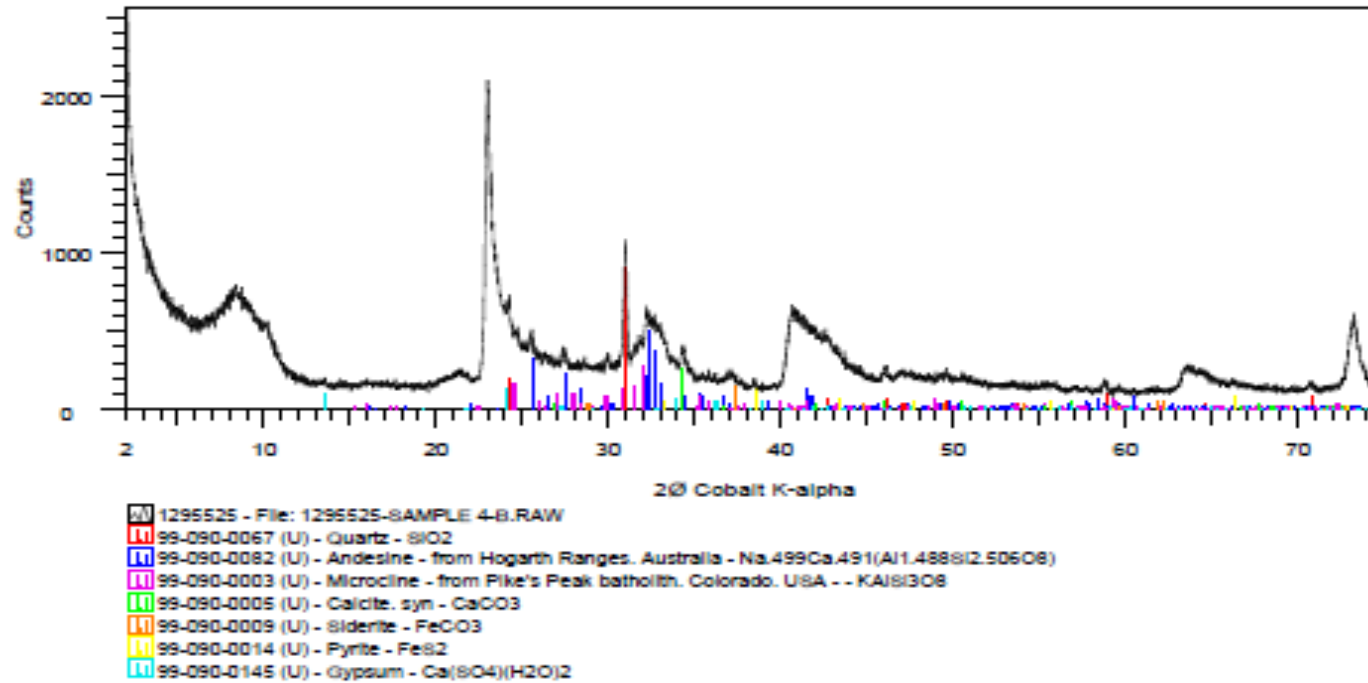
Note that we have used the more general term smectite in preference to the specific mineral term montmorillonite. Montmorillonite is a specific variety of dioctahedral smectite.

Note:

Samples will be stored for a period of eight weeks following completion of analysis and acceptance of analytical report(s) at no extra cost after which samples will be disposed of unless a specific instruction is given (with the sample analysis request/order) to store the sample beyond this period. Extended storage charges will apply.

James Hutton Limited, Craigmuckler, Aberdeen AB15 8QH, Scotland

T: +44 (0)144 928 5428 W: www.huttonltd.com



James Hutton Limited, Craigiebuckler, Aberdeen AB15 8QH, Scotland
 T: +44 (0)344 928 5428 W: www.huttonltd.com

XF009 Version 11

Page 4 of 6

Table 1: XRPD Bulk Mineralogy (weight %) by RIR Method

Labcode	Sample ID	Quartz	Plagioclase	K-feldspar	Calcite	Siderite	Pyrite	Gypsum	Muscovite	Smedite(D)	Total
1295525	SAMPLE 4-B	2.2	3.8	0.4	0.8	0.4	0.4	trace	0.8	91.8	100.0

Smedite(D) = Octahedral Smedite


AMG Superalloys UK Limited

Fullerton Road, Rotherham, South Yorkshire S60 1DL, England

ANALYTICAL SERVICES

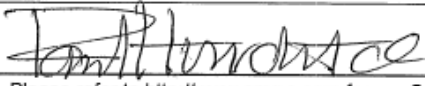
Tel. 01709-833763

Fax. 01709-830391


CERTIFICATE OF ANALYSIS

Page No. 1 of 1

Material analysed has been supplied to AMG Analytical Services for 3rd party analysis

To The James Hutton Institute Macaulay Drive Craigiebuckler Aberdeen AB15 8QH Scotland	Certificate Date	12/11/2018	Certificate No.	Lab Request No.
	Date of Receipt	02/11/2018	3804962	3806582
	Analysis Start Date	07/11/2018	Your Ref. / Order No.	
	Analysis End Date	12/11/2018	CB/00000689-XRF-GOLD	
Sample Details				
No. of Samples Submitted : 1				
FAO Ian Phillips				
Analysis Results 3821381 1295525 BENTONITE CLAY LOD@110°C 9.41 % LOI@1000°C (After LOD) 7.49 % Na2O 2.30 % MgO 2.76 % Al2O3 20.99 % SiO2 58.96 % P2O5 0.08 % K2O 0.52 % CaO 1.74 % TiO2 0.22 % Mn3O4 <0.05 % V2O5 <0.05 % Cr2O3 <0.05 % Fe2O3 4.15 % BaO 0.05 % ZrO2 0.05 % ZnO <0.05 % SrO <0.05 % ***END OF REPORT***				
Analysis on Dried Basis Material: Refractory				
Comments / Remarks Analysed using in - house documented procedures for technique(s) : LOD LOI XRF			Certificate Signed by <input type="checkbox"/> D. Williams Laboratory Manager <input checked="" type="checkbox"/> P. W. Hurditch Chief Chemist <input type="checkbox"/> H. Whitham Sales Chemist	
Signed 				

Please refer to <http://www.amg-s.com> for our Conditions of Assay

Registered Office as above. Registered in England No. 345279 V.A.T. No. GB 789 6326 65.

XRD results for Granitic Sand and Crushed Limestone

Report Number: 2018-26775

Table 1: XRPD Bulk Mineralogy (weight %) by RIR Method

Labcode	Sample ID	Quartz	K-feldspar	Plagioclase	Amphibole	Calcite	Dolomite	Bassanite	Pyrite	Clinoptilolite	Chlorite(Tri)	Muscovite	Mica(Tri)	Cristobalite/Opal	Smectite(Di)	I+/S-ML	Total
1286824	SAMPLE-1-CRL-B	7.4	1.2	1.2	-	75.5	2.0	-	0.7	-	1.7	0.2	-	-	-	10.1	100.0
1286825	SAMPLE-2-MX-B	2.4	2.2	9.5	-	1.3	-	0.8	0.1	3.8	-	-	3.2	7.8	68.9	-	100.0
1286826	SAMPLE-3-GS-B	39.8	14.0	32.3	4.9	-	-	-	-	-	3.4	3.7	1.8	-	-	-	100.0

Chlorite(Tri) = Trioctahedral Chlorite

Mica(Tri) = Trioctahedral Mica

Smectite(Di) = Dioctahedral Smectite

I+/S-ML = Illite+Illite/Smectite-Mixed Layered

James Hutton Limited, Craigiebuckler, Aberdeen AB15 8QH, Scotland
T: +44 (0)344 928 5428 W: www.huttonltd.com

Version 10

Page 4 of 9

(Note that bentonite listed in report is not the reference MX80 used in this study, it is a low-quality material provided in error)


AMG Superalloys UK Limited

Fullerton Road, Rotherham, South Yorkshire S60 1DL, England

ANALYTICAL SERVICES

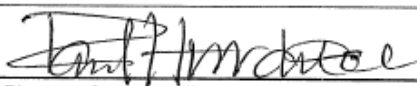
Tel. 01709-833763

Fax. 01709-830391


CERTIFICATE OF ANALYSIS

Page No. 1 of 1

Material analysed has been supplied to AMG Analytical Services for 3rd party analysis

To James Hutton Limited Macaulay Drive Craigiebuckler Aberdeen AB15 8QH Scotland	Certificate Date	05/07/2018	Certificate No.	Lab Request No.	
	Date of Receipt	27/06/2018	3802888	3803777	
	Analysis Start Date	03/07/2018	Your Ref. / Order No.		
	Analysis End Date	05/07/2018	CB/00000605		
Sample Details No. of Samples Submitted : 3					
FAO Helen Pendlowski	This Certificate replaces any test report with Request Number 3803777 previously issued				
Analysis Results					
	3812171 1286824		3812172 1286825		
				3812173 1286826	
LOD@110°C	0.21 %	LOD@110°C	1.77 %	LOD@110°C	0.10 %
LOI@1000°C (After LOD)	36.12 %	LOI@1000°C (After LOD)	6.08 %	LOI@1000°C (After LOD)	1.01 %
Na2O	0.10 %	Na2O	2.55 %	Na2O	3.33 %
MgO	1.67 %	MgO	1.85 %	MgO	1.04 %
Al2O3	2.83 %	Al2O3	18.37 %	Al2O3	12.86 %
SiO2	11.76 %	SiO2	64.23 %	SiO2	74.42 %
P2O5	0.07 %	P2O5	0.06 %	P2O5	0.05 %
K2O	0.68 %	K2O	0.60 %	K2O	2.14 %
CaO	43.95 %	CaO	2.20 %	CaO	2.25 %
TiO2	0.13 %	TiO2	0.21 %	TiO2	0.30 %
Mn3O4	<0.05 %	Mn3O4	0.06 %	Mn3O4	<0.05 %
V2O5	<0.05 %	V2O5	<0.05 %	V2O5	<0.05 %
Cr2O3	<0.05 %	Cr2O3	<0.05 %	Cr2O3	<0.05 %
Fe2O3	2.52 %	Fe2O3	3.72 %	Fe2O3	2.77 %
BaO	<0.05 %	BaO	0.12 %	BaO	0.07 %
ZrO2	<0.05 %	ZrO2	<0.05 %	ZrO2	<0.05 %
ZnO	<0.05 %	ZnO	<0.05 %	ZnO	<0.05 %
SrO	0.06 %	SrO	<0.05 %	SrO	0.05 %
END OF REPORT					
	Analysis on Dried Basis	Analysis on Dried Basis	Analysis on Dried Basis		
	Material: Non-Metallic	Material: Non-Metallic	Material: Non-Metallic		
Comments / Remarks Analysed using in - house documented procedures for technique(s) : LOD LOI XRF			Certificate Signed by <input type="checkbox"/> D. Williams Laboratory Manager <input checked="" type="checkbox"/> P. W. Hurditch Chief Chemist <input type="checkbox"/> H. Whitham Sales Chemist		
Signed 					

 Please refer to <http://www.amg-s.com> for our Conditions of Assay

Registered Office as above. Registered in England No. 345279 V.A.T. No. GB 789 6326 65.

CONFIDENTIAL REPORT

XRD Analysis

Prepared for Golder Associates

By Steven Creighton, PhD
Saskatchewan Research Council
Mining and Minerals

SRC Publication No. 10400-19C18

November 2018

CONFIDENTIAL REPORT

XRD Analysis

Prepared for Golder Associates

By Steven Creighton, PhD
Saskatchewan Research Council
Mining and Minerals

SRC Publication No. 10400-19C18

November 2018

Advanced Microanalysis Centre™
Saskatchewan Research Council
125 – 15 Innovation Blvd.
Saskatoon, SK S7N 2X8
Tel: 306-385-4066

Sample preparation

A random 0.5g aliquot of the ground sample was saturated with ethylene glycol vapours by sealing the sample powder aliquot in a sealed chamber overnight at 60°C. The sample powder was rotationally back-packed into a stainless-steel holder, inducing a preferred orientation of the clay minerals, and secured in place with a plastic backing. Comparison of data from the clay standard SWy-2 demonstrates that this sample preparation method fully saturates the clays and creates a stronger preferred orientation for smectite-rich samples compared to the traditional (USGS method) utilizing vacuum filtration of a <2µm fraction. The minimum sample thickness was 1mm – sufficient to be considered infinitely thick for X-ray diffraction using a Cu source.

XRD Analysis and data processing

Samples were irradiated with Cu K α radiation ($\lambda=1.54056\text{\AA}$) in a Bruker D4 Endeavor X-ray diffractometer (XRD) operating at 1.6kW power (40kV accelerating potential and 40mA current). The XRD is outfitted with a high speed LynxEye silicon strip detector with fluorescence background suppression. Samples were measured from 3.0 to 70° 2 θ with a 0.02° step size and 0.35 seconds dwell time.

The raw diffraction data was processed using MDI Products Jade software for mineral identification and quantification. Minerals were identified based on the observed interatomic spacing of the crystal lattices present constrained by common mineral associations. Mineral abundances were calculated using whole-pattern fitting algorithms with peak intensities scaled with internally-consistent relative intensity ratios. Non-orientable mineral abundances were quantified using patterns derived from the American Mineralogist Crystal Structure Database (AMCSD) whereas clay mineral abundances were quantified using proprietary reference patterns. The semi-preferred orientation and glycol solvation of clay minerals precludes the use of published (e.g. ICDD, AMCSD) mineral reference databases.

Detection and precision limits

The detection limit of XRD analysis is controlled by the abundance and symmetry of all the minerals present in the sample. Low symmetry minerals are harder to detect in the presence of higher symmetry minerals. The estimated detection limit for most minerals is 1-3 wt.%.

Based on repeat analyses of a secondary standards, the estimated accuracy of the clay analysis is ± 3 wt.%.

Amorphous material was observed in the sample. The broad amorphous hump in the background was removed from the modelled data by including it in the background fit. Attempts to quantify the abundance of amorphous material from XRD data have not yet proven reliable enough for inclusion in routine analyses.

Results

The following pages contain the results of the XRD mineral identification and quantitative mineral abundances.

Sample4

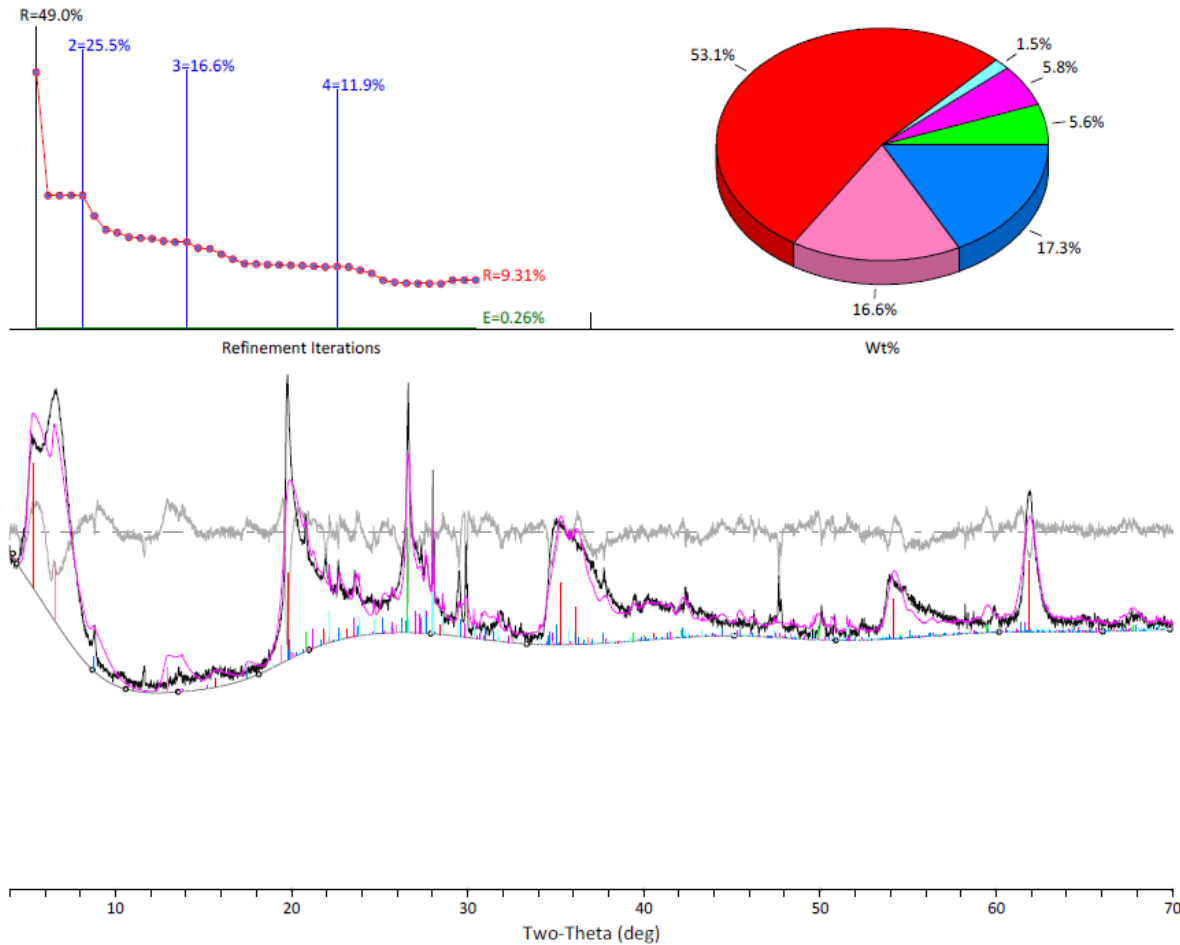
FILE: [Sample4.raw] Sample4*
 SCAN: 4.0/70.0537/0.01997/49.7(sec), Cu(40kV,40mA), I(p)=8297, 11/08/18 09:14a
 PROC: [WPF Control File]

- K-alpha2 Peak Present
 LS Weighting in 1 / Sqr(I)
 Allow Negative Isotropic B
 Allow Negative Occupancy
 Apply Anomalous Scattering
- [Diffractometer LP] Two-Theta Range of Fit = 4.0 - 70.1(deg)
 Specimen Displacement - Cos(Theta) = 0.151823(0.006163)
 Monochromator Correction for LP Factor = 1.0
 K-alpha2/K-alpha1 Intensity Ratio = 0.5

Profile Shape Function (PSF) for All Phases: Pearson-VII, Fixed-BG, Lambda=1.54059Å (Cu/K-alpha1)

Phase ID (6)	Source	I/Ic	Wt%	#L
Quartz - SiO ₂	PDF#98-091-4800	4.28(5%)	5.6 (0.4)	18
Albite - (AlSi ₃)(Na _{0.667} K _{0.333})O ₈	PDF#98-090-0615	0.56(5%)	5.8 (0.6)	171
Anorthite - Ca ₃₄ Na ₁₅ (Si _{1.17} Al _{0.83})O ₄	PDF#98-090-0968	0.59(5%)	1.5 (0.2)	283
Smectite - (Na _{0.2} Ca _{0.1})(Al _{1.3} Mg _{0.2} Fe _{0.3})Si ₄ O ₁₀ (OH)	PDF#99-003-0009	3.60(5%)	53.1 (3.3)	25
Clinochlore - Mg ₅ Al ₂ Si ₃ O ₁₈ H ₈	PDF#98-090-4198	2.00(5%)	16.6 (1.2)	255
Muscovite - K _{0.727} Na _{0.17} Ca _{0.01} Al _{2.752} Fe _{0.03} Mg _{0.022} Si _{3.128} Ti _{0.02} O ₁₂ H ₂	PDF#98-091-2074	0.40(5%)	17.3 (1.7)	205

NOTE: Fitting Halted at Iteration 39(4): R=9.31% (E=0.26%, R/E=35.15, P=74, EPS=0.5)



Golder Associates

Attention: Daniel Jones
 PO #/Project: 1895762 (2A)
 Samples: 3

SRC Geoanalytical Laboratories

125 - 15 Innovation Blvd., Saskatoon, Saskatchewan, S7N 2X8
 Tel: (306) 933-8118 Fax: (306) 933-5656 Email: geolab@src.sk.ca

Report No: G-2018-1628

Date of Report: Oct 12, 2018

ICP Whole Rock Assay
 Lithium Metaborate Fusion

Column Header Details

Aluminum in wt % (Al₂O₃)
 Calcium in wt % (CaO)
 Iron in wt % (Fe₂O₃)
 Potassium in wt % (K₂O)
 Magnesium in wt % (MgO)

Manganese in wt % (MnO)
 Sodium in wt % (Na₂O)
 Phosphorus in wt % (P₂O₅)
 Titanium in wt % (TiO₂)
 SiO₂ by ICP in wt % (SiO₂)

Barium in ppm (Ba)
 Chromium in ppm (Cr)
 Scandium in ppm (Sc)
 Strontium in ppm (Sr)
 Yttrium in ppm (Y)

Zirconium in ppm (Zr)
 Loss on Ignition in wt % (LOI)
 SUM in (SUM)

Sample Number	Al ₂ O ₃ wt %	CaO wt %	Fe ₂ O ₃ wt %	K ₂ O wt %	MgO wt %	MnO wt %	Na ₂ O wt %	P ₂ O ₅ wt %	TiO ₂ wt %	SiO ₂ wt %	Ba ppm	Cr ppm	Sc ppm	Sr ppm	Y ppm	Zr ppm	LOI wt %	SUM
SY3	11.7	8.31	6.57	4.22	2.63	0.32	4.11	0.54	0.14	59.5	445	9	8	295	726	323	N/R	98.04
Sample #4	19.6	1.79	3.70	0.49	2.43	0.01	2.04	0.07	0.20	54.3	318	5	5	243	35	307	15.1	99.73
Sample #4 R	19.5	1.75	3.72	0.47	2.44	0.01	2.03	0.06	0.19	54.2	314	4	5	240	36	302	15.2	99.57

Whole Rock Analysis: A 0.1 gram pulp is fused at 1000 C with lithium metaborate then dissolved in dilute HNO₃.
 The standard is SY3.



AMERICAN COLLOID COMPANY

Minerals Technologies Inc.
2870 Forbs Avenue | Hoffman Estates, IL 60192
Direct: 847.851.1721 | Mobile: 847.271.9474

Project Report

Project: P18-141 Analysis of Bentonite Sample
Date: 11/15/18
Requested By: Jerry Darlington
Completed By: Minerals Technologies Inc. Research and Development, Hoffman Estates

BACKGROUND

A sample of granular bentonite was given to the MTI Hoffman Estates lab for analysis. Free Swell and Fluid Loss testing were requested along with X-Ray Diffraction (XRD) and X-Ray Florescence (XRF).

Samples:

R18-1432 Rice Engineering - 55628892 MX80 Z6718A13 09/24/18

CONCLUSIONS

The sample shows a 24 hour free swell value of 27 mls along with a relative 30 minute fluid loss value of 18.6 mls. The XRD and XRF analysis suggest a sodium bentonite with evidence of small amounts of various accessory minerals such as gypsum and feldspars.

LABORATORY RESULTS

Table 1: General Data

Sample Number	Moisture As Received (%)	CEC (meq/100g)	Total Hardness (meq/100g)	Soluble Calcium (meq/100g)	Free Swell (2g/ml)
R18-1432 Rice Engineering	10.10	104	30	23	27

RHEOLOGY

Table 2: Fann Viscometer, and Gel Strength Results (22.5g / 350 ml)

Sample Number	Fann Viscometer Readings						Gel Strength (lbs/100 ft ² drill pipe)	
	600 RPM	300 RPM	200 RPM	100 RPM	6 RPM	3 RPM	10 seconds	10 minutes
R18-1432 Rice Engineering	9	5	3	2	1	1	1	1

Table 3: Calculated Viscosity Values and Fluid Loss Results

Sample Number	Apparent Viscosity	Plastic Viscosity (cPs)	Yield Point (lbs/100 ft ² drill pipe)	Yield Point/Plastic Viscosity Ratio	Fluid Loss (mls)
R18-1432 Rice Engineering	4.5	4	1	0.25	18.6

X RAY FLUORESCENCE - CHEMISTRY

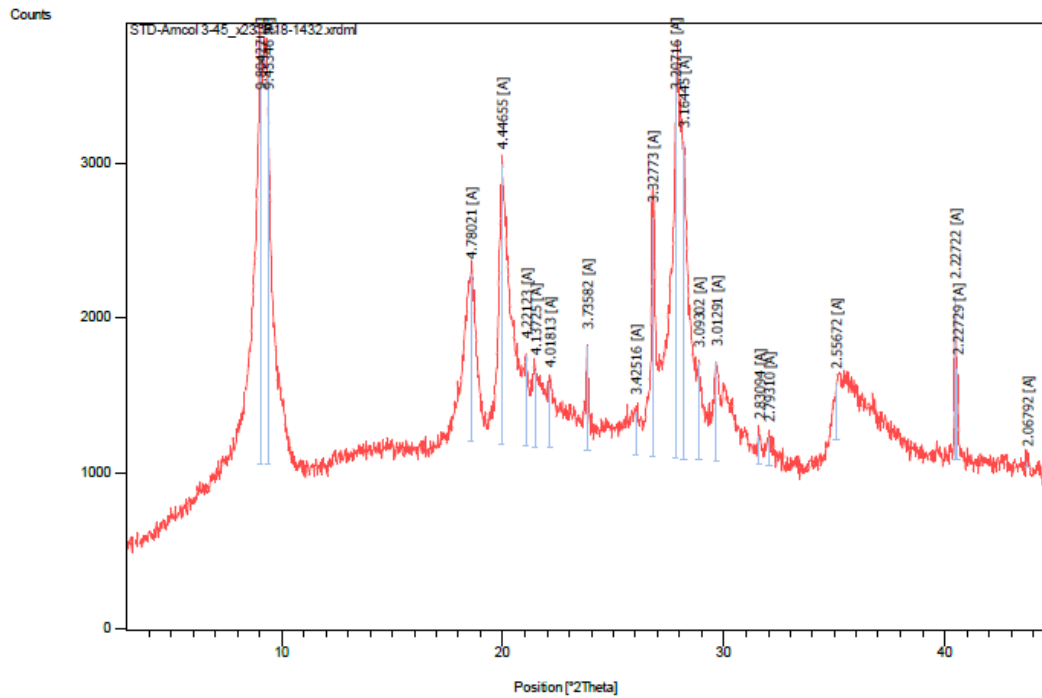
Table 4: XRF Data Normalized to 100%

ID	SiO ₂	Al ₂ O ₃	CaO	Cl	Cr ₂ O ₃	Fe ₂ O ₃	K ₂ O	MgO	MnO	Na ₂ O	P ₂ O ₅	SO ₃	TiO ₂	Total	Si/Al
R18-1432 Rice Engineering	54.13	20.51	1.20	0.03	0.03	3.47	0.36	2.70	0.02	1.97	0.03	0.21	0.22	84.88	2.33

Table 5: XRF Data Non-Normalized

ID	SiO ₂	Al ₂ O ₃	CaO	Cl	Cr ₂ O ₃	Fe ₂ O ₃	K ₂ O	MgO	MnO	Na ₂ O	P ₂ O ₅	SO ₃	TiO ₂	Total	Si/Al
R18-1432 Rice Engineering	63.77	24.17	1.41	0.04	0.04	4.09	0.43	3.19	0.02	2.32	0.03	0.25	0.25	100.00	2.33

X RAY DIFFRACTION – MINERALOGY



Pos. [°2Th.]	Height [cts]	FWHM [°2Th.]	d-spacing [Å]	Rel. Int. [%]
9.0200	2747.77	0.0836	9.80427	100.00
9.3554	2489.88	0.1004	9.45346	90.61
18.5620	1069.37	0.3011	4.78021	38.92
19.9687	1797.15	0.0669	4.44655	65.40
21.0464	586.73	0.0836	4.22123	21.35
21.4786	487.99	0.2007	4.13725	17.76
22.1233	418.40	0.2007	4.01813	15.23
23.8186	680.35	0.0502	3.73582	24.76
26.0153	278.86	0.2007	3.42516	10.15
26.7909	1534.39	0.0669	3.32773	55.84
27.8179	2529.93	0.0502	3.20716	92.07
28.2011	2033.80	0.0502	3.16445	74.02
28.8663	623.03	0.1004	3.09302	22.67
29.6512	640.63	0.1004	3.01291	23.31
31.6054	189.33	0.1004	2.83094	6.89
32.0450	177.10	0.2007	2.79310	6.45
35.0995	351.95	0.3346	2.55672	12.81
40.4681	1055.94	0.0612	2.22722	38.43
40.5719	570.23	0.0408	2.22729	20.75
43.7397	33.21	0.2040	2.06792	1.21

APPENDICES – Test Procedures

Required Tests & Lab Procedures:

Methylene Blue Determination
 Total Hardness Ca+Mg
 Free Swell Determination
 X-Ray Diffraction (XRD)
 X-Ray Fluorescence (XRF)
 Viscosity API-AV, PV, YP
 Filtrate-API

XRD: X-ray diffraction was tested using a Phillips X'Pert PW 3040-MPD diffractometer, using the AMCOL 3-45° 2θ program with the following parameters:

Start Position [°2Th.]	3.0010
End Position [°2Th.]	44.9910
Step Size [°2Th.]	0.0170
Scan Step Time [s]	29.8450
Scan Type	Continuous
PSD Mode	Scanning
PSD Length [°2Th.]	2.21
Divergence Slit Type	Automatic
Anode Material	Cu
Generator Settings	40 kV, 40 mA

Sample ground with mortar and pestle, “as received” moisture.

XRF: X-ray fluorescence testing was done on a Phillips PW 2400 x-ray spectrometer, using the ACC clay analysis program. Samples are dried to <1.0% moisture in a 110°C oven prior to testing.

Rheology: Viscosity readings were taken at various rpm off a FANN model 3A viscometer, the PV (plastic viscosity) value is given in centipoises while Gel strengths have units of lb/100ft². The slurry was prepared using 22.5g of bentonite with 350mls of water (22.5 lbs/bbl); readings were taken immediately (no aging). Fluid loss values are representative 60 minute values. Gel strengths have units of lb/100ft².

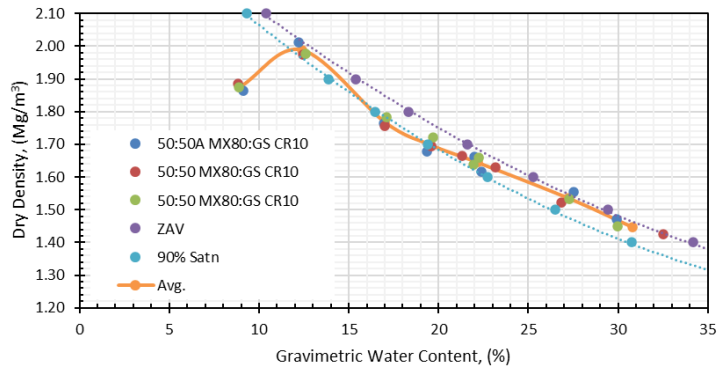
*Note: Fluid loss is reported as a relative 60 minute value.

APPENDIX B: Results of Compaction Testing

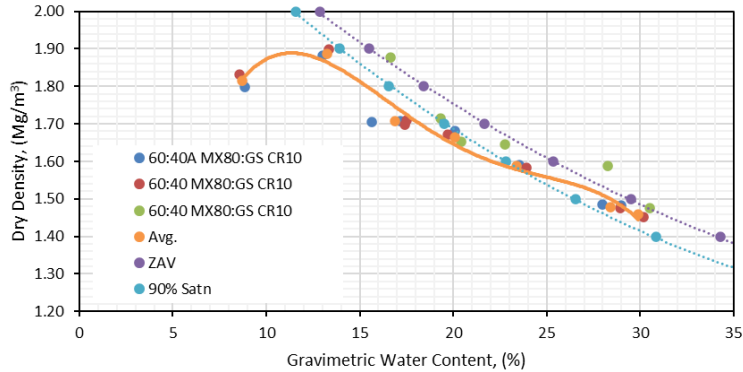
B-1 Modified Proctor: Miniature Compaction Test Results : MX80:GS CR-10 Solution

Note: The maximum dry densities shown are for raw compaction data, conversion to MPMDD value requires use of equation $MPMDD = \text{measured MDD} \cdot 0.98 + 0.11$ (Dixon et al. 1985)

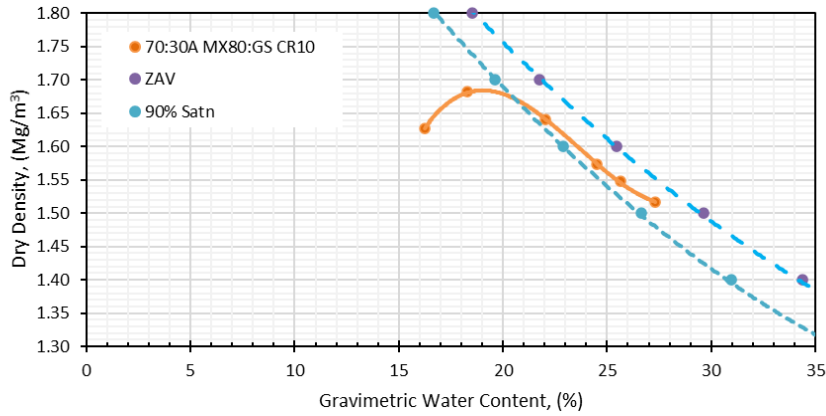
50 : 50 A				50 : 50 B				50 : 50 C			
Measured Water Content (%)	fluid / soil	Measured Dry Density (Mg/m ³)	Salt Corrected Dry Density (Mg/m ³)	Measured Water Content (%)	fluid / soil	Measured Dry Density (Mg/m ³)	Salt Corrected Dry Density (Mg/m ³)	Measured Water Content (%)	fluid / soil	Measured Dry Density (Mg/m ³)	Salt Corrected Dry Density (Mg/m ³)
9.1	9.2	1.866	1.864	8.8	8.9	1.888	1.886	8.86	8.9	1.875	1.874
12.2	12.3	2.015	2.012	12.4	12.5	1.977	1.974	12.58	12.6	1.980	1.978
17.0	17.1	1.768	1.765	17.0	17.1	1.759	1.756	17.10	17.2	1.785	1.782
19.4	19.4	1.681	1.678	19.6	19.7	1.699	1.695	19.70	19.8	1.726	1.723
22.0	22.1	1.667	1.663	21.3	21.4	1.668	1.664	21.96	22.1	1.640	1.637
22.4	22.5	1.620	1.616	23.1	23.3	1.634	1.630	22.24	22.3	1.663	1.659
27.5	27.7	1.560	1.556	26.8	27.0	1.525	1.521	27.26	27.4	1.538	1.533
29.9	30.1	1.475	1.471	32.5	32.7	1.429	1.424	29.97	30.1	1.453	1.448



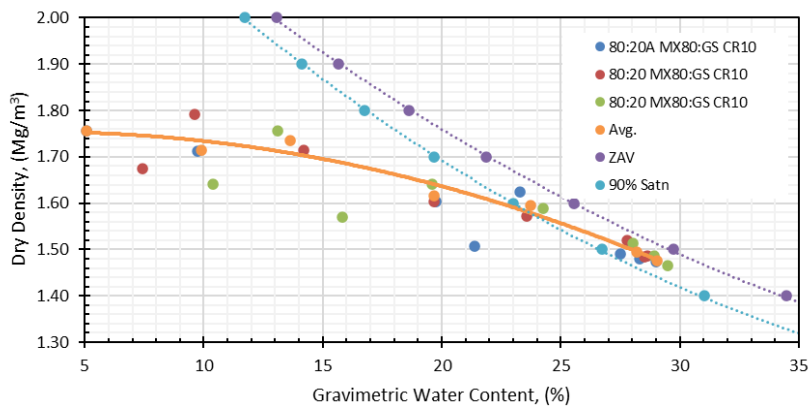
60 : 40 A				60 : 40 B				60 : 40 C			
Measured Water Content (%)	fluid / soil	Measured Dry Density (Mg/m ³)	Salt Corrected Dry Density (Mg/m ³)	Measured Water Content (%)	fluid / soil	Measured Dry Density (Mg/m ³)	Salt Corrected Dry Density (Mg/m ³)	Measured Water Content (%)	fluid / soil	Measured Dry Density (Mg/m ³)	Salt Corrected Dry Density (Mg/m ³)
8.83	8.9	1.800	1.799	8.59	8.6	1.833	1.831	13.453	13.5	1.877	1.877
12.99	13.1	1.885	1.883	13.33	13.4	1.901	1.898	16.63	16.7	1.718	1.715
15.66	15.7	1.708	1.705	17.39	17.5	1.701	1.698	19.30	19.4	1.656	1.653
17.17	17.3	1.711	1.708	17.51	17.6	1.712	1.709	20.45	20.6	1.648	1.644
20.07	20.2	1.685	1.681	19.69	19.8	1.675	1.671	22.76	22.9	1.592	1.588
23.54	23.7	1.595	1.591	23.94	24.1	1.587	1.583	28.24	28.4	1.480	1.476
27.96	28.1	1.490	1.486	28.96	29.1	1.479	1.475	30.53	30.7	1.443	1.439
28.99	29.1	1.488	1.483	30.19	30.3	1.457	1.452				



		70 : 30		
Target Water Content (%)	Measured Water Content (%)	Fluid / Soil Mass Ratio (%)	Measured Dry Density (Mg/m ³)	Salt Corrected Dry Density (Mg/m ³)
15.65	16.25	16.3	1.630	1.628
18.04	18.29	18.4	1.686	1.682
20.25	22.04	22.1	1.644	1.640
24.85	24.51	24.6	1.578	1.574
25.59	25.65	25.8	1.552	1.548
25.77	27.33	27.5	1.521	1.516



80 : 20 A				80 : 20 B				80 : 20 C			
Measured Water Content (%)	fluid / soil	Measured Dry Density (Mg/m ³)	Salt Corrected Dry Density (Mg/m ³)	Measured Water Content (%)	fluid / soil	Measured Dry Density (Mg/m ³)	Salt Corrected Dry Density (Mg/m ³)	Measured Water Content (%)	fluid / soil	Measured Dry Density (Mg/m ³)	Salt Corrected Dry Density (Mg/m ³)
9.73	9.8	1.713	1.712	9.63	9.7	1.793	1.791	10.40	10.5	1.642	1.640
5.08	5.1	1.759	1.757	14.21	14.3	1.717	1.715	13.09	13.2	1.759	1.756
19.76	19.9	1.607	1.604	7.43	7.5	1.678	1.676	15.84	15.9	1.572	1.569
21.36	21.5	1.510	1.507	19.67	19.8	1.607	1.604	19.59	19.7	1.645	1.642
23.30	23.4	1.627	1.624	23.57	23.7	1.576	1.573	24.26	24.4	1.592	1.588
27.49	27.6	1.495	1.491	27.78	27.9	1.523	1.520	28.04	28.2	1.517	1.513
28.30	28.4	1.483	1.479	28.51	28.7	1.489	1.485	28.91	29.1	1.491	1.487
29.00	29.1	1.478	1.474	28.64	28.8	1.490	1.486	29.47	29.6	1.470	1.466

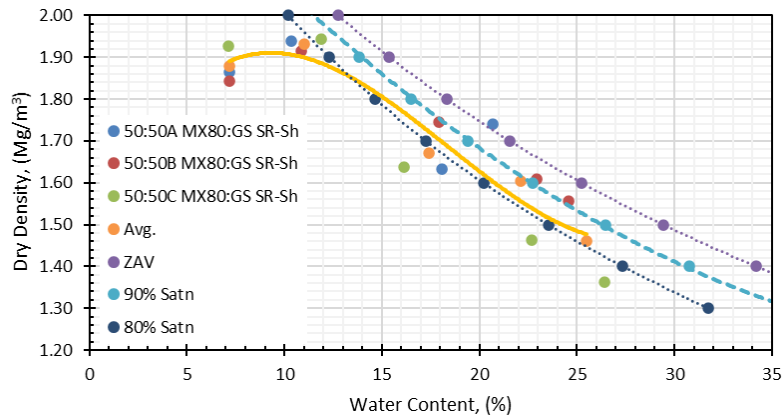


Notes:

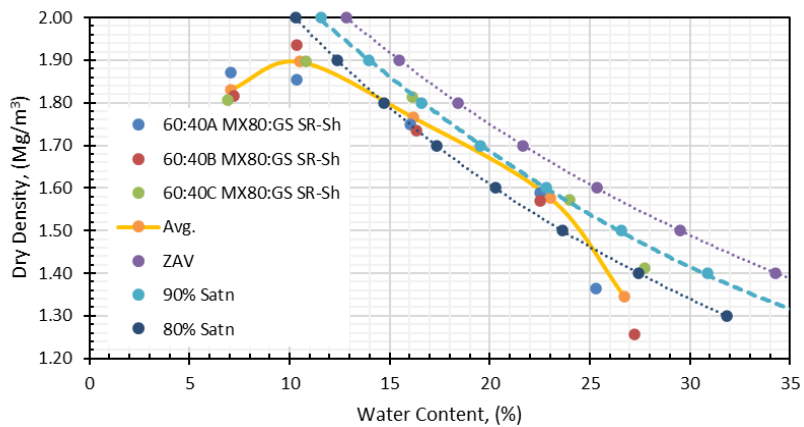
1. The maximum dry densities shown are for raw compaction data, conversion of measured maximum compacted dry density to MPMDD value requires use of equation $MPMDD = \text{measured MDD} \cdot 0.98 + 0.11$ (Dixon et al. 1985).
2. The data shown are for measured gravimetric water content and does not consider fluid mass or volume influences associated with the brine solution used in conditioning the materials

B-2 Modified Proctor: Miniature Compaction Test Results: MX80:GS – SR-Sh Solution

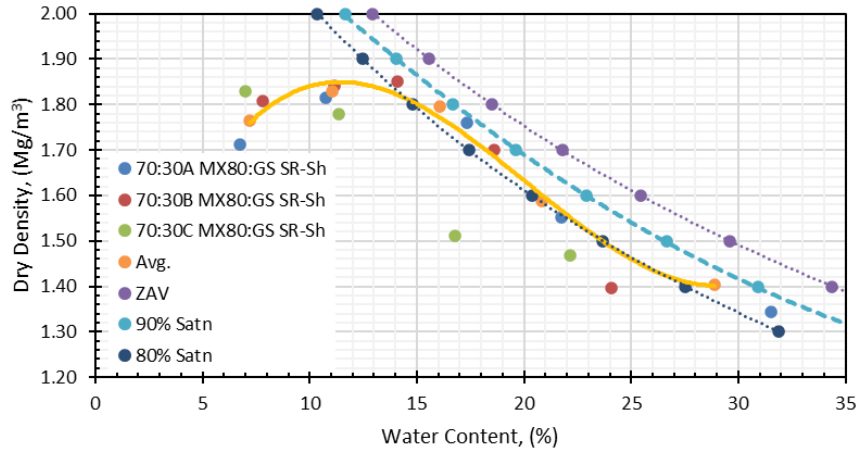
50:50A				50:50B				50:50C			
Sample Name	Measured Water Content (%)	Measured Dry Density (Mg/m ³)	Salt-Corrected Dry Density (Mg/m ³)	Sample Name	Measured Water Content (%)	Measured Dry Density (Mg/m ³)	Salt-Corrected Dry Density (Mg/m ³)	Sample Name	Measured Water Content (%)	Measured Dry Density (Mg/m ³)	Salt-Corrected Dry Density (Mg/m ³)
50/50 GS - SRSh - A - 1	7.20	1.913	1.865	50/50 GS - SRSh - A - 2	7.16	1.892	1.844	50/50 GS - SRSh - A - 3	7.12	1.976	1.927
50/50 GS - SRSh - B - 1	10.35	2.010	1.938	50/50 GS - SRSh - B - 2	10.88	1.989	1.914	50/50 GS - SRSh - B - 3	11.89	2.026	1.943
50/50 GS - SRSh - C - 1	18.09	1.740	1.633	50/50 GS - SRSh - C - 2	17.93	1.858	1.745	50/50 GS - SRSh - C - 3	16.15	1.732	1.637
50/50 GS - SRSh - D - 1	20.69	1.871	1.741	50/50 GS - SRSh - D - 2	22.95	1.743	1.610	50/50 GS - SRSh - D - 3	22.71	1.584	1.464
50/50 GS - SRSh - E - 1	sample lost			50/50 GS - SRSh - E - 2	24.56	1.693	1.556	50/50 GS - SRSh - E - 3	26.39	1.493	1.363



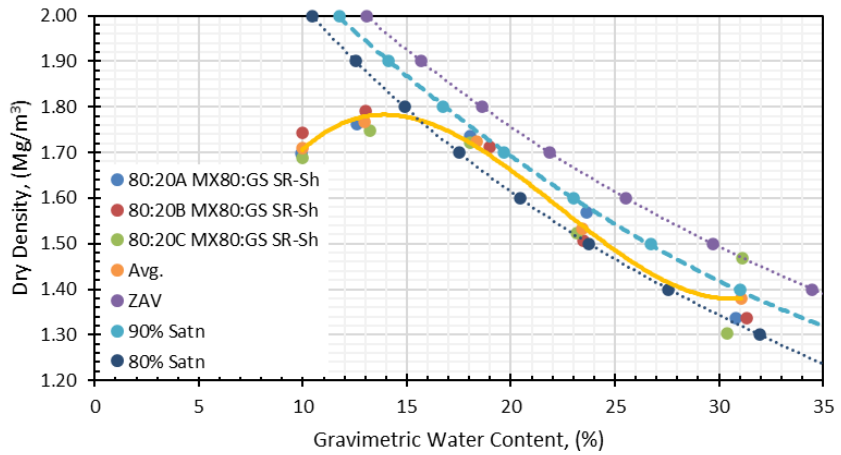
60:40A				60:40B				60:40C			
Sample Name	Measured Water Content (%)	Measured Dry Density (Mg/m ³)	Salt-Corrected Dry Density (Mg/m ³)	Sample Name	Measured Water Content (%)	Measured Dry Density (Mg/m ³)	Salt-Corrected Dry Density (Mg/m ³)	Sample Name	Measured Water Content (%)	Measured Dry Density (Mg/m ³)	Salt-Corrected Dry Density (Mg/m ³)
60/40 GS - SRSh - A - 1	7.04	1.919	1.871	60/40 GS - SRSh - A - 2	7.23	1.862	1.815	60/40 GS - SRSh - A - 3	6.93	1.851	1.806
60/40 GS - SRSh - B - 1	10.38	1.924	1.855	60/40 GS - SRSh - B - 2	10.33	2.009	1.937	60/40 GS - SRSh - B - 3	10.81	1.971	1.898
60/40 GS - SRSh - C - 1	16.03	1.851	1.750	60/40 GS - SRSh - C - 2	16.35	1.838	1.736	60/40 GS - SRSh - C - 3	16.15	1.918	1.813
60/40 GS - SRSh - D - 1	22.53	1.718	1.590	60/40 GS - SRSh - D - 2	22.52	1.698	1.571	60/40 GS - SRSh - D - 3	23.98	1.708	1.572
60/40 GS - SRSh - E - 1	25.30	1.487	1.363	60/40 GS - SRSh - E - 2	27.21	1.381	1.258	60/40 GS - SRSh - E - 3	27.73	1.554	1.413



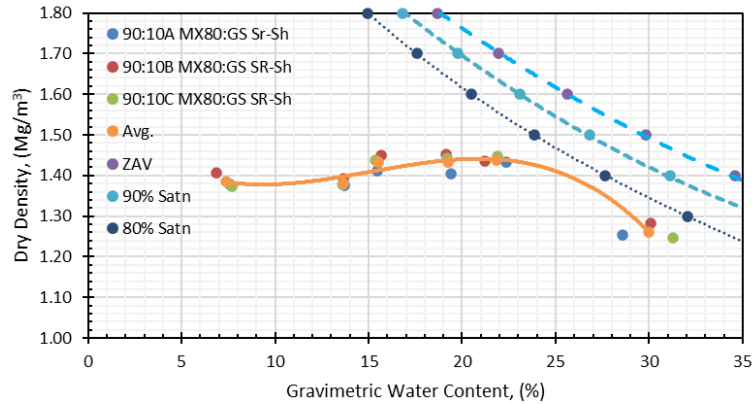
70:30A				70:30B				70:30C			
Sample Name	Measured Water Content (%)	Measured Dry Density (Mg/m ³)	Salt-Corrected Dry Density (Mg/m ³)	Sample Name	Measured Water Content (%)	Measured Dry Density (Mg/m ³)	Salt-Corrected Dry Density (Mg/m ³)	Sample Name	Measured Water Content (%)	Measured Dry Density (Mg/m ³)	Salt-Corrected Dry Density (Mg/m ³)
70/30 GS - SRSh - A - 1	6.72	1.753	1.712	70/30 GS - SRSh - A - 2	7.82	1.860	1.809	70/30 GS - SRSh - A - 3	7.00	1.821	1.776
70/30 GS - SRSh - B - 1	10.76	1.885	1.815	70/30 GS - SRSh - B - 2	11.13	1.916	1.842	70/30 GS - SRSh - B - 3	11.33	1.905	1.830
70/30 GS - SRSh - C - 1	17.35	1.869	1.759	70/30 GS - SRSh - C - 2	14.11	1.945	1.851	70/30 GS - SRSh - C - 3	16.77	1.887	1.780
70/30 GS - SRSh - D - 1	21.77	1.674	1.552	70/30 GS - SRSh - D - 2	18.62	1.814	1.700	70/30 GS - SRSh - D - 3	22.13	1.631	1.511
70/30 GS - SRSh - E - 1	31.53	1.495	1.343	70/30 GS - SRSh - E - 2	24.08	1.518	1.397	70/30 GS - SRSh - E - 3	31.10	1.634	1.469



80:20A				80:20B				80:20C			
Sample Name	Measured Water Content (%)	Measured Dry Density (Mg/m ³)	Salt-Corrected Dry Density (Mg/m ³)	Sample Name	Measured Water Content (%)	Measured Dry Density (Mg/m ³)	Salt-Corrected Dry Density (Mg/m ³)	Sample Name	Measured Water Content (%)	Measured Dry Density (Mg/m ³)	Salt-Corrected Dry Density (Mg/m ³)
80/20 GS - SRSh - A - 1	9.92	1.757	1.697	80/20 GS - SRSh - A - 2	9.96	1.806	1.744	80/20 GS - SRSh - A - 3	9.98	1.7484882	1.68783017
80/20 GS - SRSh - B - 1	12.59	1.842	1.762	80/20 GS - SRSh - B - 2	13.02	1.876	1.792	80/20 GS - SRSh - B - 3	13.21	1.8316783	1.74849796
80/20 GS - SRSh - C - 1	18.03	1.849	1.736	80/20 GS - SRSh - C - 2	18.96	1.830	1.713	80/20 GS - SRSh - C - 3	18.06	1.8348254	1.72282964
80/20 GS - SRSh - D - 1	23.66	1.703	1.569	80/20 GS - SRSh - D - 2	23.49	1.634	1.507	80/20 GS - SRSh - D - 3	23.17	1.6500909	1.52305591
80/20 GS - SRSh - E - 1	30.82	1.484	1.336	80/20 GS - SRSh - E - 2	31.34	1.487	1.336	80/20 GS - SRSh - E - 3	31.10	1.634	1.469
								80/20 GS - SRSh - E - 3	30.40	1.4464238	1.30374351



Sample Name	90 : 10 A					Sample Name	90 : 10 B					Sample Name	90 : 10 C			
	Measured Water Content (%)	Mass ratio Solution/Dry Soil (%)	Measured Dry Density (Mg/m ³)	Salt Corrected Dry Density (Mg/m ³)			Measured Water Content (%)	Mass ratio Solution/Dry Soil (%)	Measured Dry Density (Mg/m ³)	Salt Corrected Dry Density (Mg/m ³)			Measured Water Content (%)	Mass ratio Solution/Dry Soil (%)	Measured Dry Density (Mg/m ³)	Salt Corrected Dry Density (Mg/m ³)
90:10 MX80 GS - SRSh A1	7.59	9.25	1.419	1.377		90:10 MX80 GS - SRSh B1	6.87	8.37	1.449	1.406		90:10 MX80 GS - SRSh C1	7.68	9.26	1.414	1.373
90:10 MX80 GS - SRSh A2	13.71	16.71	1.446	1.375		90:10 MX80 GS - SRSh B2	13.64	16.62	1.463	1.392		90:10 MX80 GS - SRSh C2	13.62	15.74	1.447	1.377
90:10 MX80 GS - SRSh A3	15.49	18.87	1.498	1.411		90:10 MX80 GS - SRSh B3	15.66	19.08	1.541	1.451		90:10 MX80 GS - SRSh C3	15.36	19.07	1.526	1.437
90:10 MX80 GS - SRSh A4	19.38	23.62	1.503	1.404		90:10 MX80 GS - SRSh B4	19.14	23.32	1.554	1.451		90:10 MX80 GS - SRSh C4	19.22	21.85	1.544	1.442
90:10 MX80 GS - SRSh A5	22.36	27.25	1.548	1.434		90:10 MX80 GS - SRSh B5	21.23	25.88	1.550	1.436		90:10 MX80 GS - SRSh C5	21.88	24.44	1.561	1.447
90:10 MX80 GS - SRSh A6	28.57	34.82	1.383	1.255		90:10 MX80 GS - SRSh B6	30.09	36.67	1.414	1.283		90:10 MX80 GS - SRSh C6	31.29	31.48	1.374	1.247

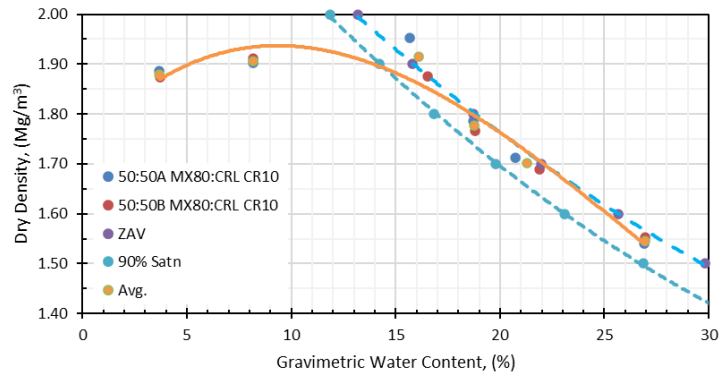


Notes:

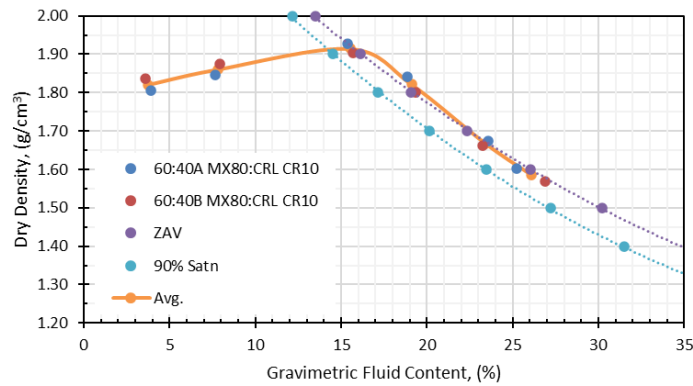
1. The maximum dry densities shown are for raw compaction data, conversion of measured maximum compacted dry density to MPMDD value requires use of equation $MPMDD = \text{measured MDD} \cdot 0.98 + 0.11$ (Dixon et al. 1985).
2. The data shown are for measured gravimetric water content and does not consider fluid mass or volume differences associated with the brine solution used in conditioning the materials

B-3 Modified Proctor: Miniature Compaction Test MX80:CRL - CR-10 Solution

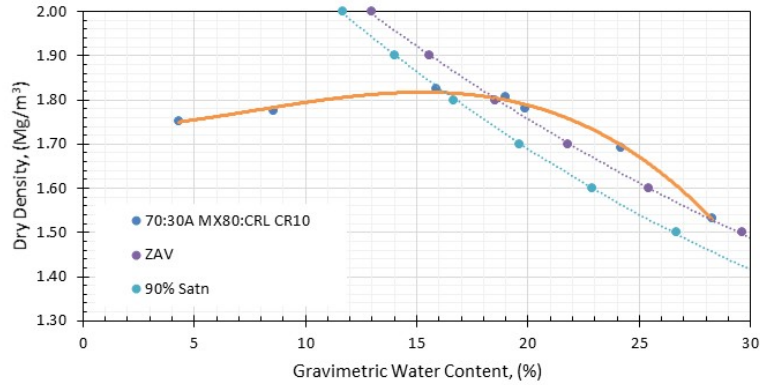
50 : 50 A				50 : 50 B			
Measured Water Content (%)	Fluid/Soil Mass Ratio (%)	Measured Dry Density (Mg/m ³)	Salt Corrected Dry Density (Mg/m ³)	Measured Water Content (%)	Fluid/Soil Mass Ratio (%)	Measured Dry Density (Mg/m ³)	Salt Corrected Dry Density (Mg/m ³)
3.7	3.7	1.886	1.885	3.7	3.7	1.875	1.874
8.2	8.2	1.904	1.902	8.2	8.2	1.912	1.911
15.7	15.8	1.957	1.953	16.5	16.6	1.878	1.875
18.7	18.8	1.791	1.786	18.8	18.9	1.771	1.767
20.7	20.8	1.717	1.712	21.9	22.0	1.694	1.690
26.9	27.1	1.545	1.540	27.0	27.1	1.557	1.552



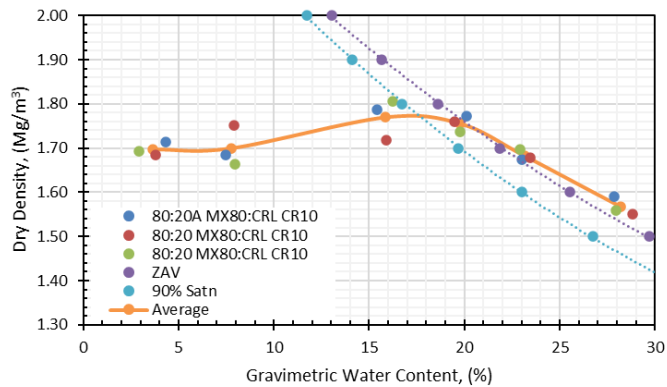
60 : 40 A				60 : 40 B			
Measured Water Content (%)	Fluid/Soil Mass Ratio (%)	Measured Dry Density (Mg/m ³)	Salt Corrected Dry Density (Mg/m ³)	Measured Water Content (%)	Fluid/Soil Mass Ratio (%)	Measured Dry Density (Mg/m ³)	Salt Corrected Dry Density (Mg/m ³)
3.90	3.9	1.806	1.805	3.58	3.6	1.838	1.837
7.61	7.6	1.848	1.846	7.90	7.9	1.877	1.875
15.30	15.4	1.930	1.927	15.61	15.7	1.906	1.902
18.75	18.8	1.846	1.842	19.26	19.4	1.805	1.801
23.45	23.6	1.678	1.673	23.14	23.3	1.667	1.663
25.13	25.3	1.607	1.602	26.78	26.9	1.575	1.570



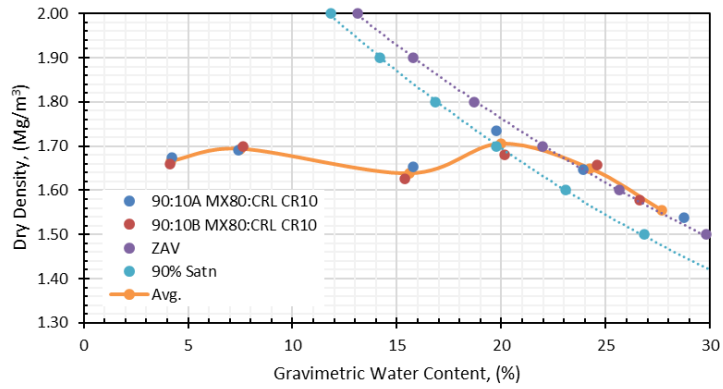
70 : 30			
Measured Water Content (%)	Fluid/Soil Mass Ratio (%)	Measured Dry Density (Mg/m ³)	Salt Corrected Dry Density (Mg/m ³)
4.30	4.3	1.754	1.753
8.54	8.6	1.778	1.776
15.90	16.0	1.827	1.824
18.97	19.1	1.811	1.807
19.86	20.0	1.786	1.782
24.20	24.3	1.697	1.692
28.25	28.4	1.537	1.532



80 : 20 A				80 : 20 B				80 : 20 C			
Measured Water Content (%)	Fluid/Soil Mass Ratio (%)	Measured Dry Density (Mg/m ³)	Salt Corrected Dry Density (Mg/m ³)	Measured Water Content (%)	Fluid/Soil Mass Ratio (%)	Measured Dry Density (Mg/m ³)	Salt Corrected Dry Density (Mg/m ³)	Measured Water Content (%)	Fluid/Soil Mass Ratio (%)	Measured Dry Density (Mg/m ³)	Salt Corrected Dry Density (Mg/m ³)
4.30	4.3	1.714	1.713	3.77	3.8	1.686	1.685	2.93	2.9	1.694	1.693
7.46	7.5	1.685	1.684	7.90	7.9	1.753	1.751	7.97	8.0	1.666	1.664
15.39	15.5	1.790	1.787	15.91	16.0	1.721	1.717	16.24	16.3	1.809	1.806
20.10	20.2	1.775	1.771	19.50	19.6	1.764	1.760	19.75	19.9	1.740	1.736
23.04	23.2	1.678	1.674	23.44	23.6	1.683	1.678	22.93	23.0	1.702	1.697
27.85	28.0	1.596	1.591	28.81	29.0	1.556	1.551	27.94	28.1	1.564	1.559



90:10 A				90:10 B			
Measured Water Content (%)	Fluid/Soil Mass Ratio (%)	Measured Dry Density (Mg/m ³)	Salt Corrected Dry Density (Mg/m ³)	Measured Water Content (%)	Fluid/Soil Mass Ratio (%)	Measured Dry Density (Mg/m ³)	Salt Corrected Dry Density (Mg/m ³)
4.21	4.2	1.674	1.673	4.12	4.1	1.661	1.660
7.41	7.4	1.690	1.688	7.62	7.7	1.701	1.699
15.76	15.8	1.653	1.650	15.40	15.5	1.630	1.627
19.75	19.8	1.734	1.731	20.17	20.3	1.684	1.680
23.91	24.0	1.646	1.642	24.57	24.7	1.662	1.658
28.74	28.9	1.538	1.533	26.61	26.7	1.582	1.577

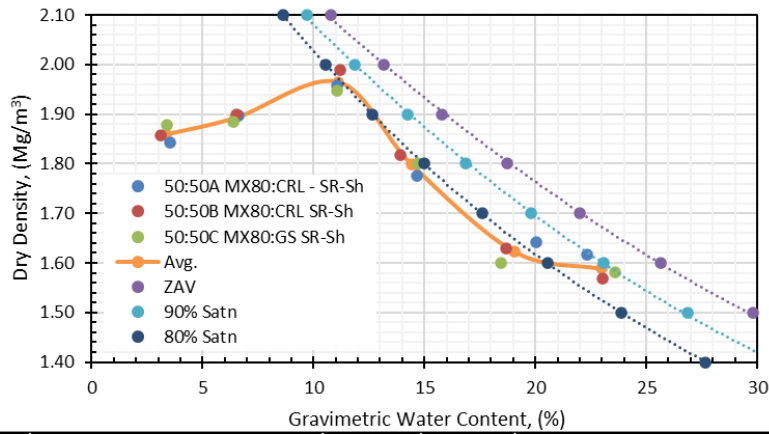


Notes:

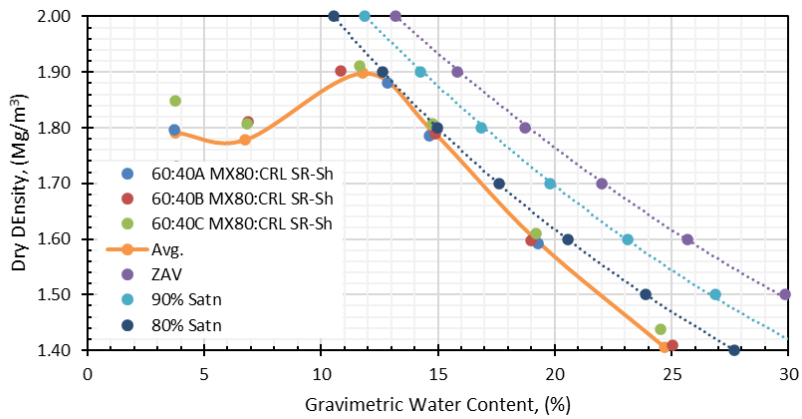
1. The maximum dry densities shown are for raw compaction data, conversion of measured maximum compacted dry density to MPMDD value requires use of equation $MPMDD = \text{measured MDD} \cdot 0.98 + 0.11$ (Dixon et al. 1985).
2. The data shown are for measured gravimetric water content and does not consider fluid mass or volume differences associated with the brine solution used in conditioning the materials

B-4 Modified Proctor: Miniature Compaction Test Data MX80:CRL – SR-Sh

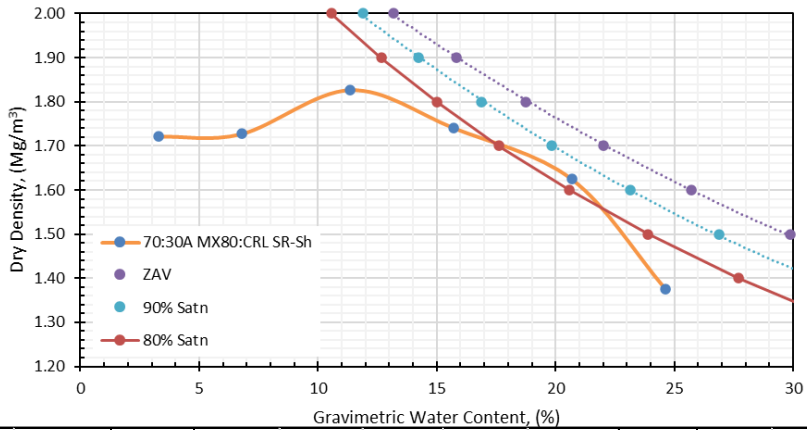
50/50A				WC mixed	50/50B				WC mixed	50/50C			
Measured Water Content (%)	Fluid/Soil Mass Ratio (%)	Measured Dry Density (Mg/m ³)	Salt Corrected Dry Density (Mg/m ³)		Measured Water Content (%)	Fluid/Soil Mass Ratio (%)	Measured Dry Density (Mg/m ³)	Salt Corrected Dry Density (Mg/m ³)		Measured Water Content (%)	Fluid/Soil Mass Ratio (%)	Measured Dry Density (Mg/m ³)	Salt Corrected Dry Density (Mg/m ³)
3.53	4.30	1.867	1.842	3.42	3.13	3.81	1.883	1.857	3.42	3.37	4.11	1.904	1.878
6.61	8.05	1.949	1.896	6.84	6.51	7.94	1.951	1.898	6.84	6.38	7.77	1.936	1.884
11.08	13.50	2.054	1.957	11.97	11.21	13.66	2.089	1.990	11.97	11.06	13.48	2.043	1.947
14.67	17.87	1.891	1.776	15.39	13.93	16.98	1.935	1.818	15.39	14.69	17.90	1.918	1.801
20.06	24.44	1.786	1.642	20.52	18.68	22.76	1.773	1.629	20.52	18.46	22.49	1.740	1.599
22.33	27.21	1.798	1.616	25.64	23.03	28.06	1.746	1.569	25.64	23.59	28.75	1.760	1.581



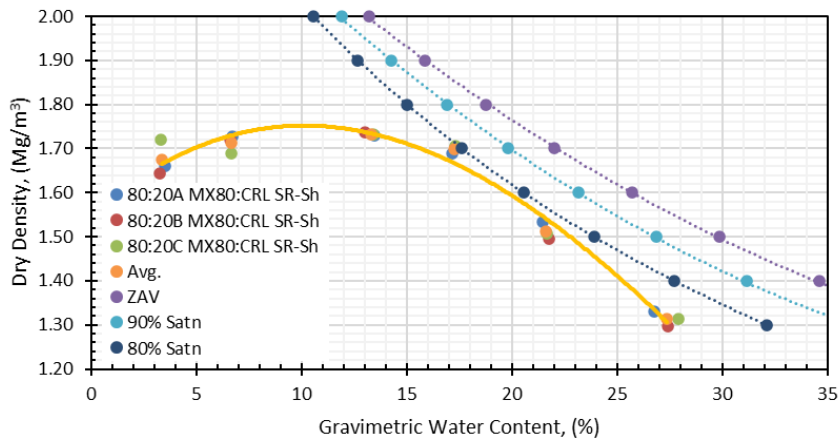
60/40A				WC mixed	60/40B				WC mixed	60/40C			
Measured Water Content (%)	Fluid/Soil Mass Ratio (%)	Measured Dry Density (Mg/m ³)	Salt Corrected Dry Density (Mg/m ³)		Measured Water Content (%)	Fluid/Soil Mass Ratio (%)	Measured Dry Density (Mg/m ³)	Salt Corrected Dry Density (Mg/m ³)		Measured Water Content (%)	Fluid/Soil Mass Ratio (%)	Measured Dry Density (Mg/m ³)	Salt Corrected Dry Density (Mg/m ³)
3.74	4.55	1.821	1.796	3.82	4.65	1.753	1.730	3.76	4.59	1.874	1.849		
6.58	8.02	1.763	1.716	6.87	8.38	1.861	1.811	6.84	8.34	1.858	1.808		
12.86	15.67	1.974	1.880	10.82	13.19	1.996	1.902	11.63	14.18	2.006	1.911		
14.62	17.82	1.901	1.786	14.91	18.17	1.906	1.790	14.75	17.98	1.925	1.808		
19.27	23.48	1.732	1.592	19.00	23.16	1.738	1.597	19.18	23.37	1.753	1.611		
24.58	29.95	1.534	1.368	25.02	30.49	1.579	1.408	24.51	29.87	1.612	1.438		



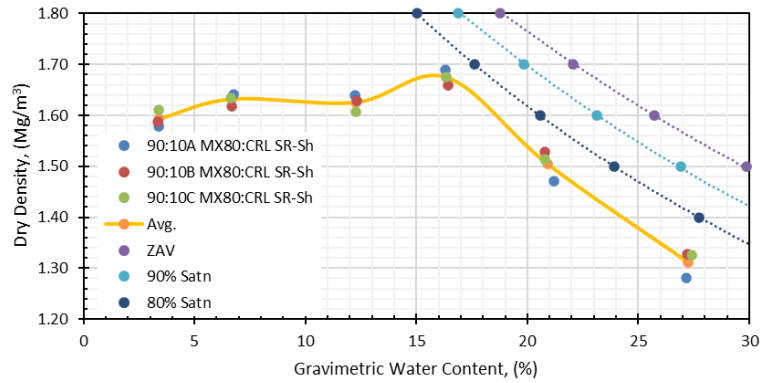
70/30				
Target water content (%)	Measured water content (%)	fluid / soil (%)	Measured Dry Density (g/cm ³)	Salt-corrected Dry Density (g/cm ³)
3.42	3.30	4.03	1.745	1.722
8.29	6.78	8.26	1.775	1.727
14.51	11.37	13.85	1.918	1.827
20.73	15.71	19.15	1.867	1.741
26.95	20.67	25.19	1.781	1.625
33.17	24.62	30.00	1.542	1.375



80/20A				80/20B					80/20C				
Measured Water Content (%)	Fluid/Soil Mass Ratio (%)	Measured Dry Density (Mg/m ³)	Salt Corrected Dry Density (Mg/m ³)	WC mixed	Measured Water Content (%)	Fluid/Soil Mass Ratio (%)	Measured Dry Density (Mg/m ³)	Salt Corrected Dry Density (Mg/m ³)	WC mixed	Measured Water Content (%)	Fluid/Soil Mass Ratio (%)	Measured Dry Density (Mg/m ³)	Salt Corrected Dry Density (Mg/m ³)
3.51	4.28	1.682	1.660	3.42	3.23	3.94	1.666	1.643	3.42	3.33	4.05	1.744	1.721
6.71	8.18	1.776	1.729	8.29	6.62	8.06	1.767	1.719	8.29	6.64	8.09	1.736	1.689
13.47	16.42	1.829	1.730	16.58	13.02	15.86	1.837	1.738	16.58	13.40	16.33	1.830	1.731
17.14	20.88	1.823	1.688	22.80	17.31	21.10	1.839	1.702	22.80	17.31	21.09	1.842	1.705
21.46	26.15	1.693	1.533	29.02	21.77	26.53	1.651	1.495	29.02	21.64	26.37	1.664	1.507
26.75	32.60	1.515	1.331	37.31	27.41	33.40	1.477	1.297	37.31	27.89	33.99	1.497	1.315



90/10A					90/10B					90/10C				
Target water content (%)	Measured water content (%)	fluid / soil (%)	Measured Dry Density (g/cm ³)	Salt-corrected Dry Density (g/cm ³)	Target water content (%)	Measured water content (%)	fluid / soil (%)	Measured Dry Density (g/cm ³)	Salt-corrected Dry Density (g/cm ³)	Target water content (%)	Measured water content (%)	fluid / soil (%)	Measured Dry Density (g/cm ³)	Salt-corrected Dry Density (g/cm ³)
3.42	3.41	4.15	1.601	1.579	3.42	3.36	4.09	1.610	1.588	3.42	3.38	4.11	1.633	1.611
8.29	6.75	8.23	1.687	1.642	8.29	6.69	8.16	1.664	1.619	8.29	6.63	8.08	1.680	1.635
16.58	12.21	14.88	1.734	1.640	16.58	12.31	15.00	1.721	1.628	16.58	12.29	14.98	1.699	1.608
22.80	16.31	19.87	1.825	1.690	22.80	16.41	20.00	1.792	1.659	22.80	16.37	19.94	1.809	1.675
29.02	21.21	25.84	1.624	1.471	29.02	20.78	25.32	1.687	1.528	29.02	20.79	25.33	1.672	1.514
37.31	27.15	33.08	1.458	1.281	37.31	27.20	33.15	1.511	1.327	37.31	27.42	33.42	1.509	1.325

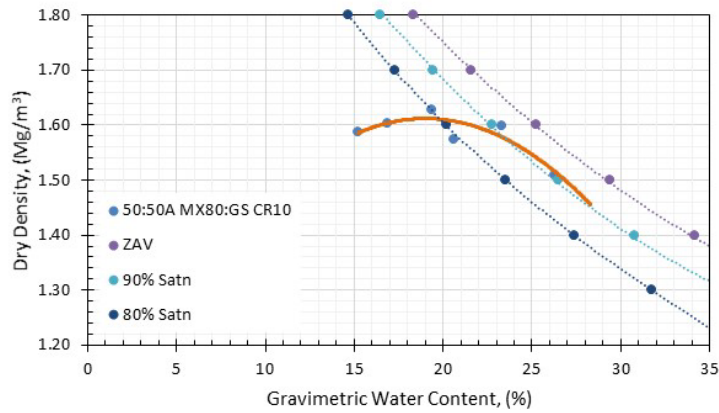


Notes:

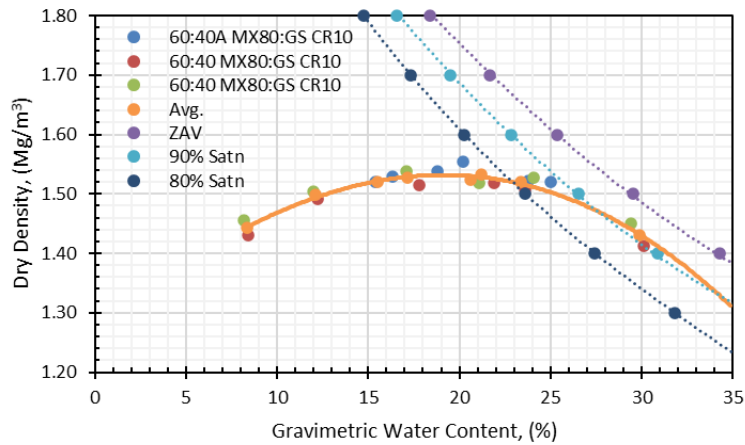
1. The maximum dry densities shown are for raw compaction data, conversion of measured maximum compacted dry density to MPMDD value requires use of equation $MPMDD = \text{measured MDD} \cdot 0.98 + 0.11$ (Dixon et al. 1985).
2. The data shown are for measured gravimetric water content and does not consider fluid mass or volume differences associated with the brine solution used in conditioning the materials

B-5 Standard Compaction Test Results MX80:GS – CR-10

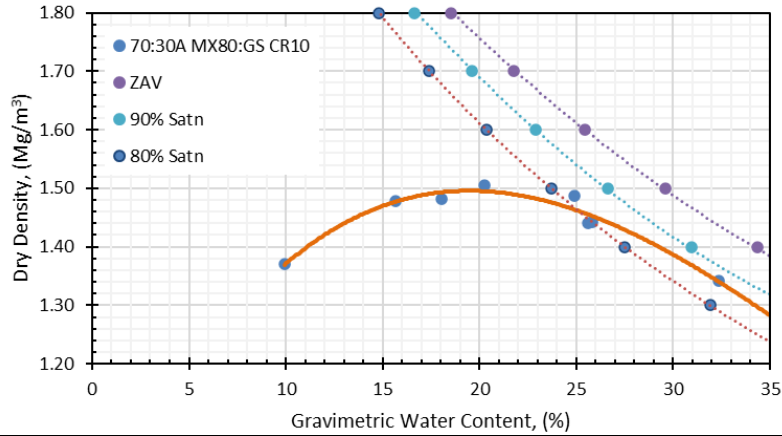
50 : 50 A				
Target Water Content (%)	Measured Water Content (%)	fluid / soil (%)	Measured Dry Density (g/cm3)	Salt-Corrected Dry Density (g/cm3)
15.66	19.4	19.5	1.631	1.628
18.06	23.3	23.4	1.603	1.600
20.08	26.3	26.4	1.513	1.510
20.27	15.2	15.3	1.590	1.586
24.88	16.9	17.0	1.608	1.604
27.64	20.6	20.7	1.580	1.575



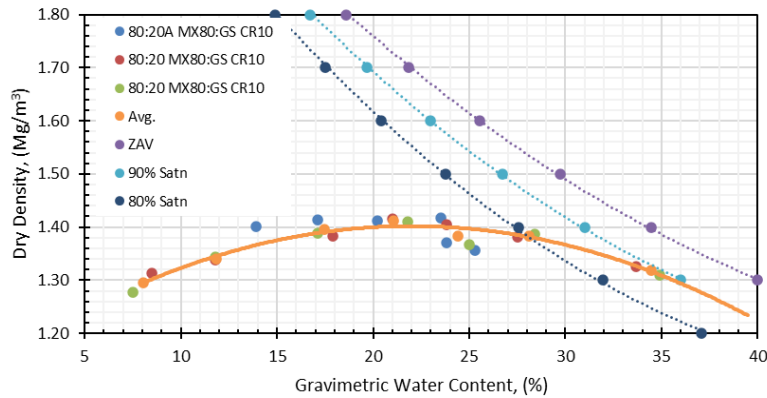
60: 40 A				60: 40 B				60: 40 C			
Measured Water Content (%)	fluid / soil (%)	Measured Dry Density (Mg/m³)	Salt-Corrected Dry Density (Mg/m³)	Measured Water Content (%)	fluid / soil (%)	Measured Dry Density (Mg/m³)	Salt-Corrected Dry Density (Mg/m³)	Measured Water Content (%)	fluid / soil (%)	Measured Dry Density (Mg/m³)	Salt-Corrected Dry Density (Mg/m³)
15.40	15.5	1.522	1.519	8.40	8.4	1.431	1.430	8.2	8.2	1.457	1.456
16.30	16.4	1.533	1.530	12.20	12.3	1.494	1.492	12.000	12.1	1.506	1.504
25.00	25.1	1.523	1.520	17.80	17.9	1.518	1.515	17.10	17.2	1.542	1.539
20.20	20.3	1.557	1.554	23.60	23.7	1.511	1.507	24.10	24.2	1.532	1.528
23.80	23.9	1.527	1.523	21.90	22.0	1.523	1.518	21.10	21.2	1.523	1.518
18.80	18.9	1.542	1.537	30.10	30.3	1.418	1.413	29.40	29.5	1.455	1.450



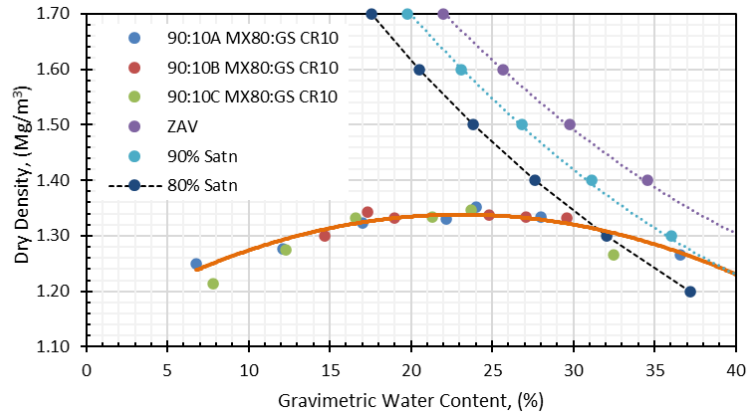
70 : 30			
Measured Water Content (%)	fluid / soil (%)	Measured Dry Density (Mg/m ³)	Salt-Corrected Dry Density (Mg/m ³)
11.50	11.6	1.372	1.370
14.50	14.6	1.480	1.477
15.80	15.9	1.485	1.482
18.60	18.7	1.509	1.506
23.40	23.5	1.492	1.488
20.40	20.5	1.444	1.440
22.30	22.4	1.446	1.442
33.60	33.8	1.347	1.342



80 : 20 A				80 : 20 B				80 : 20 C			
Measured Water Content (%)	fluid / soil (%)	Measured Dry Density (Mg/m ³)	Salt-Corrected Dry Density (Mg/m ³)	Measured Water Content (%)	fluid / soil (%)	Measured Dry Density (Mg/m ³)	Salt-Corrected Dry Density (Mg/m ³)	Measured Water Content (%)	fluid / soil (%)	Measured Dry Density (Mg/m ³)	Salt-Corrected Dry Density (Mg/m ³)
13.90	14.0	1.404	1.402	8.50	8.5	1.315	1.314	7.50	7.5	1.279	1.278
17.10	17.2	1.417	1.414	11.80	11.9	1.340	1.338	11.80	11.9	1.345	1.343
20.20	20.3	1.415	1.412	17.90	18.0	1.386	1.383	17.10	17.2	1.392	1.389
25.30	25.4	1.360	1.357	21.00	21.1	1.418	1.415	21.80	21.9	1.414	1.411
23.80	23.9	1.374	1.370	23.80	23.9	1.408	1.404	25.00	25.1	1.371	1.367
23.50	23.6	1.422	1.418	27.50	27.6	1.385	1.380	28.40	28.5	1.391	1.386
				33.70	33.9	1.331	1.326	34.90	35.1	1.315	1.310

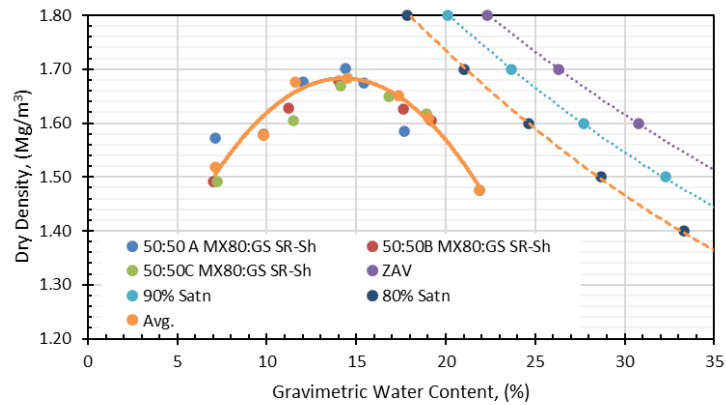


90:10 A				90:10 B				90:10 C			
Measured Water Content (%)	fluid / soil (%)	Measured Dry Density (Mg/m ³)	Salt-Corrected Dry Density (Mg/m ³)	Measured Water Content (%)	fluid / soil (%)	Measured Dry Density (Mg/m ³)	Salt-Corrected Dry Density (Mg/m ³)	Measured Water Content (%)	fluid / soil (%)	Measured Dry Density (Mg/m ³)	Salt-Corrected Dry Density (Mg/m ³)
6.80	6.8	1.249	1.247	14.70	14.8	1.301	1.300	7.80	7.8	1.214	1.213
12.10	12.2	1.276	1.273	17.30	17.4	1.344	1.342	12.30	12.4	1.277	1.275
17.00	17.1	1.323	1.320	19.00	19.1	1.334	1.331	16.60	16.7	1.334	1.331
22.20	22.3	1.331	1.327	24.80	24.9	1.340	1.337	21.30	21.4	1.337	1.334
24.00	24.1	1.352	1.348	27.10	27.2	1.337	1.333	23.70	23.8	1.351	1.347
28.00	28.1	1.334	1.329	29.60	29.7	1.336	1.332	32.50	32.7	1.270	1.266
36.60	36.8	1.265	1.260					41.80	42.0	1.204	1.199

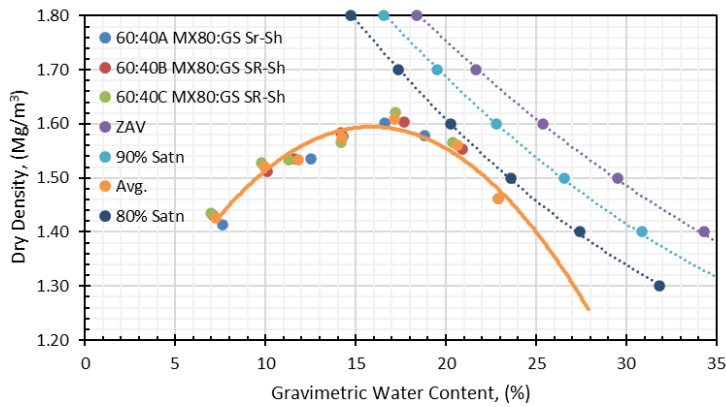


B-6 Standard Compaction Test Results MX80:GS – SR-Sh

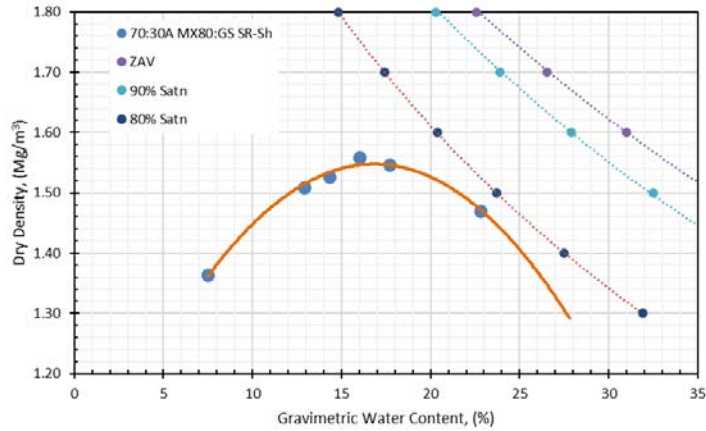
50 : 50 A				50 : 50 B				50 : 50 C			
Measured Water Content (%)	fluid / soil (%)	Measured Dry Density (Mg/m ³)	Salt-Corrected Dry Density (Mg/m ³)	Measured Water Content (%)	fluid / soil (%)	Measured Dry Density (Mg/m ³)	Salt-Corrected Dry Density (Mg/m ³)	Measured Water Content (%)	fluid / soil (%)	Measured Dry Density (Mg/m ³)	Salt-Corrected Dry Density (Mg/m ³)
7.10	8.65	1.621	1.572	7.00	8.53	1.532	1.491	7.20	8.77	1.533	1.492
12.00	14.62	1.766	1.676	9.80	11.94	1.643	1.579	9.80	11.94	1.642	1.578
14.40	17.55	1.814	1.702	11.20	13.65	1.705	1.628	11.50	14.01	1.681	1.605
15.40	18.77	1.802	1.674	14.00	17.06	1.780	1.679	14.10	17.18	1.770	1.669
17.70	21.57	1.721	1.585	17.60	21.45	1.753	1.627	16.80	20.47	1.778	1.650
21.90	26.69	1.587	1.475	19.20	23.40	1.702	1.605	18.90	23.03	1.714	1.616



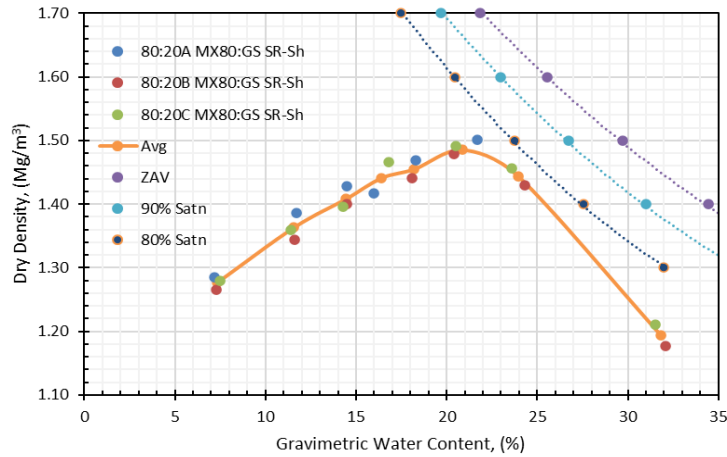
60 : 40 A				60 : 40 B				60 : 40 C			
Measured Water Content (%)	fluid / soil (%)	Measured Dry Density (Mg/m ³)	Salt-Corrected Dry Density (Mg/m ³)	Measured Water Content (%)	fluid / soil (%)	Measured Dry Density (Mg/m ³)	Salt-Corrected Dry Density (Mg/m ³)	Measured Water Content (%)	fluid / soil (%)	Measured Dry Density (Mg/m ³)	Salt-Corrected Dry Density (Mg/m ³)
7.60	9.26	1.457	1.413	7.10	8.65	1.471	1.431	7.00	8.53	1.474	1.434
12.50	15.23	1.617	1.535	10.10	12.31	1.573	1.512	9.80	11.94	1.591	1.529
14.30	17.43	1.681	1.577	11.60	14.14	1.607	1.535	11.30	13.77	1.605	1.533
16.60	20.23	1.723	1.601	14.20	17.30	1.679	1.583	14.20	17.30	1.661	1.566
18.80	22.91	1.715	1.579	17.70	21.57	1.727	1.603	17.20	20.96	1.747	1.621
22.90	27.91	1.574	1.463	20.90	25.47	1.647	1.553	20.40	24.86	1.661	1.566



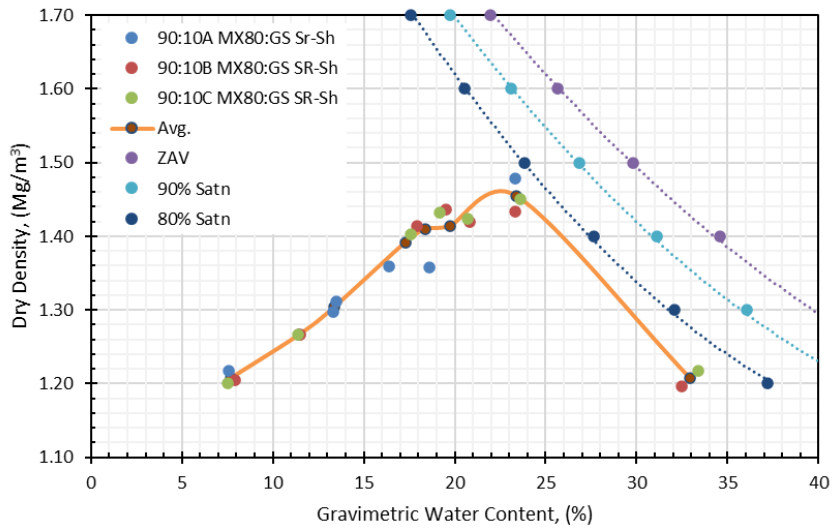
70 : 30			
Measured Water Content (%)	fluid / soil (%)	Measured Dry Density (Mg/m ³)	Salt-Corrected Dry Density (Mg/m ³)
7.50	9.14	1.402	1.364
12.90	15.72	1.57	1.509
14.30	17.43	1.598	1.526
16.00	19.50	1.653	1.559
17.70	21.57	1.666	1.546
22.80	27.78	1.559	1.470



80 : 20 A					80 : 20 B					80 : 20 C				
Target Water Content (%)	Measured Water Content (%)	fluid / soil (%)	Measured Dry Density (g/cm3)	Salt-Corrected Dry Density (g/cm3)	Target Water Content (%)	Measured Water Content (%)	fluid / soil (%)	Measured Dry Density (g/cm3)	Salt-Corrected Dry Density (g/cm3)	Target Water Content (%)	Measured Water Content (%)	fluid / soil (%)	Measured Dry Density (g/cm3)	Salt-Corrected Dry Density (g/cm3)
6.84	7.20	8.77	1.321	1.285	6.84	7.30	8.90	1.301	1.266	6.84	7.50	9.14	1.315	1.279
9.88	11.70	14.26	1.442	1.386	11.40	11.60	14.14	1.408	1.345	11.40	11.40	13.89	1.424	1.360
11.40	14.50	17.67	1.495	1.428	14.44	14.50	17.67	1.485	1.400	14.44	14.30	17.43	1.481	1.397
14.44	16.00	19.50	1.502	1.416	18.24	18.10	22.06	1.553	1.441	18.24	16.80	20.47	1.580	1.466
18.24	18.30	22.30	1.583	1.469	22.04	20.40	24.86	1.620	1.479	22.04	20.50	24.98	1.634	1.492
22.04	21.70	26.44	1.592	1.501	25.83	24.30	29.61	1.541	1.430	25.83	23.60	28.76	1.570	1.457
					32.82	32.10	39.12	1.353	1.178	32.82	31.50	38.39	1.391	1.211

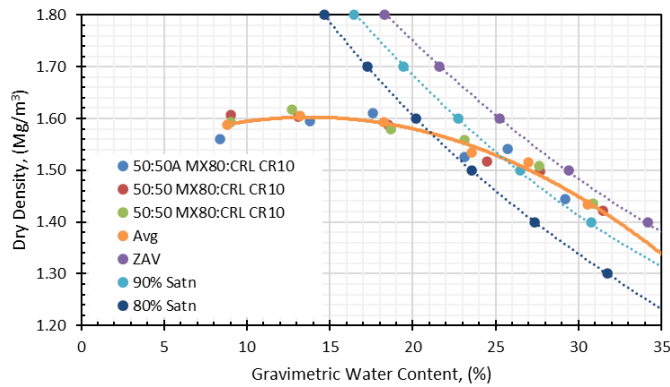


90:10 A				90:10 B				90:10 C			
Measured Water Content (%)	fluid / soil (%)	Measured Dry Density (Mg/m ³)	Salt-Corrected Dry Density (Mg/m ³)	Measured Water Content (%)	fluid / soil (%)	Measured Dry Density (Mg/m ³)	Salt-Corrected Dry Density (Mg/m ³)	Measured Water Content (%)	fluid / soil (%)	Measured Dry Density (Mg/m ³)	Salt-Corrected Dry Density (Mg/m ³)
7.60	9.26	1.251	1.217	7.90	9.63	1.238	1.205	7.50	9.14	1.234	1.201
13.30	16.21	1.350	1.297	11.50	14.01	1.327	1.267	11.40	13.89	1.326	1.266
13.50	16.45	1.374	1.312	17.90	21.81	1.500	1.415	17.60	21.45	1.487	1.402
16.40	19.99	1.442	1.360	19.50	23.76	1.548	1.437	19.20	23.40	1.544	1.433
18.60	22.67	1.463	1.358	20.80	25.35	1.555	1.420	20.70	25.23	1.560	1.424
23.30	28.39	1.568	1.479	23.30	28.39	1.545	1.434	23.60	28.76	1.563	1.450
				32.50	39.60	1.375	1.197	33.40	40.70	1.399	1.218

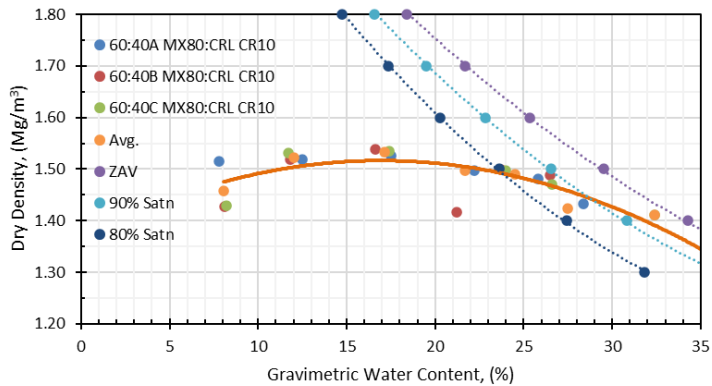


B-7 Standard Compaction Test Results MX80:CRL – CR-10

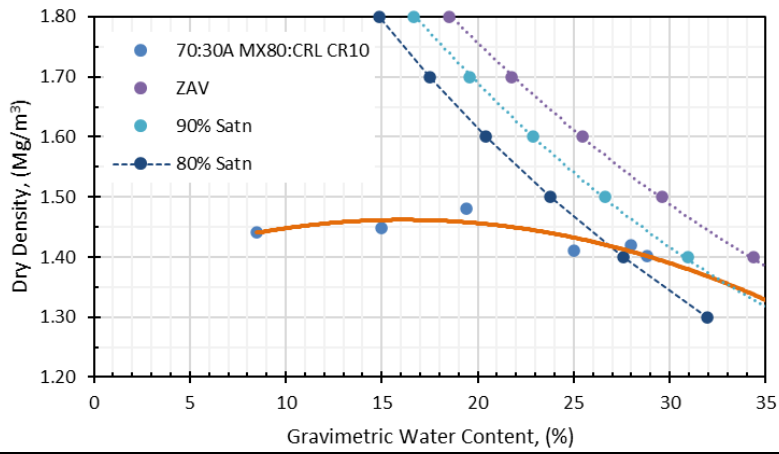
50 : 50 A				50 : 50 B				50 : 50 C			
Measured Water Content (%)	fluid / soil (%)	Measured Dry Density (Mg/m ³)	Salt-Corrected Dry Density (Mg/m ³)	Measured Water Content (%)	fluid / soil (%)	Measured Dry Density (Mg/m ³)	Salt-Corrected Dry Density (Mg/m ³)	Measured Water Content (%)	fluid / soil (%)	Measured Dry Density (Mg/m ³)	Salt-Corrected Dry Density (Mg/m ³)
8.4	8.4	1.562	1.561	9.0	9.0	1.608	1.607	9.00	9.0	1.595	1.594
13.8	13.9	1.597	1.595	13.1	13.2	1.606	1.604	12.70	12.8	1.619	1.617
17.6	17.7	1.613	1.610	18.5	18.6	1.590	1.587	18.70	18.8	1.583	1.580
23.1	23.2	1.529	1.525	24.5	24.6	1.521	1.517	23.10	23.2	1.562	1.558
25.7	25.8	1.546	1.542	27.7	27.8	1.503	1.499	27.60	27.7	1.512	1.508
29.2	29.3	1.449	1.444	31.5	31.7	1.427	1.422	30.90	31.1	1.440	1.435



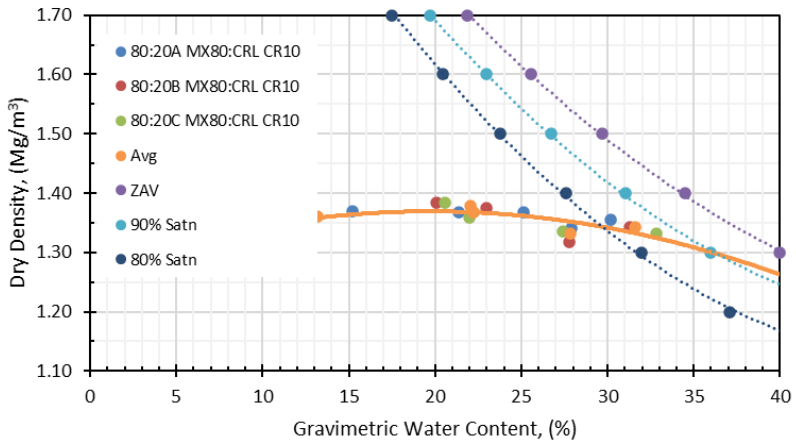
60 : 40 A					60 : 40 B					60 : 40 C				
Target Water Content (%)	Measured Water Content (%)	fluid / soil (%)	Measured Dry Density (g/cm3)	Salt-Corrected Dry Density (g/cm3)	Target Water Content (%)	Measured Water Content (%)	fluid / soil (%)	Measured Dry Density (g/cm3)	Salt-Corrected Dry Density (g/cm3)	Target Water Content (%)	Measured Water Content (%)	fluid / soil (%)	Measured Dry Density (g/cm3)	Salt-Corrected Dry Density (g/cm3)
6.45	7.80	7.8	1.517	1.516	7.37	8.10	8.1	1.429	1.428	7.37	8.20	8.2	1.430	1.429
11.98	12.50	12.6	1.520	1.518	11.06	11.80	11.9	1.521	1.519	11.06	11.70	11.8	1.534	1.532
17.51	17.50	17.6	1.528	1.525	16.58	16.60	16.7	1.542	1.539	16.58	17.40	17.5	1.537	1.534
22.11	22.20	22.3	1.500	1.496	22.11	26.50	26.6	1.492	1.488	22.11	24.00	24.1	1.501	1.497
25.80	25.80	25.9	1.485	1.481	25.80	23.70	23.8	1.504	1.500	25.80	26.60	26.7	1.474	1.470
29.48	28.40	28.5	1.437	1.432	29.48	21.20	21.3	1.421	1.416	29.48	32.40	32.6	1.415	1.410



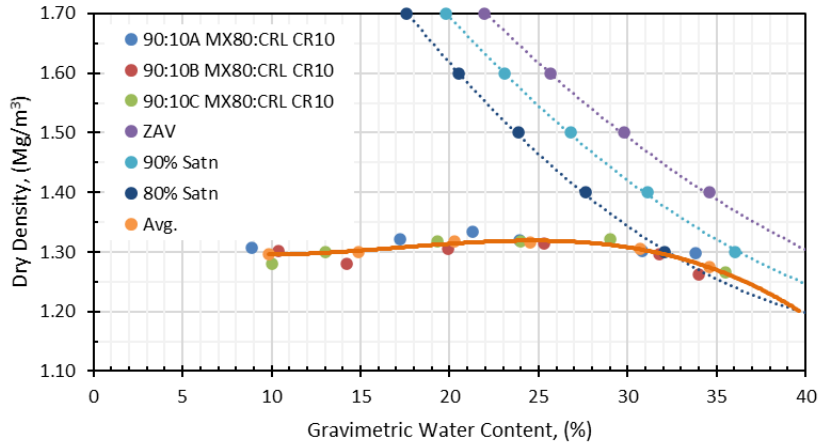
70 : 30				
Target Water Content (%)	Measured Water Content (%)	fluid / soil (%)	Measured Dry Density (g/cm3)	Salt-Corrected Dry Density (g/cm3)
6.45	8.50	8.5	1.443	1.442
11.98	15.00	15.1	1.451	1.449
17.51	19.40	19.5	1.483	1.480
22.11	28.80	28.9	1.405	1.402
25.80	28.00	28.1	1.423	1.419
29.48	25.00	25.1	1.416	1.411



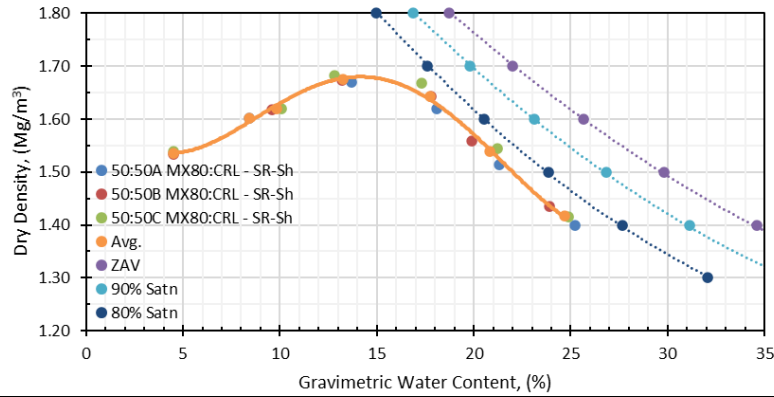
80 : 20 A				80 : 20 B				80 : 20 C			
Measured Water Content (%)	fluid / soil (%)	Measured Dry Density (Mg/m ³)	Salt-Corrected Dry Density (Mg/m ³)	Measured Water Content (%)	fluid / soil (%)	Measured Dry Density (Mg/m ³)	Salt-Corrected Dry Density (Mg/m ³)	Measured Water Content (%)	fluid / soil (%)	Measured Dry Density (Mg/m ³)	Salt-Corrected Dry Density (Mg/m ³)
10.00	10.1	1.375	1.374	9.80	9.8	1.324	1.323	9.60	9.6	1.328	1.327
15.20	15.3	1.372	1.370	12.00	12.1	1.352	1.350	12.20	12.3	1.361	1.359
25.10	25.2	1.371	1.368	20.10	20.2	1.386	1.383	20.60	20.7	1.387	1.384
21.40	21.5	1.371	1.368	23.00	23.1	1.379	1.376	22.00	22.1	1.363	1.360
27.90	28.0	1.345	1.341	27.80	27.9	1.322	1.318	27.40	27.5	1.340	1.336
30.20	30.4	1.359	1.355	31.30	31.5	1.348	1.343	32.80	33.0	1.336	1.331



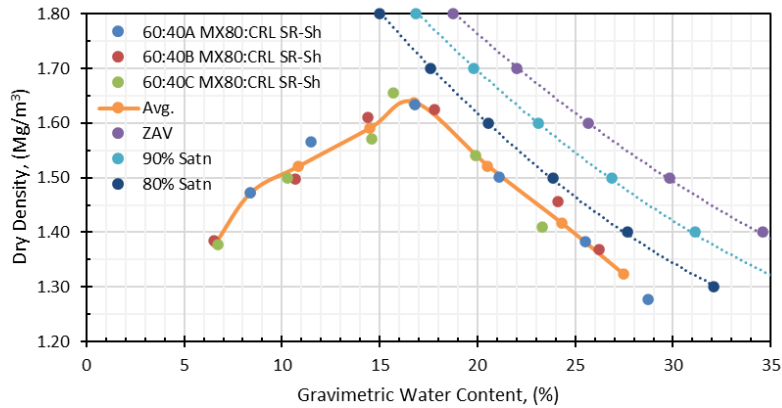
90:10A				90:10B				90:10C			
Measured Water Content (%)	fluid / soil (%)	Measured Dry Density (Mg/m ³)	Salt-Corrected Dry Density (Mg/m ³)	Measured Water Content (%)	fluid / soil (%)	Measured Dry Density (Mg/m ³)	Salt-Corrected Dry Density (Mg/m ³)	Measured Water Content (%)	fluid / soil (%)	Measured Dry Density (Mg/m ³)	Salt-Corrected Dry Density (Mg/m ³)
8.90	8.9	1.307	1.306	10.40	10.5	1.303	1.302	10.00	10.1	1.282	1.281
17.20	17.3	1.321	1.319	14.20	14.3	1.281	1.279	13.00	13.1	1.302	1.300
21.30	21.4	1.334	1.331	19.90	20.0	1.308	1.305	19.30	19.4	1.321	1.318
23.90	24.0	1.319	1.316	25.30	25.4	1.317	1.314	24.00	24.1	1.322	1.319
30.80	31.0	1.301	1.297	31.80	32.0	1.300	1.296	29.00	29.1	1.326	1.322
33.80	34.0	1.298	1.294	34.00	34.2	1.266	1.262	35.50	35.7	1.271	1.267



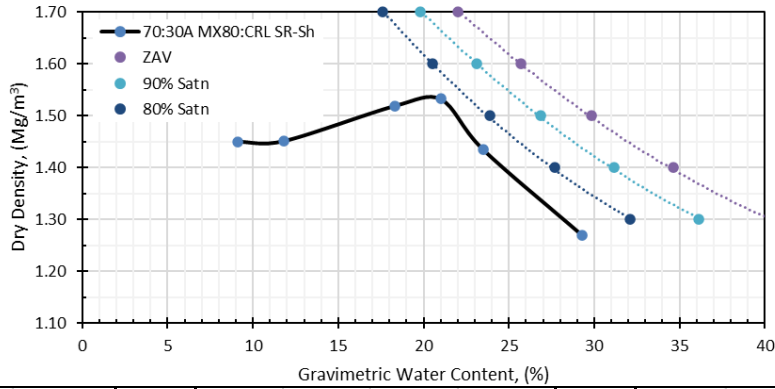
50:50 A				50:50 B				50:50 C			
Measured Water Content (%)	fluid / soil (%)	Measured Dry Density (Mg/m ³)	Salt-Corrected Dry Density (Mg/m ³)	Measured Water Content (%)	fluid / soil (%)	Measured Dry Density (Mg/m ³)	Salt-Corrected Dry Density (Mg/m ³)	Measured Water Content (%)	fluid / soil (%)	Measured Dry Density (Mg/m ³)	Salt-Corrected Dry Density (Mg/m ³)
8.40	10.24	1.642	1.603	4.50	5.48	1.561	1.533	4.50	5.48	1.567	1.539
13.70	16.69	1.748	1.669	9.60	11.70	1.679	1.619	10.10	12.31	1.681	1.620
18.10	22.06	1.739	1.619	13.20	16.09	1.770	1.674	12.80	15.60	1.778	1.682
21.30	25.96	1.658	1.514	17.80	21.69	1.770	1.643	17.30	21.08	1.798	1.669
25.20	30.71	1.559	1.400	19.90	24.25	1.701	1.558	21.20	25.83	1.686	1.544
				23.90	29.12	1.603	1.435	24.90	30.34	1.581	1.415



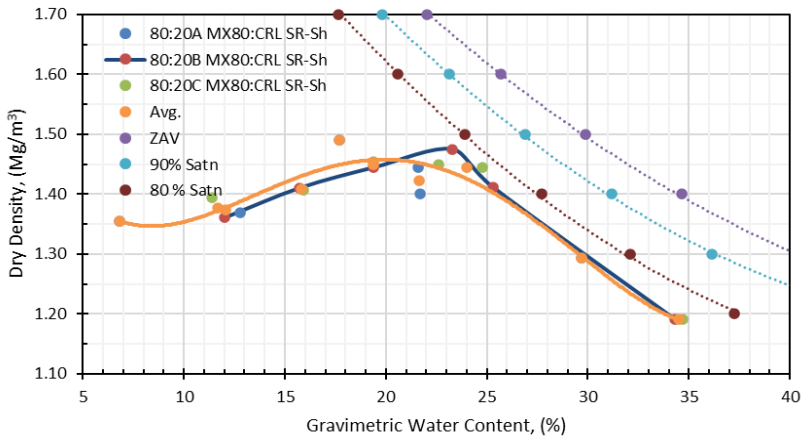
60:40 A					60:40 B					60:40 C				
Target Water Content (%)	Measured Water Content (%)	fluid / soil (%)	Measured Dry Density (g/cm3)	Salt-Corrected Dry Density (g/cm3)	Target Water Content (%)	Measured Water Content (%)	fluid / soil (%)	Measured Dry Density (g/cm3)	Salt-Corrected Dry Density (g/cm3)	Target Water Content (%)	Measured Water Content (%)	fluid / soil (%)	Measured Dry Density (g/cm3)	Salt-Corrected Dry Density (g/cm3)
6.08	8.40	10.24	1.509	1.473	6.08	6.50	7.92	1.418	1.384	6.08	6.70	8.16	1.411	1.377
11.40	11.50	14.01	1.639	1.565	10.64	10.70	13.04	1.563	1.497	10.64	10.30	12.55	1.565	1.499
17.48	16.80	20.47	1.756	1.635	15.20	14.40	17.55	1.714	1.611	15.20	14.60	17.79	1.671	1.571
22.04	21.10	25.71	1.645	1.502	18.24	17.80	21.69	1.751	1.625	18.24	15.70	19.13	1.783	1.655
25.83	25.50	31.07	1.539	1.382	22.79	24.10	29.37	1.600	1.456	22.79	19.90	24.25	1.694	1.542
31.15	28.70	34.97	1.457	1.278	27.35	26.20	31.93	1.534	1.368	27.35	23.30	28.39	1.581	1.410



70:30			
Measured Water Content (%)	fluid / soil (%)	Measured Dry Density (Mg/m ³)	Salt-Corrected Dry Density (Mg/m ³)
9.10	11.09	1.486	1.450
11.80	14.38	1.52	1.452
18.30	22.30	1.664	1.519
21.00	25.59	1.646	1.532
23.50	28.64	1.598	1.435
29.30	35.70	1.448	1.270

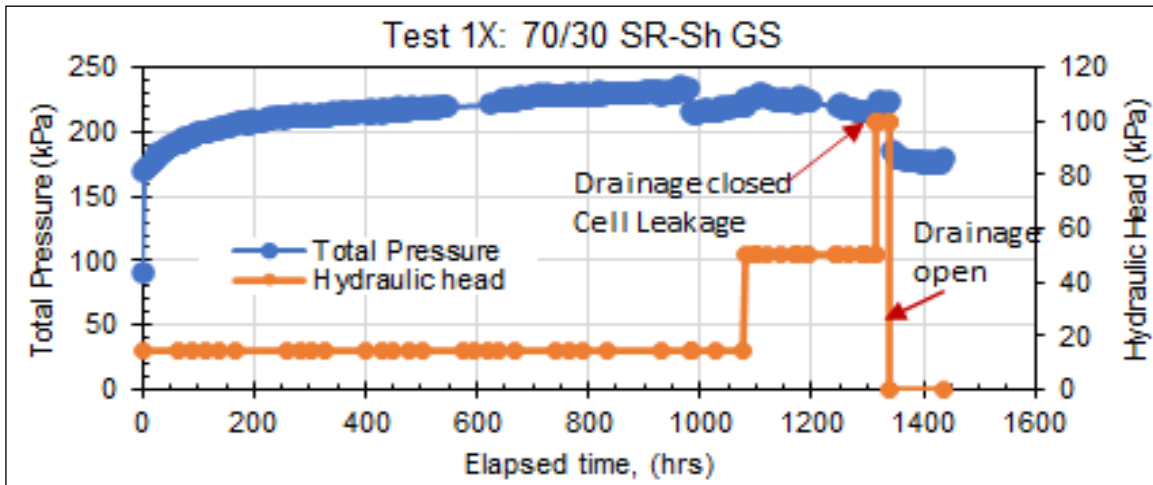


80:20 A				80:20 B				80:20 C			
Measured Water Content (%)	fluid / soil (%)	Measured Dry Density (Mg/m ³)	Salt-Corrected Dry Density (Mg/m ³)	Measured Water Content (%)	fluid / soil (%)	Measured Dry Density (Mg/m ³)	Salt-Corrected Dry Density (Mg/m ³)	Measured Water Content (%)	fluid / soil (%)	Measured Dry Density (Mg/m ³)	Salt-Corrected Dry Density (Mg/m ³)
6.80	8.29	1.389	1.356	12.00	14.62	1.394	1.361	11.40	13.89	1.428	1.394
12.80	15.60	1.433	1.369	15.70	19.13	1.472	1.410	15.90	19.38	1.468	1.406
17.70	21.57	1.600	1.490	19.40	23.64	1.537	1.445	19.40	23.64	1.547	1.454
21.60	26.32	1.582	1.444	23.30	28.39	1.600	1.475	24.80	30.22	1.567	1.445
29.70	36.19	1.440	1.293	25.30	30.83	1.561	1.411	22.60	27.54	1.603	1.449
21.70	26.44	1.597	1.401	34.30	41.80	1.353	1.191	34.70	42.29	1.353	1.191

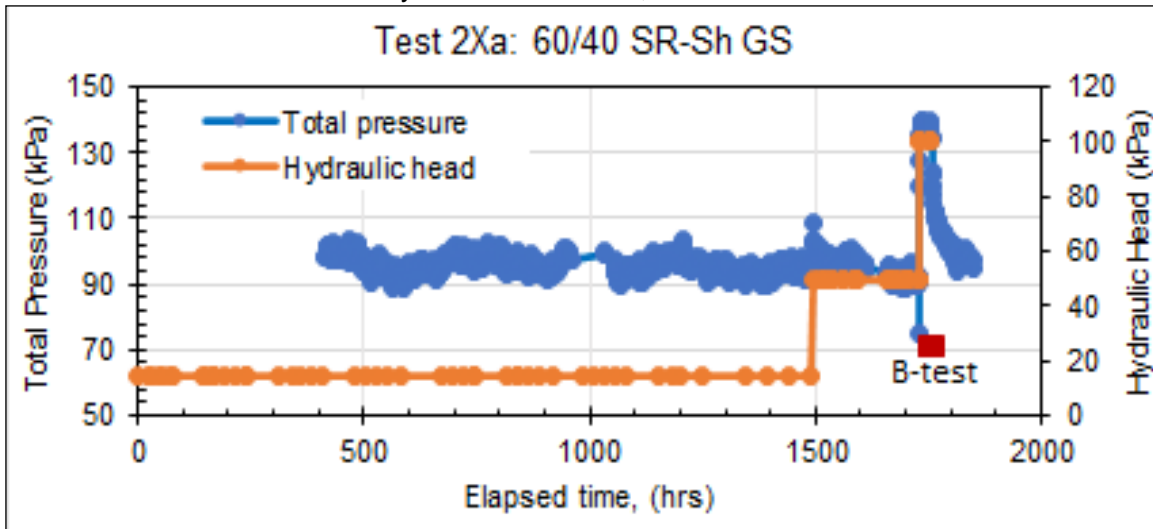


90:10 A				90:10 B				90:10 C			
Measured Water Content (%)	fluid / soil (%)	Measured Dry Density (Mg/m ³)	Salt-Corrected Dry Density (Mg/m ³)	Measured Water Content (%)	fluid / soil (%)	Measured Dry Density (Mg/m ³)	Salt-Corrected Dry Density (Mg/m ³)	Measured Water Content (%)	fluid / soil (%)	Measured Dry Density (Mg/m ³)	Salt-Corrected Dry Density (Mg/m ³)
7.70	9.38	1.327	1.295	7.20	8.77	1.276	1.245	6.20	7.56	1.292	1.261
11.20	13.65	1.371	1.309	10.80	13.16	1.340	1.284	11.40	13.89	1.320	1.265
18.20	22.18	1.490	1.387	15.20	18.52	1.398	1.314	14.90	18.16	1.385	1.302
20.90	25.47	1.543	1.409	19.20	23.40	1.486	1.370	19.20	23.40	1.487	1.371
28.80	35.10	1.455	1.307	26.50	32.29	1.512	1.358	27.30	33.27	1.517	1.362
25.10	30.59	1.536	1.347	31.60	38.51	1.394	1.227	29.90	36.44	1.440	1.267

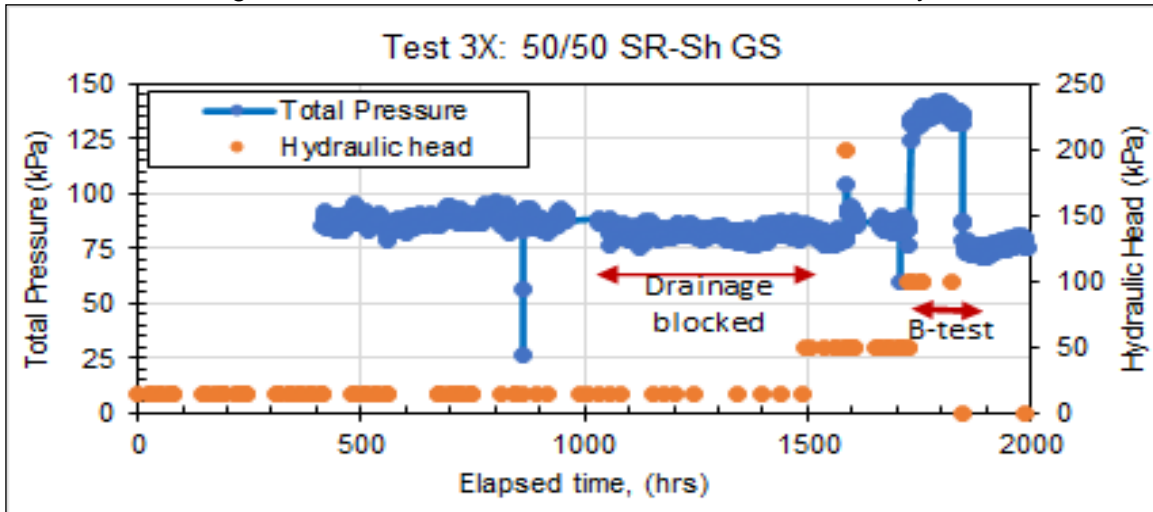
APPENDIX C: Swelling Pressure Plots

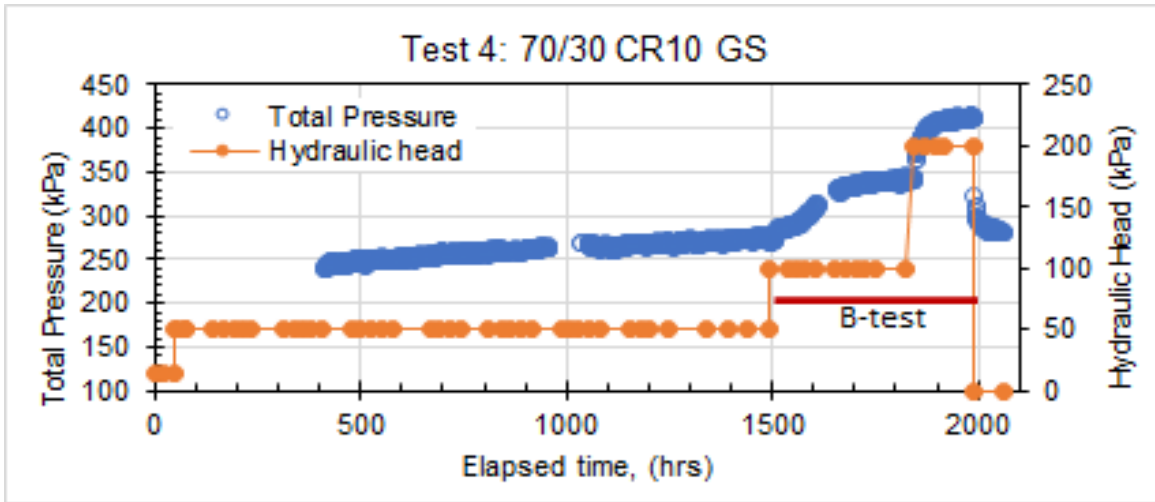


Ps is based on 0 and 15 kPa hydraulic head data,

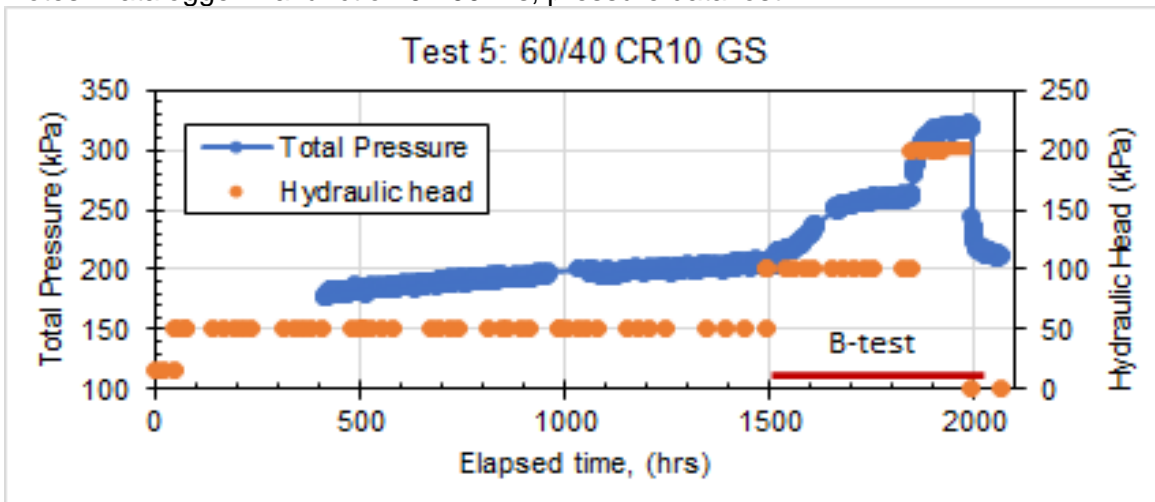


Notes: Cell leaking @ end of test @ 100 kPa. Ps is based on 15 kPa hydraulic head data.

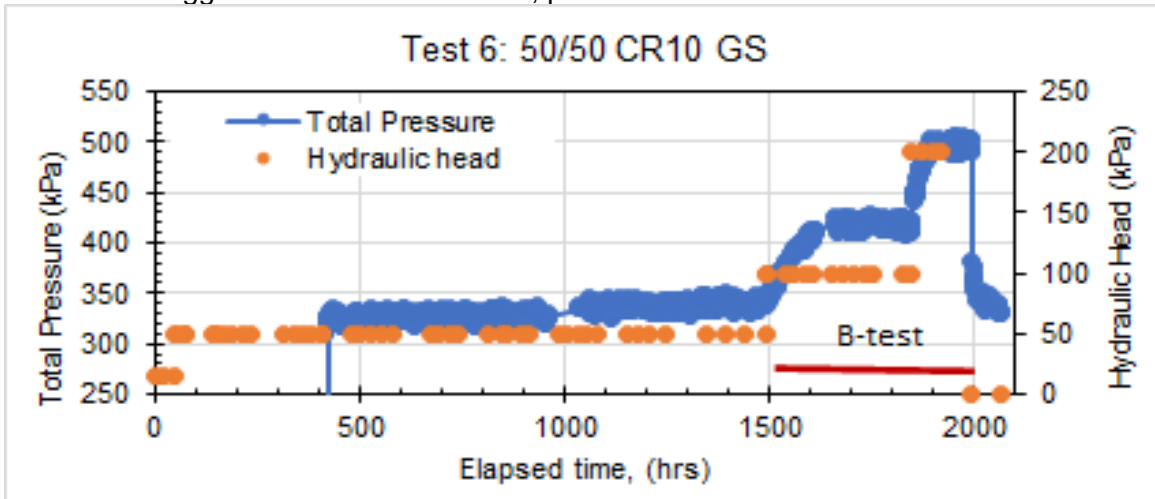




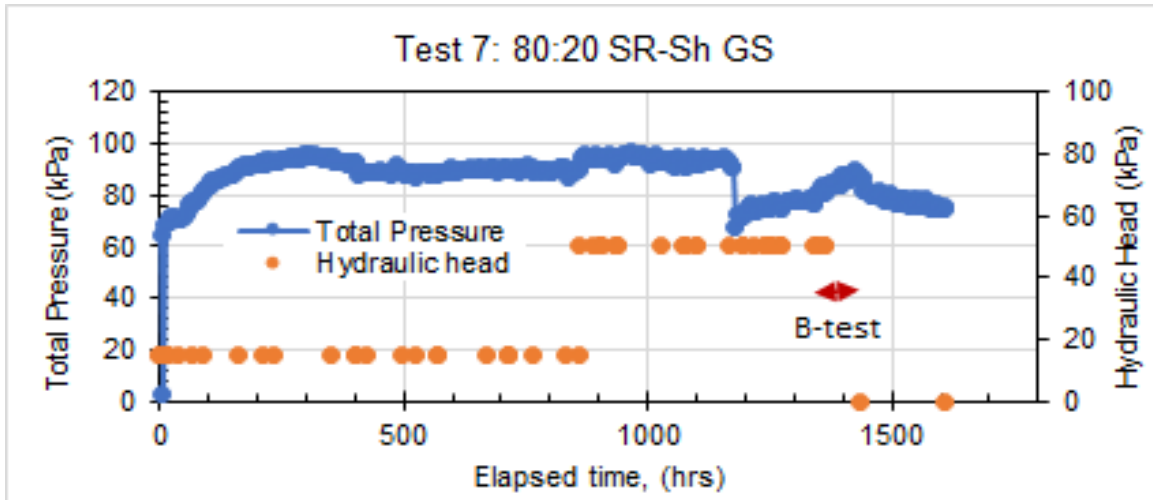
Notes: Datalogger malfunction 0-400 hrs, pressure data lost.



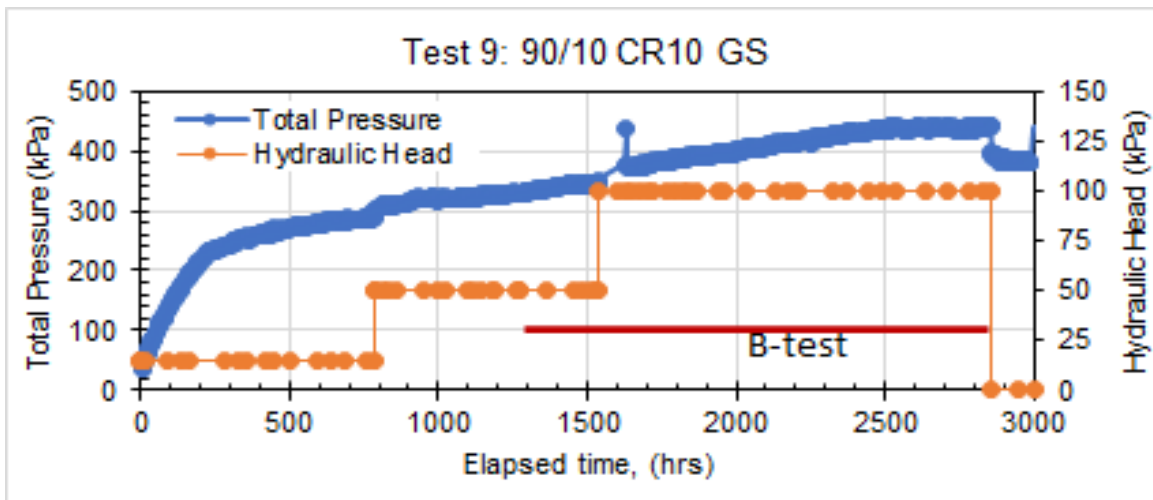
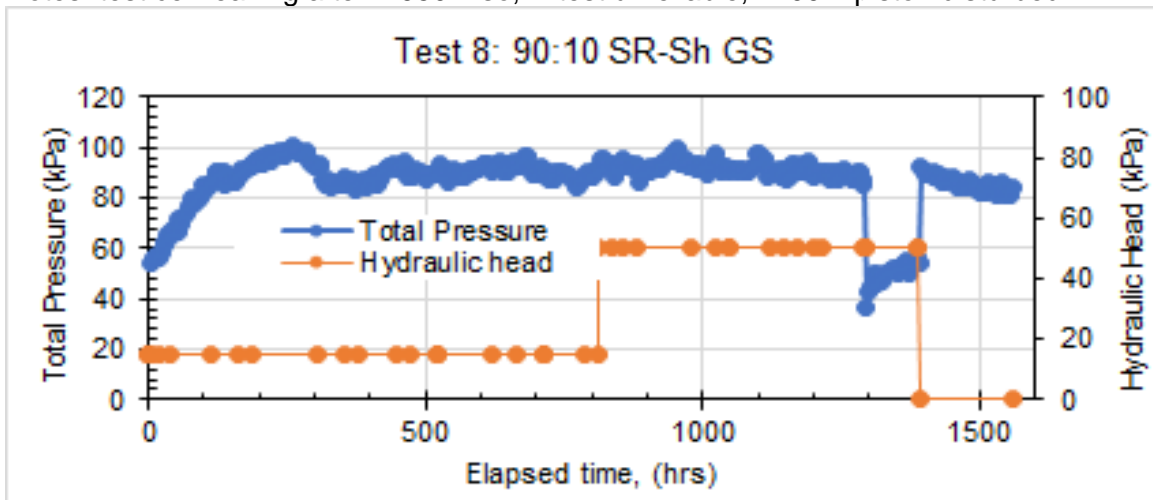
Notes: Datalogger malfunction 0-400 hrs, pressure data lost.

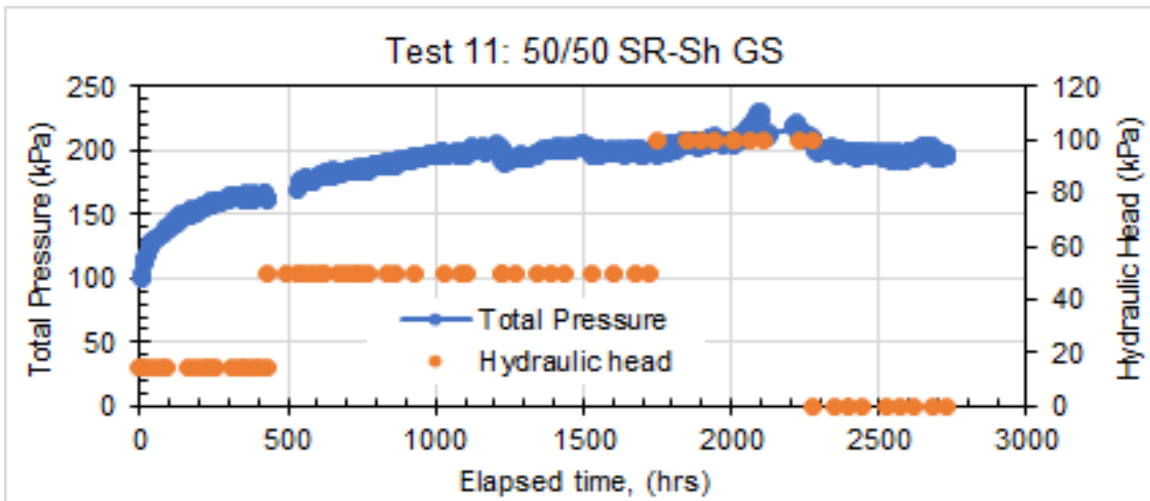
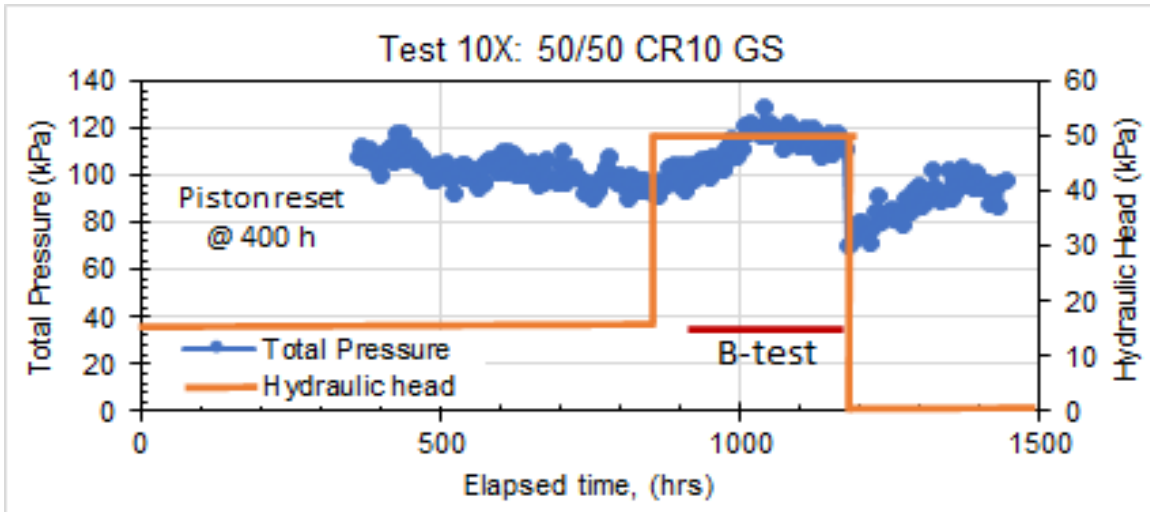


Notes: Datalogger malfunction 0-400 hrs, pressure data lost.

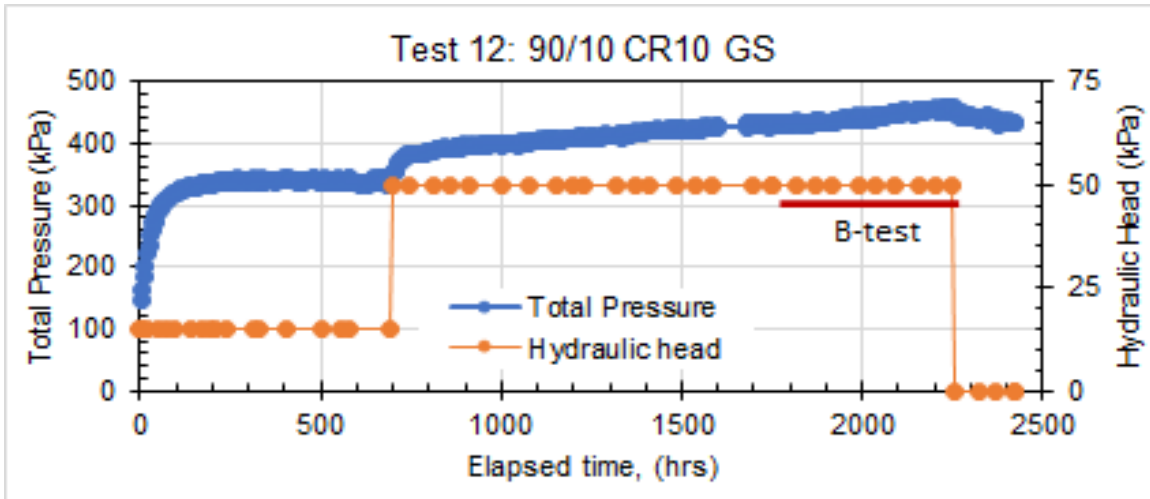


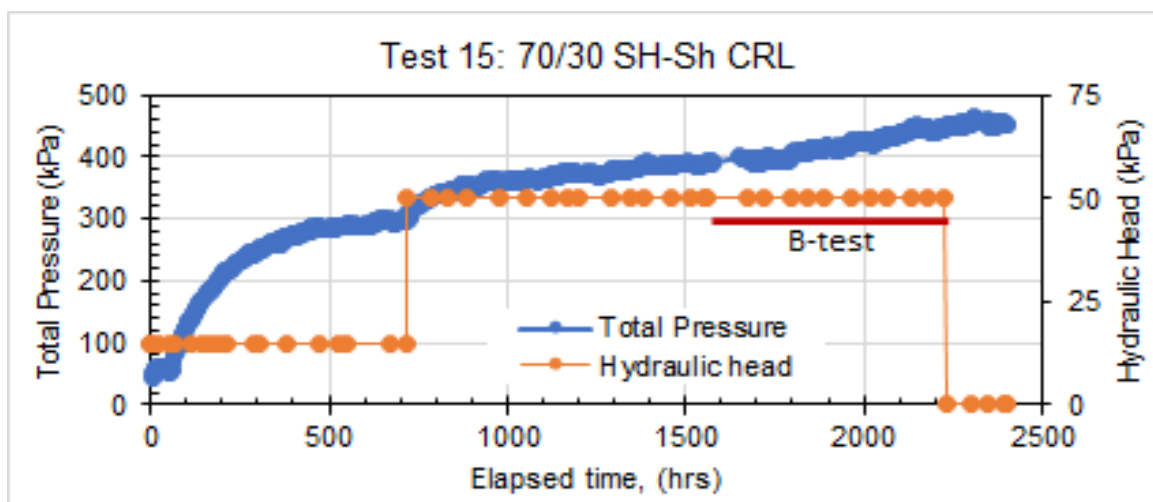
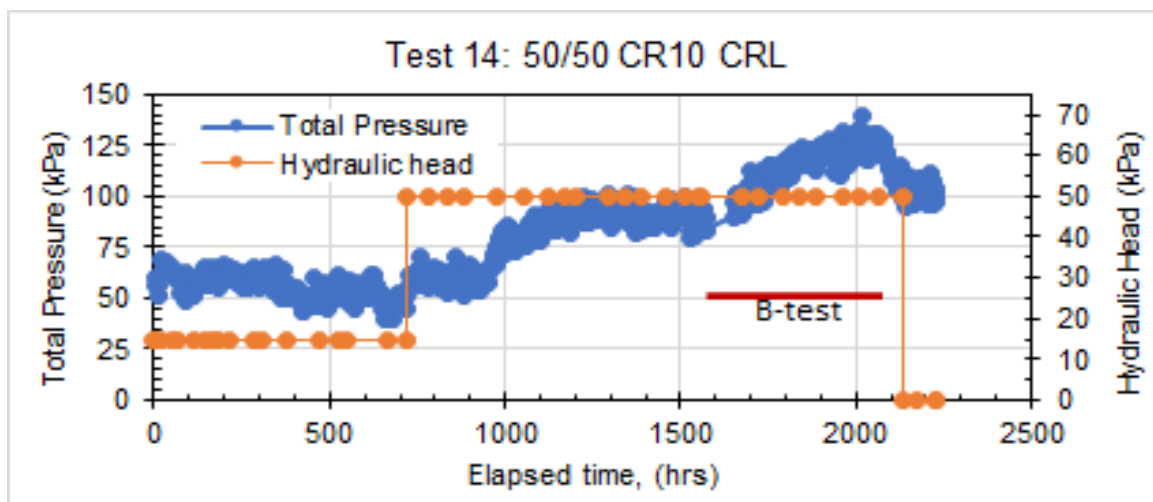
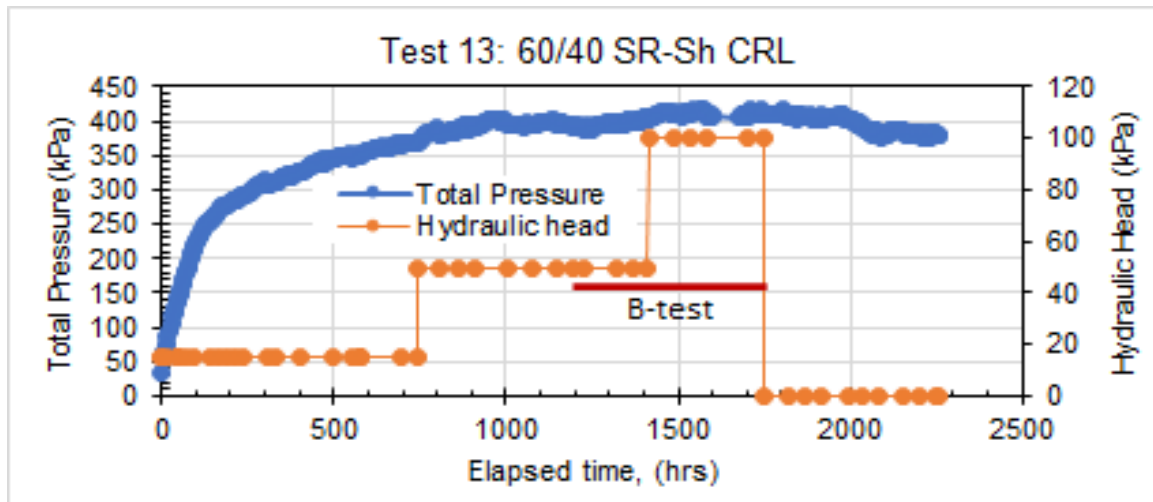
Notes: test cell leaking after ~ 950 h so, B-test unreliable, 1200 h piston disturbed

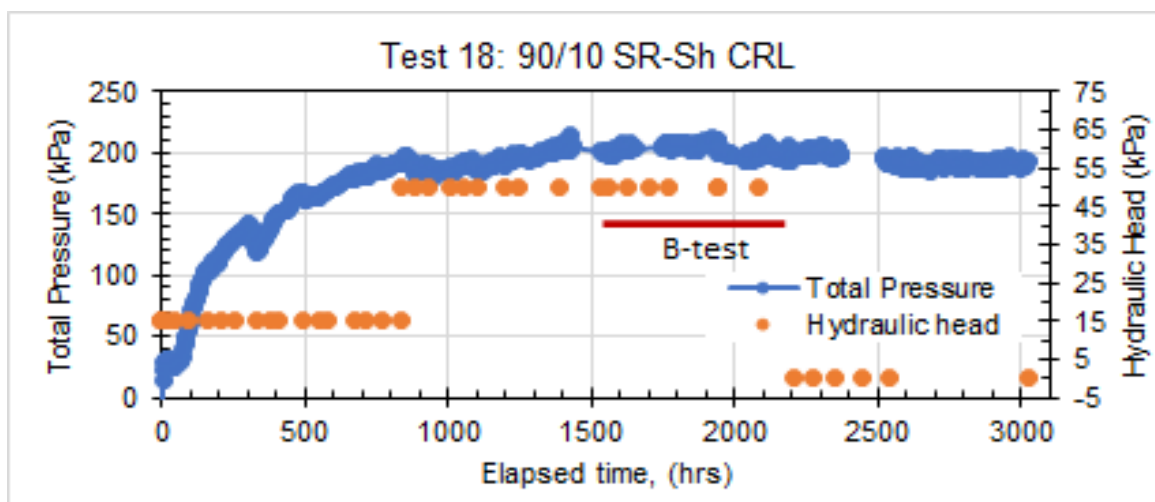
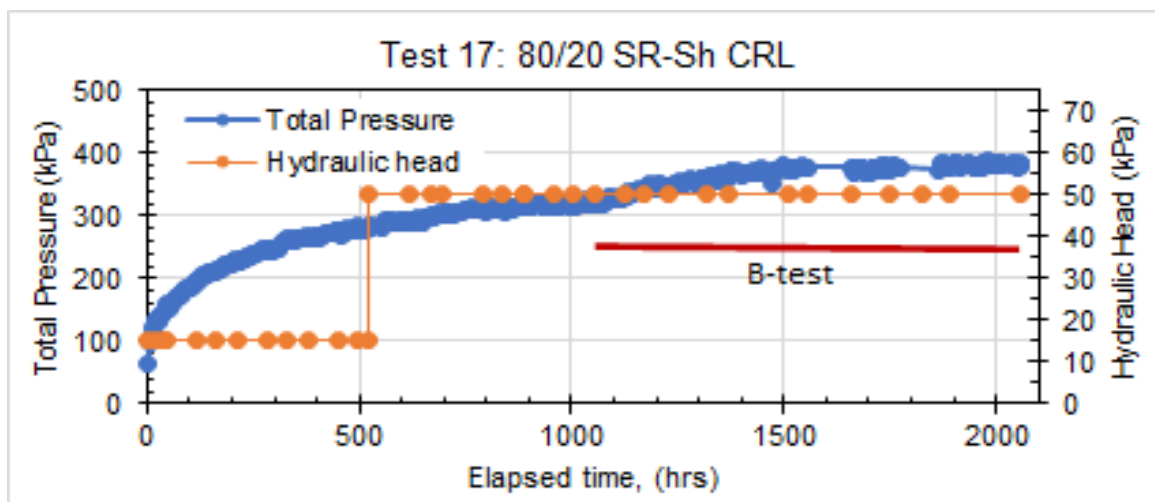
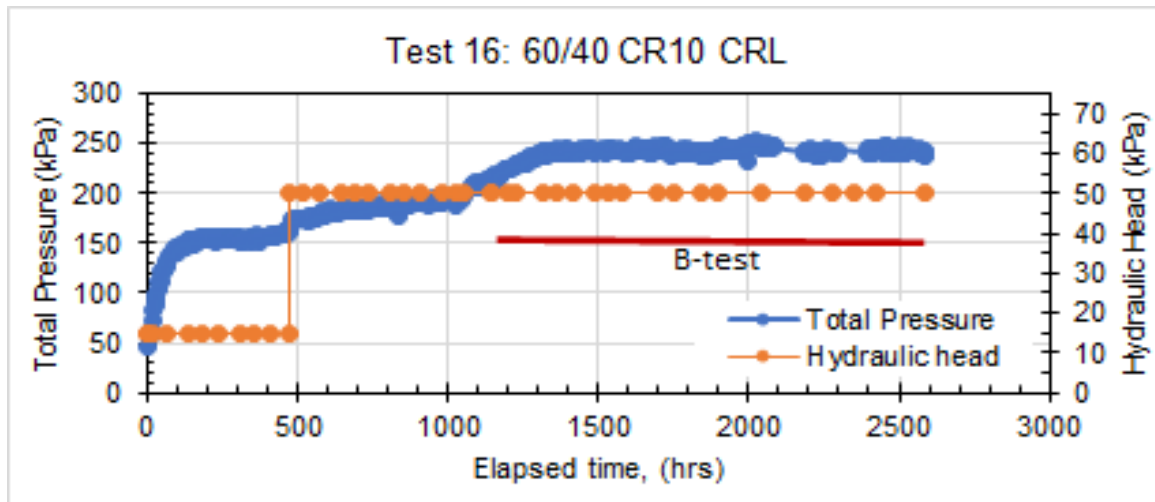


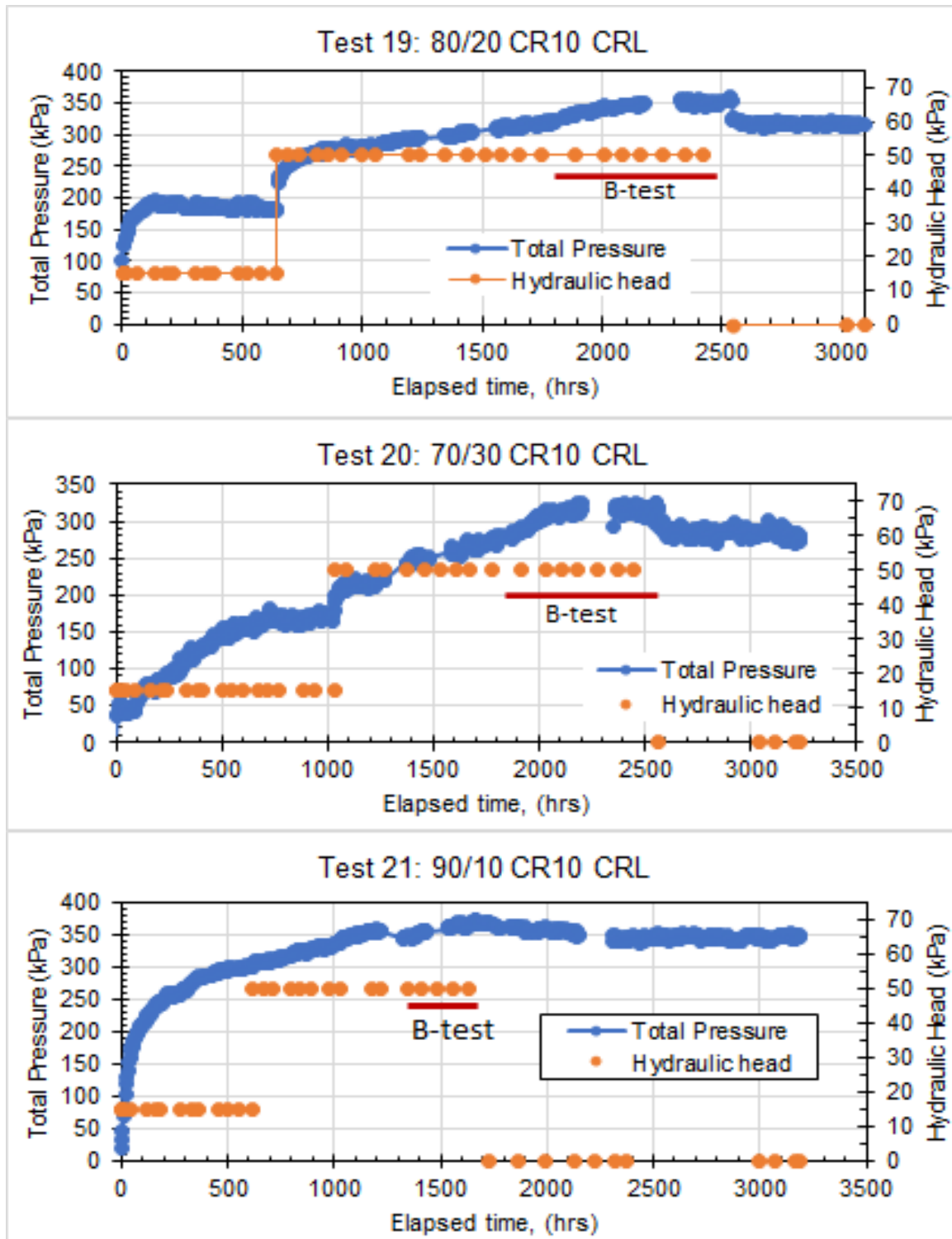


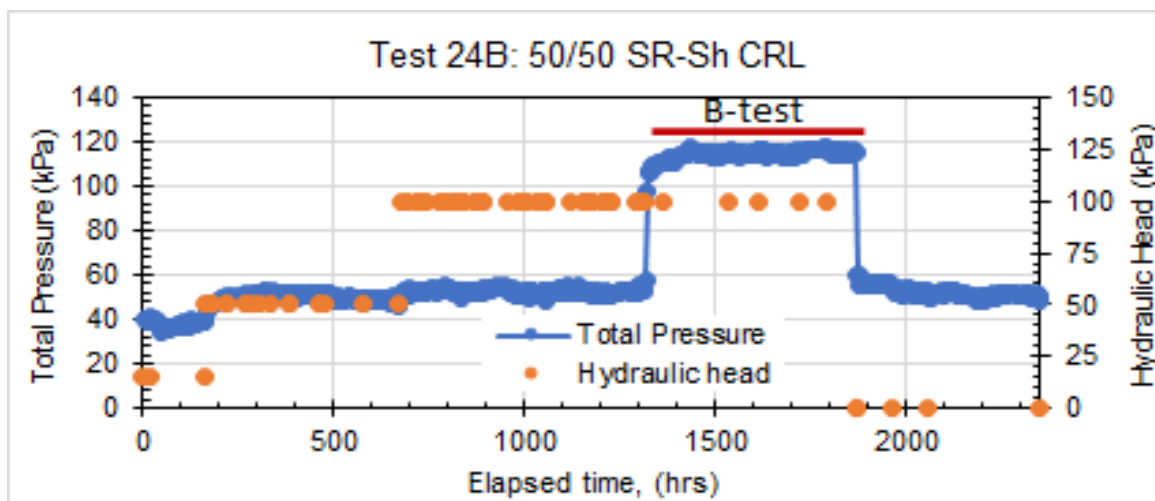
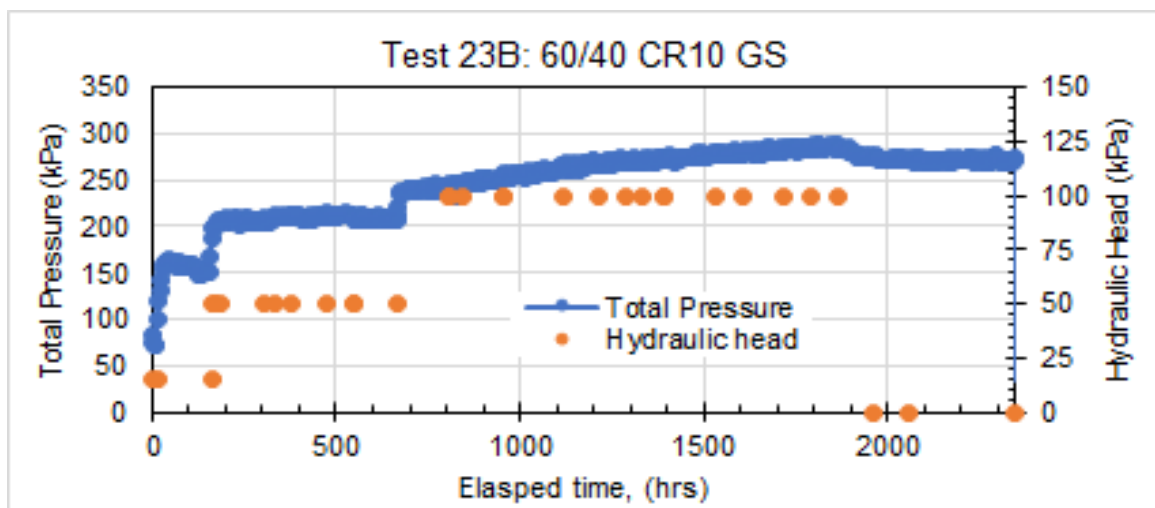
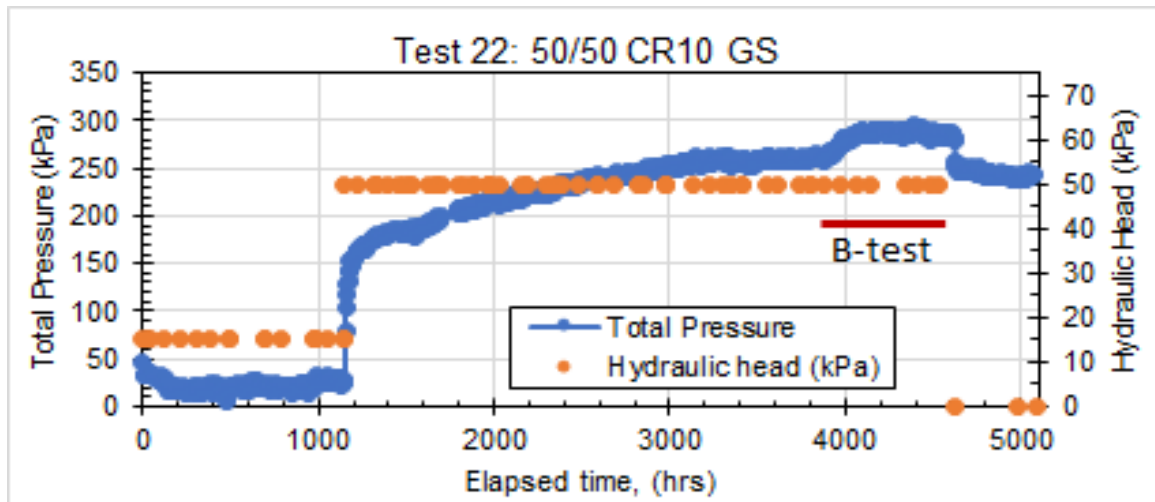
Note: Leak at piston wall, unable to do B-test, Ps based on EoT

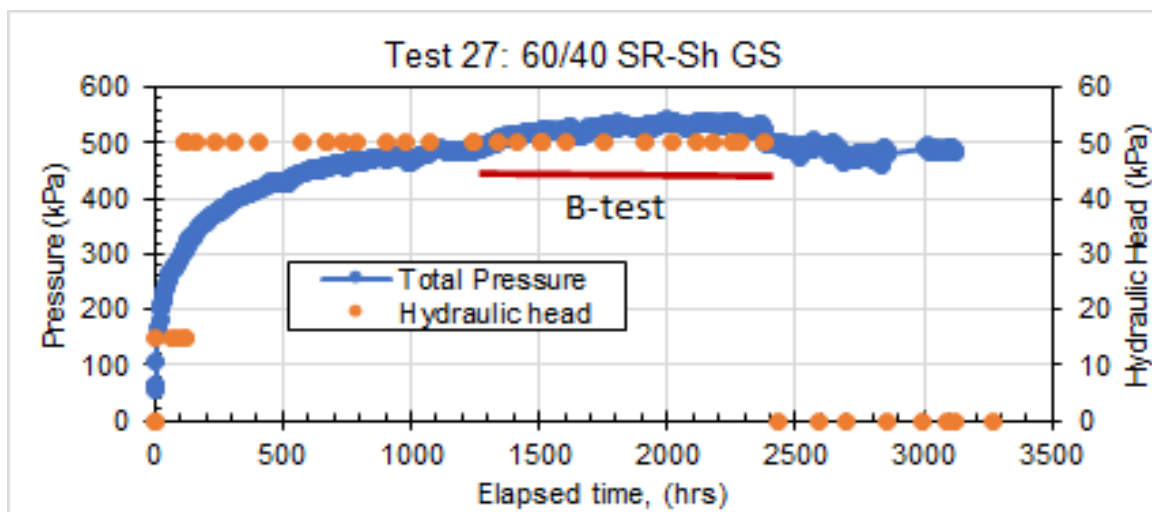
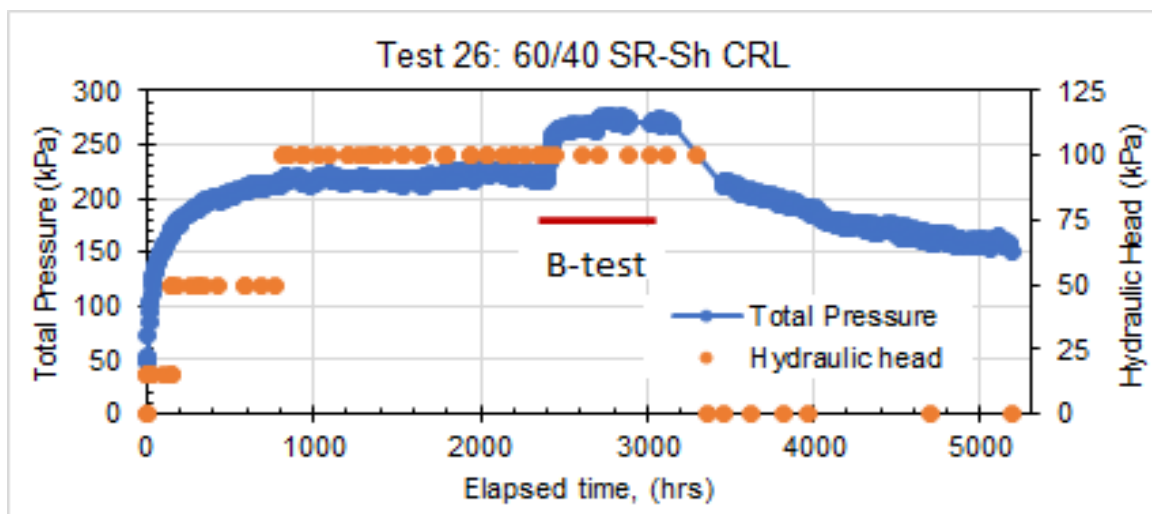
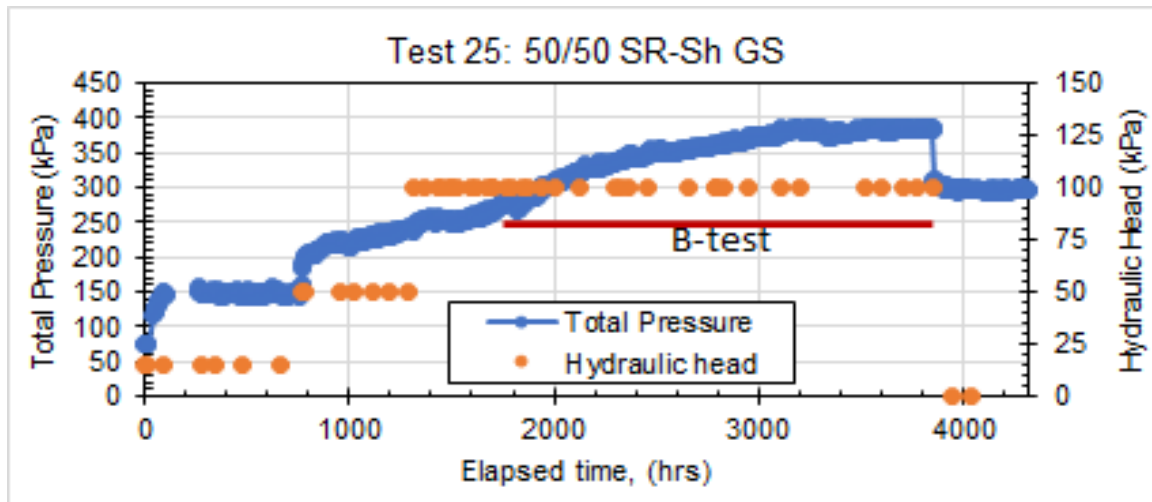


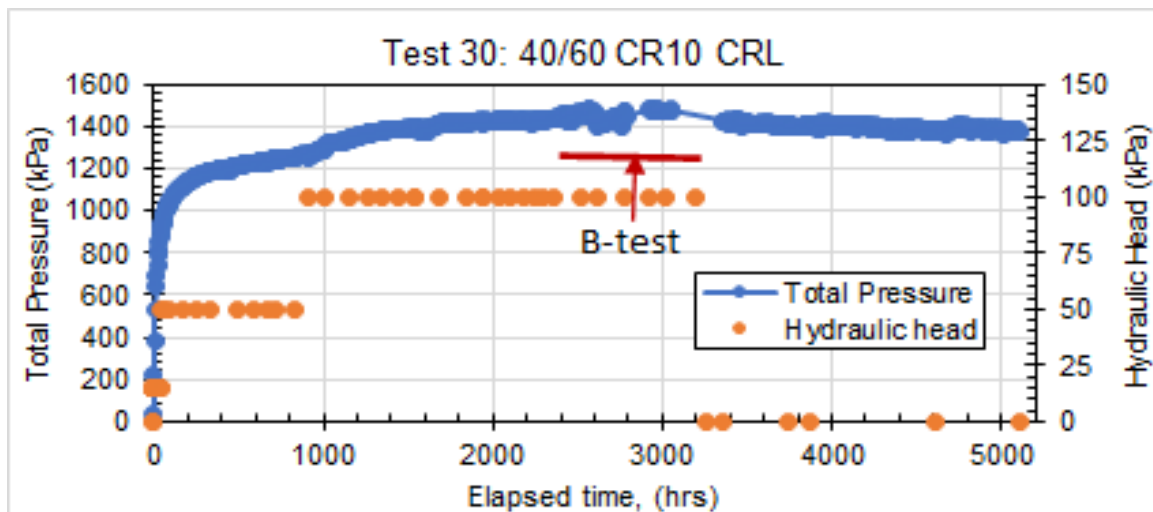
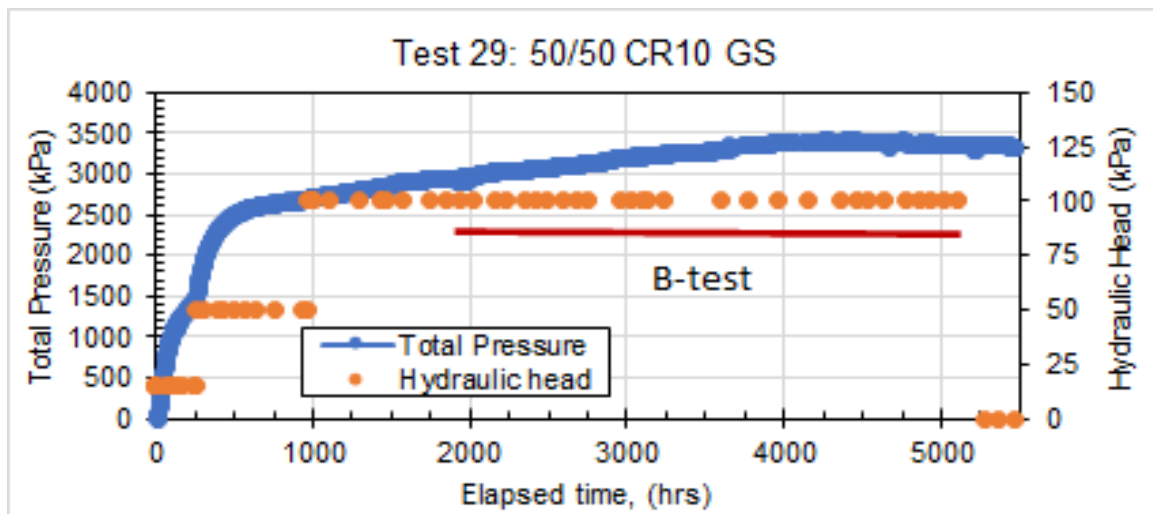
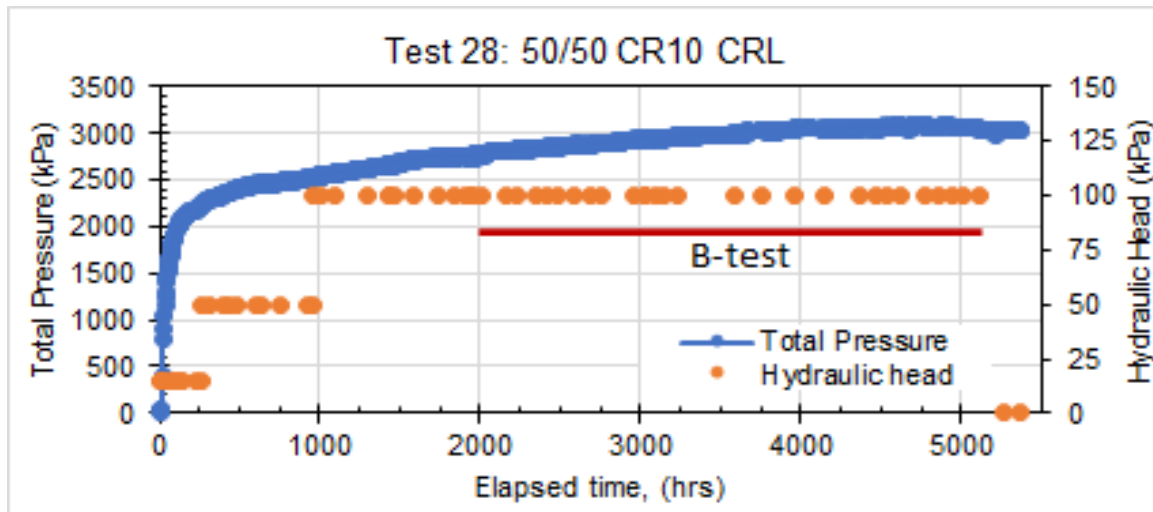


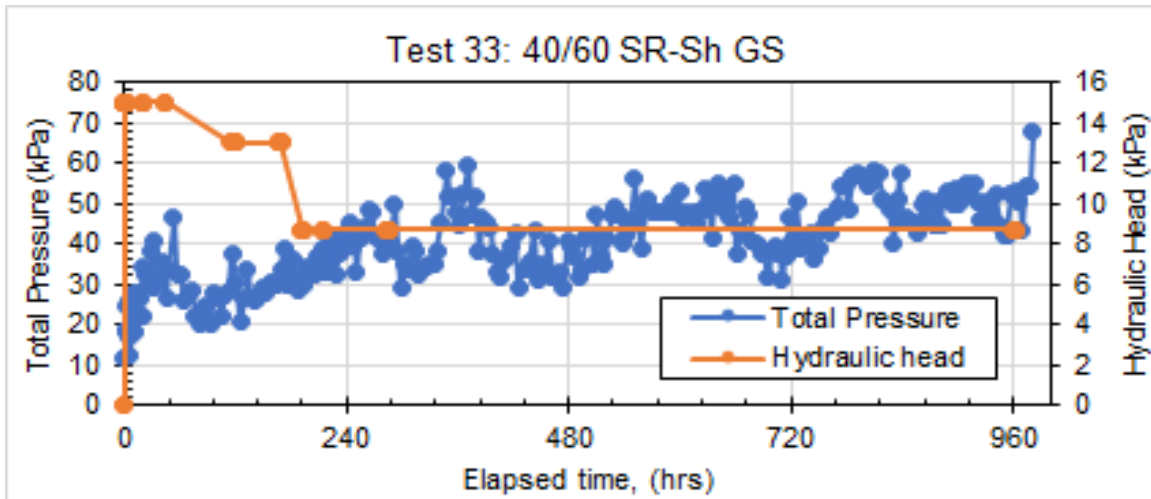
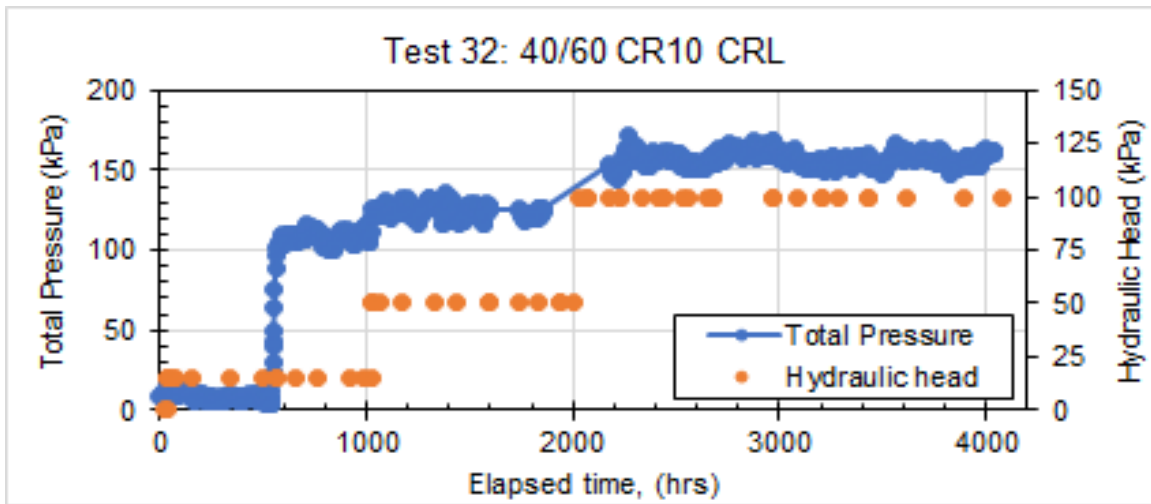
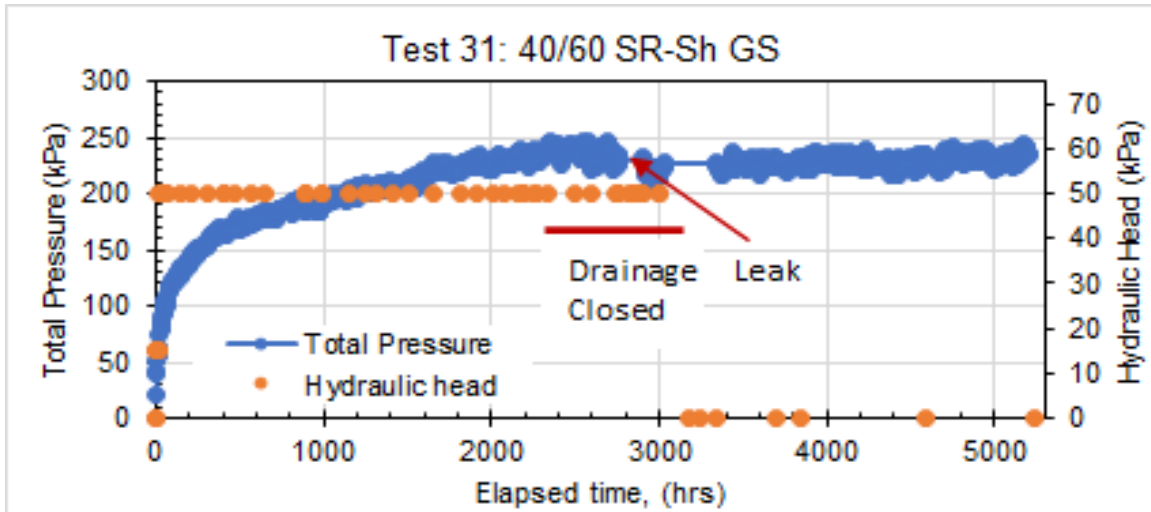




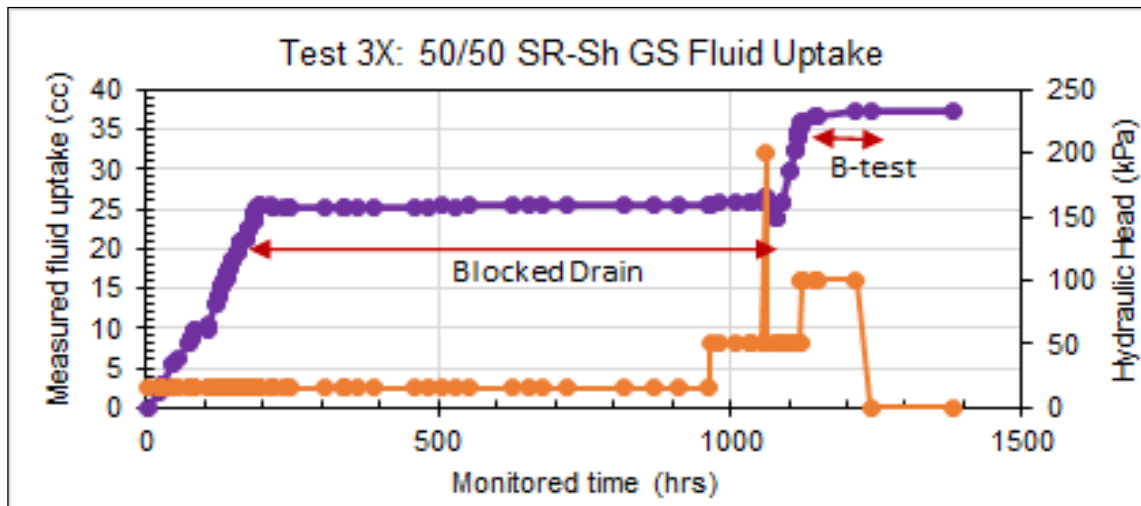
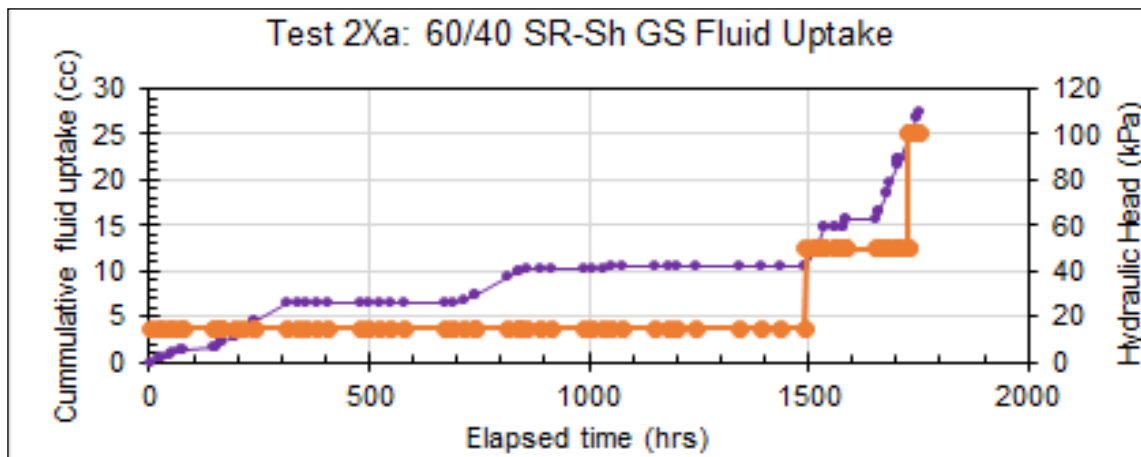
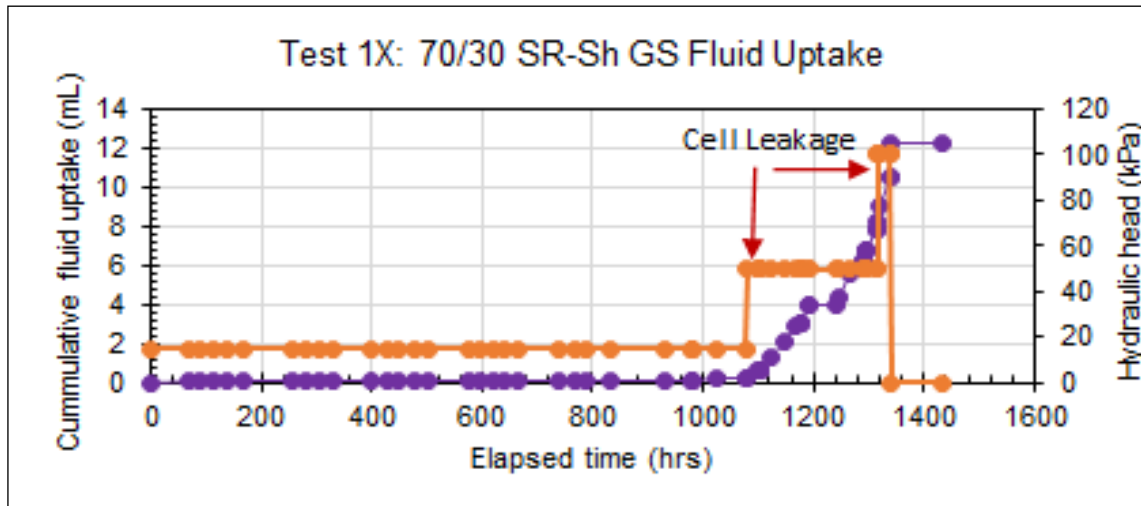


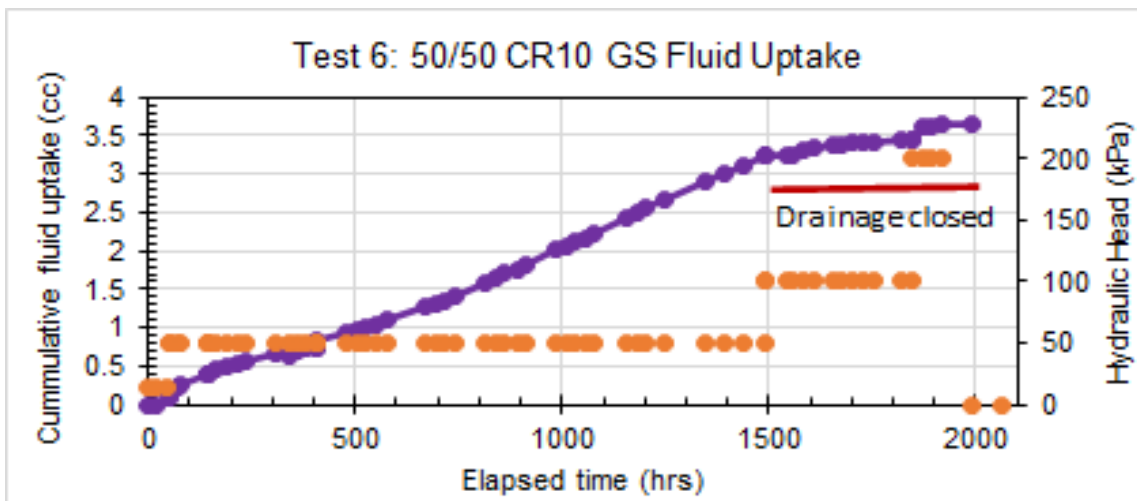
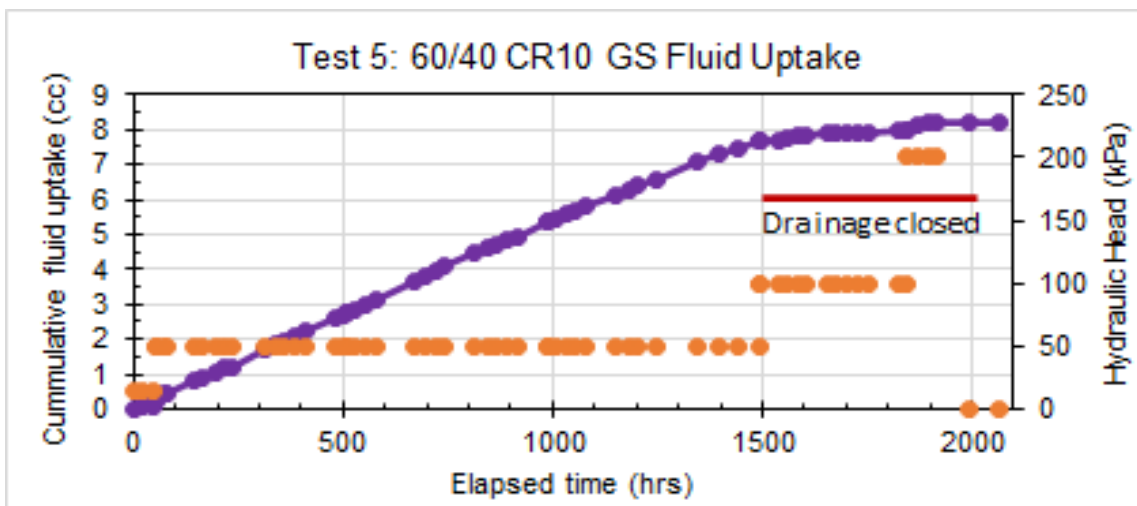
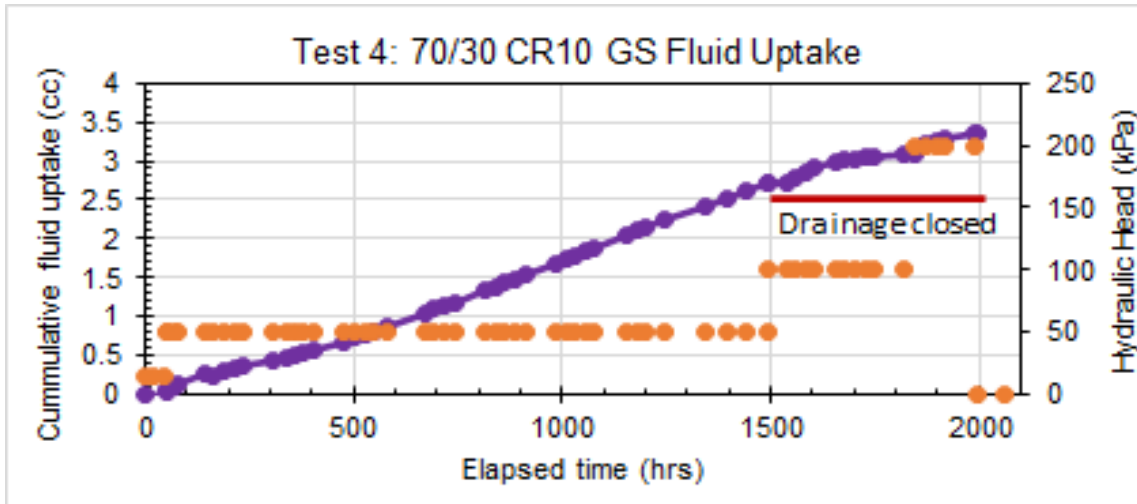




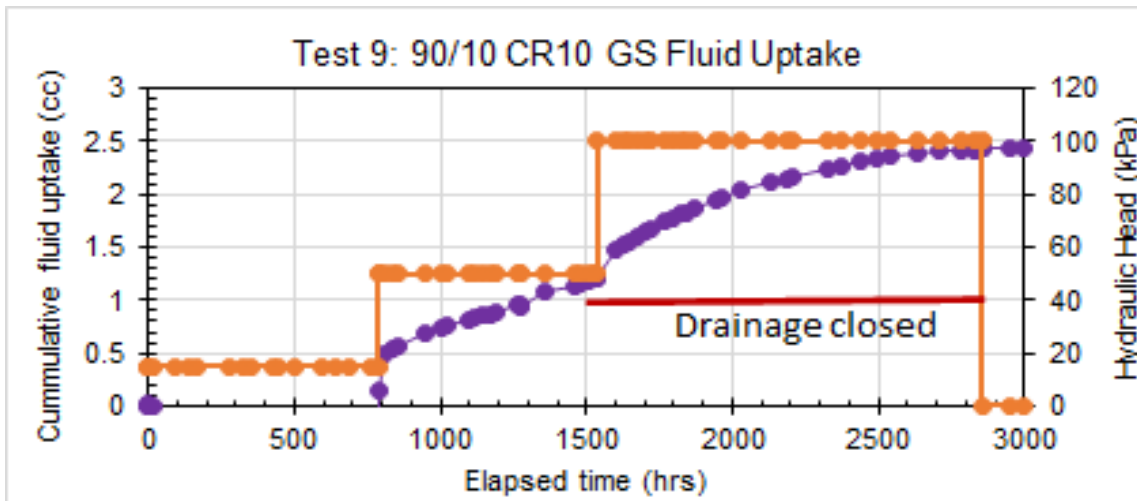
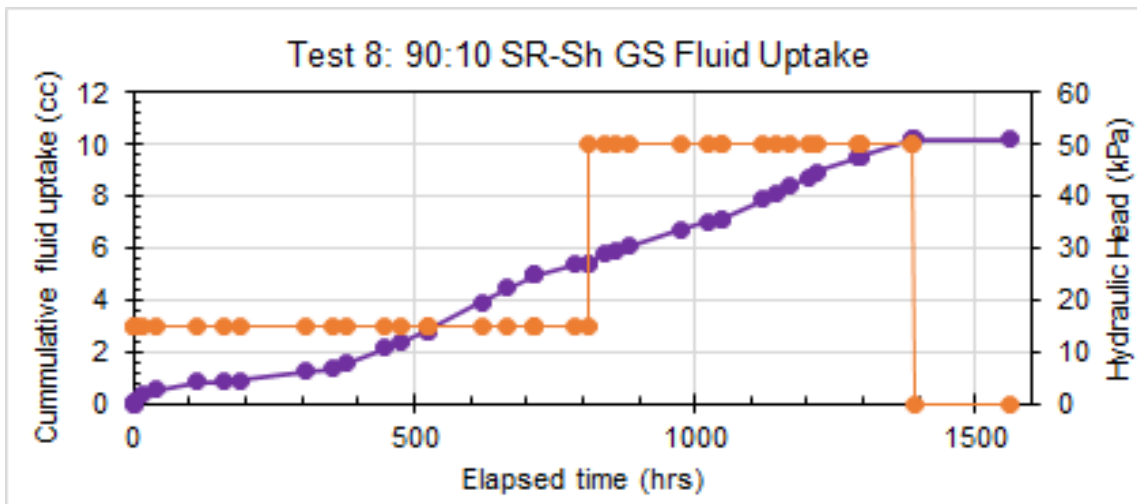
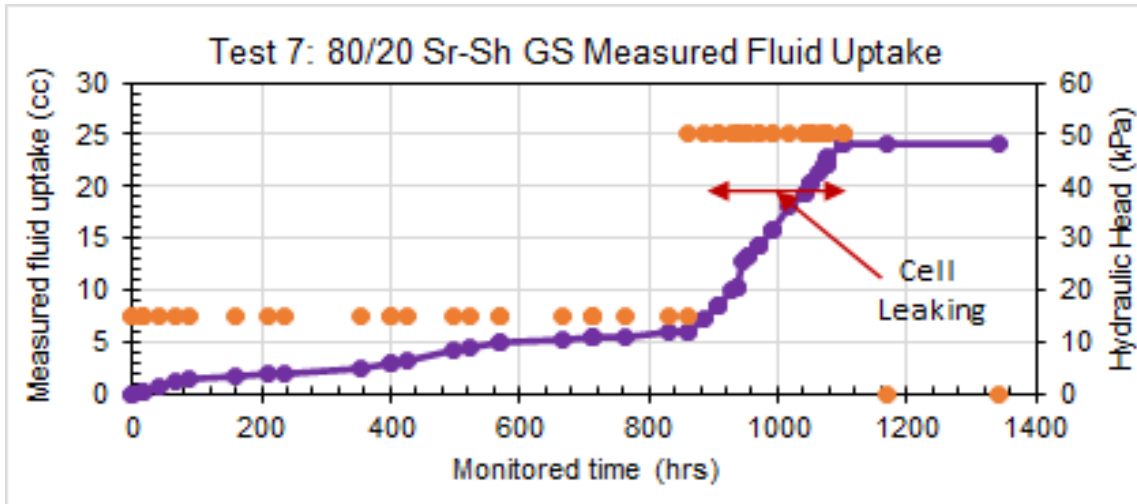


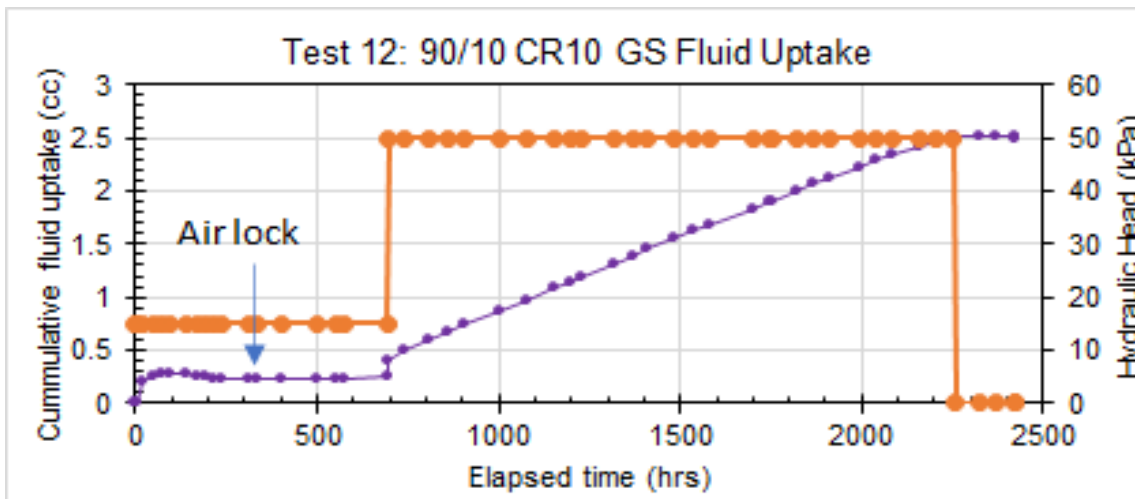
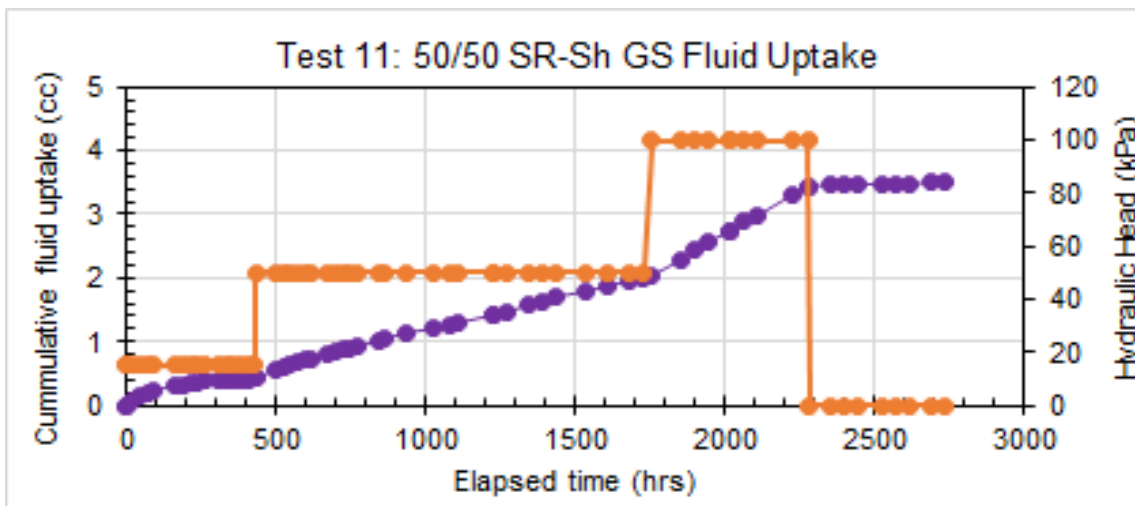
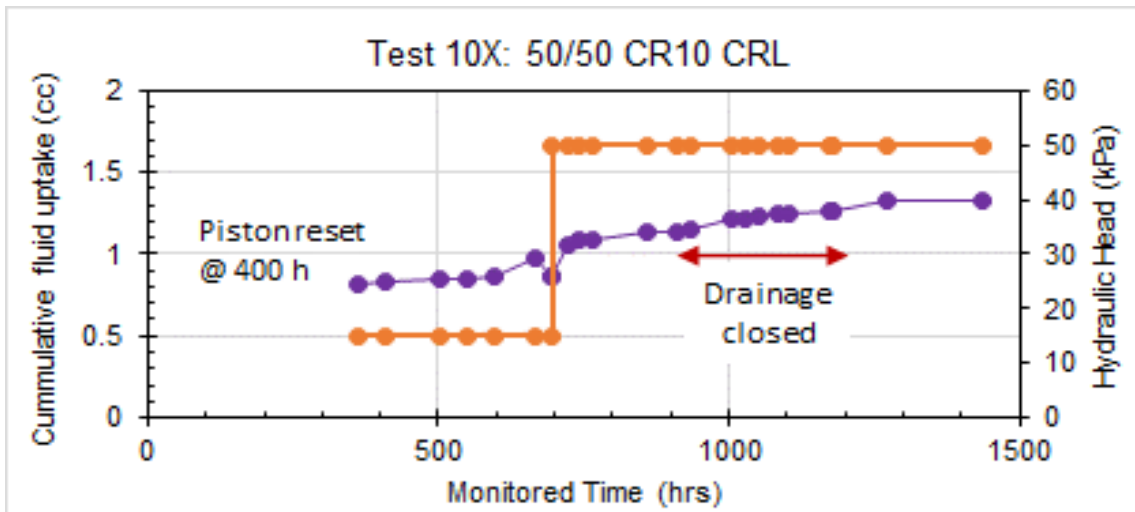
APPENDIX D: Water Uptake Measurements

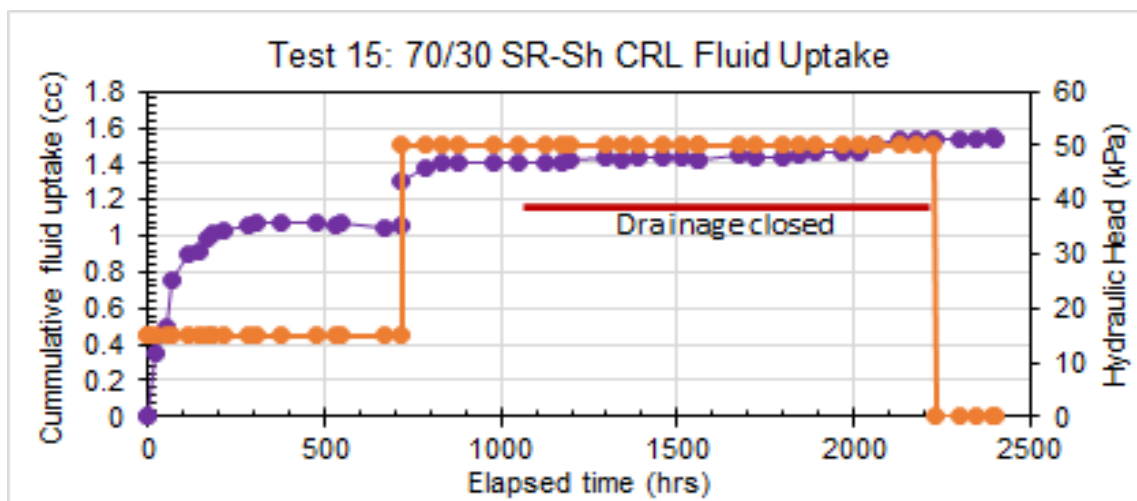
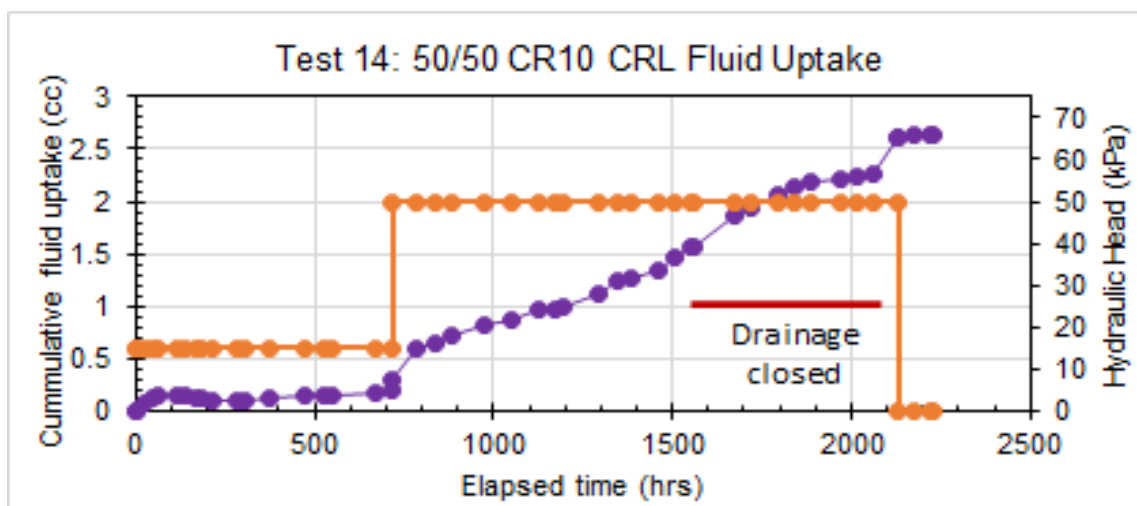
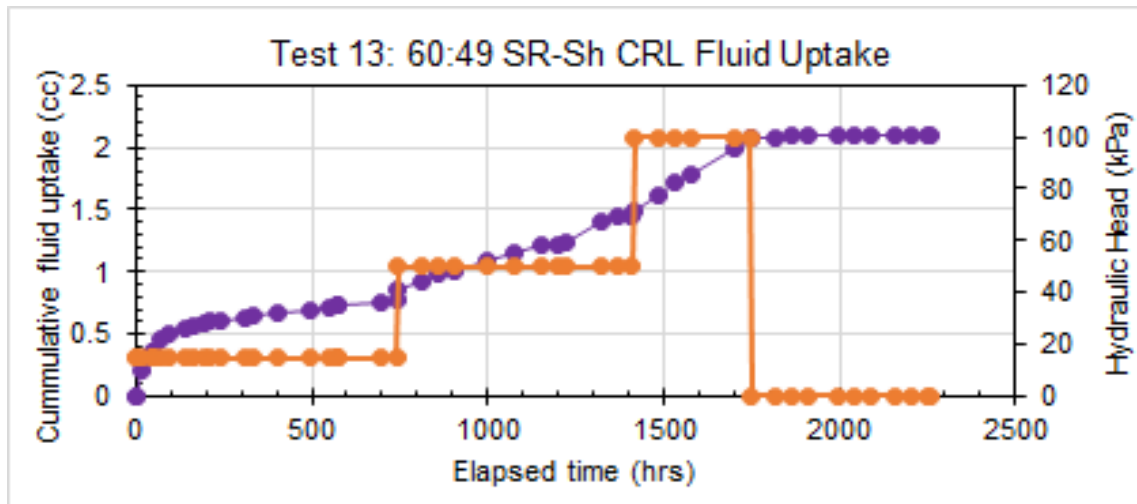


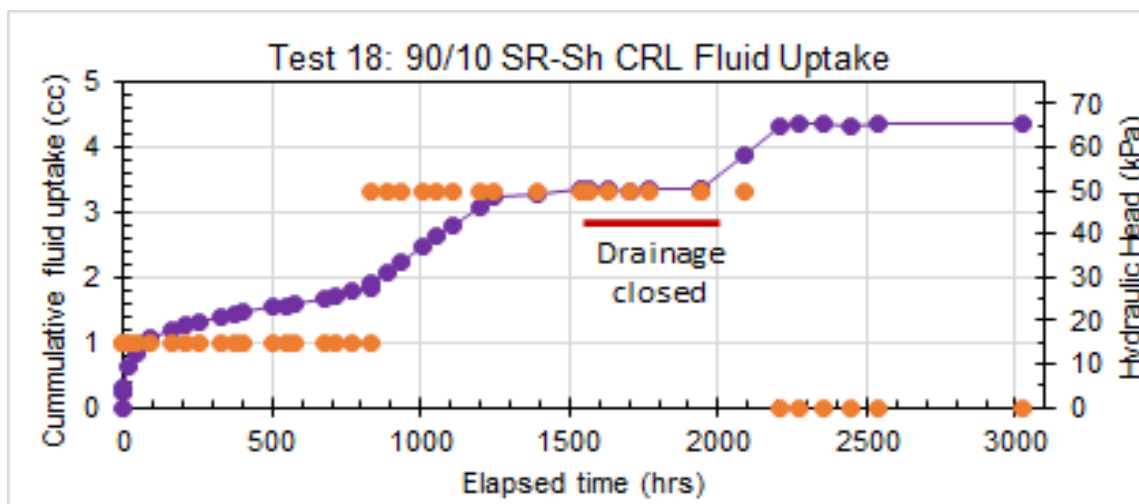
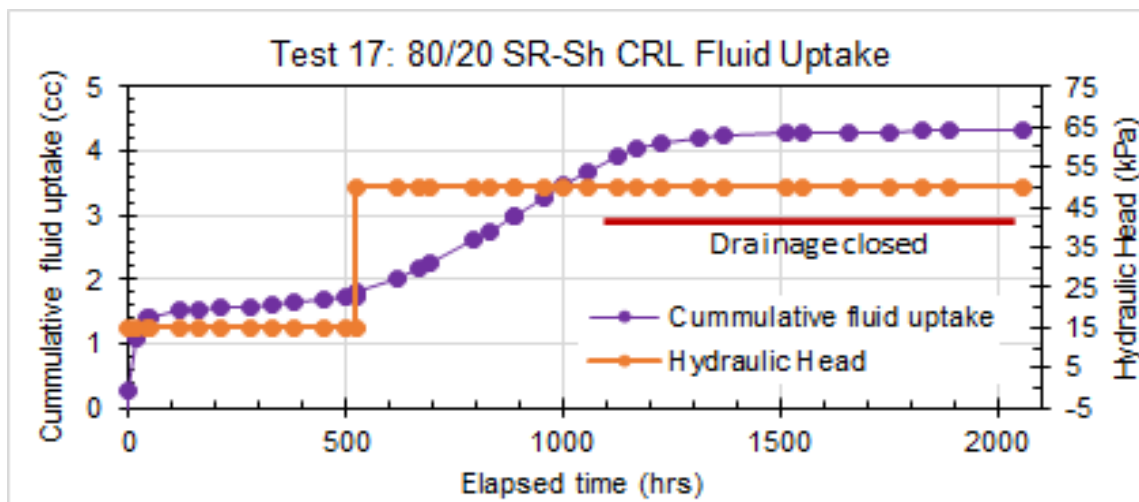
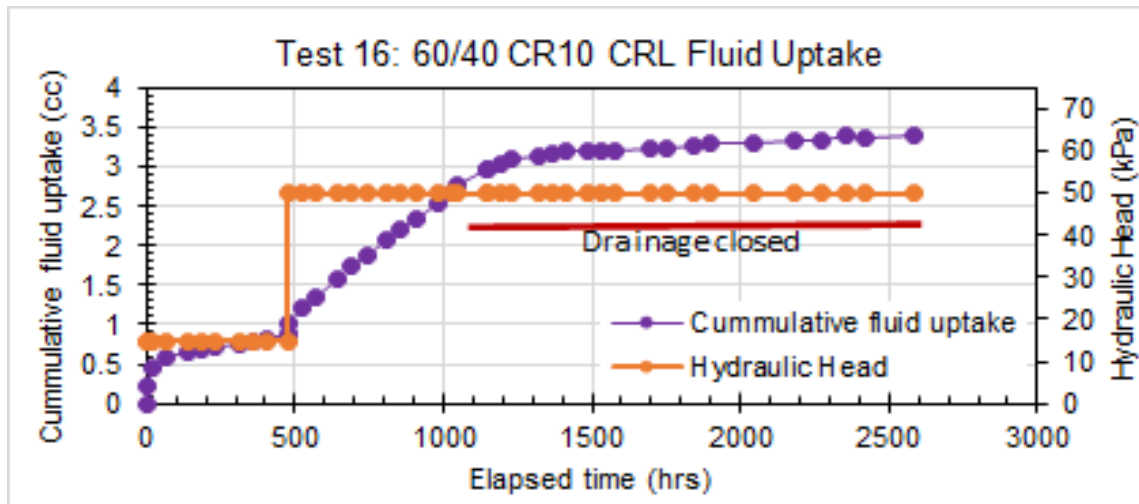


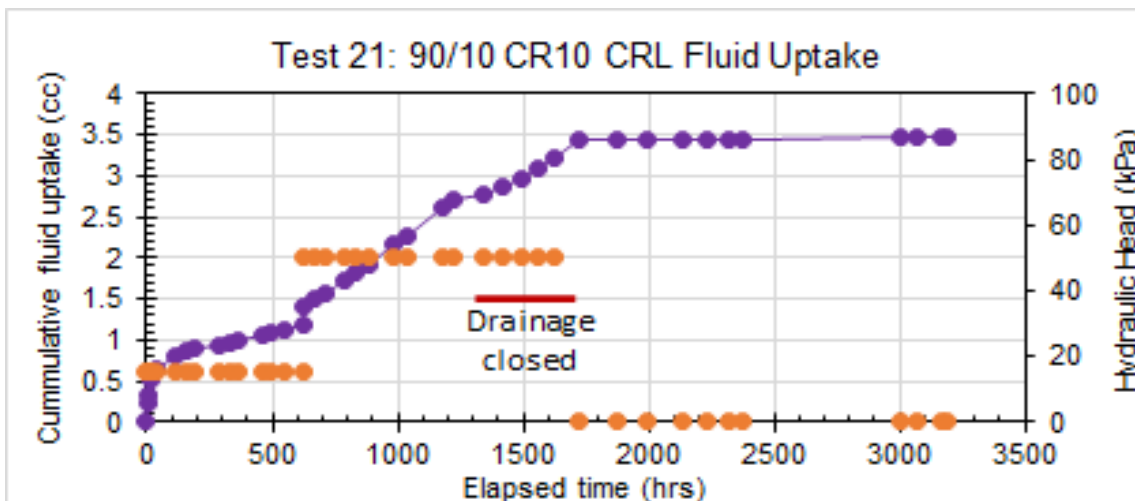
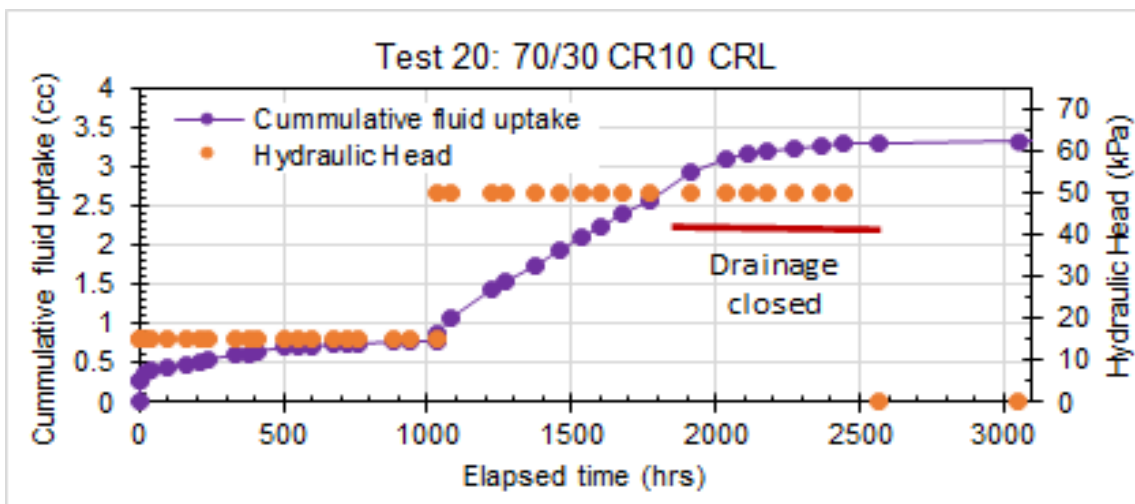
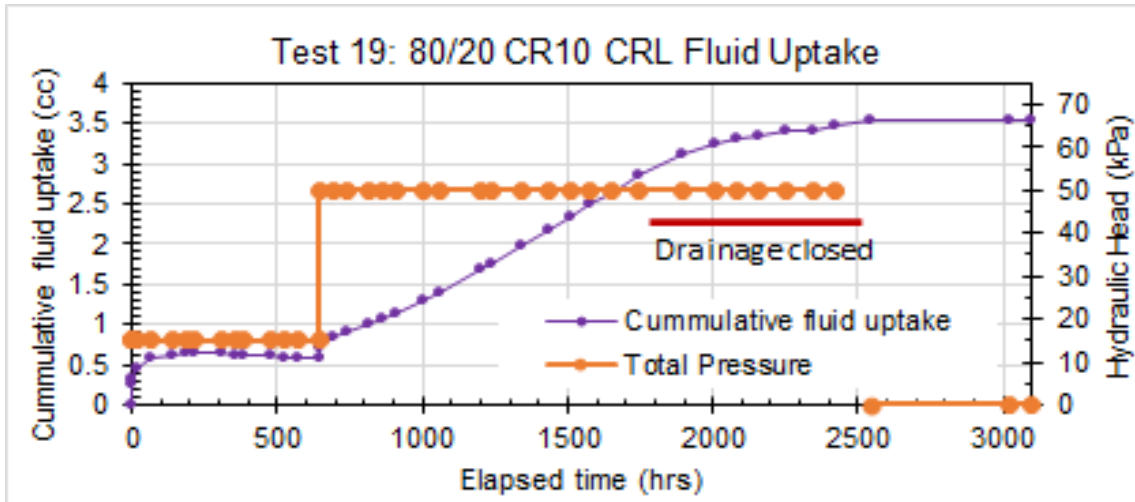
k measured @ 15 kPa head (0-800 h) is used. Brief periods where flow not monitored, hence elapsed time (Ps data) is different than monitored time (flow data)



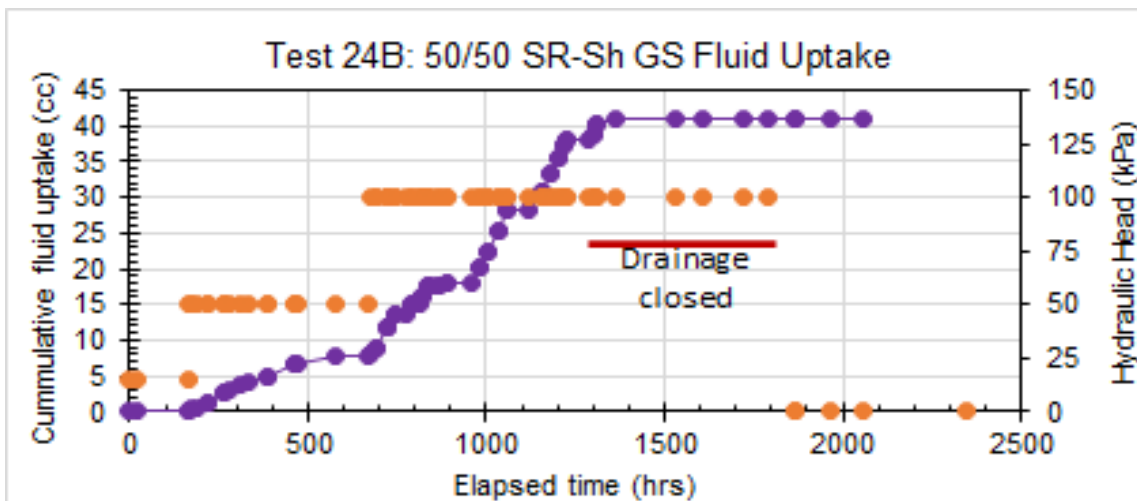
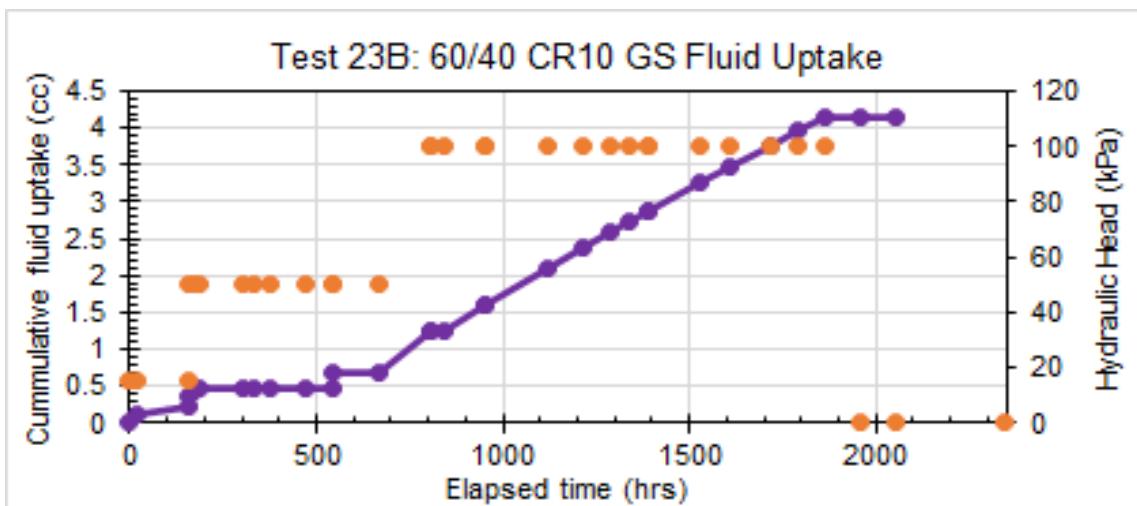
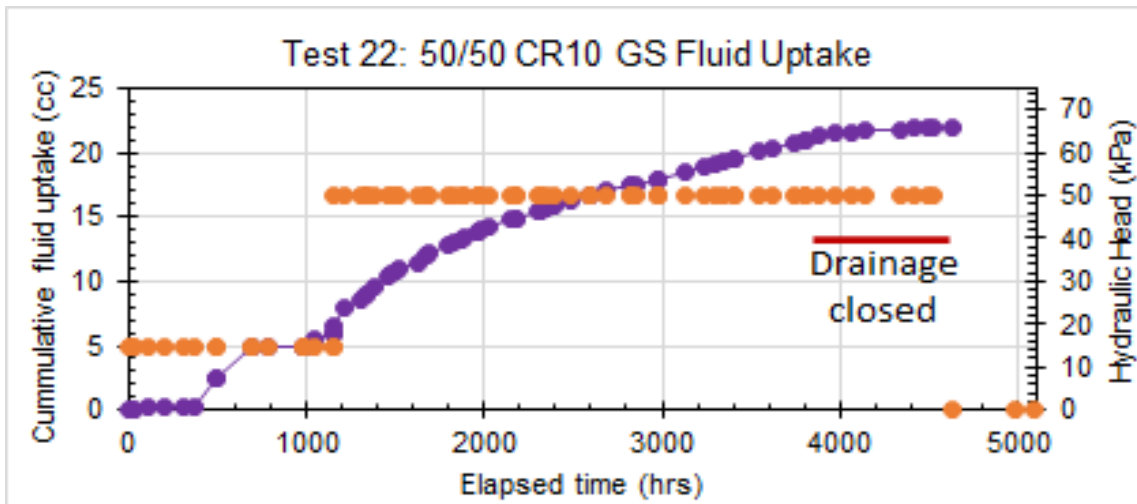


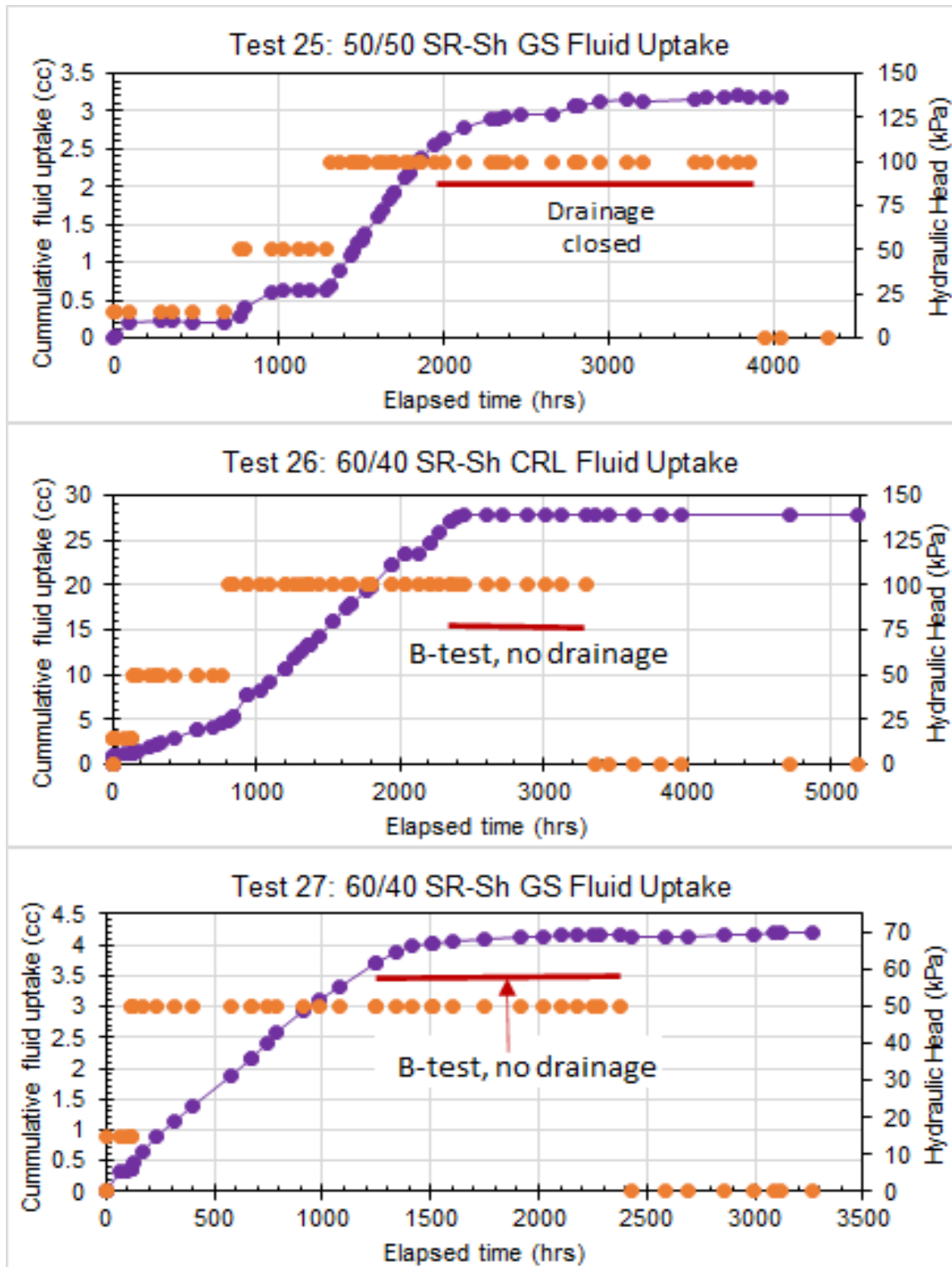


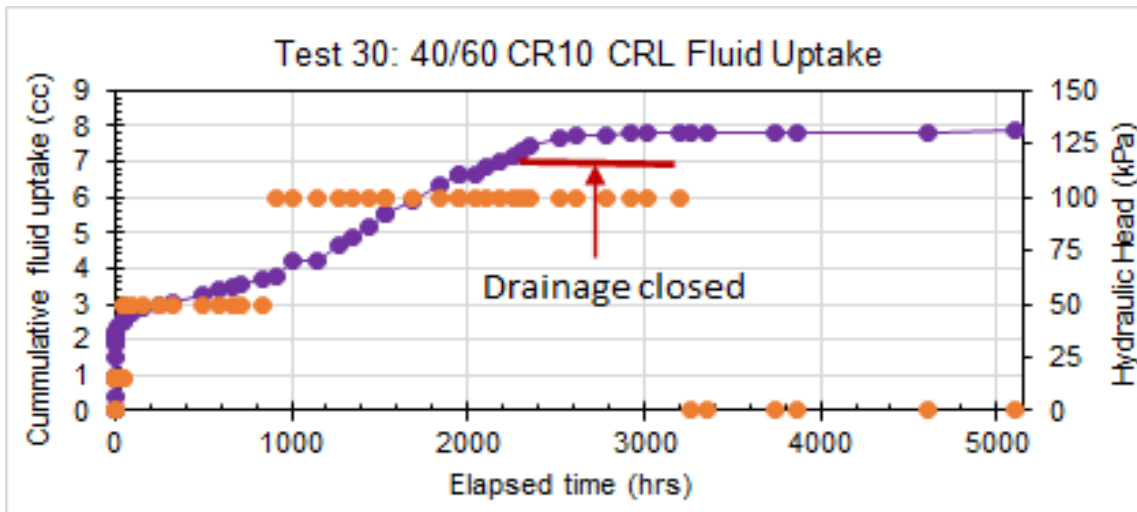
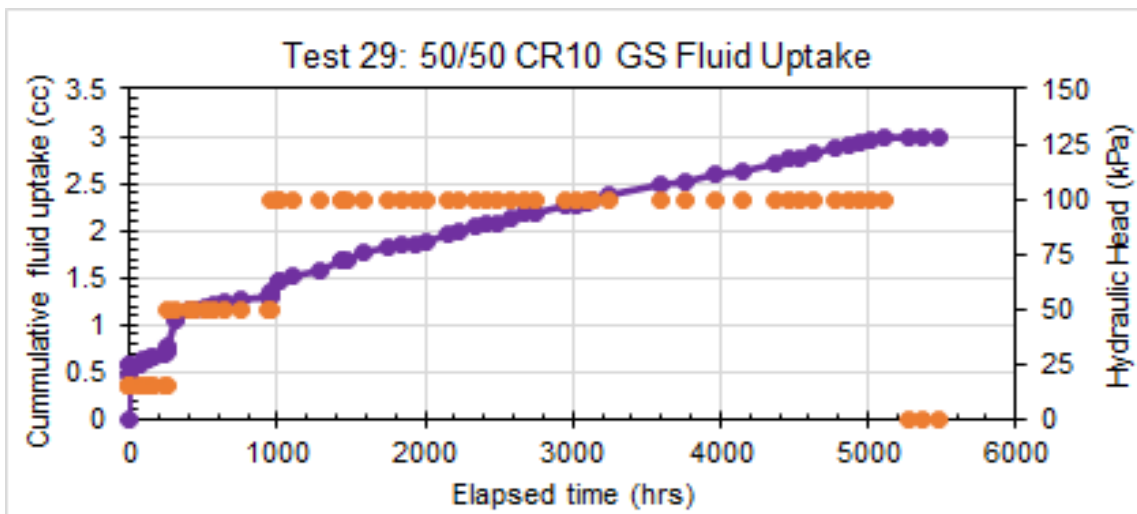
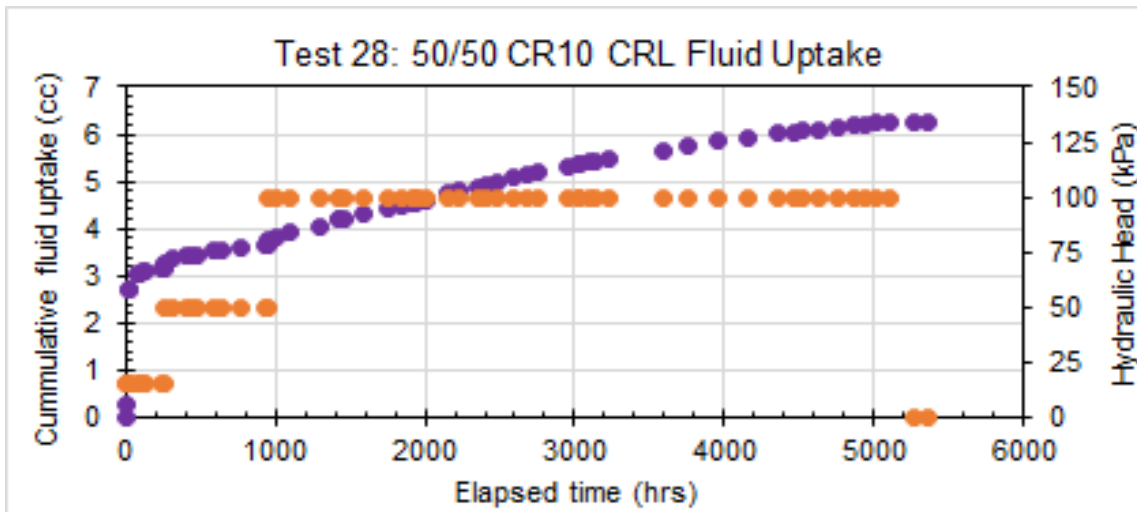


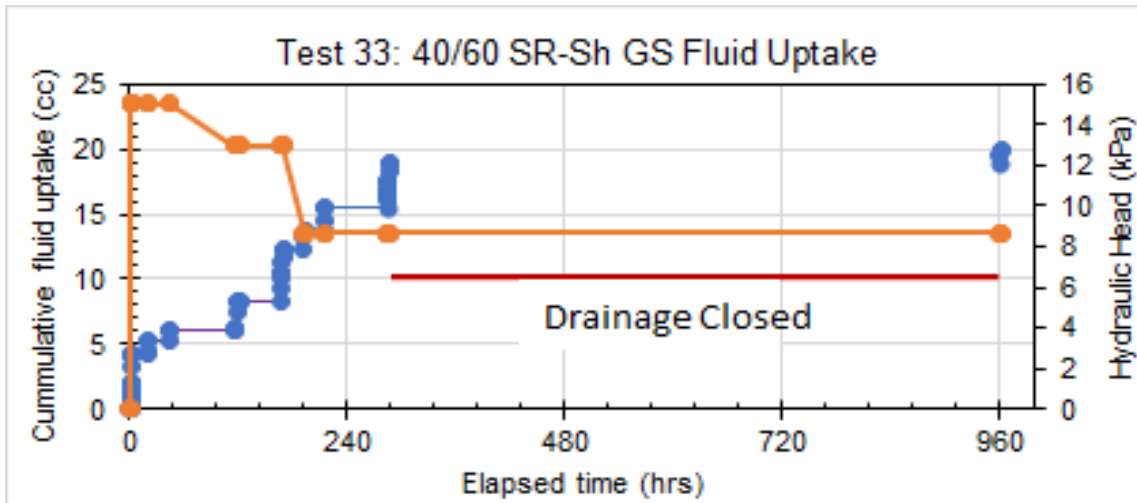
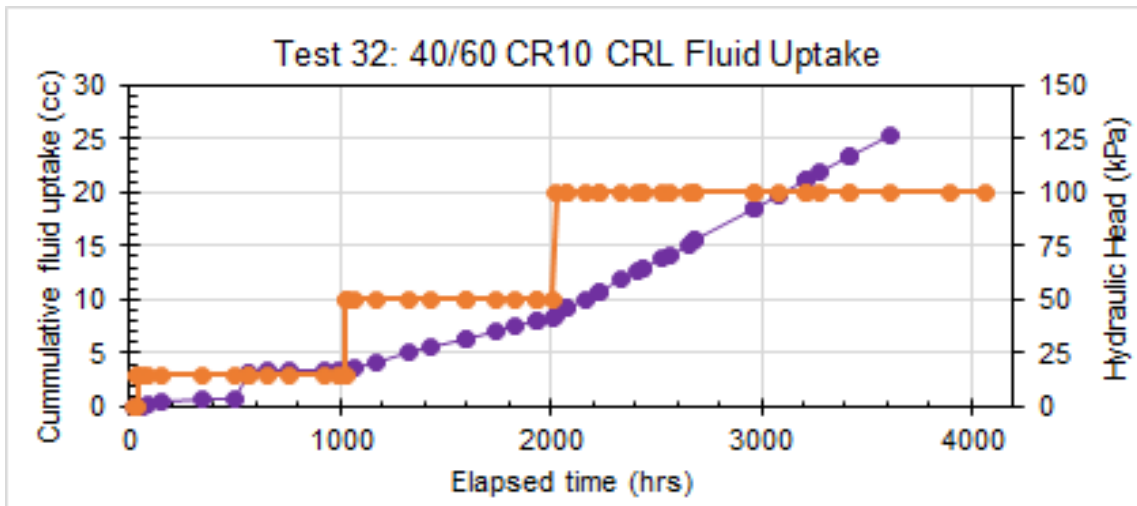
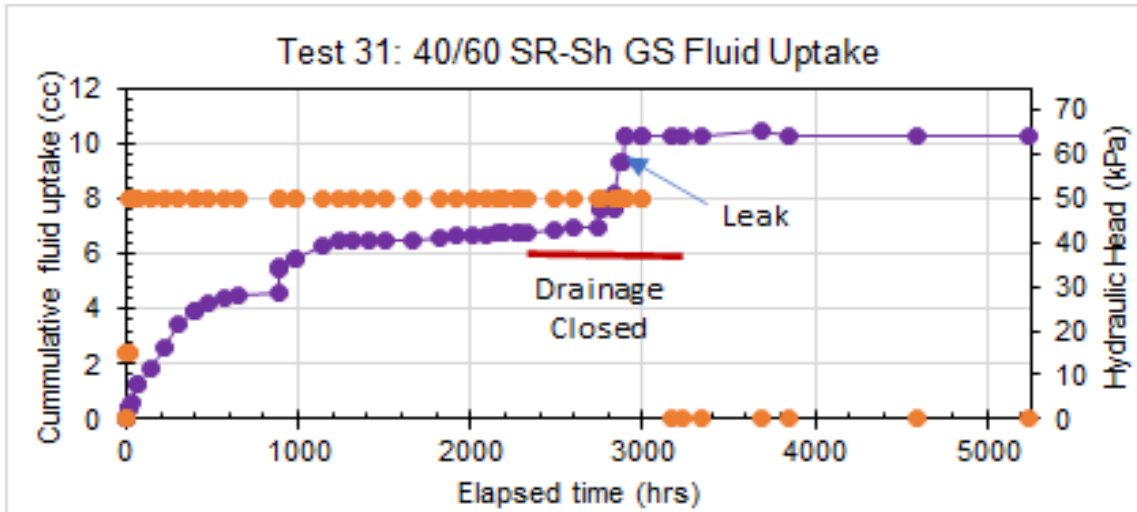


Notes: Leakage at base of cell @ 1300 h, k of specimen < than that measured









APPENDIX E: Summary of Ps and K Testing

Test #	Fluid	Sand	Dry Density (Mg/m ³)	EMDD (Mg/m ³)	Sand %	PWP kPa	Top Drain	Elapsed time (hr)	Bulk k (m/s)	Leakage k (m/s)	Corrected K (m/s)	Total P (kPa)	Ps (P-PWP)* (kPa)	Notes	
1X	SR-Sh	GS	1.51 1.54	1.132 1.162	30	15	open		4.50E-13			235	227.5	P increasing	
						50	open	980	4.10E-11		4.30E-11	225	200		
						100	open	1310	4.50E-11			225	175	cell leaking @~990 h	
						100	closed	1335		leak test			180	180	cell leaking
						0	open	1435					180	200	P increasing Defined Ps
2Xa	SR-Sh	GS	1.6 1.63	1.125 1.156	40	15			1.01E-10		3.30E-11	91	83.5		
						50		1400	4.00E-10		3.32E-10	96	71		
						100	closed	1728		6.80E-11		138	88	cell leaking	
						0	open	1756				97	97	P decreasing? Defined Ps	
3X	SR-Sh	GS	1.67 1.7	1.082 1.113	50	15			2.00E-10			80	72.5		
						50			4.00E-10		3.95E-10	82	57		
						100	Closed	1730		5.50E-12		138	88	P decreasing, inflow decreasing	
						0	open	1850				76	76	P increasing	
								1980					80	80	Defined Ps
4	CR-10	GS	1.43	1.053	60	15	open								
						50	open		3.60E-12		3.29E-12	270	245	P increasing	
						100	closed			4.00E-13		340	240	P incr. slowly, inflow decreasing	
						200	closed			2.20E-13		412	212	P increasing slowly	
						0	open					281	281	P decreasing slowly	
								260	260	Defined value					
5	CR-10	GS	1.45	0.977	40	15	open								
						50	open	50	7.50E-12		7.17E-12	201	176	P incr. slowly, inflow decreasing	
						50	open	50	6.30E-12		5.97E-12				
						100	closed	1500		3.30E-13		260	160	P incr. slowly, inflow decreasing	
						200	closed	1850		8.30E-14		320	120	P incr. slowly, inflow decreasing	
0	open	2000				212	212	P still decreasing slowly							

													200	Defined value
6	CR-10	GS	1.615	1.025	50	15 50 100 200 0	open open closed closed open	50 50 1500 1850 2000	3.30E-12	3.00E-13 8.50E-14	3.11E-12	340 410 505 331	315 310 305 331 320	P increasing pressure stable pressure stable P slight decreasing Defined value
7X	SR-Sh	GS	1.5 1.54	1.208	20	15 50 50 0	open open closed open	850 1200 1370	1.60E-11 1.30E-10	1.00E-10	1.60E-11 3.00E-11	90 95 75	82.5 70 75	P increasing P decreasing slowly P decreasing slowly
8	SR-Sh	GS	1.46 1.5	1.244 1.285	10	15 50 50 50 0	open open open closed open	800 1400	4.60E-11 1.40E-11 1.30E-11	9.10E-12	3.69E-11 4.90E-12 3.90E-12	90 90 81	82.5 65 81	P steady P decreasing P decreasing
9	CR-10	GS	1.3	1.086	10	15 50 50 100 0	open open Closed Closed open	800 1300 1550 2750	1.10E-12	2.40E-13	8.60E-13	286 330 350 445 382	278.5 305 300 345 382	P increasing P increasing P increasing P steady P decreasing
10X	CR-10	CRL	1.65	1.061	50	15 50 50 0	open open Closed open	850 900 1200	6.10E-12		6.10E-12	106 102 115 99	98.5 77 65 99 100	P steady P steady Defined value
11	SR-Sh	GS	1.88 1.9	1.32 1.345	50	15 50 50 100	open open closed? closed	500 1225 1750	4.20E-11 1.50E-12	1.40E-12 8.50E-13	6.50E-13	162 200 205	154.5 175 155	P increasing P increasing P increasing

						0	open	2275				195	195	P steady			
12	CR-10	GS	1.37	1.154	10	15	open		3.90E-13	air lock?		335	327.5	P increasing			
			1.38	1.164		50	open	700	1.90E-12		1.56E-12	435	410	P increasing			
						50	Closed	1800		3.40E-13			460	410	P increasing		
						0	open	2250					432	432	P decreasing		
												420	420	Defined value			
13	SR-Sh	CRL	1.85	1.403	40	15	open		1.90E-12		7.00E-13	370	362.5	P increasing			
			1.87	1.427		50	open	700	1.40E-12		2.00E-13	395	370	P steady			
						50	Closed	1200		1.80E-12			410	360	P increasing		
						100	Closed?	1400		1.20E-12			410	360	P steady		
						0	open	1750					380	380	P steady		
14	CR-10	CRL	1.57	0.98	50	15	open		1.10E-12		5.70E-13	48	40.5	P decreasing			
						50	open	700	1.60E-12		1.07E-12	97	72	P increasing			
						50	Closed	1550		5.30E-13			130	80	P increasing		
						0	open	2050					97	97	P decreasing		
15	SR-Sh	CRL	1.81	1.455	30	15	open		2.60E-13		1.20E-13	297	289.5	P increasing			
						1.83	1.478	50	open	700	8.20E-14			392	367	P increasing	
								50	Closed	1550		1.40E-13			447	397	P increasing
								0	open	2050					453	453	P steady
16	CR-10	CRL	1.49	1.015	40	15	open		2.70E-12		2.47E-12	162	154.5	P increasing			
						50	open	480	4.00E-12		3.77E-12	197	172	P increasing			
						50	Closed	1150		2.30E-13			241	191	P decreasing		
						0		2600						180		Defined value	
17	SR-Sh	CRL	1.66	1.375	20	15	open		2.60E-12		2.47E-12	283	275.5	P increasing			
			1.69	1.407		50	open	550	5.30E-12		5.17E-12	320	295	P increasing			
						50	Closed	1050		1.30E-13			380	330	P steady		
						0		2100									
18	SR-Sh	CRL	1.63	1.419	10	15	open		4.00E-12		3.82E-12	190	182.5	P increasing			
			1.66	1.451		50	open	850	4.10E-12		3.92E-12	215	190	P increasing			
						50	Closed	1050		1.80E-13			200	150	P increasing?		

						0	open	2100				193	193	P steady				
19	CR-10	CRL	1.35	1.06	20	15	open		3.90E-12	6.70E-13	3.23E-12	183	175.5	P increasing				
						50	open	650				316	291	P increasing				
						50	Closed	1850				360	310	P increasing?				
						0	open	2550				318	318	P decreasing				
								3250					315	Defined value				
20	CR-10	CRL	1.48	1.102	30	15	open		6.90E-13	4.80E-13	2.10E-13	171	163.5	P steady?				
						50	open	1050	2.90E-12		2.42E-12	277	252	P increasing?				
						50	Closed	1850				317	267	P steady				
						0	open	2500				284	284	P decreasing				
								3250				275	275	Defined value				
21	CR-10	CRL	1.29	1.076	10	15	open		3.30E-12	2.40E-12	9.00E-13	300	292.5	P increasing? P increasing? P steady Defined value				
						50	open	650	2.90E-12		5.00E-13	356	331					
						50	Closed	1250				374	324					
						0	open	1700				348	348					
								3200				350	350					
22	CR-10	GS	1.57	1.019	50	15	open		4.70E-12	8.20E-13	3.88E-12	270	245	airlock @ 15 kPa?				
						50	open	1100								285	235	P increasing?
						50	Closed	3800								243	243	P decreasing
						0	open	4600										P steady
																240	240	Defined value
23B	CR-10	GS	1.55	1.074	40	15	open		airlock?	8.60E-13	8.60E-13	150	142.5	P steady				
						50	open	200	8.60E-13			8.60E-13	208	183	P steady			
						100		700	1.80E-12			1.80E-12	288	238	P increasing?			
						0	open	1800					272	272	P steady			
								2400					270	270	Defined value			
24B	SR-Sh	CRL	1.83	1.26	50	15	open		2.40E-11	1.90E-11	2.39E-11	39	31.5	P increasing?				
			1.85	1.284		50	open	760				1.89E-11	47	22	P steady			
						50	open					3.69E-11						
						100	open	1300				3.70E-11	50	0	P steady			
						100	open					3.40E-11						

						100	closed	1350		9.50E-14		115	15	P steady
						0	open	1900				50	50	P steady
								2350						
25	SR-Sh	GS	1.946	1.404	50	15	open					150	142.5	no inflow airlock?
			1.966	1.43		50	open	700				241	216	no inflow airlock?
						100	open	1200	2.00E-12		1.93E-12	300	250	P increasing?
						100	closed	1600		6.80E-14		381	281	P steady
						0	open	3800				297	297	P steady
								4500						
26	SR-Sh	GS	1.87	1.426	40	15	open							
			1.844	1.395		50	open	150	8.50E-12		8.00E-12	215	190	P increasing?
						100	open	800	9.30E-12		8.80E-12	225	175	P increasing?
						100	closed	2200		5.00E-13		270	170	P steady
						0	0	5200				163	163	P decreasing
													170	Defined value
27	SR-Sh	GS	1.831	1.38	40	15	open		3.40E-12		3.30E-12	272	264.5	P increasing
			1.855	1.409		50	open	120	2.70E-12		2.60E-12	492	467	P increasing?
						50	Closed	1200		9.90E-14		535	485	P steady
						0	open	2200				485	485	P steady
								3000					485	Defined value
28	CR-10	CRL	1.89	1.333	50	15	open		2.30E-12		2.05E-12	2246	2238.5	P increasing
						50	open	230	5.70E-13		3.20E-13	2543	2518	P increasing
						100	open	900	4.70E-13		2.20E-13	2770	2720	P increasing
						100	closed	2000		2.50E-13		3075	2975	P increasing?
						0	open	5400				3032	3032	P steady
													3030	Defined value
29	CR-10	GS	1.925	1.377	50	15	open		1.00E-12		7.80E-13	1463	1455.5	P increasing
						50	open	230	2.78E-13		5.80E-14	2670	2645	P increasing
						100	open	980	3.61E-13			2960	2910	P increasing
						100	open		2.38E-13		1.80E-14			
						100	closed	2000		2.20E-13		3396	3296	P steady

						0	open	4800 5400				3327 3300	3327 3300	P decreasing Defined value
30	CR-10	CRL	1.966 1.965	1.285 1.284	60	15 50 100 100 100 0	open open open open closed open	50 900 2300 3200 5200	1.62E-12 1.89E-12 1.87E-12	1.70E-13	1.45E-12 1.72E-12 1.70E-12	1395/1250 1605/1450 1650/1485 1535-1370	1370 1555 1550 1535 1550	P increasing P steady P increasing P decreasing Defined value
31 Cell leak	SR-Sh	GS	1.915 1.936	1.219 1.246	60	50 50 0	open closed open	2500 2800 5200	4.30E-13		4.30E-13	238 246 240	213 196 240 250	P increasing P increasing P incr. (8 kPa in 1500 h) Defined value
32	CR-10	CRL	1.717	0.991	60	15 50 100 0	open open open	1000 2000 4000	6.30E-13 6.30E-12 7.40E-12		6.30E-12 7.40E-12	112 126 156	104.5 101 106 105	P steady; airlock? P steady P steady Defined value
33	SR-Sh	GS	1.69 1.72	0.964 0.995	60	15 13 9 0 0	open open open	35 26 200 286 960	9.40E-09 7.90E-09		9.40E-09 7.90E-09	35 26 40 55	27.5 19.5 35.5 55	P increasing

APPENDIX F: Summary of SWCC and Gas Permeability Test Data

SWCC data for MX80: granitic sand 50:50 CR-10 standard compaction

Capillary pressure (kPa)	dry density (g/cm ³)	void ratio	porosity	Corrected gravimetric water content (%)	Volumetric fluid content (%)	Degree of liquid saturation (%)
100	1.842	0.47	0.32	16.8	31.1	98.0
200	1.849	0.46	0.32	16.8	31.2	99.0
400	1.840	0.47	0.32	16.9	31.3	98.2
800	1.842	0.47	0.32	16.9	31.3	98.6
1450	1.853	0.46	0.31	16.7	31.2	99.5
13400	1.848	0.46	0.32	13.5	25.1	79.7
27290	1.839	0.47	0.32	11.9	21.9	68.8
58890	1.845	0.46	0.32	8.4	15.7	49.4
91610	1.854	0.46	0.31	5.1	9.5	30.2
183580	1.843	0.46	0.32	1.7	3.1	9.8

SWCC data for MX80: granitic sand 50:50 CR-10 modified compaction

Capillary pressure (kPa)	dry density (g/cm ³)	void ratio	porosity	Corrected gravimetric water content (%)	Volumetric fluid content (%)	Degree of liquid saturation (%)
100	1.577	0.71	0.42	26.4	41.8	100.4
200	1.579	0.71	0.42	26.4	42.0	101.1
400	1.581	0.71	0.41	25.8	40.9	98.7
800	1.578	0.71	0.42	25.5	40.5	97.4
1450	1.589	0.70	0.41	25.0	40.0	97.1
5600	1.584	0.70	0.41	20.9	33.3	80.5
7120	1.575	0.71	0.42	18.3	29.0	69.5
17590	1.573	0.72	0.42	13.1	20.7	49.6
71140	1.575	0.71	0.42	7.9	12.4	29.9
178460	1.565	0.72	0.42	2.6	4.2	9.9

SWCC data for MX80: crushed limestone 50:50 SR-Sh modified compaction

Capillary pressure (kPa)	dry density (g/cm ³)	void ratio	porosity	Corrected gravimetric water content (%)	Volumetric fluid content (%)	Degree of liquid saturation (%)
100	1.848	0.47	0.32	14.7	31.5	98.9
200	1.845	0.47	0.32	14.6	31.2	97.9
400	1.861	0.46	0.31	14.1	30.4	97.0
800	1.861	0.46	0.31	13.9	30.1	96.0
1450	1.861	0.46	0.31	14.3	30.9	98.8
53410	1.842	0.47	0.32	11.8	25.3	79.0
54830	1.854	0.46	0.32	10.3	22.3	70.5
66590	1.839	0.47	0.32	7.4	15.8	49.0
100620	1.849	0.47	0.32	4.4	9.5	29.8
182880	1.826	0.48	0.33	1.5	3.1	9.6

SWCC data for MX80: crushed limestone 60:40 SR-Sh modified compaction

Capillary pressure (kPa)	dry density (g/cm ³)	void ratio	porosity	Corrected gravimetric water content (%)	Volumetric fluid content (%)	Degree of liquid saturation (%)
100	1.784	0.52	0.34	16.4	34.1	99.6
200	1.784	0.52	0.34	16.4	34.0	99.5
400	1.784	0.52	0.34	16.3	33.9	99.1
800	1.784	0.52	0.34	16.2	33.5	98.1
1450	1.784	0.52	0.34	16.0	33.2	97.2
50050	1.790	0.51	0.34	13.1	27.2	80.0
55190	1.785	0.52	0.34	11.4	23.7	69.4
67470	1.788	0.52	0.34	8.2	17.0	49.9
101070	1.778	0.52	0.34	4.9	10.1	29.5
188630	1.786	0.52	0.34	1.6	3.4	10.0

Gas Permeability data for MX80: granitic sand 50:50 CR-10 standard compaction

Degree of Liquid Saturation (%)	Dry Density (g/cm ³)	Void Ratio	Porosity	Coefficient of Gas Permeability (m ²)	Gas Conductivity	
					(m/s)	(cm/s)
83.2	1.606	0.68	0.41	1.6E-14	9.3E-09	9.3E-07
73.1	1.608	0.68	0.40	1.3E-13	7.9E-08	7.9E-06
51.6	1.600	0.69	0.41	6.8E-13	4.0E-07	4.0E-05
30.4	1.588	0.70	0.41	1.2E-12	6.9E-07	6.9E-05
9.7	1.561	0.73	0.42	2.3E-12	1.3E-06	1.3E-04

Gas Permeability data for MX80: granitic sand 50:50 CR-10 modified compaction

Degree of Liquid Saturation	Dry Density	Void Ratio	Porosity	Coefficient of Gas Permeability	Gas Conductivity	
(%)	(g/cm ³)			(m ²)	(m/s)	(cm/s)
79.6	1.847	0.46	0.32	3.9E-15	2.3E-09	2.3E-07
71.6	1.863	0.45	0.31	5.9E-15	3.5E-09	3.5E-07
49.5	1.845	0.46	0.32	9.0E-14	5.3E-08	5.3E-06
29.0	1.830	0.48	0.32	1.6E-13	9.5E-08	9.5E-06
9.8	1.837	0.47	0.32	3.6E-13	2.1E-07	2.1E-05

Gas Permeability data for MX80: crushed limestone 50:50 SR-Sh modified compaction

Degree of Liquid Saturation	Dry Density	Void Ratio	Porosity	Coefficient of Gas Permeability	Gas Conductivity	
(%)	(g/cm ³)			(m ²)	(m/s)	(cm/s)
80.8	1.856	0.46	0.32	5.0E-16	3.0E-10	3.0E-08
70.5	1.854	0.46	0.32	3.1E-15	1.8E-09	1.8E-07
49.5	1.844	0.47	0.32	3.6E-14	2.1E-08	2.1E-06
29.7	1.845	0.47	0.32	1.1E-13	6.7E-08	6.7E-06
9.9	1.845	0.47	0.32	2.6E-13	1.5E-07	1.5E-05

Gas Permeability data for MX80: crushed limestone 60:40 SR-Sh modified compaction

Degree of Liquid Saturation	Dry Density	Void Ratio	Porosity	Coefficient of Gas Permeability	Gas Conductivity	
(%)	(g/cm ³)			(m ²)	(m/s)	(cm/s)
82.5	1.809	0.50	0.33	1.3E-16	7.5E-11	7.5E-09
70.5	1.794	0.51	0.34	1.7E-14	1.0E-08	1.0E-06
47.6	1.760	0.54	0.35	8.5E-14	5.0E-08	5.0E-06
29.5	1.780	0.52	0.34	1.4E-13	8.1E-08	8.1E-06
9.6	1.767	0.53	0.35	3.9E-13	2.3E-07	2.3E-05